SANDIA REPORT
SAND2012-7321
Unlimited Release
Printed September 2012

Technical Reference for Hydrogen Compatibility of Materials

C. San Marchi
B.P. Somerday

Prepared by
Sandia National Laboratories
Albuquerque, New Mexico 87185 and Livermore, California 94550

Sandia National Laboratories is a multi-program laboratory managed and operated by Sandia Corporation, a wholly owned subsidiary of Lockheed Martin Corporation, for the U.S. Department of Energy's National Nuclear Security Administration under contract DE-AC04-94AL85000.

Issued by Sandia National Laboratories, operated for the United States Department of Energy by Sandia Corporation.

Available to DOE and DOE contractors from
U.S. Department of Energy
Office of Scientific and Technical Information
P.O. Box 62
Oak Ridge, TN 37831

Telephone: (865) 576-8401
Facsimile: (865) 576-5728
E-Mail: reports@adonis.osti.gov
Online ordering: http://www.osti.gov/bridge

Available to the public from
U.S. Department of Commerce
National Technical Information Service
5285 Port Royal Rd.
Springfield, VA 22161

Telephone: (800) 553-6847
Facsimile: (703) 605-6900
E-Mail: orders@ntis.fedworld.gov
Online order: http://www.ntis.gov/help/ordermethods.asp?loc=7-4-0#online

SAND2012-7321
Unlimited Release
Printed September 2012

Technical Reference for Hydrogen Compatibility of Materials

C. San Marchi
B.P. Somerday
Hydrogen and Metallurgy Science
Sandia National Laboratories
P.O. Box 969
Livermore, California 94551-MS9404

Abstract

The Technical Reference for Hydrogen Compatibility of Materials summarizes materials data related to hydrogen-assisted fracture (also called hydrogen embrittlement) in gaseous hydrogen environments, with emphasis on hydrogen permeation and structural properties. The Technical Reference generally does not provide specific recommendations for materials selection as the suitability of a given material depends on service conditions, in particular the mechanical and environmental conditions associated with a particular component, as well as the details of the materials microstructure. In substance, the Technical Reference is a collection of stand-alone documents organized by materials class, which have been compiled into this composite report. The individual sections are occasionally updated and new sections are added; the most recent versions are available from our website at http://www.ca.sandia.gov/matlsTechRef/. This compilation updates the previous composite release: SAND2008-1163.

ACKNOWLEDGMENTS

This document was prepared with financial support from the Safety, Codes and Standards program element of the Hydrogen and Fuel Cells Program, Office of Energy Efficiency and Renewable Energy, United States Department of Energy.

Electronic copies of this report and updated sections can be requested from the authors or downloaded at http://www.sandia.gov/matlsTechRef/ .

CONTENTS

CONTENTS (cont.)

Technical Reference on Hydrogen Compatibility of Materials

Introduction

The Technical Reference on Hydrogen Compatibility of Materials summarizes materials data originating from scientific articles and institutional reports with the aim of assisting materials selection for service in hydrogen gas, with emphasis on structural materials. It is compromised of a collection of electronic documents (or sections) that are updated periodically; the latest revisions are available at http://www.ca.sandia.gov/matlsTechRef/ In addition, these documents have been assembled into a report [1] that will be revised occasionally based on substantial overall content change.

The data included in the Technical Reference reflect two primary phenomena associated with materials in hydrogen gas service: 1) permeation of hydrogen through materials, resulting in an effective leak through a structure, and 2) degradation of the mechanical properties of materials, which compromises structural integrity. The well-documented degradation phenomena consist of a number of possible mechanisms that we refer to collectively as hydrogen-assisted fracture (in the literature these are often called hydrogen embrittlement). The Technical Reference does not provide specific recommendations for materials selection as the suitability of a given material depends on service conditions, in particular the mechanical, environmental, and material conditions associated with a particular component. Examples of important mechanical, environmental, and material variables that generally contribute to hydrogen-assisted fracture include loading mode (e.g., static *vs* cyclic stress), hydrogen gas pressure, temperature, and material strength level. It is recommended that safety factors for hydrogen gas systems be established based on materials tests performed under relevant mechanical, environmental, and material conditions without significant extrapolation. For example, mechanical properties measured for a low-strength steel in low-pressure hydrogen gas should not be applied for exposure to high-pressure hydrogen gas or to the same steel in a high-strength condition. It is important to emphasize that engineering systems have been successfully designed for high-pressure hydrogen service, much of this experience is summarized in an ASME report [2].

The Technical Reference is organized by specific alloy (e.g., type 304 austenitic stainless steel) or alloy system (e.g., Cr-Mo steels) according to common and relevant nomenclature. Materials are primarily grouped by base element, such as steels or aluminum alloys, which are further distinguished by characteristics such as microstructure, composition, and heat treatment. A four-digit number (code) is assigned to each section to assist organization and revision: the first digit corresponds to the base element; steels constitute the majority of structural materials, and two distinct broad categories are used: ferritic steels (1xxx code series) and austenitic steels (2xxx code series). The second digit refers to the alloy class, and the final two digits specify the alloy or alloy system. For example, within the ferritic steels (1xxx code series), the low-alloy steels are distinguished by code numbers 12xx. At the alloy system level, the low-alloy steels include the tempered Cr-Mo steels (code 1211) and the tempered Ni-Cr-Mo steels (code 1212). When a section provides information at a level higher than the alloy family, zeros are used, such as code 1500 to designate the broad class of ferritic stainless steels.

Introduction

For the purposes of this Technical Reference, the susceptibility of structural materials to hydrogen-assisted fracture in hydrogen gas is evaluated by mechanical testing in two broad categories of environmental conditions: (1) testing in high-pressure hydrogen gas (applying stress concurrent with hydrogen gas exposure) or (2) testing in air subsequent to precharging with hydrogen (applying stress following hydrogen gas exposure). In the Technical Reference sections, these environmental conditions are referred to as *external* hydrogen and *internal* hydrogen respectively. In general, hydrogen precharging is not appropriate for ferritic steels, since the diffusion of hydrogen is relatively rapid on the time scale of typical tests (thus significant hydrogen egress can occur between hydrogen precharging and completion of testing). For some materials, such as austenitic stainless steels, testing in external hydrogen may not produce relevant data because of the slow rate of hydrogen transport in these materials. Specific guidelines for testing in external hydrogen versus testing with internal hydrogen have not been established; however, we believe that materials with hydrogen diffusivity $>10^{-10}$ m^2/s (e.g., carbon and low-alloy steels) should not be tested in air with internal hydrogen. In addition, tests in external hydrogen on materials with hydrogen diffusivity $<10^{-15}$ m^2/s (e.g., austenitic steels) may not provide lower bound properties with the possible exception of long-time tests such as sustained-load cracking. One notable exception to these recommendations is that austenitic stainless steels that form strain-induced martensite may, in some cases, be effectively tested in external hydrogen since the martensite substantially enhances hydrogen diffusion. More discussion of hydrogen transport in austenitic stainless steel can be found in Refs. [3, 4].

With regard to internal hydrogen, there are several methods of precharging materials with hydrogen, the two most common being electrolytic precharging and thermal precharging. For the purposes of the Technical Reference sections, data from electrolytic precharging are largely precluded in favor of thermal precharging because the conditions under which electrolytic precharging occurs are generally not relevant to service in high-pressure hydrogen gas. For example, the hydrogen fugacity associated with electrolytic precharging can be many orders of magnitude greater than can be obtained in hydrogen gas. In addition, since electrolytic charging is typically conducted near ambient temperature, hydrogen penetration into low-diffusivity materials is limited, often leading to large hydrogen concentration gradients near the surface of the test specimen.

1. General

Each Technical Reference *section* consists of a series of *subsections*, which have a consistent numbering system, titles, and content. Each subsection focuses on a particular characteristic or property of the alloy or alloy system represented in the section. The numbering system, title, objective and general content of the subsections are described below.

This subsection summarizes the results that follow. In particular, we emphasize the key characteristics and concepts that are important for interpreting data related to hydrogen-assisted fracture in the material that is the topic of this section.

1.1 Composition and microstructure

This subsection summarizes the characteristics of the material(s) that are referenced in the particular section of the Technical Reference. Typical compositional ranges are given using designations from the unified numbering system (UNS). The specific compositions of the materials that are cited throughout the section are also provided. In this context, we refer to

microstructure in a general sense from the perspective of product forms, processing conditions, and strength, which are also summarized when relevant. Specific microstructural details (such as phase distributions, precipitate structure, etc) are generally not provided except when essential to the following subsections.

Alloy composition is an important variable for understanding the performance of structural metals in hydrogen gas, particularly since compositional specifications tend to allow a wide range for each alloying element. It is noted, however, that alloy specifications with wide compositional ranges may be inadequate for specifying materials for hydrogen service. Indeed, this is true for applications other than hydrogen service and explains the plethora of materials specifications, such as those provided by various standards development organizations (ASME, SAE-AMS, ASTM, etc.) for specific applications. Manufacturers also typically have their own compositional specifications relevant for specific products and materials performance, which can specify tighter limits than the public domain specifications. The strength level of the alloy is also an important characteristic for pressure-bearing materials in hydrogen service as high-strength microstructures tend to be significantly more susceptible to hydrogen-assisted fracture than low-strength microstructures.

1.2 Common designations

In this subsection, we associate common names and trade names with the compositional specifications that apply to the materials from that section. The reader is referred to the UNS guide [5] and other standard references, such as the Aerospace Structural Metals Handbooks [6], for comprehensive summaries of various materials specifications that are related to common materials. In general, we have tried to avoid using trade names in favor of general common names, however, for some materials classes this is not practical.

2. Permeability, Diffusivity and Solubility

This subsection summarizes hydrogen permeability, diffusivity, and solubility data. Permeability, diffusivity and solubility collectively describe the dissolution and transport of hydrogen atoms in the lattice of a given material. The solubility (S) is a measure of hydrogen dissolved in a material at equilibrium and can be related to the concentration of hydrogen in a metal lattice (c_L) using Sievert's Law:

$$S = \frac{c_L}{f^{1/2}} \tag{1}$$

where f is the fugacity of hydrogen gas in equilibrium with the lattice (the fugacity of an ideal gas is equivalent to the pressure). Hydrogen dissociates on metal surfaces and diffuses as atomic hydrogen in metals, which accounts for the square root dependence on hydrogen fugacity. In most non-metals, hydrogen diffuses as the molecular species, thus $S \propto 1/f$. Hydrogen can be trapped by microstructural features [7], thus increasing the concentration of hydrogen dissolved in the material; this is particularly true of ferritic and martensitic steels and depends on the density and strength of trapping sites.

Introduction

The permeability (Φ) is used to calculate the steady-state flux of hydrogen permeating through a structure using Fick's first law of diffusion ($J = -D\left(dc/dx\right)$), where the permeability is defined as the product of the hydrogen diffusivity (D) and solubility:

$$\Phi \equiv DS \tag{2}$$

For example, the hydrogen flux permeating through a semi-infinite metal plate with a finite hydrogen gas pressure on one side and approximately zero pressure on the other side can be expressed as

$$J_\infty = D\frac{Sf^{1/2}}{t} = \frac{\Phi}{t} f^{1/2} \tag{3}$$

where J_∞ is the steady-state diffusional flux of hydrogen, t is the structure thickness, and f is the fugacity of hydrogen gas on the high-pressure side of the plate.

Typically, permeability and diffusivity are determined from direct measurements of the flux of hydrogen through a membrane that is pressurized with hydrogen gas on one side. This experiment must be set up such that lattice diffusion is the rate-limiting step of hydrogen transport and the equilibrium hydrogen concentrations have the correct dependence on hydrogen fugacity (generally, $\propto f^{1/2}$ for metals or $\propto f$ for non-metals). In many cases, hydrogen transport properties are measured at elevated temperature to determine the temperature dependence and to facilitate the measurements. The temperature dependence generally follows the classic exponential form:

$$A = A_0 \exp\left(\frac{-E_A}{RT}\right) \tag{4}$$

where A is the transport property of interest (permeability, diffusivity, or solubility), A_0 is a constant, E_A is an activation energy, R is the universal gas constant, and T is temperature in Kelvin. Many of the principles of permeation are reviewed in Ref. [8] in the context of metals, and an assessment of data can be found in the companion reference [9]. For polymers the reader is referred to Refs. [10, 11].

In general, permeation data are consistent in the literature, and experimental measurements are facilitate by the steady-state definition of Φ. Reported diffusivities, however, have significantly more scatter because diffusivity is determined from transient data, which are inherently more difficult to analyze than steady-state data. Since hydrogen solubility is generally determined from the ratio of the permeability and diffusivity, reported values for hydrogen solubility are dependent on the quality of the diffusivity measurement.

Electrochemical permeation measurements (ASTM G148) are not recommended for determining hydrogen transport properties in materials exposed to high-pressure hydrogen gas. However, in the absence of gas permeation data, we report effective hydrogen diffusivity (D_{eff}) from electrochemical measurements.

3. Mechanical Properties: Effects of Gaseous Hydrogen

These subsections summarize the mechanical properties that are commonly used to quantify the susceptibility of structural metals to hydrogen-assisted fracture. Results from scientific articles and institutional reports that were generated from non-standard techniques or are qualitative in nature have been precluded from these subsections

3.1 Tensile properties

Tensile properties are important for characterizing deformation and fracture in hydrogen environments. Strain rate is a particularly important test parameter as susceptibility to hydrogen-assisted fracture can be sensitive to strain rate, even in the rather narrow range from 10^{-6} to 10^{-2} 1/s [12].

3.1.1 Smooth tensile properties

Properties are reported according to definitions in ASTM E6. Except when noted yield strength refers to the 0.2% offset yield strength. If the method of determination is not given in the source article or report, it is assumed that yield strength is determined by the 0.2% offset method. The geometry of tensile specimens is assumed to follow the basic guidelines in ASTM E8.

The following nomenclature is used to summarize the deformation and fracture results from tensile tests with smooth specimens:

S_y (MPa)	0.2% offset yield strength: determined by drawing a line that has the slope of the elastic modulus and intersects the strain axis at 0.2% on a plot of the stress-strain curve; the intersection of this construction line with the flow stress is the yield strength, see ASTM E6
S_u (MPa)	tensile strength: maximum load divided by the original cross-sectional area
El_u (%)	uniform elongation: engineering strain at maximum load
El_t (%)	total elongation: engineering strain at fracture (depends on gauge length)
RA (%)	reduction of area: difference of original cross-sectional area and the minimum cross-sectional area after fracture normalized by the original cross-sectional area
RRA	relative reduction in area: ratio of RA measured for a specific test condition (external or internal hydrogen) to RA measured in air or inert environment, see ASTM G129

3.1.2 Notched tensile properties

Notched tensile specimens generate high hydrostatic tensile stresses, which can amplify the effects of hydrogen-assisted fracture. Common specimen designs are based on cylindrical tensile specimens but are modified by including a circumferential notch. ASTM G142 provides a standard notched tensile geometry for testing in high-pressure hydrogen gas; however, few studies have used this geometry. We report the notch geometry and dimensions of specimens described in the source articles and reports, including the elastic stress concentration factor. In addition, yield strength from smooth tensile tests is also reported since notch sensitivity in the absence of hydrogen will generally be a function of the material's microstructure and strength. Data measured from other notched-specimen designs, such as single-edge notched tensile specimens, are generally not included in this subsection; although when such tests demonstrate important trends, those trends are summarized.

The following nomenclature is used for notched tensile specimens:

σ_s (MPa)	notched tensile strength: maximum load divided by the original cross-sectional area at the notch, see ASTM E602
RA (%)	reduction of area: difference of original notch cross-sectional area and the minimum notch cross-sectional area after fracture normalized by the original notch cross-sectional area
K_t	elastic stress concentration factor

3.2 Fracture mechanics

We emphasize that fracture mechanics testing is imperative for the design of pressure-bearing structures with large section sizes. Fracture mechanics design methods allow safety margins against hydrogen-assisted crack propagation to be quantified. These design methods require material property inputs that are measured using fracture mechanics techniques. Proper interpretation of fracture mechanics data is critical for the design of safe structures. For example, fracture mechanics data should represent lower-bound values for a given material, environment, and testing protocol.

3.2.1 Fracture toughness

The fracture toughness of materials is measured using precracked specimens that are subjected to a constant displacement rate. Fracture toughness testing generally yields measures of both the fracture initiation and crack propagation resistances. Similar to tensile testing, the displacement rate during fracture toughness testing in hydrogen gas can affect the results. Standardized specimen geometry and testing procedures for determine of fracture toughness are outlined in ASTM E1820.

The following nomenclature is used for summarizing results from fracture toughness testing:

K_{Ic} (MPa $m^{1/2}$)	stress-intensity factor for fracture initiation under small-scale yielding, plane strain conditions
K_Q (MPa $m^{1/2}$)	value of stress-intensity factor for fracture initiation measured from specimen that does not meet dimensional requirements according to ASTM E1820
K_{JIc} (MPa $m^{1/2}$)	equivalent stress-intensity factor calculated from the J-integral value of fracture initiation toughness (J_{Ic})
J_{Ic} (kJ m^{-2})	J-integral for fracture initiation under large-scale yielding, plane strain conditions
J_Q (kJ m^{-2})	value of J-integral for fracture initiation measured from specimen that does not meet dimensional requirements according to ASTM E1820
dJ/da (MPa)	slope of the J-integral *vs* crack extension curve; a measure of the crack propagation resistance
K_{IH} (MPa $m^{1/2}$)	stress-intensity factor for fracture initiation measured in hydrogen gas; may be determined from values of the J-integral and may not meet the dimensional requirements according to ASTM E1820

3.2.2 Threshold stress-intensity factor

The threshold stress-intensity factor for sustained-load cracking (K_{TH}) is a measure of a material's resistance to hydrogen-assisted crack propagation under static loading. In general, the value of K_{TH} is not a material property, since the value of K_{TH} may depend on the geometry of the test specimen (i.e., may not be a value that is independent of specimen geometry such as K_{Ic}). One of the common test configurations is the modified bolt load compact specimen (ASTM E1681), where a constant displacement is applied with the aid of a bolt. This configuration is also referred to as the wedge-opening load (WOL) specimen. In these tests, an initial stress-intensity factor less than K_{Ic} is applied before placing the precracked specimen in the environment of interest, in this case high-pressure hydrogen gas. If susceptible to environment-assisted fracture, the precrack will extend under decreasing stress-intensity factor until the crack arrests at the threshold value.

The time for initiation of crack propagation can be unpredictable, possibly requiring many thousands of hours. Therefore, the lack of an environmental cracking response may not imply that the applied stress-intensity factor is less than the threshold. Thus, crack advance and arrest is the only unambiguous method of determining a threshold value.

More specifics of the method recommended for testing in gaseous hydrogen can be found in the ASME Boiler and Pressure Vessel Code, Section VIII, Division 3, Article KD-10.

3.3 Fatigue

Fatigue is a material failure mode particular to cyclic loading. The effects of hydrogen gas on fatigue properties have not been extensively investigated for most alloy classes. Fatigue is arguably the most important failure mechanism in structures subjected to cyclic stress, therefore this failure mechanism must be considered in the design of hydrogen gas components subjected to pressure cycling. Given the importance of this failure mode, more efforts are needed to measure fatigue properties of materials in hydrogen gas. Frequency of the load cycle and the ratio of minimum load to maximum load (R-ratio) are two important variables that have been shown to affect fatigue properties measured in hydrogen gas.

3.3.1 Low-cycle and high-cycle fatigue

Perhaps the most common fatigue testing method involves smooth cylindrical specimens, which are used to generate the so-called S-N curves. The S-N curves are plots of alternating stress amplitude (S) *vs* number of cycles to failure (N). The number of cycles to failure includes both crack initiation and propagation.

3.3.2 Fatigue crack propagation

Although results from fatigue testing of smooth specimens do not separate fatigue crack initiation and propagation, testing of fracture mechanics specimens can provide data solely on fatigue crack propagation. Precracked specimens are tested using fracture mechanics methods (ASTM E647) to generate plots of fatigue crack growth rate (crack extension per load cycle, da/dN) as a function of stress intensity factor range (ΔK). These data can be used to quantify design margins that accommodate the propagation of known defects in pressure-bearing structures or that eliminate the propagation of critical defects all together.

3.4 Creep

Creep is a high-temperature failure mode, where materials can deform and ultimately fracture under static loading. Although creep may not be a consideration for most hydrogen infrastructure components, effects of hydrogen could be strongly manifested in creep due to the low strain rates typically involved and the fact that hydrogen solubility increases with temperature.

3.5 Impact

Notched-bar impact tests, such as Charpy impact, are standard methods of estimating fracture toughness in steels (ASTM E23). Due to the nature of strain rate effects on hydrogen-assisted fracture, impact testing is not the most effective method for quantifying hydrogen-assisted fracture in materials. Consequently, correlations between impact properties and fracture toughness are not appropriate for assessing hydrogen-assisted fracture.

3.6 Disk rupture testing

The disk rupture test is a qualitative assessment of susceptibility to hydrogen-assisted fracture. This method involves pressurizing identical membranes of material with hydrogen gas and with inert gas (such as helium) until the membranes fail. The ratio of the burst pressure in inert gas to the burst pressure in hydrogen gas is an index of susceptibility to hydrogen-assisted fracture (ASTM F1459). These tests do not provide data that are used to quantify the safety margins of components in hydrogen gas systems; however, disk rupture tests can be used as a simple screening tool for evaluating the relative susceptibility of materials to hydrogen-assisted fracture.

4. Fabrication

In the 4.x subsections, we describe specific processing variables and metallurgical features that should be considered in assessing susceptibility to hydrogen-assisted fracture. Primary processing (forging, cold-working, etc.) as well as subsequent heat treatment are important variables. For example, aging of A-286 (precipitation-strengthened austenitic stainless steel) significantly impacts the ductility in this alloy, and appears to increase the susceptibility to hydrogen-assisted fracture. Welding is another important fabrication variable, particularly in ferritic steels where martensite can form during heating and cooling at the weld. Martensite is known to be vulnerable to hydrogen-assisted fracture.

5. References

1. C San Marchi and BP Somerday. Technical Reference on Hydrogen Compatibility of Materials (SAND2008-1163). Sandia National Laboratories, Livermore CA (2008).
2. ASME. Hydrogen Standardization Interim Report for Tanks, Piping, and Pipelines (STP/PT-003). American Society of Mechanical Engineers (ASME), New York (2005).
3. C San Marchi, BP Somerday and SL Robinson. Permeability, Solubility and Diffusivity of Hydrogen Isotopes in Stainless Steels at High Gas Pressure. Int J Hydrogen Energy 32 (2007) 100-116.
4. C San Marchi, BP Somerday, X Tang and GH Schiroky. Effects of alloy composition and strain hardening on tensile fracture of hydrogen-precharged type 316 stainless steels. Int J Hydrogen Energy 33 (2007) 889-904.

5. ASTM DS-56H, Metals and Alloys in the UNIFIED NUMBERING SYSTEM (SAE HS-1086 OCT01). American Society for Testing and Materials (Society of Automotive Engineers) (2001).
6. WF Brown, H Mindlin and CY Ho. Aerospace Structural Metals Handbook. West Lafayette IN: CINDAS/UASF CRDA Handbooks Operation, Purdue University (1998).
7. JP Hirth. Effects of hydrogen on the properties of iron and steel. Metall Trans 11A (1980) 861-890.
8. AD LeClaire. Permeation of Gases Through Solids: 1. Principles. Diffusion and Defect Data 33 (1983) 1-66.
9. AD LeClaire. Permeation of Gases Through Solids: 2. An assessment of measurements of the steady-state permeability of H and its isotopes through Fe, Fe-based alloys, and some commercial steels. Diffusion and Defect Data 34 (1983) 1-35.
10. SA Stern, B Krishnakumar and SM Nadakatti. Permeability of Polymers to Gases and Vapors. in: JE Mark, editor. Physical Properties of Polymers Handbook. Woodbury NY: American Institute of Physics (1996).
11. S Pauly. Permeability and Diffusion Data. in: J Brandrup, EH Immergut and EA Grulke, editors. Polymer Handbook, fourth edition. New York: John Wiley and Sons (1999).
12. EJ Vesely, RK Jacobs, MC Watwood and WB McPherson. Influence of Strain Rate on Tensile Properties in High-Pressure Hydrogen. in: AW Thompson and NR Moody, editors. Hydrogen Effects in Materials. Proceedings of the Fifth International Conference on the Effect of Hydrogen on the Behavior of Materials (Moran WY, 1994), volume Warrendale PA: TMS (1996) p. 363-374.

This page intentionally left blank.

Technical Reference on Hydrogen Compatibility of Materials

Plain Carbon Ferritic Steels:

C-Mn Alloys (code 1100)

1. General

Carbon and alloy steels can be categorized by a variety of characteristics such as composition, microstructure, strength level, material processing, and heat treatment [1]. The carbon and alloy steel categories selected for the Technical Reference on Hydrogen Compatibility of Materials are based on characteristics of the steels as well as available data. In this chapter, the steels are distinguished by the primary alloying elements, i.e., carbon and manganese. Data on the compatibility of carbon steels with hydrogen gas exist primarily for the following alloys: A515 Gr. 70, A516 Gr. 70, A106 Gr. B, A106 Gr. C, SA 105, and the 10xx steels. In addition, a substantial amount of data has been generated for the API 5L steels, grades X42 to X80. Since a full range of properties in hydrogen gas is not available for each steel, data for all carbon steels are presented in this chapter. Although plain carbon ferritic steels exhibit some metallurgical differences, the basic trends in the data are expected to apply generally to this class of steels.

Carbon steels are attractive structural materials in applications such as pipelines because the steels can be formed and welded, and adequate mechanical properties can be achieved through normalizing heat treatments or hot rolling. The API 5L steels may contain additional alloying elements, such as small quantities of niobium and vanadium. These "microalloying" additions as well as processing through controlled rolling impart a combination of elevated strength and improved low-temperature fracture resistance.

Despite the attractive properties of carbon steels, these materials must be used judiciously in structures exposed to hydrogen gas. Hydrogen gas degrades the tensile ductility of carbon steels, particularly in the presence of stress concentrations. Additionally, hydrogen gas lowers fracture toughness, and certain metallurgical conditions can render the steels susceptible to crack extension under static loading. Hydrogen gas also accelerates fatigue crack growth, even at relatively low hydrogen gas partial pressures, suggesting that small fractions of hydrogen in gas blends must be considered in fatigue life assessments. The severity of these manifestations of hydrogen embrittlement depends on mechanical, environmental, and material variables. Variables that influence behavior in hydrogen gas include loading rate, load cycle frequency, gas pressure, gas composition, and the presence of welds. Control over these variables may allow carbon steels to be applied safely in hydrogen gas environments. For example, limiting the magnitude and frequency of load cycling can improve the compatibility of carbon steels with hydrogen gas.

This chapter presents a range of data for carbon steels in hydrogen gas, including tensile and crack growth properties. The crack growth data emphasize fracture mechanics properties, since pipeline design can benefit from defect-tolerant design principles, particularly for hydrogen environments.

1.1 Composition and microstructure

Table 1.1.1 lists the allowable composition ranges for carbon steels covered in this chapter. Table 1.1.2 summarizes the compositions and product forms of steels from hydrogen compatibility studies reported in this chapter. Table 1.1.3 details the heat treatments applied to steels in Table 1.1.2. Additionally, Table 1.1.3 includes the yield strength, ultimate tensile strength, total elongation, and reduction of area that result from the heat treatments.

1.2 Common designations

A515 Gr. 70: UNS K03103, ASTM A515 (70)
A516 Gr. 70: UNS K02700, ASTM A516 (70)
A106 Gr. B: ASTM A106 (B)
A106 Gr. C: ASTM A106 (C)
SA 105 Gr. II: ASME SA-105, ASTM A105
1020: UNS G10200, AISI 1020, ASTM A830 (1020)
1042: UNS G10420, AISI 1042, ASTM A830 (1042)
1080: UNS G10800, AISI 1080, ASTM A830 (1080)
X42: API 5L X42
X52: API 5L X52
X60: API 5L X60
X65: API 5L X65
X70: API 5L X70
X80: API 5L X80

2. Permeability, Diffusivity and Solubility

The permeability and solubility of hydrogen in 10xx carbon steels are mildly affected by carbon content and microstructure [2]. In a single study, permeation experiments were conducted on six carbon steels over the temperature range 500 to 900 K and gas pressure range 0.01 to 0.7 MPa [2]. The hydrogen permeability *vs* temperature relationships are plotted in Figure 2.1 (also listed in Table 2.1) for the normalized microstructures and show that permeability systematically decreases as carbon content increases. The difference in the permeability for 1010 steel compared to 1095 steel is about a factor of three over the entire temperature range examined.

The solubility of hydrogen in 10xx carbon steels was determined from the ratio of permeability and diffusivity [2]. Solubility *vs* temperature relationships are given in Table 2.1 and plotted in Figure 2.2 and demonstrate a trend similar to permeability, where solubility generally decreases as carbon content increases. The difference in the solubility for 1010 steel compared to 1095 steel is about a factor of two over the entire temperature range examined.

Permeability and solubility *vs* temperature relationships were reported for three different microstructures [2]: normalized, spheroidized, and quenched and tempered. The permeability was nearly identical for the three microstructures over the temperature range examined. The solubility was highest in the normalized microstructure and lowest in the quenched and tempered microstructure, but the difference was less than a factor of two over the temperature range.

The solubility is the Sievert's constant in Sievert's law and thus can be used to calculate the concentration of hydrogen in the metal lattice. At lower temperatures, hydrogen segregates to

defects in metals, and the total hydrogen concentration is the sum of hydrogen in the lattice and hydrogen at defects. The solubility relationships in Table 2.1 can be used to calculate the lattice hydrogen concentration in carbon steels but not the total hydrogen concentration. More information on calculating total hydrogen concentrations in steels at lower temperatures can be found in Ref. [3].

3. Mechanical Properties: Effects of Gaseous Hydrogen

3.1 Tensile properties

3.1.1 Smooth tensile properties

Measurement of smooth tensile properties of carbon steels in high-pressure hydrogen gas demonstrates that hydrogen degrades reduction of area but not ultimate tensile strength. Tables 3.1.1.1 and 3.1.1.2 summarize properties measured in 6.9 and 69 MPa hydrogen gas for a wide range of carbon steels [4-6]. The reduction of area measurements in hydrogen gas are remarkably consistent, where most values range from 35 to 47% independent of hydrogen gas pressure. Although these absolute values remain relatively high in hydrogen gas, the loss of reduction of area relative to values measured in air or inert gas can be as high as 50%. The most notable exception to the general reduction of area trend is the high-carbon steel 1080, which exhibits a reduction of area as low as 6% in hydrogen gas. However, the reduction of area for 1080 in nitrogen gas (14%) is also relatively low.

3.1.2 Notched tensile properties

High-pressure hydrogen severely degrades the reduction of area of carbon steels when measurements are conducted using notched specimens. In addition, hydrogen mildly reduces tensile strength in notched specimens. Table 3.1.2.1 summarizes data for a range of carbon steels tested in 6.9 MPa hydrogen gas [4]. Similar to trends from smooth specimens, the reduction of area values from notched specimens are in a consistent range (5 to 9%). However, the reduction of area loss measured from notched specimens is much more pronounced than the reduction of area loss measured from smooth specimens; e.g., the reduction of area loss from notched specimens can be as high as 80% in hydrogen gas. The reduction of notched tensile strength is generally less than 15% for specimens tested in hydrogen gas.

Measurements for notched specimens in 69 MPa hydrogen gas (Table 3.1.2.2) [7] show trends similar to measurements in 6.9 MPa hydrogen gas, however absolute values cannot be compared directly since the notch geometries are different. Nonetheless, Table 3.1.2.2 shows that hydrogen induces reduction of area losses as high as 70%. Notched tensile strength losses are as high as 25% in hydrogen gas.

3.2 Fracture mechanics

3.2.1 Fracture toughness

The fracture toughness and crack propagation resistance of carbon steels are lower in high-pressure hydrogen gas compared to properties measured in air or inert gas. Table 3.2.1.1 lists fracture toughness and crack propagation resistance results for a range of carbon steels tested in hydrogen gas up to 35 MPa pressure [5, 6, 8-11]. At a constant pressure of 6.9 MPa, the fracture toughness is degraded by as much as 50% in hydrogen gas. However, absolute fracture

toughness remains high, where most values are near 100 MPa·$m^{1/2}$. Hydrogen has a more pronounced effect on crack propagation resistance; dJ/da values measured in hydrogen gas can be 90% lower than values measured in air or inert gas.

The fracture toughness measured in hydrogen gas is sensitive to both the loading rate and gas pressure. Figure 3.2.1.1 shows that the fracture toughness for X42 steel in 4 MPa hydrogen gas is constant at displacement rates from $3x10^{-5}$ to $3x10^{-4}$ mm/s but then increases by 30% as the displacement rate increases to $3x10^{-3}$ mm/s [11]. Figure 3.2.1.2 displays the fracture toughness *vs* hydrogen gas pressure data for X42 and A516 steel from Table 3.2.1.1 [8, 9, 11]. For both sets of data, fracture toughness decreases as gas pressure increases but appears to be approaching a lower limiting value. Fracture toughness values are higher for A516 compared to X42, but this difference may be due in part to the higher loading rate for tests on A516.

Fracture toughness can depend sensitively on gas composition, as illustrated in Figure 3.2.1.3 [6]. In this figure, fracture toughness measurements are shown for X42 and X70 steels in nitrogen, methane, and hydrogen, as well as mixtures of hydrogen, methane, carbon monoxide, and carbon dioxide. The results for hydrogen and nitrogen are the same data from Table 3.2.1.1. The data in Figure 3.2.1.3 show that methane does not adversely affect fracture toughness, however a mixture of methane and hydrogen causes a reduction in fracture toughness. Furthermore, fracture toughness is not degraded in gas mixtures containing hydrogen and carbon monoxide. In these cases, carbon monoxide hinders hydrogen uptake into the steel and precludes hydrogen-assisted fracture [6], at least on the time scale of the fracture toughness test.

3.2.2 Threshold stress-intensity factor

Subcritical crack extension can occur when materials are exposed to static loading and hydrogen gas concurrently. Testing was conducted on A106 Gr. B and X70 steels to assess the resistance of these materials to subcritical cracking in 6.9 and 4.1 MPa hydrogen gas partial pressures, respectively [6, 9]. Subcritical crack extension was not detected for either steel. Similarly, testing was conducted on A516 and A106 Gr. C steels to measure the threshold stress-intensity factor for subcritical crack extension (i.e., K_{TH}) at high hydrogen gas pressures [12]. As summarized in Table 3.2.2.1., no crack extension was measured at the reported stress-intensity factors.

3.3 Fatigue

3.3.1 Low-cycle and high-cycle fatigue

No known published data in hydrogen gas.

3.3.2 Fatigue crack propagation

Hydrogen gas enhances the fatigue crack growth rate of carbon steels. Figure 3.3.2.1 shows crack growth rate (da/dN) *vs* stress-intensity factor range (ΔK) relationships for a range of carbon steels in approximately 7 MPa hydrogen gas [6, 10, 13-16]. Several general trends are apparent from the data in Figure 3.3.2.1. The fatigue crack growth rates in hydrogen become increasingly greater relative to crack growth rates in air or inert gas as ΔK increases. In the higher range of ΔK, fatigue crack growth rates are at least ten-fold greater than crack growth rates in air or inert gas. While the da/dN vs ΔK relationships in air and inert gas are remarkably similar, the da/dN

vs ΔK relationships in hydrogen are noticeably more varied. In the higher range of ΔK, crack growth rates in hydrogen can vary by more than a factor of 10.

The da/dN *vs* ΔK relationships in hydrogen gas can be affected by numerous variables, including gas pressure, load ratio, load cycle frequency, and gas composition. The effects of these variables are described in the following paragraphs.

Effect of gas pressure

Fatigue crack growth rates generally increase as hydrogen gas pressure increases [13, 16]. Figure 3.3.2.2 shows da/dN vs ΔK relationships for 1020 steel in hydrogen gas from 0.02 to 7 MPa and for SA 105 steel in hydrogen gas from 7 to 100 MPa [13, 16]. The effect of hydrogen gas pressure on crack growth rates appears to depend on ΔK. At higher ΔK, the da/dN vs ΔK relationships measured in hydrogen merge, suggesting that crack growth rates are not as sensitive to gas pressure at these ΔK levels. At lower ΔK, crack growth rates can increase by more than a factor of 10 as gas pressure increases from 0.02 MPa to 100 MPa.

The da/dN vs ΔK relationship for 1020 steel in 0.02 MPa hydrogen gas is particularly striking. At this low gas pressure (less than 1 atmosphere), the crack growth rate can be a factor of 10 greater than the crack growth rate in air. This result indicates that gases containing even low partial pressures of hydrogen may accelerate fatigue crack growth in carbon steels.

Effect of load ratio

The cyclic load ratio (R, defined as the ratio of the minimum and maximum loads in the load cycle) does not control fatigue crack growth rates in hydrogen gas [10]. Figure 3.3.2.3 shows crack growth rates measured for X42 steel in hydrogen gas as a function of load ratio at a fixed ΔK. While the crack growth rate is independent of load ratio for values between 0.1 and 0.4, the crack growth rate increases at higher load ratios. This increase in crack growth rates is controlled not by the load ratio but by the maximum stress-intensity factor (K_{max}) in the load cycle. Since $\Delta K = K_{max}(1-R)$, an increase in R at fixed ΔK requires that K_{max} increase as well. The crack growth rate accelerates at higher load ratios because K_{max} is approaching the fracture toughness in hydrogen gas (e.g., the values in Table 3.2.1.1) [10].

Although Figure 3.3.2.3 shows that crack growth rates in hydrogen gas are not a function of load ratio in the range from 0.1 to 0.4, crack growth rates in nitrogen are a strong function of load ratio. Thus, as load ratio increases from 0.1 to 0.4, hydrogen has less effect on crack growth rate relative to the crack growth rate in nitrogen. The varying effect of load ratio on crack growth rates in hydrogen and nitrogen has been attributed to crack closure. It has been suggested that plasticity-induced crack closure is less pronounced in hydrogen compared to environments such as nitrogen [10].

Other measurements of fatigue crack growth rates in hydrogen gas indicate that da/dN *vs* ΔK relationships do not depend on load ratio. The da/dN *vs* ΔK relationships for 1020 steel in 7 MPa hydrogen gas are nearly identical at load ratios of 0.15 and 0.37 [13].

Effect of load cycle frequency

Fatigue crack growth rates in hydrogen gas generally increase as the load cycle frequency decreases. This trend is illustrated in Figure 3.3.2.4, which displays da/dN *vs* ΔK relationships

for SA 105 steel in 100 MPa hydrogen gas over a range of load cycle frequencies from 0.001 to 1 Hz [16]. As frequency decreases from 1 to 0.001 Hz, the crack growth rate increases by about a factor of 5.

Additional data for SA 105 steel in 100 MPa hydrogen gas demonstrate that the load cycle profile can be important as well. Figure 3.3.2.5 shows fatigue crack growth rates plotted against the cycle duration (reciprocal of frequency) [16]. These data were generated using two different load profiles, where the time to reach maximum load was either 0.5 or 100 seconds. While the fatigue crack growth rate generally increases as the cycle duration increases, crack growth rates for the 100 second ramp appear to increase more rapidly than crack growth rates for the 0.5 second ramp.

The effect of load cycle frequency on fatigue crack growth rates in hydrogen gas has been demonstrated for other steels. Fatigue crack growth rates for 1020 steel in 0.14 MPa hydrogen gas decreased as frequency increased from 1 to 10 Hz [13].

Effect of gas composition

Additives to hydrogen gas can reduce fatigue crack growth rates, however this phenomenon has not been explored at low load cycle frequencies. Figure 3.3.2.6 shows da/dN *vs* ΔK relationships for X42 steel in 6.9 MPa hydrogen gas containing three different additives: oxygen, sulfur dioxide, or carbon monoxide [6]. In each case, the gas additive lowers the fatigue crack growth rate to the crack growth rate measured in nitrogen, at least for the relatively high frequency (1 Hz) used in the study.

The effect of hydrogen gas mixtures on fatigue crack growth was also explored for 1020 steel at a load cycle frequency of 1 Hz and low total gas pressure. Figure 3.3.2.7 shows da/dN *vs* ΔK relationships for three gas mixtures: hydrogen and carbon dioxide, hydrogen and natural gas, and hydrogen and water [17]. The addition of carbon dioxide to hydrogen has no effect on fatigue crack growth rates, as the da/dN *vs* ΔK relationship for the gas mixture is similar to the relationship for pure hydrogen. The crack growth rate in water plus hydrogen is lower than the crack growth rate in pure hydrogen; however, hydrogen plus water vapor raises the crack growth rate above the crack growth rate in pure water vapor. Finally, the crack growth rate in hydrogen plus natural gas is similar to the crack growth rate in pure hydrogen. In addition, the crack growth rate in pure natural gas is nearly the same as the crack growth rate in air.

3.4 Recent mechanical property measurements

3.4.1 Fracture toughness

The fracture toughness was measured for X60 and X80 steels in 5.5 and 21 MPa hydrogen gas [18, 19]. Although fracture toughness values were notably higher for the X80 steel compared to the X60 steel (Table 3.2.1.1), values for both steels were comparable to others listed in Table 3.2.1.1, i.e., near 100 $MPa \cdot m^{1/2}$. The varying hydrogen gas pressure did not significantly affect fracture toughness for either the X60 steel or the X80 steel.

3.4.2 Fatigue crack propagation

Figure 3.4.2.1 and Figure 3.4.2.2 show crack growth rate (da/dN) *vs* stress-intensity factor range (ΔK) relationships for X60 and X80 steels in hydrogen gas [18, 19]. These relationships were measured at two gas pressures (5.5 and 21 MPa) and two R ratios (0.1 and 0.5) for each

steel. The general trends of the fatigue crack growth rates in Figure 3.4.2.1 and Figure 3.4.2.2 are similar to the trends in Figure 3.3.2.1, i.e., crack growth rates in hydrogen become increasingly greater relative to crack growth rates in air as ΔK increases. The magnitudes of the fatigue crack growth rates are also similar, as demonstrated by including data for A516 steel from Figure 3.3.2.1 in the plots for X60 and X80 in Figure 3.4.2.1 and Figure 3.4.2.2.

The effects of R ratio and gas pressure on the da/dN *vs* ΔK relationships for X60 and X80 steels are not readily established from the data in Figure 3.4.2.1 and Figure 3.4.2.2. In the higher ΔK range, increasing R ratio leads to modestly higher crack growth rates but varying gas pressure has essentially no effect on crack growth rates. In the lower ΔK range, the only clear trend for the X80 steel is that crack growth rates are highest in 21 MPa hydrogen gas at R=0.5. For the X60 steel at lower ΔK, crack growth rates appear higher for R=0.5 but the effect of gas pressure is not clear.

4. Fabrication

4.1 Heat treatment

Heat treating A516 steel to produce different microstructures does not significantly affect fatigue crack growth rates in hydrogen gas [14, 15]. The da/dN *vs* ΔK curves for A516 in three different heat treatment conditions (see Table 1.1.3) are plotted in Figure 4.1.1. The heat treatments produced the following three microstructures: ferrite plus pearlite with a 35 μm prior austenite grain size, ferrite plus pearlite with a 180 μm prior austenite grain size, and bainite plus continuous grain boundary ferrite with a 200 μm prior austenite grain size. The yield strengths of these microstructures are between 305 and 415 MPa (see Table 1.1.3). Despite the wide range in microstructures, the da/dN *vs* ΔK relationships are nearly identical at higher ΔK. The primary difference in the da/dN *vs* ΔK relationships is a mild shift in the threshold stress-intensity range (ΔK_{TH}) values, i.e., ΔK_{TH} varies from 8 to 11.5 MPa $\cdot m^{1/2}$ [14, 15].

An unexpected result was found when comparing the fatigue crack growth responses of X42 and 1080 steels in 6.9 MPa hydrogen gas [5]. The reduction of area (Table 3.1.1.1) and fracture toughness (Table 3.2.1.1) in hydrogen gas are lower for the 1080 steel compared to the X42 steel, but fatigue crack growth rates in 1080 steel are less affected by hydrogen gas. This is demonstrated from the da/dN *vs* ΔK relationships in Figure 4.1.2. It was suggested that hydrogen facilitates fatigue crack growth in the ferrite phase, so that fatigue crack growth rates are higher in the X42 steel with a ferrite plus pearlite microstructure compared to the 1080 steel with a fully pearlitic microstructure [5] .

4.2 Properties of welds

The tensile, fracture toughness, and fatigue crack growth properties of carbon steel welds have been measured in hydrogen gas. These properties are considered in the following paragraphs.

Tensile properties

A large amount of data has been generated for the tensile properties of carbon steel welds in 6.9 MPa hydrogen gas. Properties from both smooth and notched tensile specimens are summarized in Tables 4.2.1 through 4.2.4.

The trends for smooth tensile specimen properties of welds in hydrogen gas are similar to those for the base metals (section 3.1.1). Table 4.2.1 lists measurements from tensile specimens that were oriented perpendicular to the weld [4, 20]. Most reduction of area values range from 30 to 40%, which represent reduction of area losses of approximately 50% from values measured in air. These reduction of area properties were measured primarily for shielded metal arc and submerged arc welds. The lowest reduction of area values (12 to 20%) were measured for an electric resistance weld, a gas tungsten arc weld, and a gas metal arc weld. The weld with the reduction of area of 12% fractured in the transition zone between the heat affected zone and the base metal. Some of the highest reduction of area values measured (66 to 77%) were from specimens that fractured in the fusion zone.

Other smooth tensile specimens were tested in an orientation parallel to the weld, where the specimens were centered either in the fusion zone or heat affected zone. Table 4.2.2 shows that reduction of area values in hydrogen gas are mostly in the range 38 to 47% [20]. These values are generally greater than those measured from specimens oriented perpendicular to the weld.

Weld properties measured from notched tensile specimens in hydrogen gas are remarkably consistent, independent of specimen orientation relative to the weld. Tables 4.2.3 and 4.2.4 show that reduction of area values are in the range 9 to 17%, which represent reduction of area losses of 50 to 70% from values measured in air [4, 20]. In addition, hydrogen lowers the tensile strength by less than 15%. The reduction of area properties for welds are better than the properties reported for base metals (section 3.1.2) when measured using notched tensile specimens. The notched tensile strength properties for welds and base metals are similar.

Fracture toughness

The fracture toughness of welds in hydrogen gas depends on the type of weld and location of crack propagation, as summarized in Table 4.2.5. The fracture toughness and crack propagation resistance of submerged arc welds in X60 steel are high when crack propagation is in the fusion zone [8]. The fracture toughness of the weld fusion zone (103 $MPa \cdot m^{1/2}$) is equal to the fracture toughness of the base metal (Table 3.2.1.1). Furthermore, the crack propagation resistance of the weld fusion zone (267 MPa) exceeds the crack propagation resistance of the base metal (43 MPa, Table 3.2.1.1). In contrast, the fracture toughness of the heat affected zone was low and could not be measured reliably, since cracks ultimately propagated in a rapid, subcritical manner. The fracture toughness of the heat affected zone in electric resistance welded X42 was measured, and this value (48 $MPa \cdot m^{1/2}$) was lower than the fracture toughness of the base metal (107 $MPa \cdot m^{1/2}$, Table 3.2.1.1). No subcritical crack propagation was measured in the X42 weld heat affected zone when tested under static load in 6.9 MPa hydrogen gas [6].

Fatigue crack propagation

Welds in X60 steel are not more susceptible to fatigue crack growth than the base metal in 6.9 MPa hydrogen gas [14]. Figure 4.2.1 shows that the da/dN *vs* ΔK relationships for the fusion zone and heat affected zone of a submerged arc weld are nearly identical to the da/dN *vs* ΔK relationship for the base metal.

5. References

1. "Classification and Designation of Carbon and Low-Alloy Steels," in *Metals Handbook, Properties and Selection: Irons, Steels, and High-Performance Alloys*, 10th ed., vol. 1, ASM International, Materials Park OH, 1990, pp. 140-194.
2. VL Gadgeel and DL Johnson, "Gas-Phase Hydrogen Permeation and Diffusion in Carbon Steels as a Function of Carbon Content from 500 to 900 K," *Journal of Materials for Energy Systems*, vol. 1, 1979, pp. 32-40.
3. JP Hirth, "Effects of Hydrogen on the Properties of Iron and Steel," *Metallurgical Transactions A*, vol. 11A, 1980, pp. 861-890.
4. WR Hoover, JJ Iannucci, SL Robinson, JR Spingarn, and RE Stoltz, "Hydrogen Compatibility of Structural Materials for Energy Storage and Transmission," SAND80-8202, Sandia National Laboratories, Livermore, CA, 1980.
5. HJ Cialone and JH Holbrook, "Microstructural and Fractographic Features of Hydrogen-Accelerated Fatigue-Crack Growth in Steels," in *Microstructural Science: Welding, Failure Analysis, and Metallography*, vol. 14, MR Louthan, I LeMay, and GF VanderVoort, Eds., American Society for Metals, Metals Park, OH, 1987, pp. 407-422.
6. HJ Cialone and JH Holbrook, "Sensitivity of Steels to Degradation in Gaseous Hydrogen," in *Hydrogen Embrittlement: Prevention and Control, ASTM STP 962*, L Raymond, Ed., American Society for Testing and Materials, Philadelphia, 1988, pp. 134-152.
7. RJ Walter and WT Chandler, "Influence of Gaseous Hydrogen on Metals Final Report," NASA-CR-124410, NASA, Marshall Space Flight Center AL, 1973.
8. WR Hoover, SL Robinson, RE Stoltz, and JR Spingarn, "Hydrogen Compatibility of Structural Materials for Energy Storage and Transmission Final Report," SAND81-8006, Sandia National Laboratories, Livermore CA, 1981.
9. SL Robinson and RE Stoltz, "Toughness Losses and Fracture Behavior of Low Strength Carbon-Manganese Steels in Hydrogen," in *Hydrogen Effects in Metals*, IM Bernstein and AW Thompson, Eds., The Metallurgical Society of AIME, Warrendale, PA, 1981, pp. 987-995.
10. HJ Cialone and JH Holbrook, "Effects of Gaseous Hydrogen on Fatigue Crack Growth in Pipeline Steel," *Metallurgical Transactions A*, vol. 16A, 1985, pp. 115-122.
11. F Gutierrez-Solana and M Elices, "High-Pressure Hydrogen Behavior of a Pipeline Steel," in *Current Solutions to Hydrogen Problems in Steels*, CG Interrante and GM Pressouyre, Eds., American Society for Metals, Metals Park, OH, 1982, pp. 181-185.
12. AW Loginow and EH Phelps, "Steels for Seamless Hydrogen Pressure Vessels," *Corrosion*, vol. 31, 1975, pp. 404-412.
13. HG Nelson, "On the Mechanism of Hydrogen-Enhanced Crack Growth in Ferritic Steels," in *Proceedings of the Second International Conference on Mechanical Behavior of Materials*, ASM, Metals Park, OH, 1976, pp. 690-694.
14. HF Wachob, "The Influence of Microstructure on the Resistance of Low Strength Ferrous Alloys to Gas Phase Hydrogen Degradation," NASA-CR-166334, Failure Analysis Associates, Palo Alto, CA, 1981.
15. HF Wachob and HG Nelson, "Influence of Microstructure on the Fatigue Crack Growth of A516 in Hydrogen," in *Hydrogen Effects in Metals*, IM Bernstein and AW Thompson, Eds., The Metallurgical Society of AIME, Warrendale, PA, 1981, pp. 703-711.

16. RJ Walter and WT Chandler, "Cyclic-Load Crack Growth in ASME SA-105 Grade II Steel in High-Pressure Hydrogen at Ambient Temperature," in *Effect of Hydrogen on Behavior of Materials*, AW Thompson and IM Bernstein, Eds., The Metallurgical Society of AIME, Warrendale, PA, 1976, pp. 273-286.
17. HG Nelson, "Hydrogen-Induced Slow Crack Growth of a Plain Carbon Pipeline Steel Under Conditions of Cyclic Loading," in *Effect of Hydrogen on Behavior of Materials*, AW Thompson and IM Bernstein, Eds., The Metallurgical Society of AIME, Warrendale, PA, 1976, pp. 602-611.
18. C SanMarchi, BP Somerday, KA Nibur, DG Stalheim, T Boggess, and S Jansto, "Fracture and Fatigue of Commercial Grade API Pipeline Steels in Gaseous Hydrogen," in *Proceedings of the ASME 2010 Pressure Vessels & Piping Division / K-PVP Conference PVP2010*, Bellevue, Washington, 2010, PVP2010-25825.
19. D Stalheim, T Boggess, C SanMarchi, S Jansto, B Somerday, and G Muralidharan, "Microstructure and Mechanical Property Performance of Commercial Grade API Pipeline Steels in High Pressure Gaseous Hydrogen," in *Proceedings of IPC 2010 8th International Pipeline Conference*, Calgary, Alberta, 2010, IPC2010-31301.
20. WR Hoover, "Hydrogen Compatibility of Structural Materials for Energy Storage and Transmission," SAND79-8200, Sandia National Laboratories, Livermore, CA, 1979.
21. "Metals & Alloys in the Unified Numbering System," Standard SAE HS-1086/2004, 10th ed., SAE International, Warrendale, PA, 2004.
22. "Standard Specification for Seamless Carbon Steel Pipe for High-Temperature Service," Standard A 106/A 106M-04b, ASTM International, West Conshohocken PA, 2004.
23. "Standard Specification for Carbon Steel Forgings for Piping Applications," Standard A 105/A 105M-05, ASTM International, West Conshohocken, PA, 2005.
24. "Specification for Line Pipe," API Specification 5L, American Petroleum Institute, Washington DC, 1999.

Table 1.1.1. Allowable composition ranges (wt%) for carbon steels.

Steel	Specification	Fe	C	Mn	P	S	Si	Other	Ref.
A515 Gr. 70	UNS K03101	Bal	0.31 max	0.90 max	0.035 max	0.040 max	0.13 0.33	—	[21]
A516 Gr. 70	UNS K02700	Bal	0.27 max	0.79 1.30	0.035 max	0.040 max	0.13 0.45	—	[21]
A106 Gr. B	ASTM A106 (B)	Bal	0.30 max	0.29 1.06	0.035 max	0.035 max	0.10 min	—	[22]
A106 Gr. C	ASTM A106 (C)	Bal	0.35 max	0.29 1.06	0.035 max	0.035 max	0.10 min	—	[22]
SA 105 Gr. II	ASTM A105	Bal	0.35 max	0.60 1.05	0.035 max	0.040 max	0.10 0.35	—	[23]
1020	UNS G10200	Bal	0.18 0.23	0.30 0.60	0.030 max	0.050 max	—	—	[21]
1042	UNS G10420	Bal	0.40 0.47	0.60 0.90	0.030 max	0.050 max	—	—	[21]
1080	UNS G10800	Bal	0.75 0.88	0.60 0.90	0.030 max	0.050 max	—	—	[21]
X42†	API 5L X42	Bal	0.22 max	1.30 max	0.025 max	0.015 max	—	Nb+Ti+V<0.15	[24]
X52†	API 5L X52	Bal	0.22 max	1.40 max	0.025 max	0.015 max	—	Nb+Ti+V<0.15	[24]
X60†	API 5L X60	Bal	0.22 max	1.40 max	0.025 max	0.015 max	—	Nb+Ti+V<0.15‡	[24]
X65†	API 5L X65	Bal	0.22 max	1.45 max	0.025 max	0.015 max	—	Nb+Ti+V<0.15‡	[24]
X70†	API 5L X70	Bal	0.22 max	1.65 max	0.025 max	0.015 max	—	Nb+Ti+V<0.15‡	[24]
X80†	API 5L X80	Bal	0.22 max	1.85 max	0.025 max	0.015 max	—	Nb+Ti+V<0.15‡	[24]

† composition limits for welded product in Product Specification Level 2 (PSL 2)

‡ other compositions may be established by agreement between purchaser and manufacturer, but limit of Nb+Ti+V<0.15 must be satisfied

Table 1.1.2. Compositions (wt%) of carbon steels in hydrogen compatibility studies.

Steel	Product form	Fe	C	Mn	P	S	Si	Other	Ref.
A515 Gr. 70	0.95 cm plate	Bal	0.27	0.71	0.011	0.018	0.19	—	[7]
A516 Gr. 70	1.25 cm plate	Bal	0.22	1.10	0.009	0.023	0.21	—	[14, 15]
A516 Gr. 70	nr	Bal	0.24	1.12	0.013	0.022	0.21	<0.04 Al, Cr, Mo, Ni	[12]
A516 Gr. 70 (U.S. grade)	2.5 cm plate	Bal	0.21	1.04	0.012	0.020	0.21	—	[4, 8, 9, 20]
A516 (Japan grade)	plate	Bal	0.26	0.79	0.013	0.033	0.17	—	[4]
A106 Gr. B	pipeline	nr							[4, 20]
A106 Gr. C	nr	Bal	0.26	1.06	0.011	0.023	0.23	—	[12]
SA 105 Gr. II	59 cm OD, 37 cm ID hemisphere	Bal	0.23	0.62	0.010	0.015	0.15	—	[16]
1020	3.8 cm plate	nr							[13, 17]
1020	0.95 cm rod	Bal	0.17	0.47	0.011	0.037	—	—	[7]
1042	0.95 cm rod	Bal	0.44	0.76	0.008	0.020	0.20	—	[7]
1080	rail web section	Bal	0.85	0.79	0.007	0.042	0.173	—	[5]
X42	30.5 cm OD, 28.6 cm ID pipeline	Bal	0.26	0.82	0.020	0.026	0.014	<0.04 Cr, Cu, Mo, Ni ; <0.005 Al, Sn	[5, 6, 10]
X42	nr	Bal	0.10	0.70	0.033	0.022	0.26	0.17 Co, 0.15 Cr	[11]
X52	pipeline	Bal	0.14	0.98	0.015	0.012	0.29	<0.012 Al, Nb	[4, 20]
X60	pipeline	Bal	0.26	1.39	0.006	0.022	0.03	0.050 V	[4, 20]
X60	1.25 cm plate	Bal	0.12	1.29	0.014	0.016	0.25	<0.03 Cr, Cu, Mo, Nb, Ni, V	[8, 14]
X65	pipeline	Bal	0.22	1.23	—	—	0.11	0.020 Nb	[4, 20]
X70	101.6 cm OD, 98.6 ID pipeline	Bal	0.09	1.50	0.008	0.006	0.31	<0.42 Al, Cr, Cu, Mo; <0.084 Nb, Ni, Sn	[6]
X70	pipeline	Bal	0.11	1.44	0.013	0.002	0.27	<0.30 Cu, Ni; <0.09 Al, Nb, V	[4, 20]
X70 (Arctic grade)	pipeline	Bal	0.06	1.70	0.010	0.009	0.20	0.30 Mo, 0.062 Nb	[4, 20]
X60	plate	Bal	0.03	1.14	0.008	0.001	0.18	0.16 Cr, 0.14 Ni, 0.084 Nb, 0.034 Al, 0.014 Ti	[18, 19]
X80	plate	Bal	0.05	1.52	0.007	0.003	0.12	0.25 Cr, 0.14 Ni, 0.092 Nb, 0.036 Al, 0.012 Ti	[18, 19]

nr = not reported; ID = inner diameter; OD = outer diameter

Table 1.1.3. Heat treatments and mechanical properties of carbon steels in hydrogen compatibility studies.

Steel	Heat treatment	S_y (MPa)	S_u (MPa)	RA (%)	Ref.
A515 Gr. 70	HR	338	504	66	[7]
A516 Gr. 70 (F+P, GS = 35 μm)	N 1173 K/45 min + FC	330	565	—	[14, 15]
A516 Gr. 70 (F+P, GS = 180 μm)	N 1473 K/45 min + FC	305	—	—	
A516 Gr. 70 (B, GS = 200 μm)	A 1473 K/45 min + ISQ + T 723 K/90 min	415	—	—	
A516 Gr. 70	HR	290	572	62	[12]
A516 Gr. 70 (U.S. grade)	HR	375	535	69	[4, 8, 9, 20]
A516 (Japan grade)	nr	364	566	72	[4]
A106 Gr. B	nr	462	559	58	[4, 20]
A106 Gr. C	N 1130 K/75 min + AC	345	558	68	[12]
SA 105 Gr. II	SR 894 K/240 min + 0.9 K/min cool	269	462	63	[16]
1020	HR	207	379	—	[13, 17]
1020	HR	373	490	65	[7]
1042	N 1172 K/60 min + AC	400†	621†	59†	[7]
1080	N 1123 K/60 min + FC	414†	814†	16†	[5]
X42	HR	366	511	56	[5, 6, 10]
X42	nr	280	415	58	[11]
X52	nr	414	609	60	[4, 20]
X60	nr	427	594	49	[4, 20]
X60	nr	473	675	62	[8, 14]
X65	nr	504	605	57	[4, 20]
X70	CR	584	669	57	[6]
X70	nr	626	693	77	[4, 20]
X70 (Arctic grade)	nr	697	733	77	[4, 20]
X60	nr	434	486	88†	[18, 19]
X80	nr	565	600	81†	[18, 19]

nr = not reported; A = austenitize; AC = air cool; B = bainite; CR = controlled rolled; F = ferrite; FC = furnace cool; GS = grain size; ISQ = isothermal quench; HR = hot rolled; N = normalized; P = pearlite; SR = stress relief

† properties measured in high-pressure nitrogen or helium gas

Table 2.1. Hydrogen permeability (Φ) and solubility (S) *vs* temperature relationships for carbon steels and iron.*

Material	Temp. range (K)	Pressure range (MPa)	$\Phi = \Phi_o \exp(-E_\Phi / RT)$		$S = S_o \exp(-E_S / RT)$		Ref.
			Φ_o $\left(\frac{\text{mol H}_2}{\text{m} \cdot \text{s} \cdot \text{MPa}^{1/2}}\right)$	E_Φ $\left(\frac{\text{kJ}}{\text{mol}}\right)$	S_o $\left(\frac{\text{mol H}_2}{\text{m}^3 \cdot \text{MPa}^{1/2}}\right)$	E_S $\left(\frac{\text{kJ}}{\text{mol}}\right)$	
Iron	500 - 900	0.01 - 0.7	2.513×10^{-5}	31.69	180.1	23.66	[2]
1010			3.442×10^{-5}	34.18	202.4	24.70	
1020			3.77×10^{-5}	35.07	159.0	23.54	
1035			3.603×10^{-5}	36.16	188.6	24.63	
1050			2.097×10^{-5}	34.13	82.89	21.10	
1065			1.602×10^{-5}	34.73	65.63	21.54	
1095			1.039×10^{-5}	33.43	41.98	19.28	

* Diffusivity (D) can be obtained from the ratio of permeability and solubility, i.e., $D = \Phi / S$

Table 3.1.1.1. Smooth tensile properties of carbon steels in 6.9 MPa hydrogen gas at room temperature. Properties in either air or nitrogen gas are included for comparison. The tensile specimen orientation is longitudinal (L) unless otherwise specified.

Steel	Test environment	Strain rate (s^{-1})	S_y (MPa)	S_u (MPa)	El_t (%)	RA (%)	Ref.
A516 (U.S. grade)	Air 6.9 MPa H_2	~ $3x10^{-4*}$	375 364	535 551	17 19	69 43	[4]
A516 (Japan grade)	Air 6.9 MPa H_2	~ $3x10^{-4*}$	364 359	566 571	22 18	72 37	[4]
A106 Gr. B	Air 6.9 MPa H_2	~ $3x10^{-4*}$	462 503	559 576	14 11	58 50	[4]
1080	6.9 MPa N_2 6.9 MPa H_2	$1x10^{-4}$	414 421	814 794	12 7.5	16 7.2	[5]
1080 (T)	6.9 MPa N_2 6.9 MPa H_2		414 407	814 787	10 7.4	14 6.5	
X42	Air 6.9 MPa H_2	$1x10^{-4}$	366 331	511 483	21 20	56 44	[5, 6, 10]
X42 (T)	Air 6.9 MPa H_2		311 338	490 476	21 19	52 41	
X52	Air 6.9 MPa H_2	~ $3x10^{-4*}$	414 429	609 597	19 15	60 37	[4]
X60	Air 6.9 MPa H_2	~ $3x10^{-4*}$	427 422	594 590	13 10	49 27	[4]
X65	Air 6.9 MPa H_2	~ $3x10^{-4*}$	504 506	605 611	15 15	57 36	[4]
X70	Air 6.9 MPa H_2	$1x10^{-4}$	584 548	669 659	20 20	57 47	[6]
X70 (T)	Air 6.9 MPa H_2		613 593	702 686	19 15	53 38	
X70	Air 6.9 MPa H_2	~ $3x10^{-4*}$	626 566	693 653	16 14	77 37	[4]
X70 (Arctic grade)	Air 6.9 MPa H_2	~ $3x10^{-4*}$	697 695	733 733	14 12	77 37	[4]

T = transverse oriented specimen

* calculated based on displacement rate and specimen gauge length

Table 3.1.1.2. Smooth tensile properties of carbon steels in 69 MPa hydrogen gas at room temperature. Properties in air and/or helium gas are included for comparison.

Steel	Test environment	Strain rate* (s^{-1})	S_y (MPa)	S_u (MPa)	El_t (%)	RA (%)	Ref.
1042	69 MPa He 69 MPa H_2	$3.3x10^{-5}$	400† -	621 614	29 22	59 27	[7]
1020‡	Air 69 MPa He 69 MPa H_2	$3.3x10^{-5}$	373† 283† 276†	490 435 428	— 40 32	65 68 45	[7]
A515	Air 69 MPa He 69 MPa H_2	$3.3x10^{-5}$	338† 276† 297†	504 448 442	— 42 29	66 67 35	[7]

* strain rate in elastic range
† defined at deviation from linearity on load *vs* time plot
‡ prestrained under tension in air immediately prior to testing

Table 3.1.2.1. Notched tensile properties of carbon steels in 6.9 MPa hydrogen gas at room temperature. Properties in air are included for comparison.

Steel	Specimen	Test environment	Displ. rate (mm/s)	S_y* (MPa)	σ_s (MPa)	RA (%)	Ref.
A516 (U.S. grade)	(a)	Air 6.9 MPa H_2	$8.5x10^{-3}$	375 364	759 629	30 5.4	[4]
A106 Gr. B	(a)	Air 6.9 MPa H_2	$8.5x10^{-3}$	462 503	618 619	26 8.0	[4]
X52	(a)	Air 6.9 MPa H_2	$8.5x10^{-3}$	414 429	818 707	15 7.0	[4]
X60	(a)	Air 6.9 MPa H_2	$8.5x10^{-3}$	427 422	847 782	23 8.4	[4]
X65	(a)	Air 6.9 MPa H_2	$8.5x10^{-3}$	504 506	806 758	21 6.1	[4]
X70	(a)	Air 6.9 MPa H_2	$8.5x10^{-3}$	626 566	946 845	45 8.7	[4]
X70 (Arctic grade)	(a)	Air 6.9 MPa H_2	$8.5x10^{-3}$	697 695	1027 949	42 8.6	[4]

* yield strength of smooth tensile specimen
(a) V-notched specimen: 90^o included angle; minimum diameter = 2.44 mm; maximum diameter = 2.87 mm; notch root radius = 0.025 to 0.051 mm.

Table 3.1.2.2. Notched tensile properties of carbon steels in 69 MPa hydrogen gas at room temperature. Properties in air and/or helium gas are included for comparison.

Steel	Specimen	Test environment	Displ. rate (mm/s)	S_y* (MPa)	σ_s (MPa)	RA (%)	Ref.
1042	(a)	69 MPa He 69 MPa H_2	~ $4x10^{-4}$	400 —	1056 793	8.5 2.8	[7]
1020§	(a)	Air 69 MPa He 69 MPa H_2	~ $4x10^{-4}$	373 283 276	787 724 621	12 14 8.3	[7]
A515	(a)	69 MPa He 69 MPa H_2	~ $4x10^{-4}$	276 297	731 559	8.1 2.3	[7]

* yield strength of smooth tensile specimen

(a) V-notched specimen: 60^o included angle; minimum diameter = 3.81 mm; maximum diameter = 7.77 mm; notch root radius = 0.024 mm. Nominal stress concentration factor (K_t) = 8.4.

Table 3.2.1.1. Fracture toughness for carbon steels in hydrogen gas at room temperature. The fracture toughness in air, nitrogen, or helium is included for comparison. The crack propagation direction is parallel to the longitudinal orientation of the material product form.

Steel	S_y† (MPa)	RA† (%)	Test environment	Displ. rate (mm/s)	K_{Ic} (MPa $\cdot m^{1/2}$)	K_{IH}‡ (MPa $\cdot m^{1/2}$)	dJ/da (MPa)	Ref.
A516	375	69	Air 3.5 MPa H_2 6.9 MPa H_2 20.7 MPa H_2 34.5 MPa H_2	$8.5x10^{-3}$	166*	 131 113 98 90	516 47 55 54 57	[8, 9]
1080	414	16	6.9 MPa N_2 6.9 MPa H_2	$2.5x10^{-4}$ - $2.5x10^{-3}$	111	 81	42 13	[5]
X42	366	56	6.9 MPa N_2 6.9 MPa H_2	$2.5x10^{-4}$ - $2.5x10^{-3}$	178*	 107	70 63	[5, 6, 10]
X42	280	58	Air 2.0 MPa H_2 4.0 MPa H_2 6.5 MPa H_2 7.0 MPa H_2 8.0 MPa H_2 10.0 MPa H_2 12.2 MPa H_2 16.0 MPa H_2	$\leq 3.3x10^{-4}$	147*	 101-128 85 69 73# 59# 53# 57# 46#	111 — 36 31 — — — — —	[11]
X60	473	62	6.9 MPa He 6.9 MPa H_2	$8.5x10^{-3}$	142	 104	123 43	[8]
X70	584	57	6.9 MPa N_2 6.9 MPa H_2	$2.5x10^{-4}$ - $2.5x10^{-3}$	197	 95	251 23	[6]
X60	434	88	5.5 MPa H_2 21 MPa H_2	$8.3x10^{-5}$ - $8.3x10^{-4}$	—	85 82	—	[18]
X80	565	81	5.5 MPa H_2 21 MPa H_2	$8.3x10^{-5}$ - $8.3x10^{-4}$	—	105 102	—	[18]

† yield strength and reduction of area of smooth tensile specimen in air

‡ calculated from relationship $K = \sqrt{JE/1-\nu^2}$

* reported fracture toughness may not be valid plane strain measurement

\# measured from burst tests on pipes with machined flaws

Table 3.2.2.1. Threshold stress-intensity factor for carbon steels in high-pressure hydrogen gas at 286 K. The crack propagation direction is parallel to the longitudinal orientation of the material product form.

Steel	S_y† (MPa)	RA† (%)	K_{Ic}† (MPa ·$m^{1/2}$)	Test environment	K_{TH} (MPa ·$m^{1/2}$)	Ref.
A516	290	62	*	69 MPa H_2	NCP 82	[12]
A106 Gr. C	345	68	*	97 MPa H_2	NCP 55	[12]

NCP = no crack propagation
† properties measured in air
* specimen dimensions precluded valid measurement

Table 4.2.1. Smooth tensile properties of carbon steel welds in 6.9 MPa hydrogen gas at room temperature. Properties in air are included for comparison. The tensile specimen orientation is perpendicular to the weld.

Steel / Weld	Test environment	Strain rate (s^{-1})	S_y (MPa)	S_u (MPa)	El_t (%)	RA (%)	Fracture location	Ref.
A106 Gr. B / SMA	Air 6.9 MPa H_2	~ $3x10^{-4}$*	393 385	615 553	21 14	77 40	nr	[4]
X52 / ERW	Air 6.9 MPa H_2	~ $3x10^{-4}$*	513 499	633 621	10 6.1	40 20	nr	[4]
X65 / SA	Air 6.9MPa H_2	~ $3x10^{-4}$*	516 505	633 624	13 10	56 30	nr	[4]
X70 / SA (Arctic grade)	Air 6.9 MPa H_2	~ $3x10^{-4}$*	649 643	686 678	12 9.5	69 37	nr	[4]
A516 / SMA	Air Air 6.9 MPa H_2 6.9 MPa H_2 6.9 MPa H_2 6.9 MPa H_2	nr	338 386 366 373 462 435	531 545 524 545 531 552	23 13 17 18 14 12	72 69 31 48 77 66	BM FZ BM FZ FZ FZ	[20]
A516 / GTA	Air 6.9 MPa H_2 6.9 MPa H_2	nr	435 435 462	593 593 580	16 15 6	71 38 20	BM BM FZ	[20]
A516 / GMA	Air 6.9 MPa H_2	nr	373 386	573 517	23 3	73 12	FZ TZ	[20]

nr = not reported; BM = base metal; ERW = electric resistance weld; FZ = fusion zone; GMA = gas metal arc; GTA = gas tungsten arc; SA = submerged arc; SMA = shielded metal arc; TZ = transition zone
* calculated based on displacement rate and specimen gauge length

Table 4.2.2. Smooth tensile properties of A516 steel welds in 6.9 MPa hydrogen gas at room temperature. Properties in air are included for comparison. The tensile specimen orientation is parallel to the weld.

Steel / Weld	Test environment	Strain rate (s^{-1})	S_y (MPa)	S_u (MPa)	El_t (%)	RA (%)	Specimen location	Ref.
A516 / SMA	Air	nr	424	505	25	82	FZ	[20]
	Air		483	593	13	66	HAZ	
	6.9 MPa H_2		444	528	15	46	FZ	
	6.9 MPa H_2		386	559	15	38	HAZ	
A516 / GTA	Air	nr	600	690	13	67	FZ	[20]
	Air		421	566	26	64	HAZ	
	6.9 MPa H_2		517	600	8.7	44	FZ	
	6.9 MPa H_2		497	600	15	58	HAZ	
A516 / GMA	Air	nr	600	690	17	67	FZ	[20]
	Air		331	559	27	70	HAZ	
	6.9 MPa H_2		580	676	11	42	FZ	
	6.9 MPa H_2		407	566	18	47	HAZ	

nr = not reported; FZ = fusion zone; GMA = gas metal arc; GTA = gas tungsten arc; HAZ = heat affected zone; SMA = shielded metal arc

Table 4.2.3. Notched tensile properties of carbon steel welds in 6.9 MPa hydrogen gas at room temperature. Properties in air are included for comparison. The notched tensile specimen orientation is perpendicular to the weld.

Steel / Weld	Specimen	Test environment	Displ. rate (mm/s)	S_y* (MPa)	σ_s (MPa)	RA (%)	Ref.
A106 Gr. B / SMA	(a)	Air	$8.5x10^{-3}$	393	719	49	[4]
		6.9 MPa H_2		385	603	14	
X70 / SA (Arctic grade)	(a)	Air	$8.5x10^{-3}$	649	1002	35	[4]
		6.9 MPa H_2		643	973	10	
X70 / SMA (Arctic grade)	(a)	Air	$8.5x10^{-3}$	551	1025	20	[4]
		6.9 MPa H_2		595	901	9.0	

SA = submerged arc; SMA = shielded metal arc

* yield strength of smooth tensile specimen

(a) V-notched specimen: 90^o included angle; minimum diameter = 2.44 mm; maximum diameter = 2.87 mm; notch root radius = 0.025 to 0.051 mm.

Table 4.2.4. Notched tensile properties of A516 steel welds in 6.9 MPa hydrogen gas at room temperature. Properties in air are included for comparison. The notched tensile specimen orientation is parallel to the weld.

Steel / Weld	Specimen	Test environment	Displ. rate (mm/s)	S_y* (MPa)	σ_s (MPa)	RA (%)	Specimen location	Ref.
A516 / SMA	(a)	Air	nr	424	738	62	FZ	[20]
		Air		483	828	32	HAZ	
		6.9 MPa H_2		444	642	10	FZ	
		6.9 MPa H_2		386	842	17	HAZ	
A516 / GTA	(a)	Air	nr	600	945	36	FZ	[20]
		Air		421	821	32	HAZ	
		6.9 MPa H_2		517	800	17	FZ	
		6.9 MPa H_2		497	697	9	HAZ	
A516 / GMA	(a)	Air	nr	600	945	25	FZ	[20]
		Air		331	780	34	HAZ	
		6.9 MPa H_2		580	835	12	FZ	
		6.9 MPa H_2		407	655	10	HAZ	

nr = not reported; FZ = fusion zone; GMA = gas metal arc; GTA = gas tungsten arc; HAZ = heat affected zone; SMA = shielded metal arc

* yield strength of smooth tensile specimen

(a) V-notched specimen: 90^o included angle; minimum diameter = 2.27 mm; maximum diameter = 2.87 mm; notch root radius = 0.051 mm.

Table 4.2.5. Fracture toughness for carbon steel welds in hydrogen gas at room temperature. The fracture toughness in nitrogen or helium is included for comparison.

Steel / Weld	S_y † (MPa)	Test environment	Displ. rate (mm/s)	K_{Ic} ‡ (MPa ·$m^{1/2}$)	K_{IH} ‡ (MPa ·$m^{1/2}$)	dJ/da (MPa)	Specimen location	Ref.
X42 / ERW	366	6.9 MPa N_2 6.9 MPa H_2	$2.5x10^{-4}$ - $2.5x10^{-3}$	67	48	97 69	HAZ HAZ	[6]
X60 / SA (1 pass)	473	6.9 MPa He 6.9 MPa He 6.9 MPa H_2 6.9 MPa H_2	$8.5x10^{-3}$	188* 205*	103 109#	452 171 267 §	FZ HAZ FZ HAZ	[8]
X60 / SA (2 pass)		6.9 MPa He 6.9 MPa He 6.9 MPa H_2 6.9 MPa H_2		188* 77	103 §	452 253 267 §	FZ HAZ FZ HAZ	

ERW = electric resistance weld; FZ = fusion zone; HAZ = heat affected zone;
SA = submerged arc

† yield strength of base metal from smooth tensile specimen in air

‡ calculated from relationship $K = \sqrt{JE/1-\nu^2}$

* reported fracture toughness may not be valid plane strain measurement

\# calculated from J-integral value at onset of rapid, subcritical crack extension

§ not measured due to rapid, subcritical crack extension

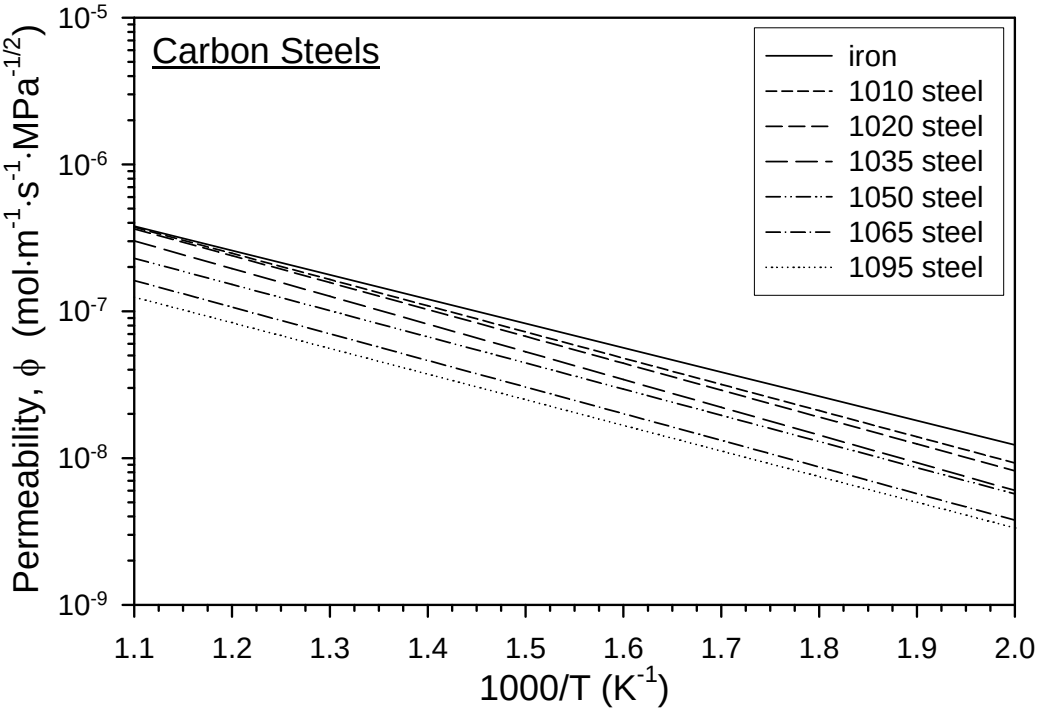

Figure 2.1. Permeability *vs* temperature relationships for carbon steels and iron [2].

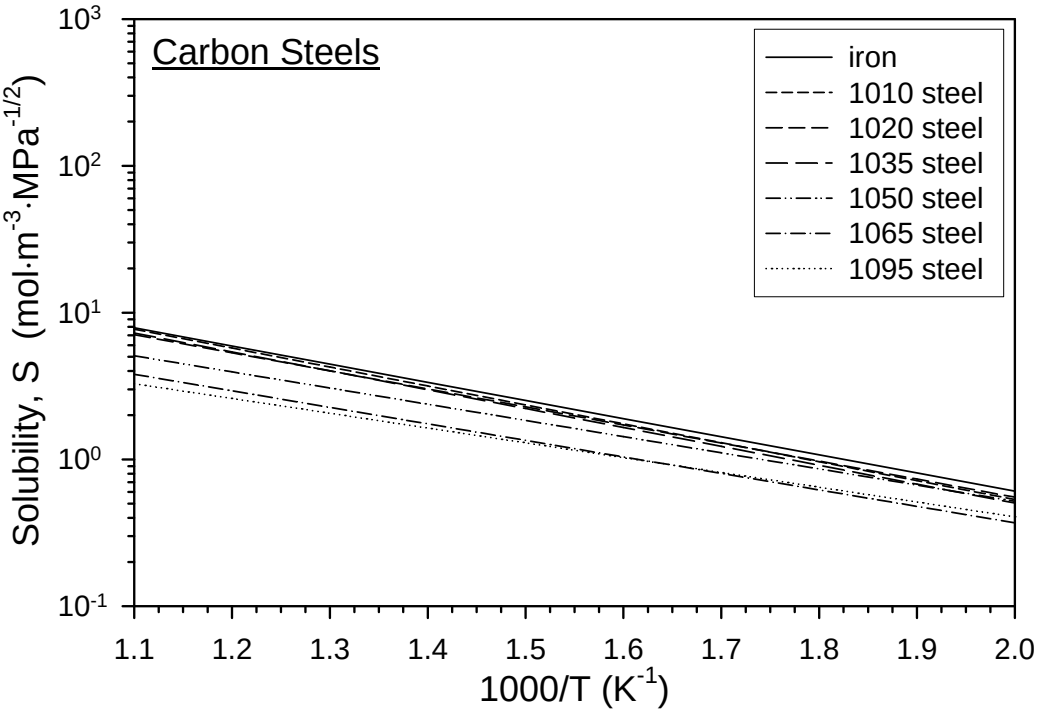

Figure 2.2. Solubility *vs* temperature relationships determined from permeability and diffusivity *vs* temperature relationships for carbon steels and iron [2].

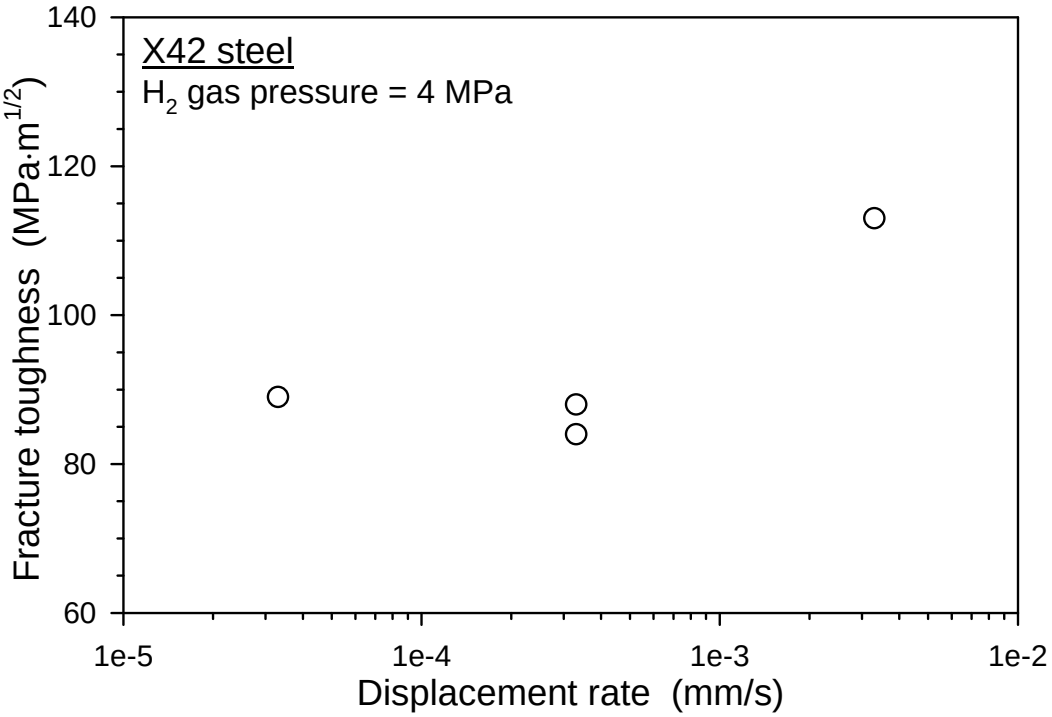

Figure 3.2.1.1. Effect of displacement rate on fracture toughness in hydrogen gas for X42 steel [11].

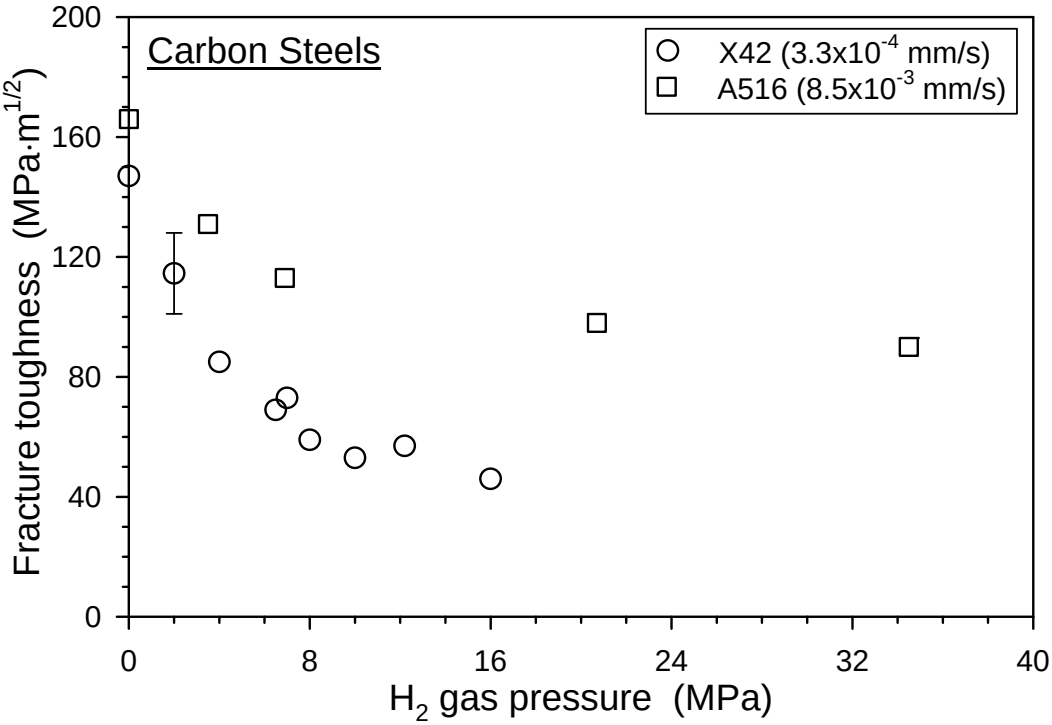

Figure 3.2.1.2. Effect of hydrogen gas pressure on fracture toughness for carbon steels [8, 9, 11]. The displacement rate used in the fracture toughness tests is indicated for each steel.

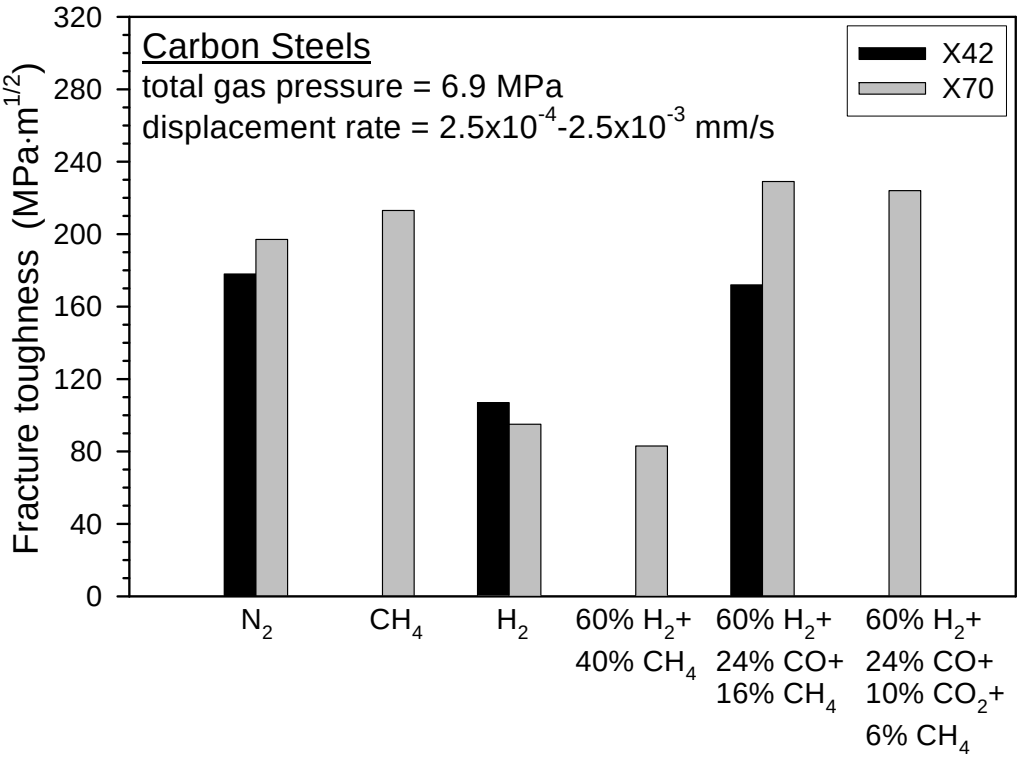

Figure 3.2.1.3. Effect of gas composition on fracture toughness for carbon steels [6].

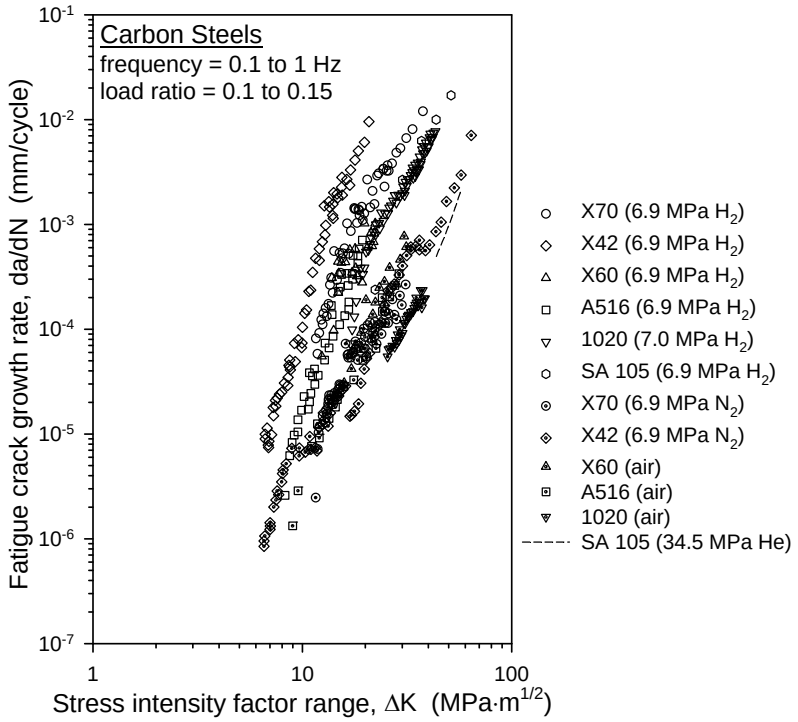

Figure 3.3.2.1. Fatigue crack growth rate *vs* stress-intensity factor range relationships for carbon steels in hydrogen gas [6, 10, 13-16]. Fatigue crack growth rate data in air, nitrogen, or helium are included for comparison.

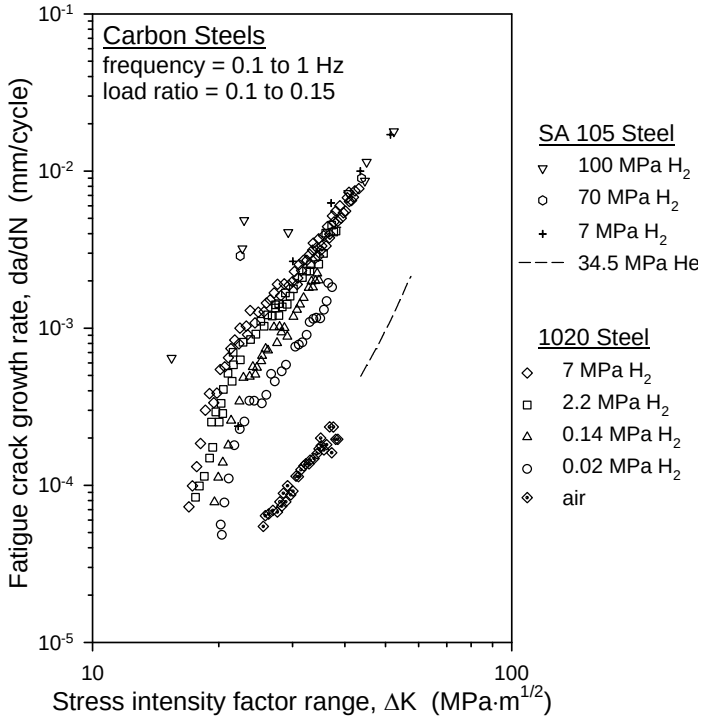

Figure 3.3.2.2. Effect of hydrogen gas pressure on fatigue crack growth rate *vs* stress-intensity factor range relationships for carbon steels [13, 16]. Fatigue crack growth rate data in air or helium gas are included for comparison.

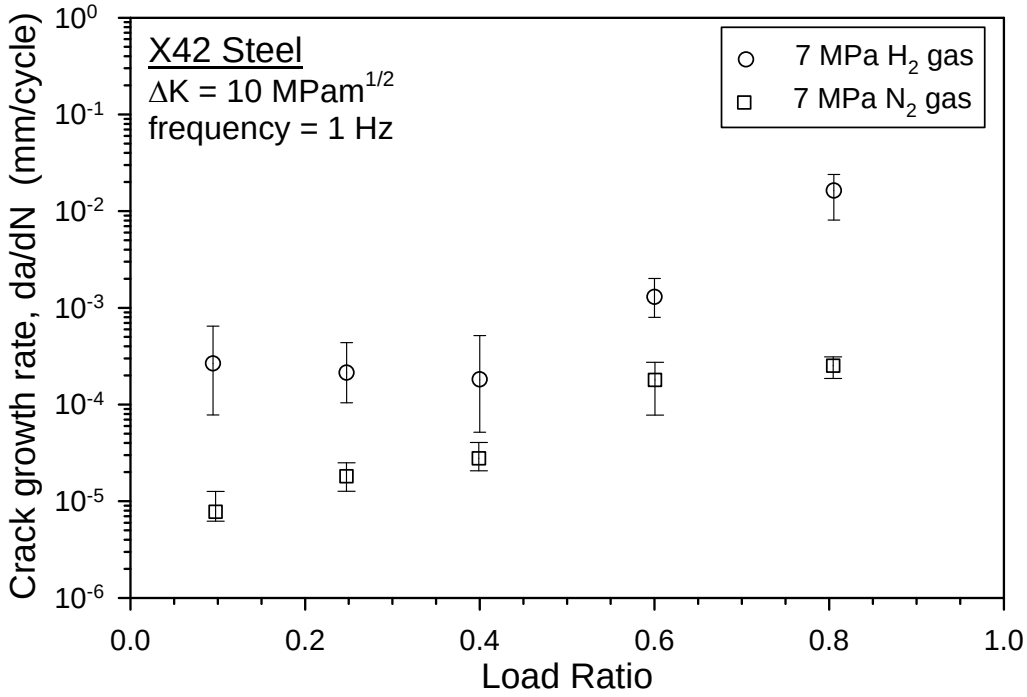

Figure 3.3.2.3. Effect of load ratio on fatigue crack growth rate for X42 steel in hydrogen gas at fixed stress-intensity factor range [10]. Fatigue crack growth rate data in nitrogen gas are included for comparison.

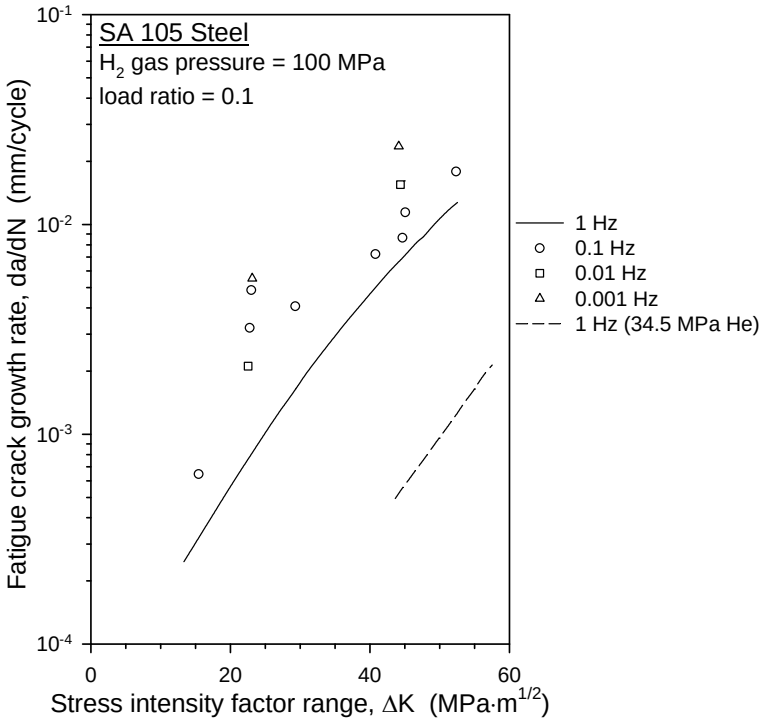

Figure 3.3.2.4. Effect of load cycle frequency on fatigue crack growth rate *vs* stress-intensity factor range relationships for SA 105 steel in hydrogen gas [16]. Fatigue crack growth rate data in helium gas are included for comparison.

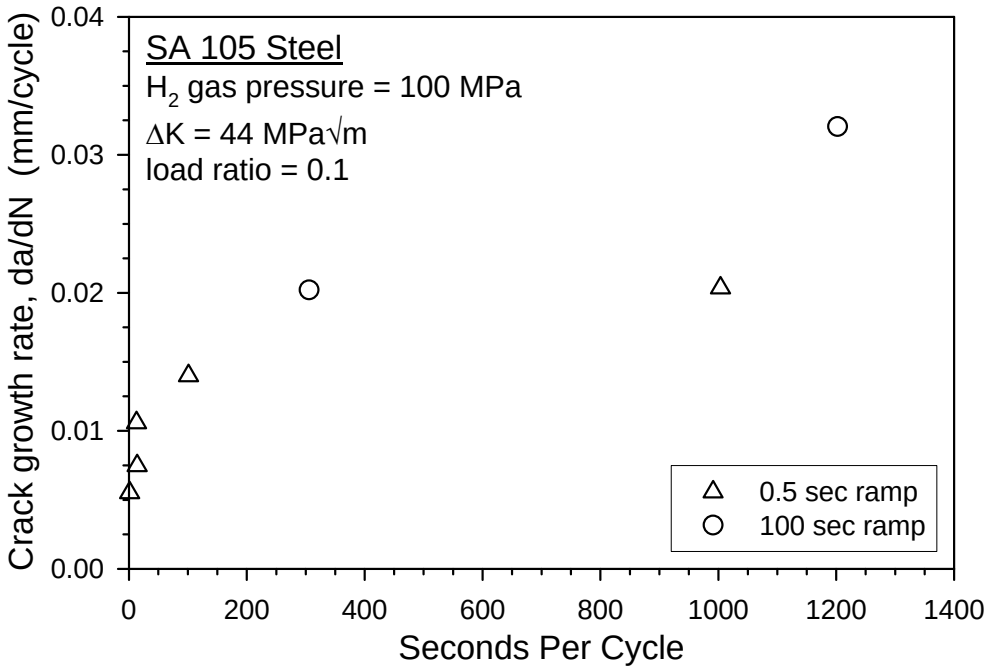

Figure 3.3.2.5. Effect of load cycle duration on fatigue crack growth rate for SA 105 steel in hydrogen gas at fixed stress-intensity factor range [16]. Data for two different loading ramp rates are displayed.

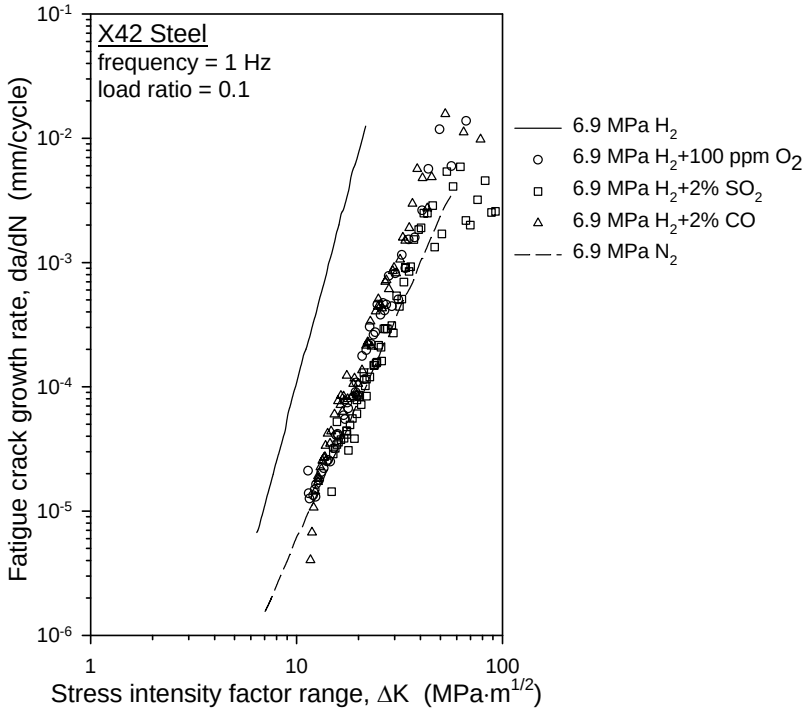

Figure 3.3.2.6. Effect of hydrogen gas composition on fatigue crack growth rate *vs* stress-intensity factor range relationships for X42 steel [6]. Fatigue crack growth rate data in nitrogen gas are included for comparison.

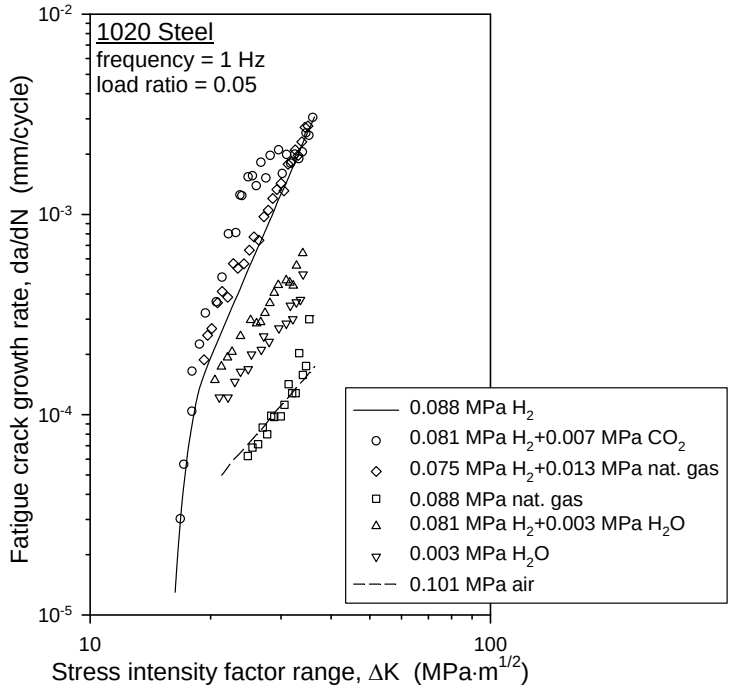

Figure 3.3.2.7. Effect of gas composition on fatigue crack growth rate *vs* stress-intensity factor range relationships for 1020 steel in low-pressure hydrogen gas [17]. Fatigue crack growth rate data in natural gas, water, and air are included for comparison.

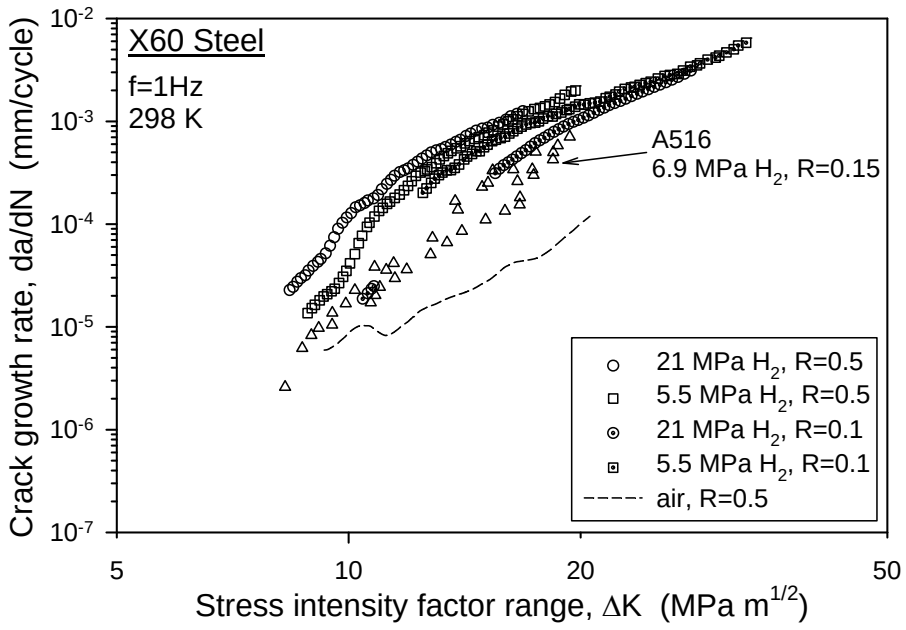

Figure 3.4.2.1. Fatigue crack growth rate *vs* stress-intensity factor range relationships for X60 steel in hydrogen gas [18]. These relationships were measured at two gas pressures and two R ratios. Two additional sets of data are included for comparison: data for X60 in air and data for A516 steel in hydrogen gas from Figure 3.3.2.1.

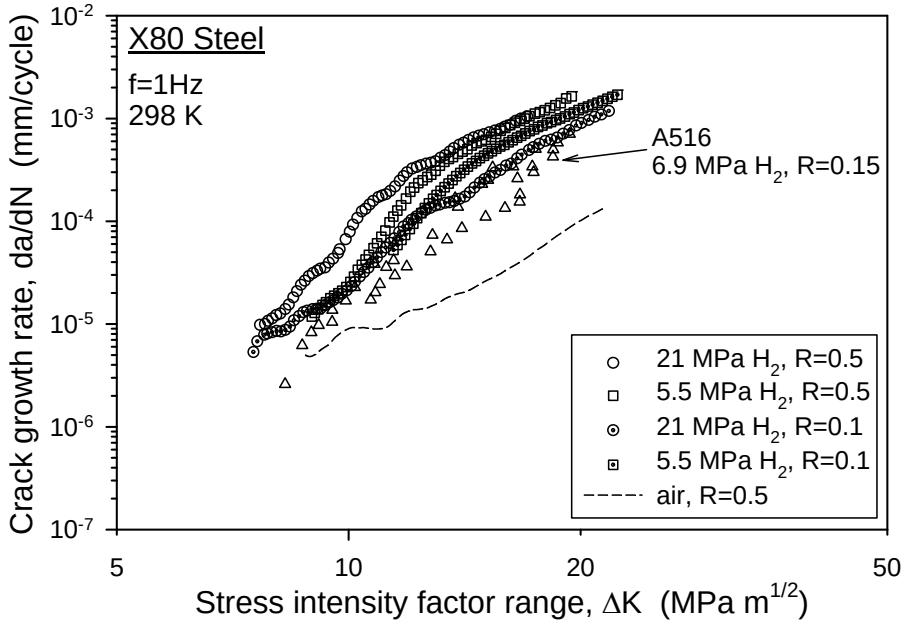

Figure 3.4.2.2. Fatigue crack growth rate *vs* stress-intensity factor range relationships for X80 steel in hydrogen gas [18]. These relationships were measured at two gas pressures and two R ratios. Two additional sets of data are included for comparison: data for X80 in air and data for A516 steel in hydrogen gas from Figure 3.3.2.1.

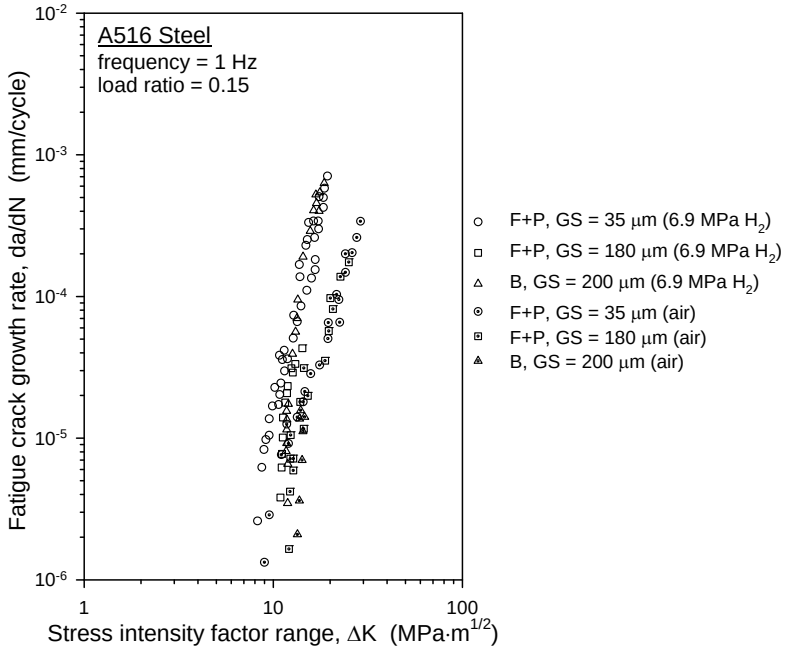

Figure 4.1.1. Effect of microstructure on fatigue crack growth rate *vs* stress-intensity factor range relationships for A516 steel in hydrogen gas [15]. Data are shown for both ferrite plus pearlite and bainitic microstructures at different grain sizes. Fatigue crack growth rate data in air are included for comparison. B = bainite; F = ferrite; GS = grain size; P = pearlite.

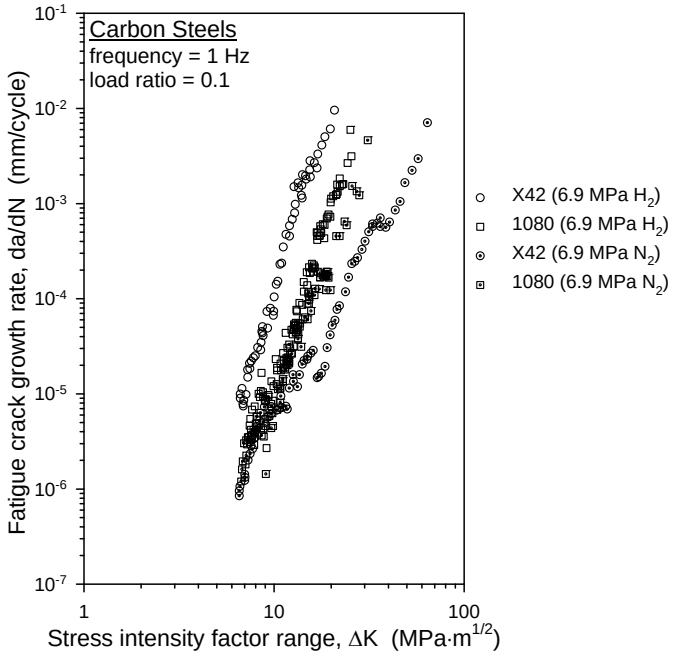

Figure 4.1.2. Effect of microstructure on fatigue crack growth rate *vs* stress-intensity factor range relationships for carbon steels in hydrogen gas [5]. Fatigue crack growth rate data in nitrogen gas are included for comparison.

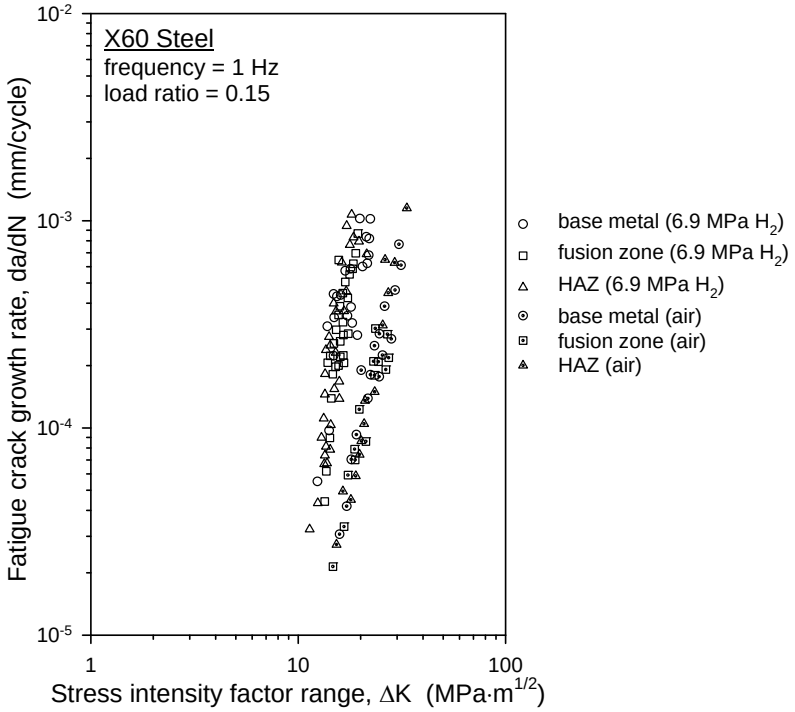

Figure 4.2.1. Fatigue crack growth rate *vs* stress-intensity factor range relationships for welded X60 steel in hydrogen gas [14]. Data are shown for both the fusion zone and heat-affected zone of the weld as well as the base metal. Fatigue crack growth rate data in air are included for comparison.

This page intentionally left blank.

Technical Reference on Hydrogen Compatibility of Materials

Low-Alloy Ferritic Steels:

Tempered Fe-Cr-Mo Alloys (code 1211)

1. General

Carbon and alloy steels can be categorized by a variety of characteristics such as composition, microstructure, strength level, material processing, and heat treatment [1]. The carbon and alloy steel categories selected for the Technical Reference for Hydrogen Compatibility of Materials are based on characteristics of the steels as well as available data. In this chapter, the steels are distinguished by the primary alloying elements, i.e., chromium (< 2.5 wt%) and molybdenum (< 1.25 wt%). Additionally, data in this chapter pertain to steels that were heat treated by heating in the austenite phase field (austenitizing), cooling, then tempering at intermediate temperatures to achieve the final mechanical properties. Data on the compatibility of Cr-Mo steels with hydrogen gas exist primarily for the following alloys: 4130, 4140, 4145, 4147, and 2.25Cr-1Mo. Since a full range of data is not available for each steel, data for all Cr-Mo steels are presented in this chapter. Although the steels exhibit some metallurgical differences, many of the data trends are expected to apply to each steel.

The Cr-Mo steels are attractive structural materials in applications such as pressure vessels because of combinations of strength and toughness that can be achieved through tempering. However, the tempered Cr-Mo steels must be used judiciously in structures exposed to hydrogen gas. Hydrogen gas degrades the tensile properties of Cr-Mo steels, particularly in the presence of stress concentrations. Additionally, hydrogen gas lowers fracture toughness and renders the steels susceptible to crack extension under static loading. Hydrogen gas also accelerates fatigue crack growth. The severity of these manifestations of hydrogen embrittlement depends on material and environmental variables. Important variables include yield strength, hydrogen gas pressure, and temperature. Control over these variables individually or in combination may allow Cr-Mo steels to be applied safely in hydrogen gas environments. For example, limiting steel yield strength can improve resistance to hydrogen embrittlement.

This chapter emphasizes fracture mechanics properties, since pressure vessel design codes employ defect-tolerant design principles, particularly for hydrogen environments. Not all fracture mechanics data for Cr-Mo steels have been generated for material and environmental conditions that reflect conditions anticipated for applications in a hydrogen energy infrastructure. For example, some data pertain to high-strength steels exposed to low hydrogen gas pressures. In these cases, the data can provide insight into trends for Cr-Mo steels exposed to hydrogen gas, but the data are not intended for use in calculating design margins. Additional materials testing is needed to assure that hydrogen compatibility data are obtained for the specific combination of mechanical, material, and environmental variables required in any given application.

1.1 Composition and microstructure

Table 1.1.1 lists the allowable composition ranges for Cr-Mo steels covered in this chapter. Table 1.1.2 summarizes the compositions of steels from hydrogen compatibility studies reported in this chapter. Table 1.1.3 details the heat treatments applied to steels in Table 1.1.2.

Additionally, Table 1.1.3 includes the yield strength, ultimate tensile strength, reduction of area, and fracture toughness that result from the heat treatments.

1.2 Common designations

4130: UNS G41300, AISI 4130, AMS 6370, ASTM A29 (4130), SAE J404 (4130)
4140: UNS G41400, AISI 4140, AMS 6382, ASTM A29 (4140), SAE J404 (4140)
4145: UNS G41450, AISI 4145, ASTM A29 (4145), SAE J404 (4145)
4147: UNS G41470, AISI 4147, ASTM A29 (4147)
2.25Cr-1Mo: UNS K21590, ASTM A335 (P22)

2. Permeability, Diffusivity and Solubility

The permeability of 4130 to hydrogen gas (0.01 to 3 MPa pressure) was measured over the temperature range 373 to 873 K [2]. Permeation was measured for two conditions of 4130: normalized (ferrite + carbide microstructure) as well as quenched and tempered (martensitic microstructure). The temperature dependence of permeability (ϕ) was reported as [2]:

Normalized 4130 $$\phi = 2.91\text{x}10^{-5}\frac{\text{mol H}_2}{\text{m}\cdot\text{s}\cdot\sqrt{\text{MPa}}}\exp\left(\frac{-39.7\frac{\text{kJ}}{\text{mol}}}{RT}\right)$$

Quenched and tempered 4130 $$\phi = 3.64\text{x}10^{-5}\frac{\text{mol H}_2}{\text{m}\cdot\text{s}\cdot\sqrt{\text{MPa}}}\exp\left(\frac{-35.2\frac{\text{kJ}}{\text{mol}}}{RT}\right)$$

Hydrogen solubility relationships were also generated from the permeation studies on 4130. The solubility (S) of hydrogen in 4130 as a function of temperature was reported as [2]:

Normalized 4130 $$S = 82.5\frac{\text{mol H}_2}{\text{m}^3\cdot\sqrt{\text{MPa}}}\exp\left(\frac{-27.1\frac{\text{kJ}}{\text{mol}}}{RT}\right)$$

Quenched and tempered 4130 $$S = 102\frac{\text{mol H}_2}{\text{m}^3\cdot\sqrt{\text{MPa}}}\exp\left(\frac{-27.2\frac{\text{kJ}}{\text{mol}}}{RT}\right)$$

Employing these solubility relationships in Sievert's law yields the concentration of hydrogen in the steel lattice. At lower temperatures, the total hydrogen concentration is not accurately determined from the solubility relationship and Sievert's law. At these temperatures, hydrogen segregates to defects in the steel, and the total hydrogen concentration is the sum of hydrogen in the lattice and hydrogen at defects. More information on calculating total hydrogen concentrations in steels at lower temperatures is in Ref. [3].

3. Mechanical Properties: Effects of Gaseous Hydrogen

3.1 Tensile properties

3.1.1 Smooth tensile properties

Measurement of smooth tensile properties of 4140 in high-pressure hydrogen gas demonstrates that hydrogen severely degrades reduction of area but not ultimate tensile strength. Table 3.1.1.1 shows that reduction of area measured in high-pressure hydrogen gas is 80% lower compared to the measurement in high-pressure helium gas [4].

3.1.2 Notched tensile properties

High-pressure hydrogen significantly reduces tensile strength in 4140 when measurements are conducted using notched specimens. In addition, the yield strength of 4140 dictates the severity of tensile strength degradation measured from notched specimens. Table 3.1.2.1 shows that tensile strength is 60% lower in hydrogen compared to the value in helium for high-strength 4140 [4]. For low-strength 4140, tensile strength is 15% lower in hydrogen.

The absolute reduction of area measured in hydrogen gas depends on the yield strength of 4140. Table 3.1.2.1 shows that reductions of area are 0.9% and 7.1% for high-strength and low-strength 4140, respectively. Hydrogen lowers reduction of area by 70% and 50% compared to values in helium for high-strength and low-strength 4140, respectively.

3.2 Fracture mechanics

3.2.1 Fracture toughness

The fracture toughness of 2.25Cr-1Mo in hydrogen gas (K_{IH}) is significantly lower than the fracture toughness in argon (K_{Ic}). Table 3.2.1.1 shows that K_{IH} is about 75% lower than K_{Ic} for hydrogen gas pressures between 1 and 10 MPa [5]. Absolute values of K_{IH} are between 48 and 54 MPa$\sqrt{m}$.

3.2.2 Threshold stress-intensity factor

The critical stress-intensity factor for hydrogen-assisted crack extension under static loading is termed a threshold (i.e., K_{TH}). Values of K_{TH} are sensitive to material and environmental variables. The trends in K_{TH} as a function of these variables are described below.

Effect of yield strength

Yield strength is a critical material variable governing K_{TH}. Increasing yield strength can dramatically lower K_{TH} [6-9], as demonstrated in Figure 3.2.2.1 for high-strength 4130 tested in low-pressure (0.08 MPa) hydrogen gas. The K_{TH} values decrease by a factor of three as yield strength increases in the range 1050 to 1330 MPa.

The dominant effect of yield strength is also observed for lower-strength steels tested in high-pressure hydrogen gas [8]. Table 3.2.2.1 summarizes K_{TH} values for 4130, 4145, and 4147 in high-pressure hydrogen gas. The K_{TH} values are also plotted as a function of yield strength (670 to 1055 MPa) for the lowest and highest hydrogen gas pressures, i.e., 21 and 97 MPa (Figure 3.2.2.2). While both plots show that K_{TH} decreases as yield strength increases, the yield strength dependence is more pronounced at the lower gas pressure. In addition, the K_{TH} values appear to converge at higher yield strength.

Effect of gas pressure

Hydrogen gas pressure is a critical environmental variable governing K_{TH}. The prevailing trend is that K_{TH} decreases as gas pressure increases. This trend is demonstrated from the K_{TH} *vs* gas pressure plots constructed for high-strength (S_y = 1330 MPa) 4130 steel at three temperatures in Figure 3.2.2.3 [6, 7]. For the two higher temperatures, K_{TH} appears to approach lower limiting values as hydrogen gas pressure increases. The lower limiting K_{TH} increases as temperature increases.

Values of K_{TH} are more sensitive to hydrogen gas pressure for lower-strength steels, as illustrated in Figure 3.2.2.4. The plots in Figure 3.2.2.4 were constructed from data in Table 3.2.2.1 for two steels having widely varying yield strengths: 4130 with 635 MPa yield strength and 4147 with 870 MPa yield strength. While K_{TH} is less sensitive to gas pressure in the higher-strength steel, absolute values of K_{TH} are lower.

Effect of temperature

At elevated temperature K_{TH} is greater than at ambient temperature, while at sub-ambient temperature K_{TH} is reduced. Measurements in low-pressure hydrogen gas show that K_{TH} increases by 40 to 50% in 4130 at two yield strength levels as absolute temperature increases 50 K above ambient (Figure 3.2.2.5) [6, 7]. The K_{TH} decreases by 25 to 30% as temperature decreases 70 K below ambient.

3.3 Fatigue

3.3.1 Low-cycle and high-cycle fatigue

No known published data in hydrogen gas.

3.3.2 Fatigue crack propagation

Hydrogen gas enhances the fatigue crack growth rate (da/dN). The effect of hydrogen gas on the crack growth rate *vs* stress-intensity factor range (ΔK) relationship for 2.25Cr-1Mo steel is demonstrated in Figure 3.3.2.1 [5]. The crack growth rates in hydrogen gas exceed those in argon gas at ΔK levels greater than 10 MPa$\sqrt{m}$. The ratio of crack growth rates in hydrogen and argon environments becomes more pronounced as ΔK increases. The fatigue crack growth rates are nearly insensitive to the magnitude of hydrogen gas pressure in the range 1 to 4 MPa.

The fatigue crack growth rate of 2.25Cr-1Mo steel in hydrogen gas is not a strong function of loading frequency in the range 0.05 to 5 Hz (Figure 3.3.2.2) [5]. The data suggest that crack growth rates in both hydrogen gas and argon gas mildly decline as frequency increases.

Additives to hydrogen gas can cause fatigue crack growth rates to increase or decrease. Figure 3.3.2.3 summarizes the effects of various additives on the fatigue crack growth rate of 2.25Cr-1Mo steel in hydrogen gas [5]. The results are reported as the ratio of the crack growth rate in hydrogen gas with a given additive and the crack growth rate in hydrogen gas only. The data show that O_2 and CO gas additives retard fatigue crack growth rates, while H_2O, CH_3SH and H_2S gas additives accelerate fatigue crack growth rates.

3.4 Creep

No known published data in hydrogen gas.

3.5 Impact

No known published data in hydrogen gas.

4. Fabrication

The hydrogen compatibility of the heat-affected zone and fusion zone of welds must be considered. Performance of welds should not be gauged based on data for base metal.

5. References

1. "Classification and Designation of Carbon and Low-Alloy Steels", in *Metals Handbook, Properties and Selection: Irons, Steels, and High-Performance Alloys*, 10th ed., vol. 1, ASM International, Materials Park OH, 1990, pp. 140-194.
2. HG Nelson and JE Stein, "Gas-Phase Hydrogen Permeation Through Alpha Iron, 4130 Steel, and 304 Stainless Steel from Less Than 100 ^{o}C to Near 600 ^{o}C," NASA TN D-7265, NASA, Washington DC, 1973.
3. JP Hirth, "Effects of Hydrogen on the Properties of Iron and Steel", *Metallurgical Transactions A*, vol. 11A, 1980, pp. 861-890.
4. RJ Walter and WT Chandler, "Effects of High-Pressure Hydrogen on Metals in Ambient Temperatures Final Report," R-7780-1 (NASA contract NAS8-14), Rocketdyne, Canoga Park CA, 1969.
5. S Fukuyama and K Yokogawa, "Prevention of Hydrogen Environmental Assisted Crack Growth of 2.25Cr-1Mo Steel by Gaseous Inhibitors", in *Pressure Vessel Technology*, vol. 2, Verband der Technischen Uberwachungs-Vereine, Essen, Germany, 1992, pp. 914-923.
6. HG Nelson and DP Williams, "Quantitative Observations of Hydrogen-Induced, Slow Crack Growth in a Low Alloy Steel," NASA TMX-62,253, NASA Ames Research Center, Moffett Field CA, 1973.
7. HG Nelson and DP Williams, "Quantitative Observations of Hydrogen-Induced, Slow Crack Growth in a Low Alloy Steel", in *Stress Corrosion Cracking and Hydrogen Embrittlement of Iron Base Alloys*, RW Staehle, J Hochmann, RD McCright, and JE Slater, eds., NACE, Houston TX, 1977, pp. 390-404.
8. AW Loginow and EH Phelps, "Steels for Seamless Hydrogen Pressure Vessels", *Corrosion*, vol. 31, 1975, pp. 404-412.
9. S Hinotani, F Terasaki, and K Takahashi, "Hydrogen Embrittlement of High Strength Steels in High Pressure Hydrogen Gas at Ambient Temperature", *Tetsu-To-Hagane*, vol. 64, 1978, pp. 899-905.
10. *Metals & Alloys in the Unified Numbering System*, Standard SAE HS-1086/2004, 10th ed., SAE International, Warrendale PA, 2004.

Table 1.1.1. Allowable compositional ranges (wt%) for Cr-Mo steels.

Steel	Specification	Fe	Cr	Mo	C	Mn	Si	P	S	Other	Ref.
4130	UNS G41300	Bal	0.80 1.10	0.15 0.25	0.28 0.33	0.40 0.60	0.15 0.35	0.035 max	0.040 max	—	[10]
4140	UNS G41400	Bal	0.80 1.10	0.15 0.25	0.38 0.43	0.75 1.00	0.15 0.35	0.035 max	0.040 max	—	[10]
4145	UNS G41450	Bal	0.80 1.10	0.15 0.25	0.43 0.48	0.75 1.00	0.15 0.35	0.035 max	0.040 max	—	[10]
4147	UNS G41470	Bal	0.80 1.10	0.15 0.25	0.45 0.50	0.75 1.00	0.15 0.35	0.035 max	0.040 max	—	[10]
2.25Cr-1Mo	UNS K21590	Bal	2.00 2.50	0.90 1.10	0.15 max	0.30 0.60	0.50 max	0.030 max	0.030 max	—	[10]

Table 1.1.2. Compositions (wt%) of Cr-Mo steels in hydrogen compatibility studies.

Steel	Fe	Cr	Mo	C	Mn	Si	P	S	Other	Ref.
4130	Bal	0.70	0.20	0.30	—	—	—	—	—	[2]
4140	Bal	0.93	0.20	0.40	0.83	0.31	0.009	0.014	—	[4]
2.25Cr-1Mo	Bal	2.46	0.94	0.12	0.50	0.03	—	0.008	—	[5]
4130	Bal	1	0.2	0.30	—	—	—	—	—	[6, 7]
4130	Bal	1.12	0.19	0.37	0.58	0.27	0.006	0.014	—	[8]
4145	Bal	0.85	0.17	0.46	0.85	0.27	0.009	0.025	—	[8]
4147	Bal	0.99	0.18	0.47	0.98	0.26	0.012	0.011	—	[8]

Table 1.1.3. Heat treatments and mechanical properties of Cr-Mo steels in hydrogen compatibility studies.

Steel	Heat treatment	S_y (MPa)	S_u (MPa)	RA (%)	K_{Ic} (MPa$\sqrt{m}$)	Ref.
4140 (low strength)	A 1116 K/60 min + OQ + T 977 K/120 min + AC	642	745	68	—	[4]
4140 (high strength)	A 1116 K/60 min + WQ + T 755 K/120 min	1235†	1283†	48†	—	[4]
2.25Cr-1Mo	A 1193 K/120 min + AC + T 963 K/1440 min	430	555	—	206	[5]
4130	A 1116 K + WQ + (523 K < T < 813 K)/120 min	1050 1330	1140 1600	—	—	[6, 7]
4130	A 1144 K/120 min + OQ + T 908 K/120 min + AC	635	820	67	125*	[8]
4145 (low strength)	A 1144 K/60 min + OQ + T 866 K/60 min + AC	670	895	57	153*	[8]
4145 (high strength)	A 1116 K/30 min + WQ + T 839 K/60 min + AC	1055	1130	54	114*	[8]
4147	A 1144K/90 min + OQ + (905 K < T < 941 K)/60 min + AC	725 870	905 1005	60 64	155 160*	[8]

A = austenitize; AC = air cool; OQ = oil quench; T = temper; WQ = water quench

* not reported as standardized K_{Ic} measurement

† properties measured in high-pressure helium gas

Table 3.1.1.1. Smooth tensile properties of Cr-Mo steels in high-pressure helium gas and high-pressure hydrogen gas at room temperature.

Steel	Test environment	Strain rate (s^{-1})	S_y (MPa)	S_u (MPa)	El_t (%)	RA (%)	Ref.
4140	69 MPa He 69 MPa H_2	$3.3x10^{-5}$*	1235† —	1283 1228	14‡ 2.6‡	48 8.8	[4]

* strain rate up to S_y
† defined at deviation from linearity on load *vs* time plot
‡ based on 32 mm gauge length

Table 3.1.2.1. Notched tensile properties of Cr-Mo steels in air, high-pressure helium gas and high-pressure hydrogen gas at room temperature.

Steel	Specimen	Test environment	Displ. rate (mm/s)	S_y* (MPa)	σ_s (MPa)	RA (%)	Ref.
4140 (low strength)	(a)	air 69 MPa He 69 MPa H_2	~ $4x10^{-4}$	642 — —	1345 1259 1074	10 14 7.1	[4]
4140 (high strength)	(a)	69 MPa He 69 MPa H_2	~ $4x10^{-4}$	1235 —	2160 862	2.8 0.9	[4]

* yield strength of smooth tensile specimen
(a) V-notched specimen: 60^o included angle; minimum diameter = 3.81 mm; maximum diameter = 7.77 mm; notch root radius = 0.024 mm. Nominal stress concentration factor (K_t) = 8.4.

Table 3.2.1.1. Values of fracture toughness for Cr-Mo steel in hydrogen gas.

Steel	S_y† (MPa)	RA† (%)	K_{Ic} (MPa√m)	Test environment	Displ. rate (mm/s)	K_{IH} (MPa√m)	Ref.
2.25Cr-1Mo	430	—	206	1.1 MPa H_2 4.0 MPa H_2 9.9 MPa H_2	$1.7x10^{-3}$	54 52 48	[5]

† yield strength and reduction of area of smooth tensile specimen in air

Table 3.2.2.1. Values of threshold stress-intensity factor for Cr-Mo steels in high-pressure hydrogen gas at 286 K.

Steel	S_y† (MPa)	RA† (%)	K_{Ic} (MPa√m)	Test environment	K_{TH} (MPa√m)	Ref.
4130	635	67	125*	21 MPa H_2 41 MPa H_2 62 MPa H_2 69 MPa H_2 97 MPa H_2	88 68 45 32 52	[8]
4145	670	57	153*	21 MPa H_2 41 MPa H_2 62 MPa H_2 69 MPa H_2 97 MPa H_2	72 67 55 60 31	[8]
4145	1055	54	114*	21 MPa H_2 41 MPa H_2	22 19	[8]
4147	725	64	155*	21 MPa H_2 41 MPa H_2 62 MPa H_2 97 MPa H_2	97 93 66 46	[8]
4147	780	60	158*	21 MPa H_2 41 MPa H_2 62 MPa H_2 97 MPa H_2	123 41 45 30	[8]
4147	870	61	160*	21 MPa H_2 41 MPa H_2 62 MPa H_2 97 MPa H_2	38 30 24 23	[8]

† yield strength and reduction of area of smooth tensile specimen in air

* not reported as standardized K_{Ic} measurement

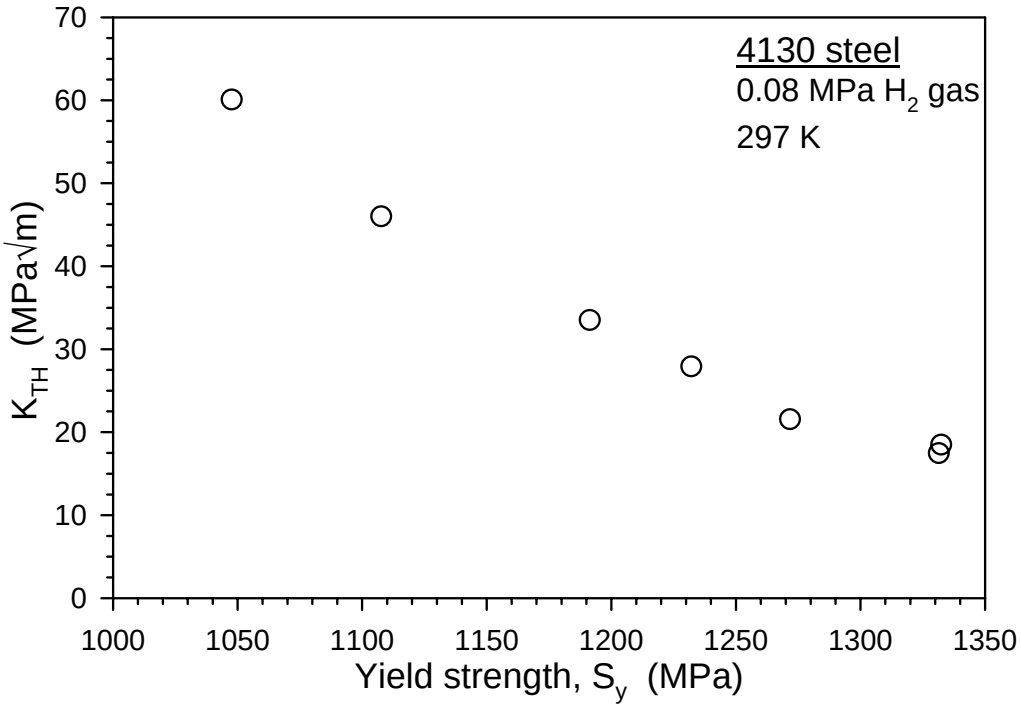

Figure 3.2.2.1. Effect of yield strength on threshold stress-intensity factor for crack extension in low-pressure hydrogen gas for 4130 steel [6, 7].

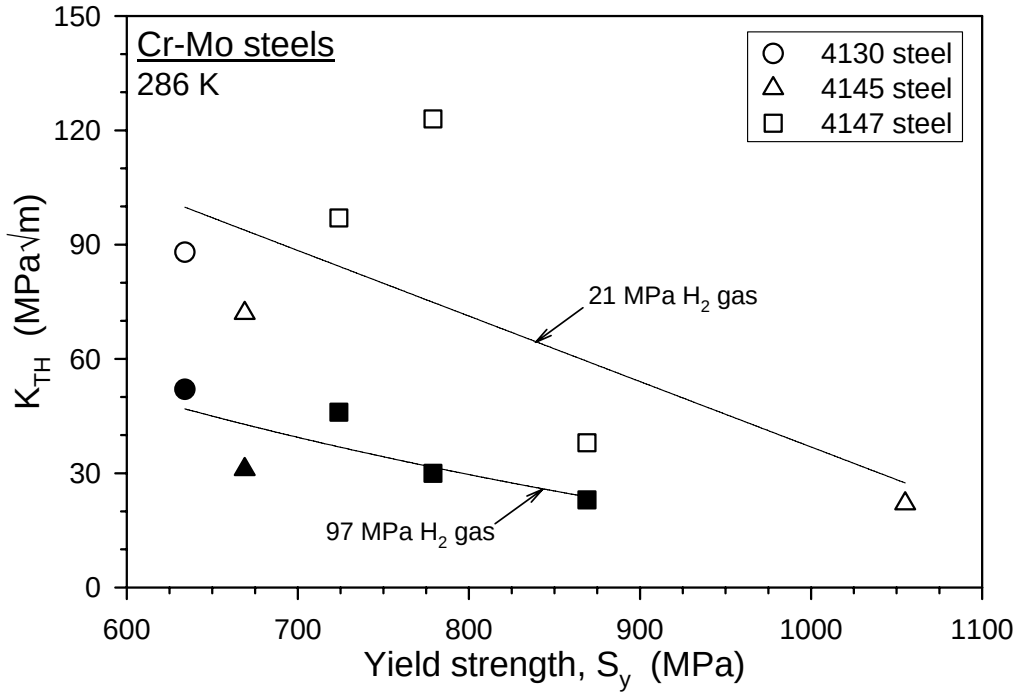

Figure 3.2.2.2. Effect of yield strength on threshold stress-intensity factor for crack extension in high-pressure hydrogen gas for Cr-Mo steels [8]. Open symbols (21 MPa H_2 gas) and filled symbols (97 MPa H_2 gas) represent data from Table 3.2.2.1.

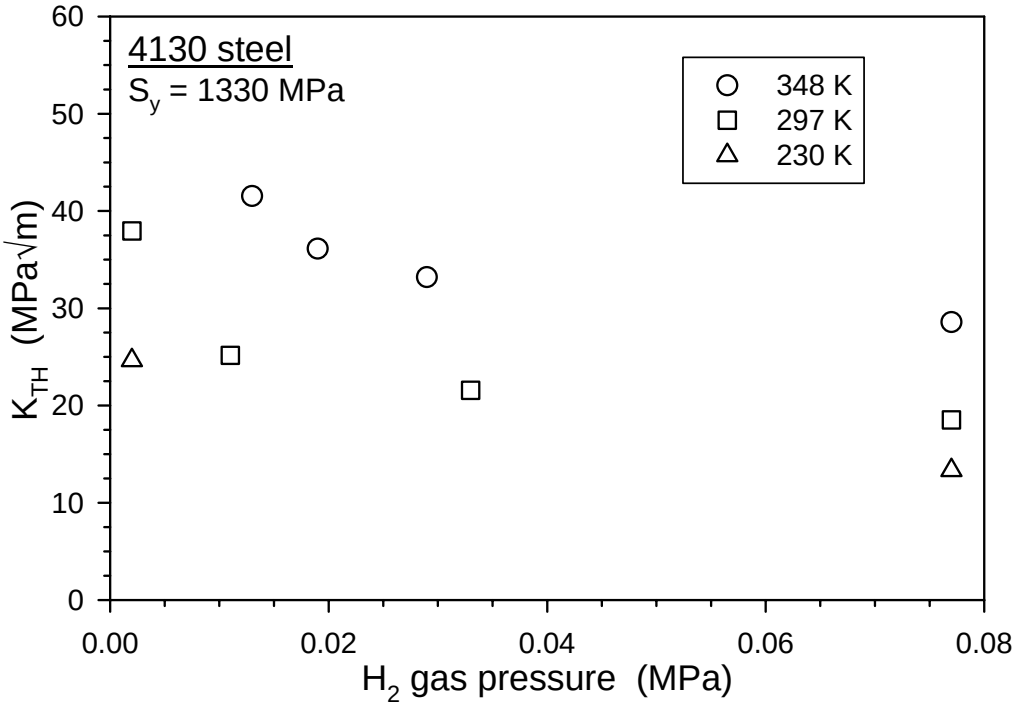

Figure 3.2.2.3. Effect of low hydrogen gas pressures on threshold stress-intensity factor for crack extension in high-strength 4130 steel [6, 7]. Results are shown for three temperatures.

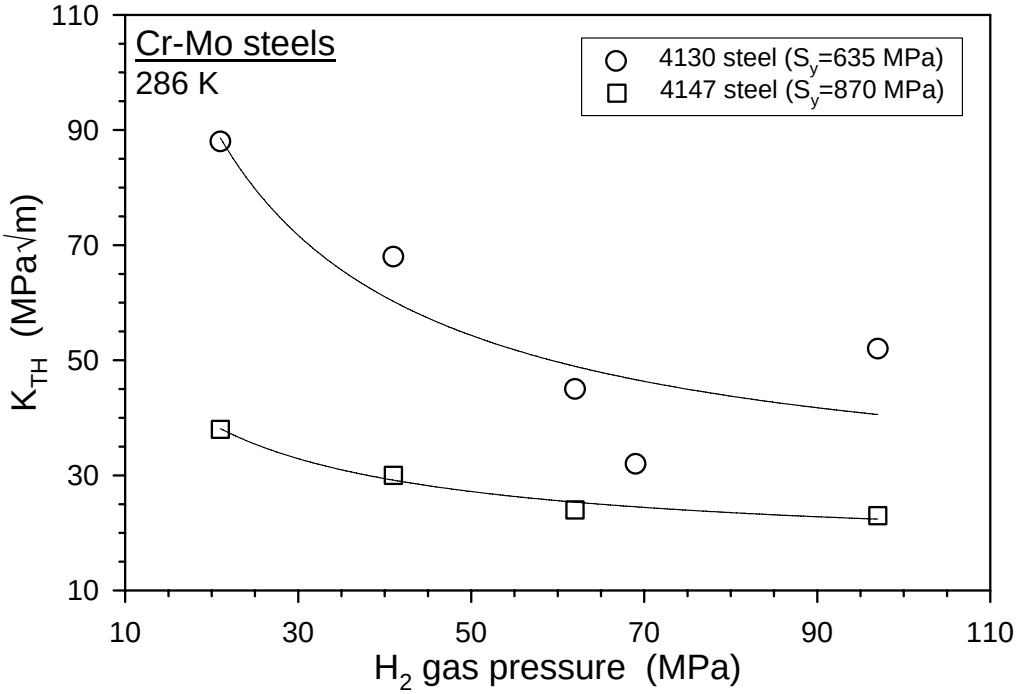

Figure 3.2.2.4. Effect of high hydrogen gas pressures on threshold stress-intensity factor for crack extension in Cr-Mo steels [8]. Data are for two steels with relatively low and high yield strengths from Table 3.2.2.1.

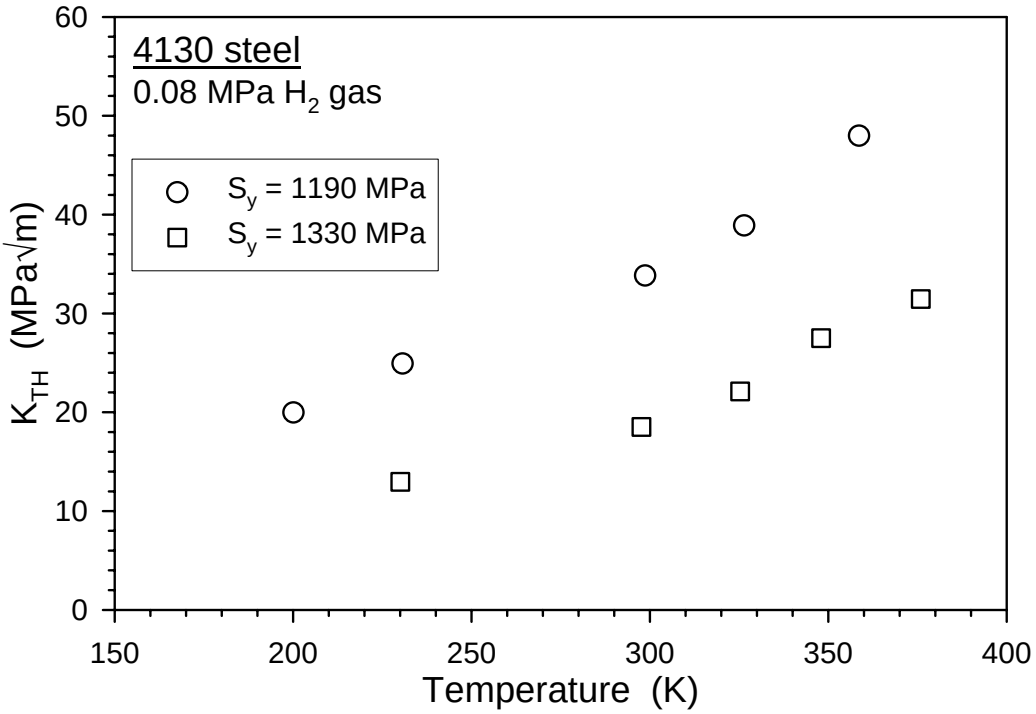

Figure 3.2.2.5. Effect of temperature on threshold stress-intensity factor for crack extension in low-pressure hydrogen gas for 4130 steel [6, 7]. Results are shown for two yield strengths.

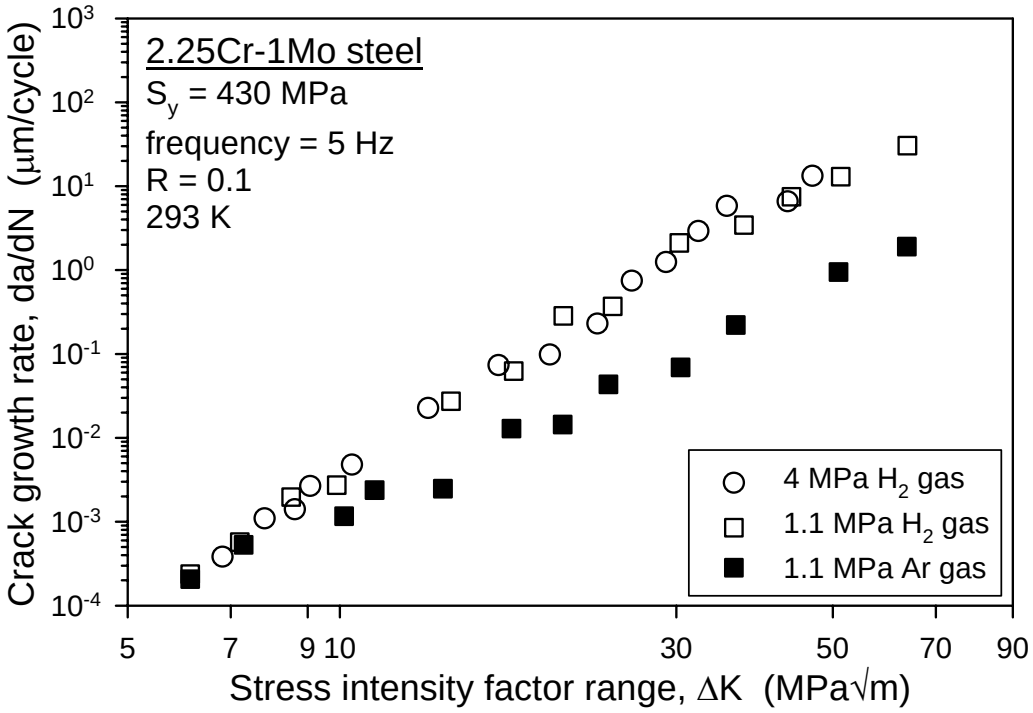

Figure 3.3.2.1. Fatigue crack growth rate as a function of stress-intensity factor range for 2.25Cr-1Mo steel in hydrogen and argon gases [5].

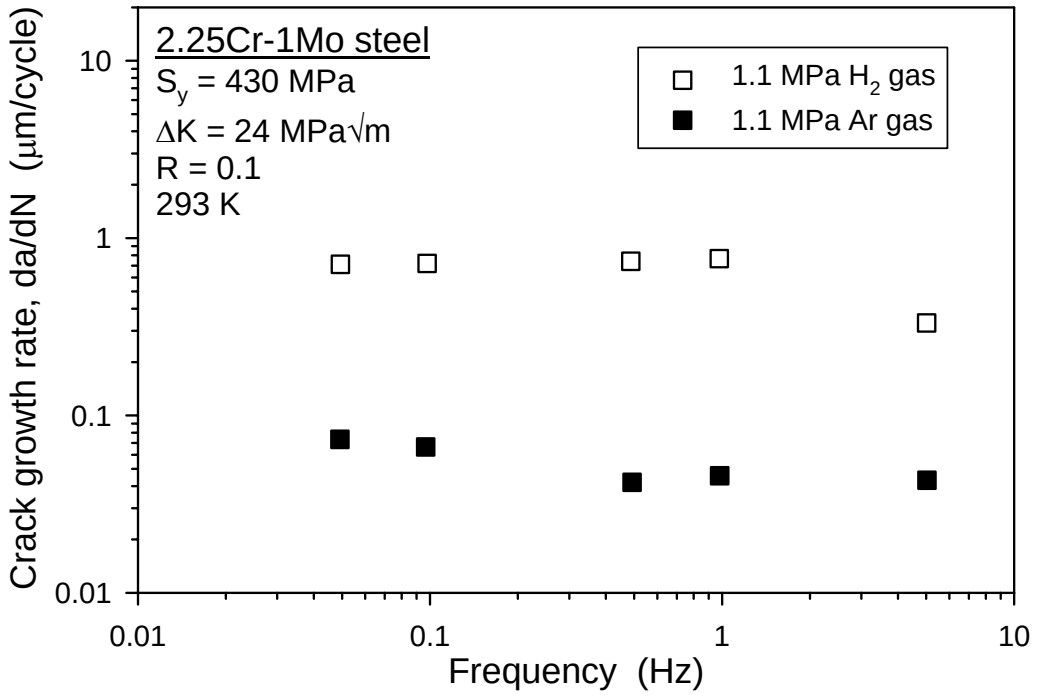

Figure 3.3.2.2. Fatigue crack growth rate as a function of load cycling frequency for 2.25Cr-1Mo steel at fixed stress-intensity factor range [5].

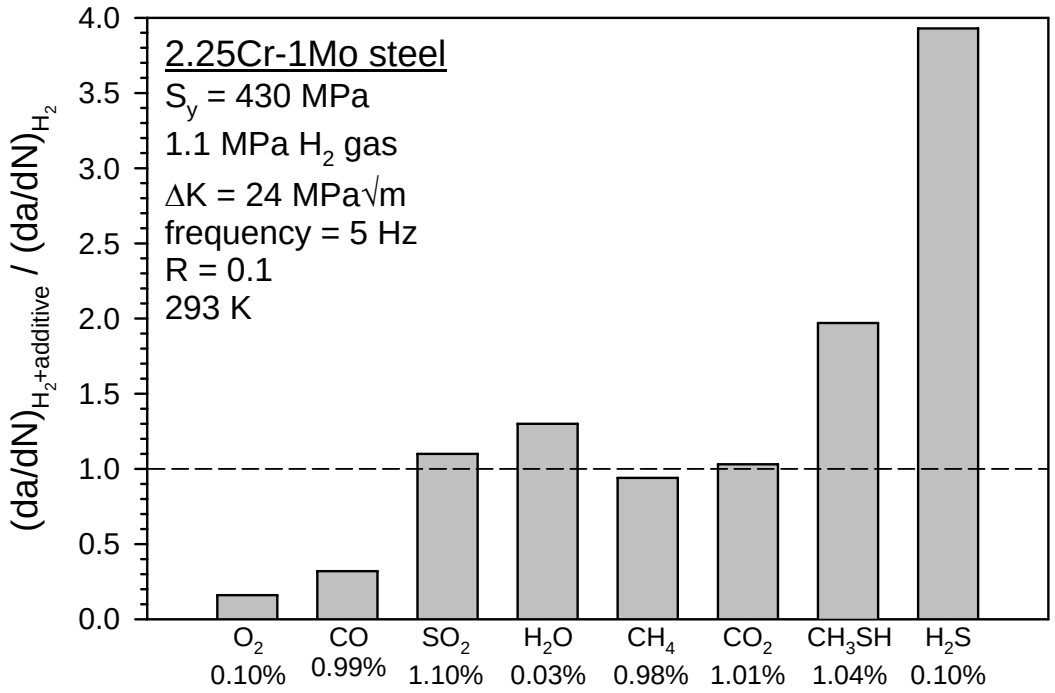

Figure 3.3.2.3. Ratio of fatigue crack growth rate in hydrogen gas with additives to fatigue crack growth rate in hydrogen gas at fixed stress-intensity factor range for 2.25Cr-1Mo steel [5]

This page intentionally left blank.

Technical Reference on Hydrogen Compatibility of Materials

Low-Alloy Ferritic Steels:

Tempered Fe-Ni-Cr-Mo Alloys (code 1212)

1. General

Carbon and alloy steels can be categorized by a variety of characteristics such as composition, microstructure, strength level, material processing, and heat treatment [1]. The carbon and alloy steel categories selected for the Technical Reference for Hydrogen Compatibility of Materials were based on characteristics of the steels as well as available data. In this chapter, the steels are distinguished by the primary alloying elements, i.e., nickel (< 5.5 wt%), chromium (< 2.0 wt%), and molybdenum (< 0.75 wt%). Additionally, data in this chapter pertain to steels that were heat treated by heating in the austenite phase field (austenitizing), rapidly cooling (quenching) to form martensite, then tempering at intermediate temperatures to achieve the final mechanical properties. Hydrogen compatibility data exist primarily for the following Ni-Cr-Mo steels: 4340, HY-80, HY-100, HY-130, and A517 (F). Since a full range of data is not available for each steel, data for all Ni-Cr-Mo steels are presented in this chapter. Although the steels exhibit some metallurgical differences, many of the data trends are expected to apply to each steel.

The Ni-Cr-Mo steels are attractive structural materials in applications such as pressure vessels because of combinations of strength and toughness that can be achieved through quenching and tempering. However, the quenched and tempered Ni-Cr-Mo steels must be used judiciously in structures exposed to hydrogen gas. Hydrogen gas degrades the strength and ductility of Ni-Cr-Mo steels, particularly in the presence of stress concentrations. Additionally, hydrogen gas lowers fracture toughness and renders the steels susceptible to crack extension under static loading. Hydrogen gas also accelerates fatigue crack growth. The severity of these manifestations of hydrogen embrittlement depends on mechanical, material, and environmental variables. Important variables include loading rate, yield strength, steel composition, hydrogen gas pressure, and temperature. Control over these variables individually or in combination may allow Ni-Cr-Mo steels to be applied safely in hydrogen gas environments. For example, limiting steel yield strength and tailoring concentrations of manganese and silicon can improve resistance to hydrogen embrittlement.

This chapter emphasizes fracture mechanics properties, since pressure vessel design codes employ defect-tolerant design principles, particularly for hydrogen environments. Most fracture mechanics data for Ni-Cr-Mo steels have been generated for material and environmental conditions that do not reflect conditions anticipated for applications in a hydrogen energy infrastructure. For example, much of the data pertains to high-strength steels exposed to low hydrogen gas pressures. This chapter reports general data trends that must be considered for all Ni-Cr-Mo steels exposed to hydrogen gas, but much of the data is not intended for use in calculating design margins. Additional materials testing is needed to assure that hydrogen compatibility data are obtained for the specific combination of mechanical, material, and environmental variables required in any given application.

1.1 Composition and microstructure

Table 1.1.1 lists the allowable composition ranges for Ni-Cr-Mo steels covered in this chapter. Table 1.1.2 summarizes the compositions of steels from hydrogen compatibility studies reported in this chapter. Table 1.1.3 details the heat treatments applied to steels in Table 1.1.2. Additionally, Table 1.1.3 includes the yield strength, ultimate tensile strength, reduction of area, and fracture toughness that result from the heat treatments.

1.2 Common designations

4340: UNS G43400, AISI 4340, AMS 6415, ASTM A29 (4340), SAE J404 (4340)
HY-80: UNS K31820, MIL-S-23009 (HY80), ASTM A372 (K)
HY-100: UNS K32045, MIL-S-23009 (HY100)
HY-130: MIL-S-24512
A517 (F), T-1: UNS K11567, ASTM A517 (F)

2. Permeability, Diffusivity and Solubility

The permeability of annealed A517 (F) to low-pressure hydrogen gas was measured over the temperature range 260 to 700 K [2]. The annealed microstructure consisted of ferrite + pearlite rather than tempered martensite. The composition of the A517 (F) steel was not provided. The temperature dependence of permeability (ϕ) was reported as [2]:

$$\phi = 1.5\text{x}10^{-4}\,\frac{\text{mol H}_2}{\text{m}\cdot\text{s}\cdot\sqrt{\text{MPa}}}\exp\left(\frac{-39.3\,\frac{\text{kJ}}{\text{mol}}}{RT}\right) \qquad (1)$$

3. Mechanical Properties: Effects of Gaseous Hydrogen

3.1 Tensile properties

3.1.1 Smooth tensile properties

Measurements from smooth tensile specimens of several Ni-Cr-Mo steels in high-pressure hydrogen gas demonstrate that hydrogen degrades reduction of area but not ultimate tensile strength. Table 3.1.1.1 shows that reduction of area values measured in high-pressure hydrogen gas are 15% lower compared to values measured in high-pressure helium gas for both HY-100 and HY-80 [3]. The reduction of area for A517 (F) is approximately the same in air and hydrogen gas; however, comparison of properties measured in high-pressure hydrogen gas to properties measured in air must account for the effect of hydrostatic pressure on reduction of area, yield strength, and tensile strength [3].[1] The lower tensile strengths for HY-80 and A517 (F) in hydrogen gas compared to values in air result from the effect of hydrostatic pressure.

[1] Hydrostatic pressure imposed by high-pressure gas can reduce the yield and tensile strengths and increase the elongation and reduction of area of metals. Mild changes in tensile properties measured in high-pressure hydrogen gas compared to those measured in air may result from the effect of hydrostatic pressure on material deformation and not an environmental effect of hydrogen.

The reduction of area measured in high-pressure hydrogen gas is sensitive to tensile specimen surface condition. Tensile data in Table 3.1.1.2 reflect an attempt to study the role of surface oxides on tensile fracture in high-pressure hydrogen gas [3]. The surfaces of smooth specimens from A517 (F) steel were abraded with a tool to expose fresh metal, then the specimens were tested in tension. The abrasion and testing procedures were conducted in different combinations of environments. The results in Table 3.1.1.2 show that abrasion followed by testing in hydrogen gas decreases the reduction of area for all abrasion environments and elapsed times after abrasion. The reduction of area measured in hydrogen gas was governed by the presence of surface grooves and irregularities produced by the abrading tool. The reduction of area measured in hydrogen gas 2 days following abrasion (RA = 46%) was higher than the reduction of area measured 0.5 hr following abrasion (RA = 39%), suggesting that surface oxides reformed in the former case and increased the ductility. But the dominant effect of abrasion was to produce fine surface discontinuities that degraded the reduction of area in hydrogen gas.

3.1.2 Notched tensile properties

The reduction of area and tensile strength of Ni-Cr-Mo steels are more severely affected by hydrogen when measured from notched tensile specimens compared to smooth tensile specimens. Table 3.1.2.1 shows that reduction of area values measured from notched specimens in high-pressure hydrogen gas are 50 to 60% lower compared to values measured in high-pressure helium gas for HY-100 and HY-80 [3]. In addition, hydrogen gas degrades the reduction of area for A517 (F) by 70% compared to the value in air. The decrease in reduction of area for A517 (F) in hydrogen gas is likely to be more severe when accounting for the effect of hydrostatic pressure. The tensile strengths of HY-100, HY-80, and A517 (F) are lower by 20 to 30% in high-pressure hydrogen gas compared to values in high-pressure helium gas (Table 3.1.2.1) [3].

Variation in notch acuity does not significantly affect reduction of area and tensile strength in high-pressure hydrogen gas, as illustrated for A517 (F) steel in Table 3.1.2.2 [3]. Hydrogen reduces tensile strength compared to values in helium by approximately the same magnitude (20 to 25%) for specimens with stress concentration factors of 3.8, 5.8, and 8.4. Additionally, reduction of area in hydrogen is lower by 70 to 80% compared to values in air for all stress concentration factors.

3.2 Fracture mechanics

3.2.1 Fracture toughness

The fracture toughness in hydrogen gas (K_{IH}) strongly depends on loading rate. Figure 3.2.1.1 shows K_{IH} data that were produced for 4340 in low-pressure hydrogen gas using standardized procedures [4, 5]. The K_{IH} decreases by a factor of two as loading rate decreases over three orders of magnitude. For each loading rate, K_{IH} is less than the fracture toughness, K_{Ic} (Table 1.1.3).

3.2.2 Threshold stress-intensity factor

The critical stress-intensity factor for hydrogen-assisted crack extension under static loading is termed a threshold (i.e., K_{TH}). Values of K_{TH} are sensitive to material and environmental variables. The trends in K_{TH} as a function of these variables are described below.

Effect of yield strength

Yield strength is a critical material variable governing K_{TH}. The consistent trend is that K_{TH} decreases as yield strength increases [6-10]. The effect of yield strength can be quite dramatic, as demonstrated in Figure 3.2.2.1 for three 4340 steels tested in low-pressure (0.11 MPa) hydrogen gas [6]. The K_{TH} values decrease by a factor of four to eight for the different steels as yield strength increases in the range 1145 to 1875 MPa. The higher K_{TH} for steel B7 compared to steels B6 and B2 is attributed to effects of steel composition, but yield strength still governs K_{TH} in steel B7.

The dominant effect of yield strength is also observed for steels tested in high-pressure hydrogen gas [10]. Table 3.2.2.1 summarizes K_{TH} values for HY-80, A517 (F), and HY-130 in high-pressure (21 to 97 MPa) hydrogen gas. For constant gas pressure, K_{TH} consistently decreases as steel yield strength increases in the range 585 to 940 MPa.

Effect of steel composition

The segregation of impurity elements to grain boundaries facilitates hydrogen-assisted intergranular fracture and lowers K_{TH}. The impurity elements and heat treatment practices that promote temper embrittlement in alloy steels also exacerbate hydrogen-assisted fracture [11].

The common alloying elements manganese and silicon influence the tendency for impurity elements to segregate to grain boundaries. The segregated impurity elements act in concert with hydrogen to cause intergranular fracture, but the bulk concentrations of manganese and silicon govern K_{TH} [6]. The dominant effects of manganese and silicon on K_{TH} are illustrated in Figures 3.2.2.2 and 3.2.2.3 [6, 12]. In Figure 3.2.2.2, K_{TH} values for steels based on 4340 are plotted *vs* the sum of bulk manganese, silicon, sulfur, and phosphorus concentrations. Examination of the steel compositions associated with individual data points in Figure 3.2.2.2 reveals that K_{TH} is most sensitive to manganese and silicon. Values of K_{TH} measured in low-pressure hydrogen gas decrease by a factor of five as manganese and silicon increase, then K_{TH} reaches a lower limiting value. Low bulk concentrations of sulfur and phosphorus are not sufficient for increasing K_{TH}. In Figure 3.2.2.3, results for HY-130 in low-pressure hydrogen gas show that steel A with low manganese and silicon has consistently higher K_{TH} than steel F.

The dominant effects of bulk manganese and silicon concentrations and secondary roles of bulk sulfur and phosphorus concentrations are supported by results from Sandoz [7, 13]. In this study, the concentrations of chromium, molybdenum, manganese, cobalt, carbon, sulfur, and phosphorus were individually varied in steels based on 4340. Tests in low-pressure hydrogen gas demonstrated that increases in manganese from 0.07 to 2.65 wt% decreased K_{TH} (Figure 3.2.2.4). In contrast, increases in sulfur and phosphorus concentrations in the range 0.002 to 0.027 wt% did not affect K_{TH}. Other results showed that variations in chromium and molybdenum did not affect K_{TH}. Variations in carbon had no effect on K_{TH} except at concentrations (i.e., 0.53 wt%) above the composition limit for 4340, where K_{TH} increased.

A notable result from the Sandoz study [7, 13] is that elements not included in the 4340 steel specification (Table 1.1.1) can improve K_{TH}. As cobalt was added to 4340 in concentrations from 0.39 to 2.83 wt%, K_{TH} was increased by 50% (Figure 3.2.2.4).

Effect of thermal aging

Aging in the tempering temperature window for extended times can lower K_{TH}. The effects of extended aging following quenching and tempering are demonstrated for two HY-130 steels in low-pressure hydrogen gas (Figure 3.2.2.3) [12]. Both steels suffer a sharp decline in K_{TH} after 50 hours of aging. In particular, K_{TH} for the steel with high manganese and silicon (steel F) decreases by a factor of two. As aging time increases up to 1000 hours, K_{TH} continues to decrease for both steels. The decrease in K_{TH} as a function of aging time has been attributed to the thermally activated process of impurity segregation [14]. As described in the previous section, impurities that segregate to grain boundaries act in concert with hydrogen to promote intergranular fracture and lower K_{TH}.

Effect of austenitizing temperature

Limited data suggest that austenitizing temperature does not significantly affect K_{TH} (Figure 3.2.2.5) [15]. In the study represented in Figure 3.2.2.5, increasing the austenitizing temperature increased the prior austenite grain size but did not significantly alter the amount of retained austenite or the yield strength after tempering. The K_{TH} values were defined at a crack growth rate of approximately $7x10^{-4}$ mm/s from experiments in low-pressure hydrogen gas. Because of scatter in crack growth rate data [15] and low absolute values of K_{TH}, it is difficult to make firm conclusions from the data.

Effect of gas pressure

Hydrogen gas pressure is a critical environmental variable governing K_{TH}. The prevailing trend is that K_{TH} decreases as gas pressure increases [6, 9, 10, 16, 17]. The K_{TH} *vs* gas pressure trends are influenced by other environmental and material variables such as temperature and yield strength. The K_{TH} *vs* gas pressure plots constructed for 4340 steel (1070 MPa yield strength) at three temperatures in Figure 3.2.2.6 [9] are typical for Ni-Cr-Mo steels. The plots for the two higher temperatures show that K_{TH} decreases and approaches a lower limiting value as gas pressure increases. The plots are shifted to higher K_{TH} values as temperature increases.

Results do not reveal a consistent effect of yield strength on the relationship between K_{TH} and gas pressure. Data indicate that K_{TH} for high-strength 4340 approaches a lower limiting value at relatively low gas pressures [6, 16, 17], as illustrated in Figure 3.2.2.7. In contrast, K_{TH} for the lower-strength steel HY-130 (940 MPa yield strength) is still affected by gas pressure in the range 21 to 97 MPa (Table 3.2.2.1) [10]. These sets of data suggest that K_{TH} in lower-strength Ni-Cr-Mo steels does not approach a lower limiting value until much higher gas pressures. However, K_{TH} values for lower-strength A517 (F) (760 MPa yield strength) do not vary as a function of gas pressure between 21 MPa and 97 MPa (Table 3.2.2.1) [10]. Despite the uncertain effect of yield strength on the relationship between K_{TH} and gas pressure, it must be emphasized that absolute values of K_{TH} decrease as yield strength increases for all gas pressure ranges as described previously.

Effect of temperature

The K_{TH} can increase markedly as temperature increases above ambient [9, 16, 18]. The K_{TH} *vs* temperature data in Figure 3.2.2.8 for 4340 in low-pressure hydrogen gas show that absolute temperatures only 75 K above ambient increase K_{TH} by a factor of three, while absolute temperatures 65 K below ambient do not affect K_{TH} [16]. A similar effect of elevated temperature on K_{TH} is observed in Figure 3.2.2.6 [9].

3.3 Fatigue

3.3.1 Low-cycle and high-cycle fatigue

Hydrogen did not affect the low-cycle fatigue strength of A517 (F) [3]. Two smooth tensile specimens were each subjected to 3000 load cycles in 69 MPa hydrogen gas and did not exhibit failure. The specimens were cycled over a stress range from 20 to 780 MPa at a frequency of 0.14 Hz.

3.3.2 Fatigue crack propagation

Hydrogen gas enhances the fatigue crack growth rate (da/dN) [17, 19]. The effect of high-pressure hydrogen gas on the crack growth rate *vs* stress-intensity factor range (ΔK) relationship for HY-100 steel is demonstrated in Figure 3.3.2.1 [17]. The crack growth rates in hydrogen gas exceed those in helium gas at all ΔK levels. The ratio of crack growth rates in hydrogen and helium environments becomes more pronounced as ΔK increases and reaches a value of about 20 at the highest ΔK levels.

Fatigue crack growth rates increase as hydrogen gas pressure increases, as illustrated for HY-100 in Figure 3.3.2.2 [17]. The data show that da/dN (at fixed $\Delta K = 55$ MPa$\sqrt{m}$) increases continuously as gas pressure increases.

Hydrogen can accelerate fatigue crack growth in lower-strength steels more than higher-strength steels [19]. Fatigue crack growth measurements in low-pressure hydrogen gas show that crack growth rates are higher in HY-80 compared to HY-130 (Figure 3.3.2.3). At higher ΔK levels, da/dN in HY-80 exceeds da/dN in HY-130 by a factor of 10. Crack growth rates in air are similar for the HY-80 and HY-130 steels. The effect of yield strength on fatigue crack growth indicated in Figure 3.3.2.3 is opposite to the effect of yield strength on K_{TH} (e.g., Figure 3.2.2.1).

3.4 Creep

No known published data in hydrogen gas.

3.5 Impact

No known published data in hydrogen gas.

4. Fabrication

4.1 Properties of welds

The hydrogen compatibility of the heat-affected zone and fusion zone of welds must be considered. Performance of welds should not be gauged based on data for base metal.

5. References

1. "Classification and Designation of Carbon and Low-Alloy Steels", in *Metals Handbook, Properties and Selection: Irons, Steels, and High-Performance Alloys*, 10th ed., vol. 1, ASM International, Materials Park OH, 1990, pp. 140-194.
2. MR Louthan, RG Derrick, JA Donovan, and GR Caskey, "Hydrogen Transport in Iron and Steel", in *Effect of Hydrogen on Behavior of Materials*, AW Thompson and IM Bernstein,

eds., The American Institute of Mining, Metallurgical, and Petroleum Engineers, New York NY, 1976, pp. 337-347.
3. RJ Walter and WT Chandler, "Effects of High-Pressure Hydrogen on Metals in Ambient Temperatures Final Report," R-7780-1 (NASA contract NAS8-14), Rocketdyne, Canoga Park CA, 1969.
4. WG Clark and JD Landes, "An Evaluation of Rising Load K_{Iscc} Testing", in *Stress Corrosion - New Approaches, ASTM STP 610*, ASTM, Philadelphia PA, 1976, pp. 108-127.
5. "Standard Test Method for Measurement of Fracture Toughness," Standard E 1820-01, ASTM International, West Conshohocken PA, 2002.
6. N Bandyopadhyay, J Kameda, and CJ McMahon, "Hydrogen-Induced Cracking in 4340-Type Steel: Effects of Composition, Yield Strength, and H_2 Pressure", *Metallurgical Transactions A*, vol. 14A, 1983, pp. 881-888.
7. G Sandoz, "A Unified Theory for Some Effects of Hydrogen Source, Alloying Elements, and Potential on Crack Growth in Martensitic AISI 4340 Steel", *Metallurgical Transactions*, vol. 3, 1972, pp. 1169-1176.
8. S Hinotani, F Terasaki, and K Takahashi, "Hydrogen Embrittlement of High Strength Steels in High Pressure Hydrogen Gas at Ambient Temperature", *Tetsu-To-Hagane*, vol. 64, 1978, pp. 899-905.
9. GC Story, "Hydrogen Assisted Cracking of a Low Alloy Steel - Pressure, Temperature and Yield Strength Effects on the Threshold Fracture Toughness", PhD dissertation, University of California-Davis, Davis CA, 1980.
10. AW Loginow and EH Phelps, "Steels for Seamless Hydrogen Pressure Vessels", *Corrosion*, vol. 31, 1975, pp. 404-412.
11. CJ McMahon, "Hydrogen-Induced Intergranular Fracture of Steels", *Engineering Fracture Mechanics*, vol. 68, 2001, pp. 773-788.
12. Y Takeda and CJ McMahon, "Strain Controlled vs Stress Controlled Hydrogen Induced Fracture in a Quenched and Tempered Steel", *Metallurgical Transactions A*, vol. 12A, 1981, pp. 1255-1266.
13. G Sandoz, "The Effects of Alloying Elements on the Susceptibility to Stress-Corrosion Cracking of Martensitic Steels in Salt Water", *Metallurgical Transactions*, vol. 2, 1971, pp. 1055-1063.
14. CL Briant, HC Feng, and CJ McMahon, "Embrittlement of a 5 Pct Nickel High Strength Steel by Impurities and Their Effects on Hydrogen-Induced Cracking", *Metallurgical Transactions A*, vol. 9A, 1978, pp. 625-633.
15. M Nakamura and E Furubayashi, "Effect of Grain Size on Crack Propagation of High Strength Steel in Gaseous Hydrogen Atmosphere", *Materials Science and Technology*, vol. 6, 1990, pp. 604-610.
16. WG Clark, "Effect of Temperature and Pressure on Hydrogen Cracking in High Strength Type 4340 Steel", *Journal of Materials for Energy Systems*, vol. 1, 1979, pp. 33-40.
17. RJ Walter and WT Chandler, "Influence of Gaseous Hydrogen on Metals Final Report," NASA-CR-124410, NASA, Marshall Space Flight Center AL, 1973.
18. S Pyun and H Lie, "Relationship Between Hydrogen-Assisted Crack Propagation Rate and the Corresponding Crack Path in AISI 4340 Steel", *Steel Research*, vol. 61, 1990, pp. 419-425.

19. WG Clark, "The Effect of Hydrogen Gas on the Fatigue Crack Growth Rate Behavior of HY-80 and HY-130 Steels", in *Hydrogen in Metals*, IM Bernstein and AW Thompson, eds., ASM, Metals Park OH, 1974, pp. 149-164.
20. *Metals & Alloys in the Unified Numbering System*, Standard SAE HS-1086/2004, 10th ed., SAE International, Warrendale PA, 2004.
21. "Military Specification Steel Forgings, Alloy, Structural, High Yield Strength (HY-130)," Specification MIL-S-24512, 1975.

Table 1.1.1. Allowable composition ranges (wt%) for Ni-Cr-Mo steels.

Steel	Specification	Fe	Ni	Cr	Mo	C	Mn	Si	P	S	Other	Ref.
4340	UNS G43400	Bal	1.65 2.00	0.70 0.90	0.20 0.30	0.38 0.43	0.60 0.80	0.15 0.30	0.035 max	0.040 max	—	[20]
HY-80	UNS K31820	Bal	2.00 3.25	1.00 1.80	0.20 0.60	0.18 max	0.10 0.40	0.15 0.35	0.015 max	0.008 max	0.25 max Cu 0.03 max V 0.02 max Ti	[20]
HY-100	UNS K32045	Bal	2.25 3.50	1.00 1.80	0.20 0.60	0.20 max	0.10 0.40	0.15 0.35	0.015 max	0.008 max	0.25 max Cu 0.03 max V 0.02 max Ti	[20]
HY-130	MIL-S-24512	Bal	4.75 5.25	0.40 0.70	0.30 0.65	0.12 max	0.60 0.90	0.20 0.35	0.010 max	0.010 max	0.25 max Cu 0.05<V<0.10 0.02 max Ti	[21]
A517 (F)	UNS K11567	Bal	0.70 1.00	0.40 0.65	0.40 0.60	0.10 0.20	0.60 1.00	0.15 0.35	0.035 max	0.040 max	0.15<Cu<0.50 0.03<V<0.08 0.0005<B<0.006	[20]

Table 1.1.2. Compositions (wt%) of Ni-Cr-Mo steels in hydrogen compatibility studies.

Steel	Fe	Ni	Cr	Mo	C	Mn	Si	P	S	Other	Ref.
HY-100	Bal	2.57	1.67	0.42	0.16	0.32	0.22	0.010	0.019	0.05 Cu 0.002 V 0.001 Ti	[3]
HY-80	Bal	2.49	1.46	0.43	0.13	0.30	0.22	0.016	0.021	0.05 Al 0.002 V 0.001 Ti	[3]
A517 (F)	Bal	0.79	0.54	0.43	0.16	0.80	0.21	0.010	0.016	0.04 V 0.002 B	[3]
4340	Bal	2.54	0.86	0.39	0.36	0.76	0.25	0.010	0.010	0.093 V	[4, 16]
modified 4340 (steel B7)	Bal	1.82	0.81	0.25	0.37	0.007	0.002	0.003	0.003	0.002 Cu	[6]
4340 (steel B6)	Bal	1.80	0.75	0.26	0.37	0.72	0.32	0.003	0.005	—	[6]
4340 (steel B2)	Bal	1.72	0.73	0.22	0.39	0.68	0.08	0.009	0.016	0.046 Al 0.05 V 0.04 Nb	[6]
modified 4340 (steel 43Mn)	Bal	1.82	0.75	0.30	0.24	0.07 2.65	0.27	0.003	0.01	—	[7, 13]
modified 4340 (steel 43Co)	Bal	1.74	0.85	0.26	0.30	0.79	0.32	0.001	0.004	0.39<Co<2.83	[7, 13]
4340	Bal	1.75	0.79	0.26	0.41	0.76	0.28	0.008	0.004	0.14 Cu	[9]
HY-80	Bal	2.26	1.46	0.30	0.16	0.28	0.22	0.011	0.016	0.016 Al 0.005 V	[10]
A517 (F)	Bal	0.87	0.53	0.43	0.17	0.79	0.23	0.010	0.016	0.27 Cu 0.031 Al 0.039 V 0.003 B	[10]
HY-130	Bal	4.91	0.58	0.58	0.11	0.85	0.27	0.009	0.007	0.021 Al 0.05 V	[10]
HY-130 (steel A)	Bal	4.90	0.51	0.50	0.14	0.02	0.03	0.004	0.005	0.075 V 0.300 Al 0.002 N 0.0018 Sn	[12]
HY-130 (steel F)	Bal	4.97	0.48	0.50	0.13	0.90	0.36	0.004	0.006	0.079 V 0.025 Al 0.002 N 0.0009 Sn	[12]
4340	Bal	1.74	0.67	0.22	0.44	0.74	0.28	0.015	0.006	—	[15]
4340	Bal	1.81	0.82	0.22	0.39	0.63	0.27	0.008	0.017	—	[17]
HY-100	Bal	2.86	1.40	0.41	0.16	0.31	0.20	0.012	0.019	0.13Cu 0.003 Ti 0.003 V	[17]
HY-80	Bal	2.99	1.68	0.41	0.18	0.30	0.20	0.018	0.013	0.005 V	[19]
HY-130	Bal	4.96	0.57	0.41	0.12	0.79	0.35	0.004	0.005	0.057 V	[19]

Table 1.1.3. Heat treatments and mechanical properties of Ni-Cr-Mo steels in hydrogen compatibility studies.

Steel	Heat treatment	S_y (MPa)	S_u (MPa)	RA (%)	K_{Ic} (MPa$\sqrt{m}$)	Ref.
HY-100	specification MIL-S-16216G	730	845	65	—	[3]
HY-80	specification MIL-S-16216G	620	735	69	—	[3]
A517 (F)	A 1158 K/30 min + WQ + T 936 K/60 min	765	835	63	—	[3]
4340	A 1122 K/240 min + WQ + T 833 K/240 min + WQ	1235	1340	46	154 176	[4, 16]
mod. 4340 (steel B7)	A 1123 K/60 min + OQ + (373 K < T < 798 K)/60 min	1200 1860	—	—	45 105	[6]
4340 (steel B6)		1160 1860	—	—	40 90	
4340 (steel B2)		1145 1875	—	—	45 105	
mod. 4340 (steel 43Mn)	A 1255 K + Q + DT 689 K/(60 min + 60 min)	1165	1305	—	115*	[7, 13]
mod. 4340 (steel 43Co)	A 1255 K + Q + (672 K < DT < 727 K)/(60 min + 60 min)	1275	1415	—	115*	[7, 13]
4340	A 1323 K/90 min + OQ + SR 473 K/60 min + WQ + TA 198 K/180 min + T 838 K/90 min + WQ	1070	1190	52	—	[9]
HY-80	A 1177 K/90 min + WQ + T 997 K/90 min + WQ	585	690	77	125*	[10]
A517 (F)	A 1177 K/60 min + WQ + 938 K/90 min + WQ	760	835	66	157*	[10]
HY-130	A 1089 K/90 min + WQ + 900 K/90 min + WQ	940	985	70	185*	[10]
HY-130 (steel A)	A 1273 K/120 min + WQ + T 898 K/120 min + WQ	1040	—	—	—	[12]
HY-130 (steel F)		1000	—	—	—	
4340	(1123 K < A < 1523 K)/15 min + 1123 K/10 min + OQ + T 473 K/60 min	1550	2000	0 40	35 50*	[15]
4340	A 1089 K/60 min + OQ + T 644 K/120 min	1380	—	—	—	[17]
HY-100	—	765	855	70	—	[17]
HY-80	A 1172 K + WQ + T 950 K + WQ	655	780	70	—	[19]
HY-130	A 1089 K + WQ + T 866 K + WQ	965	1020	67	—	[19]

A = austenitize; DT = double temper; OQ = oil quench; Q = quench; SR = stress relieve; T = temper; TA = transform austenite; WQ = water quench

* not reported as standardized K_{Ic} measurement

Table 3.1.1.1. Smooth tensile properties of Ni-Cr-Mo steels in air, high-pressure helium gas, and high-pressure hydrogen gas at room temperature.

Steel	Test environment	Strain rate (s^{-1})	S_y (MPa)	S_u (MPa)	El_t (%)	RA (%)	Ref.
HY-100	69 MPa He 69 MPa H_2	$3.3x10^{-5}$*	669† —	780 793	20‡ 18‡	76 63	[3]
HY-80	air 69 MPa He 69 MPa H_2	$3.3x10^{-5}$*	642† 566† 587†	738 676 683	— 23‡ 20‡	64 70 60	[3]
A517 (F)	air 69 MPa H_2	$3.3x10^{-5}$*	835† 745†	897 842	18‡ 18‡	67 65	[3]

* strain rate up to S_y
† defined at deviation from linearity on load *vs* time plot
‡ based on 32 mm gauge length

Table 3.1.1.2. Smooth tensile properties of A517 (F) steel in air and high-pressure hydrogen gas at room temperature as a function of surface preparation.

Steel	Abrading environment	Time after abrading before H_2 contact	Test environment	Strain rate* (s^{-1})	S_y† (MPa)	S_u (MPa)	El_t‡ (%)	RA (%)	Ref.
A517 (F)	no abrasion		air	$3.3x10^{-5}$	835	897	18	67	[3]
	air	n/a	air		835	890	18	64	
	no abrasion		69 MPa H_2		745	842	18	65	
	air	0.5 hr	69 MPa H_2		766	856	12	39	
	air	2 days	69 MPa H_2		731	835	14	46	
	69 MPa H_2	n/a	69 MPa H_2		738	821	13	43	

* strain rate up to S_y
† defined at deviation from linearity on load *vs* time plot
‡ based on 32 mm gauge length

Table 3.1.2.1. Notched tensile properties of Ni-Cr-Mo steels in air, high-pressure helium gas and high-pressure hydrogen gas at room temperature.

Steel	Specimen	Test environment	Displ. rate (mm/s)	S_y* (MPa)	σ_s (MPa)	RA (%)	Ref.
HY-100	(a)	69 MPa He 69 MPa H_2	~ $4x10^{-4}$	669 —	1546 1132	7.3 3.8	[3]
HY-80	(a)	69 MPa He 69 MPa H_2	~ $4x10^{-4}$	566 587	1311 1069	8.6 3.6	[3]
A517 (F)	(a)	air 69 MPa He[a] 69 MPa H_2	~ $4x10^{-4}$	835 — 745	1628 1532[b] 1194	7.4 5.7 2.1	[3]

* yield strength of smooth tensile specimen (Table 3.1.1.1)

[a] contaminated with hydrogen

[b] estimated from strength measured in air and effect of hydrostatic pressure

(a) V-notched specimen: 60^o included angle; minimum diameter = 3.81 mm; maximum diameter = 7.77 mm; notch root radius = 0.024 mm. Stress concentration factor (K_t) = 8.4.

Table 3.1.2.2. Notched tensile properties as a function of notch acuity for A517 (F) steel in air, high-pressure helium gas, and high-pressure hydrogen gas at room temperature.

Steel	Specimen	Test environment	Displ. rate (mm/s)	σ_s (MPa)	RA (%)	Ref.
A517 (F)	K_t = 3.8†	air 69 MPa He 69 MPa H_2	~ $4x10^{-4}$	1677 1566 1249	13 12 2.8	[3]
	K_t = 5.8†	air 69 MPa He 69 MPa H_2		1677 1587 1187	11 12 2.0	
	K_t = 8.4†	air 69 MPa He[a] 69 MPa H_2		1628 1532[b] 1194	7.4 5.7 2.1	

K_t = stress concentration factor

† V-notched specimen: 60^o included angle; minimum diameter = 3.81 mm; maximum diameter = 7.77 mm; notch root radius = 0.117, 0.051, and 0.024 mm for K_t = 3.8, 5.8, and 8.4, respectively.

[a] contaminated with hydrogen

[b] estimated from strength measured in air and effect of hydrostatic pressure

Table 3.2.2.1. Values of threshold stress-intensity factor for Ni-Cr-Mo steels in high-pressure hydrogen gas at 286 K.

Steel	S_y† (MPa)	RA† (%)	K_{Ic} (MPa√m)	Test environment	K_{TH} (MPa√m)	Ref.
HY-80	585	77	125*	69 MPa H_2 97 MPa H_2	NCP 116 NCP 89	[10]
A517 (F)	760	66	157*	21 MPa H_2 41 MPa H_2 62 MPa H_2 69 MPa H_2 97 MPa H_2	86 67 77 70 81	[10]
HY-130	940	70	185*	21 MPa H_2 41 MPa H_2 69 MPa H_2	36 32 24	[10]

NCP = no crack propagation at given stress intensity factor

† yield strength and reduction of area of smooth tensile specimen in air

* not reported as standardized K_{Ic} measurement

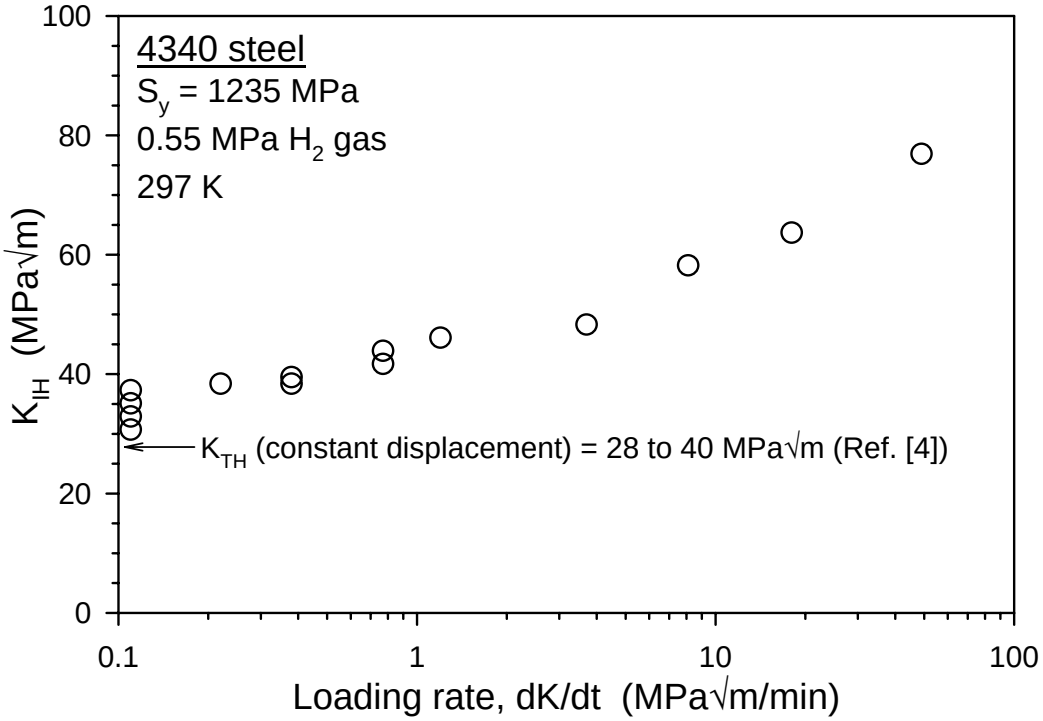

Figure 3.2.1.1. Effect of loading rate on fracture toughness in low-pressure hydrogen gas for 4340 steel [4].

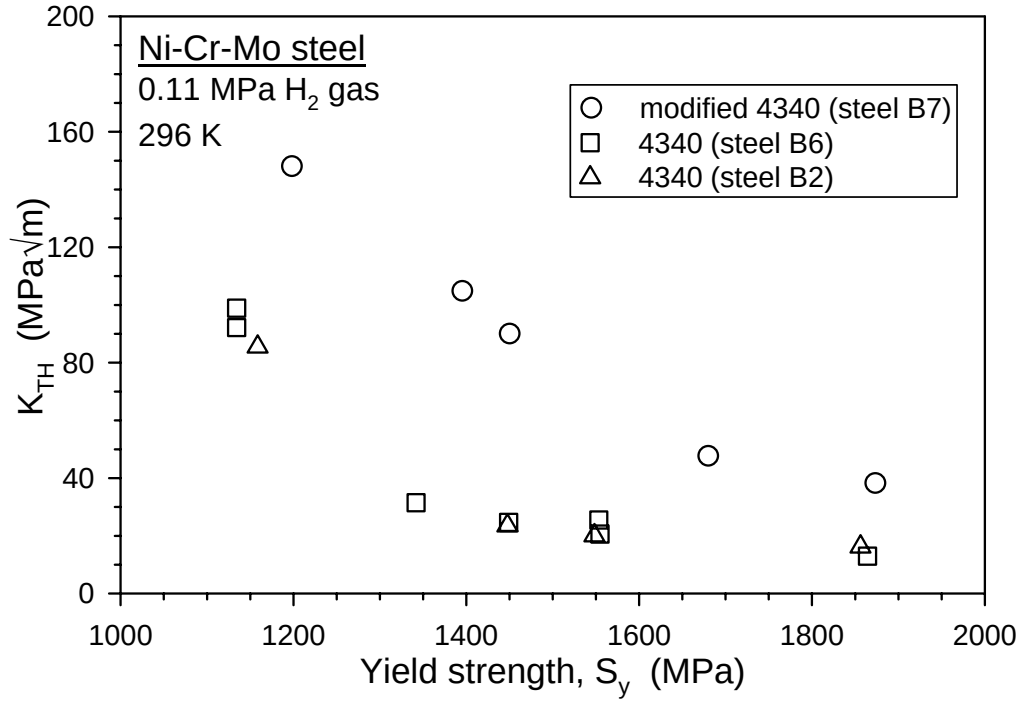

Figure 3.2.2.1. Effect of yield strength on threshold stress-intensity factor for crack extension in low-pressure hydrogen gas for steels based on 4340 [6].

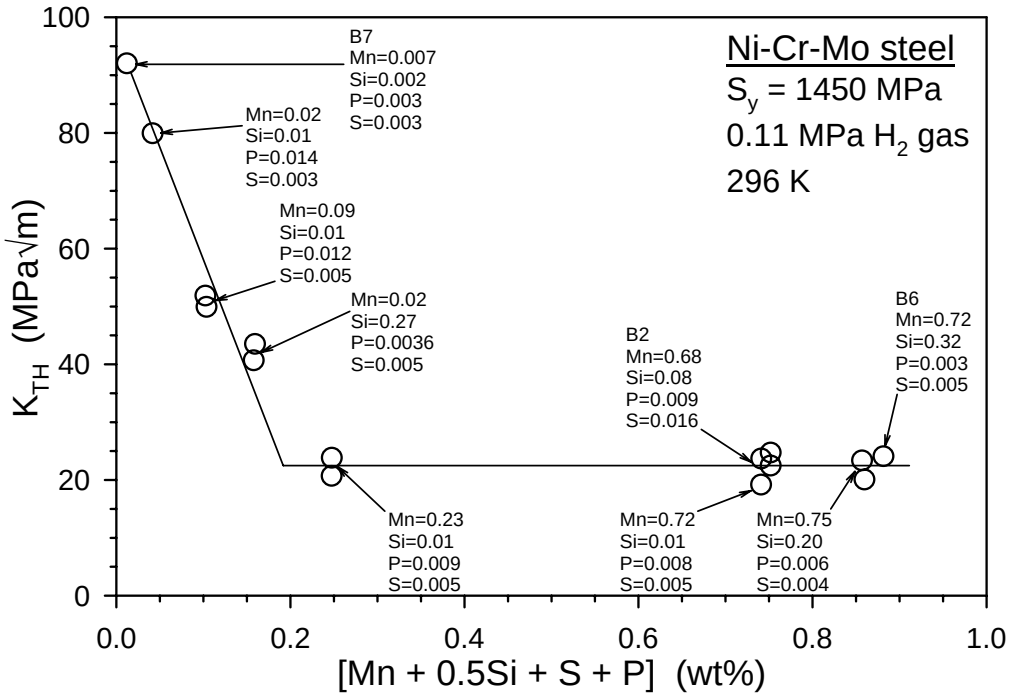

Figure 3.2.2.2. Effect of manganese, silicon, phosphorus, and sulfur content on threshold stress-intensity factor for crack extension in low-pressure hydrogen gas for steels based on 4340 [6].

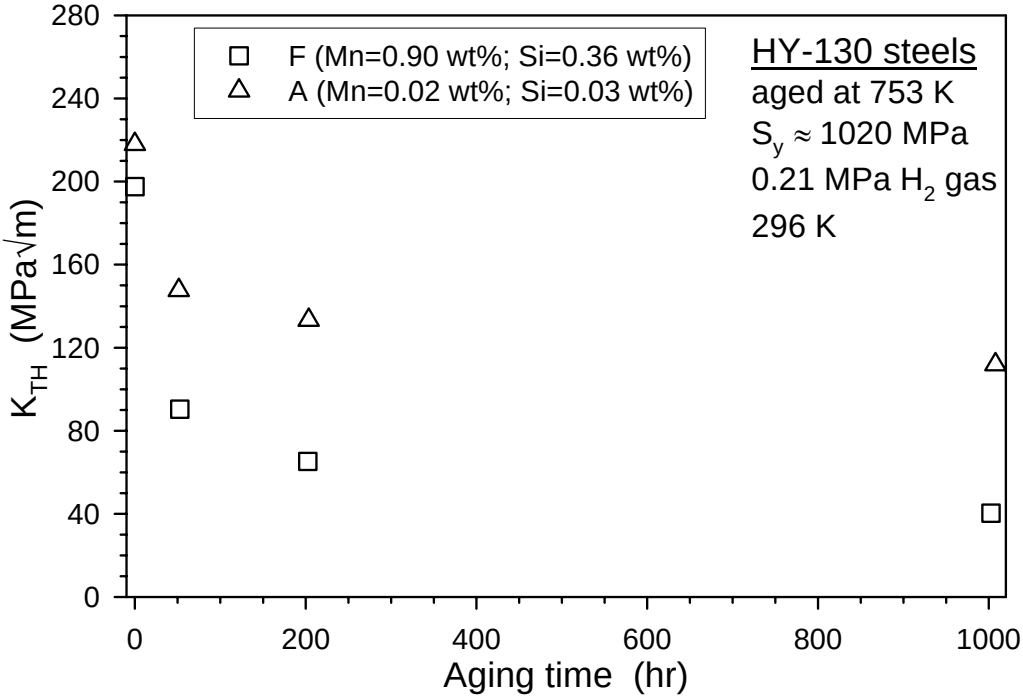

Figure 3.2.2.3 Effect of aging time at 753 K on the threshold stress-intensity factor for crack extension in low-pressure hydrogen gas for HY-130 steels [12].

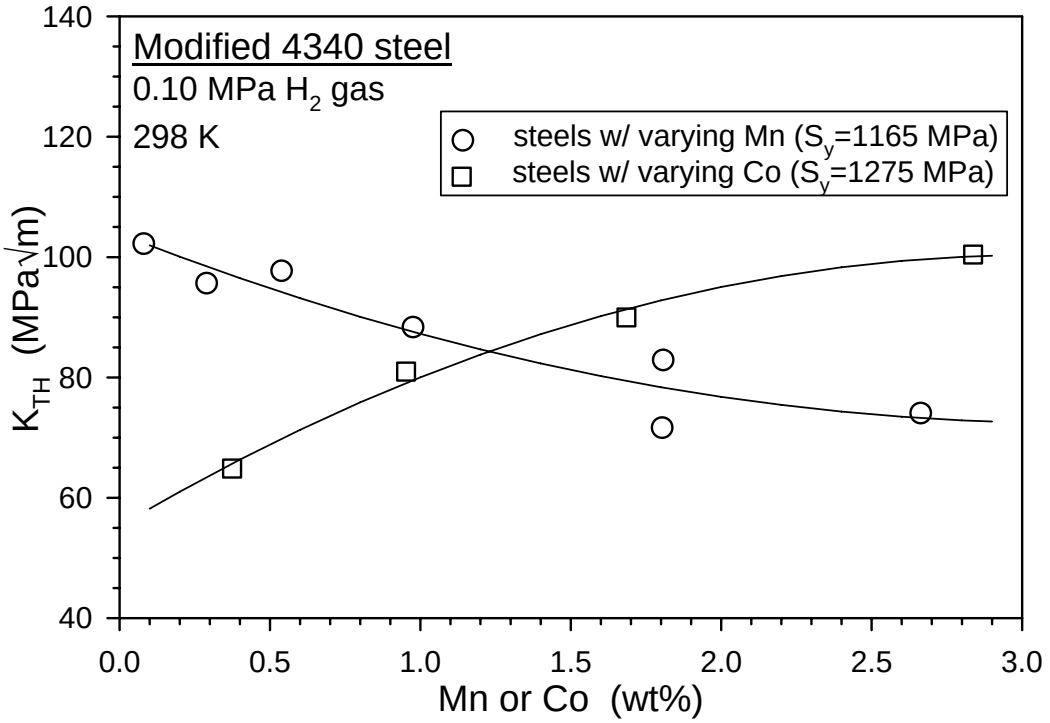

Figure 3.2.2.4. Effect of manganese or cobalt content on threshold stress-intensity factor for crack extension in low-pressure hydrogen gas for modified 4340 steels [7].

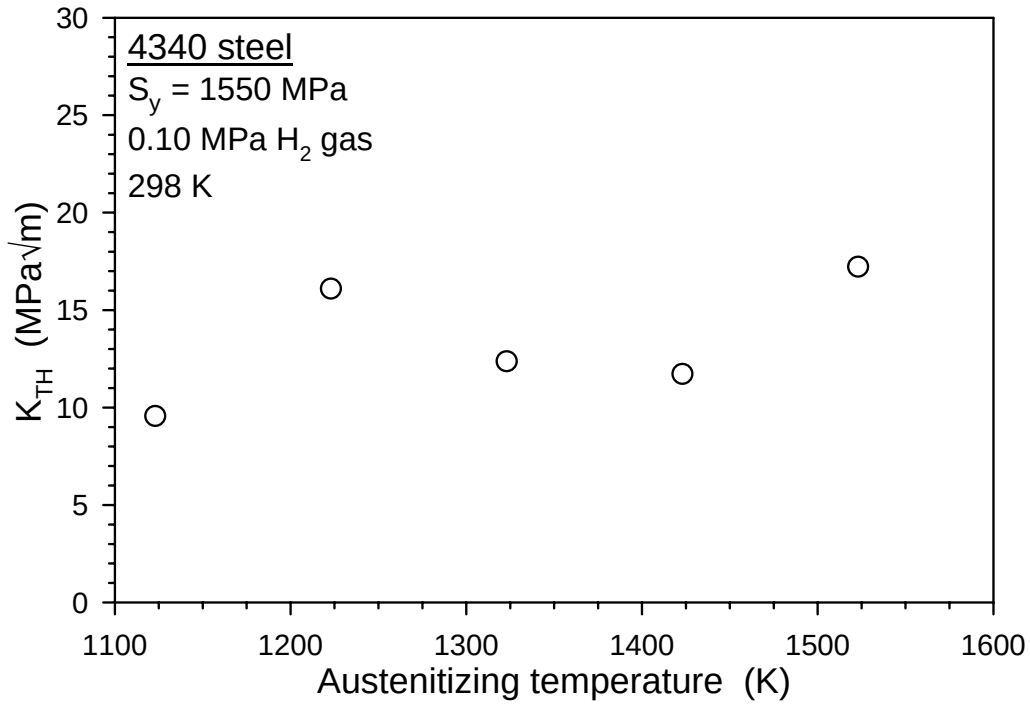

Figure 3.2.2.5. Effect of austenitizing temperature on threshold stress-intensity factor for crack extension in low-pressure hydrogen gas for 4340 steel [15].

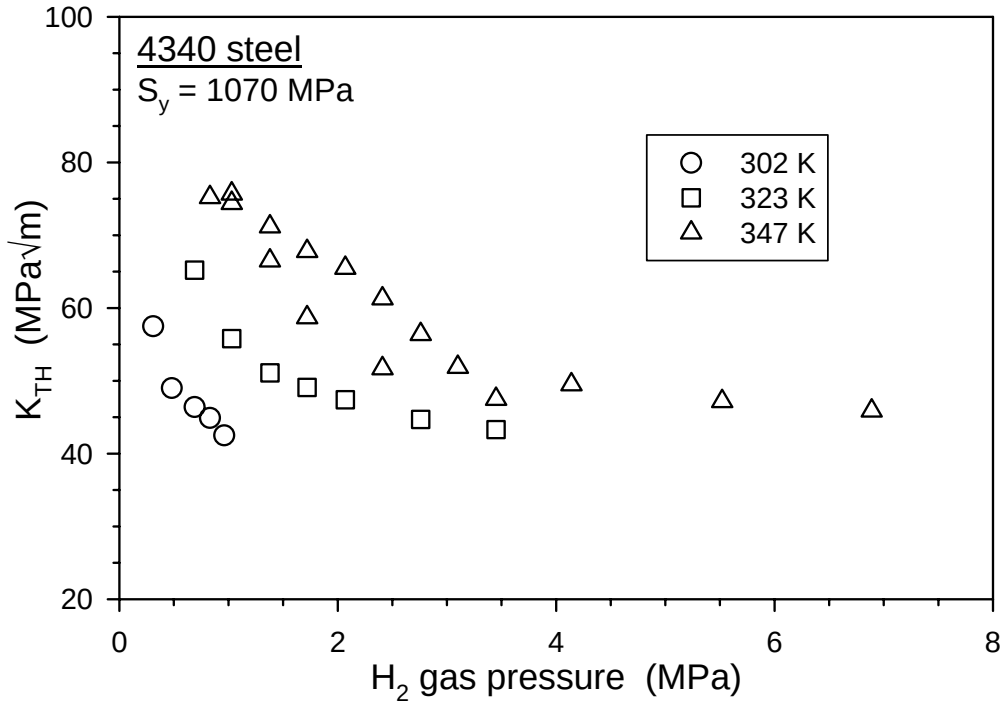

Figure 3.2.2.6. Effect of hydrogen gas pressure on threshold stress-intensity factor for crack extension in 4340 steel [9]. Data are shown for three temperatures.

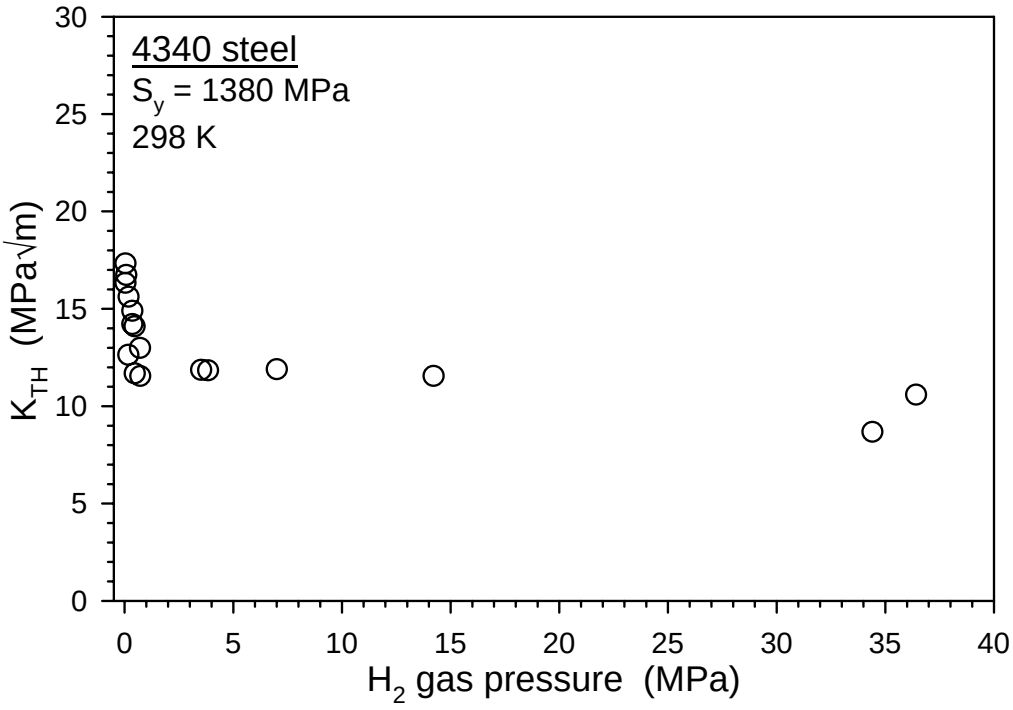

Figure 3.2.2.7. Effect of hydrogen gas pressure on threshold stress-intensity factor for crack extension in high-strength 4340 steel [17].

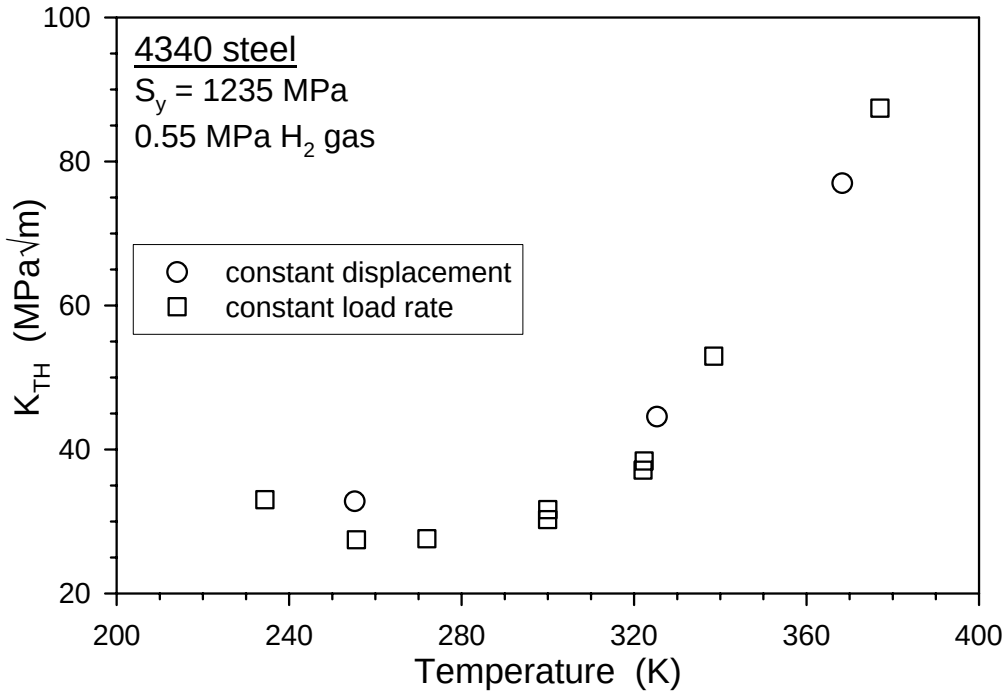

Figure 3.2.2.8. Effect of temperature on threshold stress-intensity factor for crack extension in low-pressure hydrogen gas for 4340 steel [16]. Two loading modes were used to generate the data: constant displacement and constant load rate (dK/dt = 0.1 to 0.2 MPa√m/min).

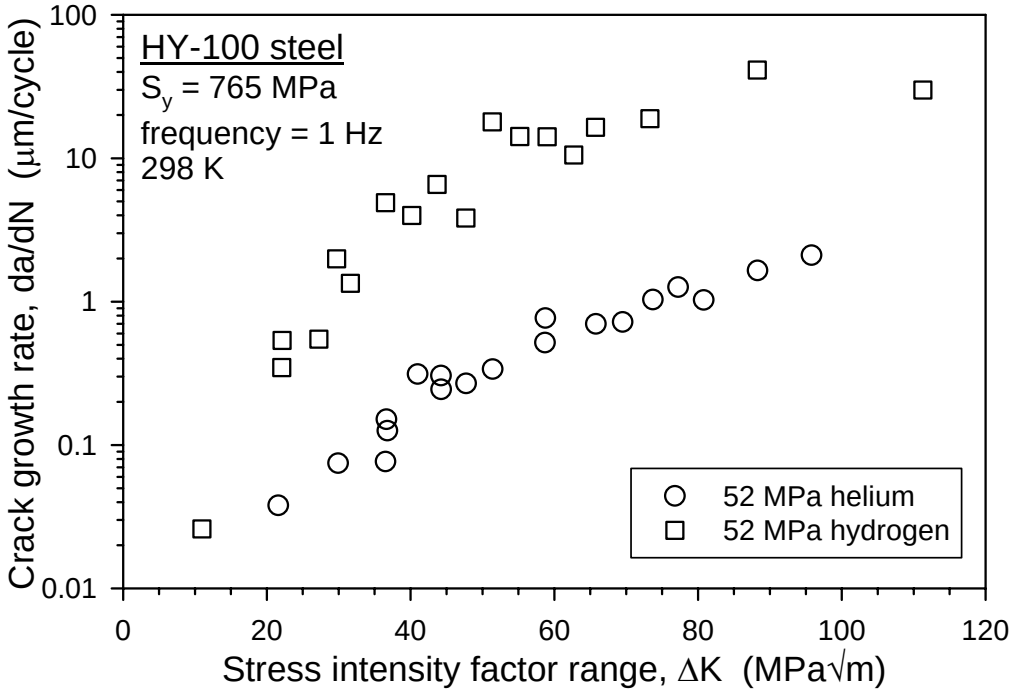

Figure 3.3.2.1. Fatigue crack growth rate as a function of stress-intensity factor range for HY-100 steel in high-pressure hydrogen and helium gases [17].

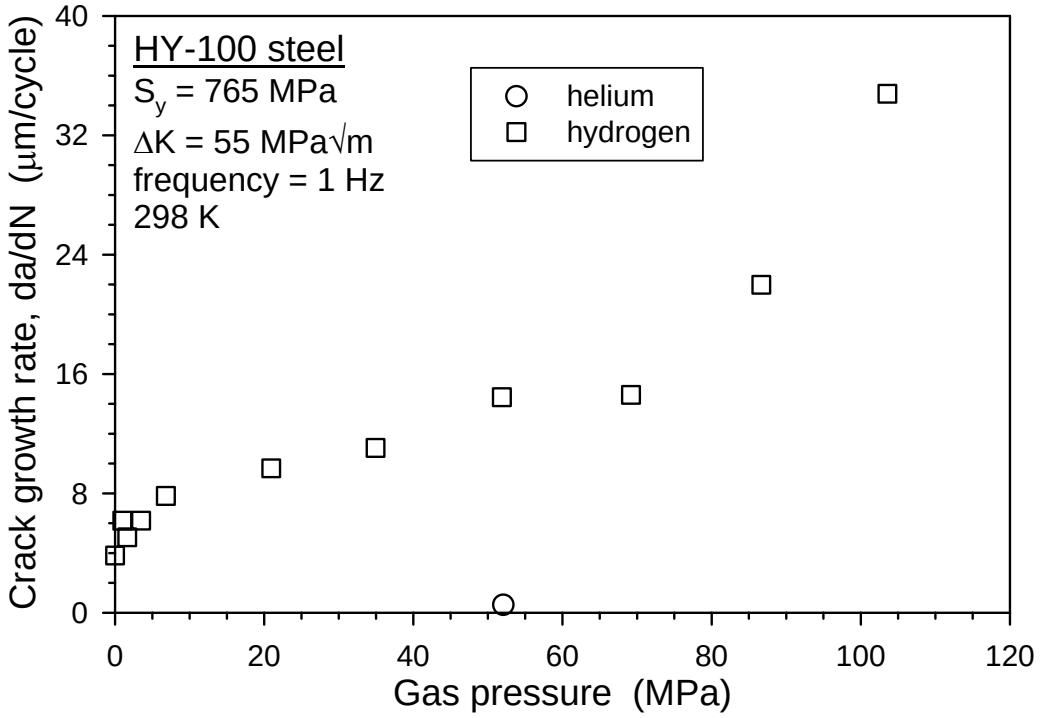

Figure 3.3.2.2. Fatigue crack growth rate as a function of hydrogen gas pressure for HY-100 steel at fixed stress-intensity factor range [17].

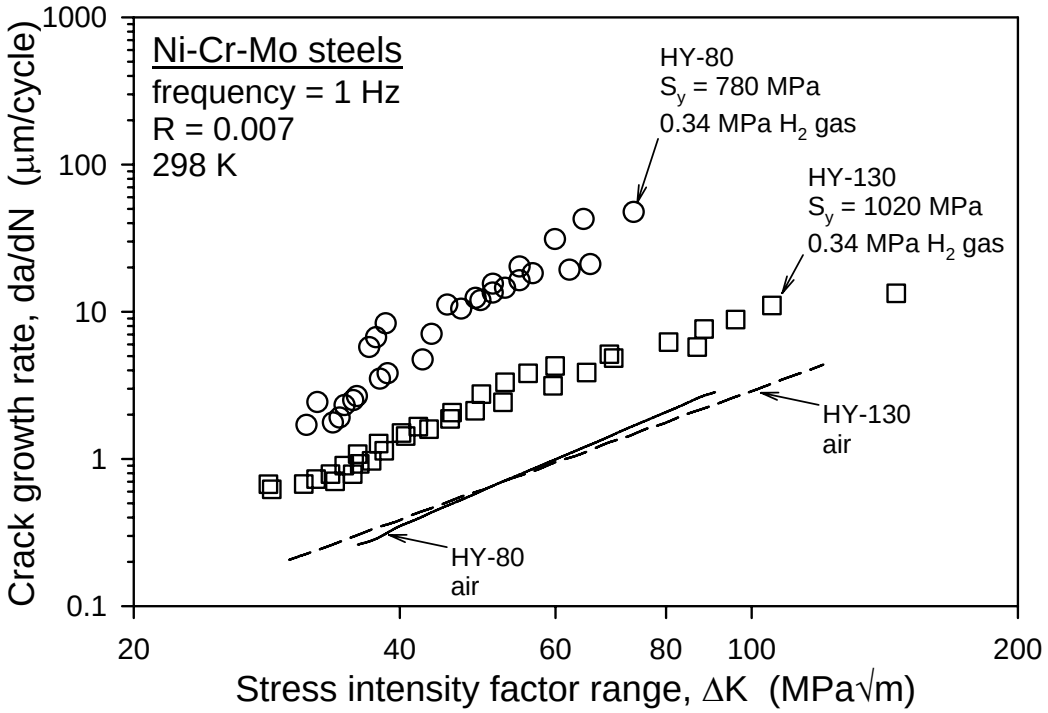

Figure 3.3.2.3. Fatigue crack growth rate as a function of stress-intensity factor range for HY-80 and HY-130 steels in air and low-pressure hydrogen gas [19].

This page intentionally left blank.

Technical Reference on Hydrogen Compatibility of Materials

High-Alloy Ferritic Steels:

9Ni-4Co (code 1401)

1. General

9Ni-4Co is a high strength, tempered martensitic steel used primarily in the aerospace industry [1, 2]. Screening tests indicate that this alloy is not appropriate for use in gaseous hydrogen environments [3-5]. Fatigue data indicate that gaseous additives can reduce the embrittling effects of gaseous hydrogen on 9Ni-4Co [6]; however, further study is required to determine the viability and practicality of such an approach.

1.1 Composition and microstructure

Table 1.1.1 lists the compositional range for 9Ni-4Co steel.

1.2 Common designations

HP9-4-20, UNS K91472
similar alloys: HP9-4-30 (UNS K91283), HP9-4-25 (UNS91122)

2. Permeability, Diffusivity and Solubility

Permeability of hydrogen in 9Ni-4Co is reported to be similar to pure iron and 4130 steel [7, 8]. The temperature dependence of permeability is reported in Ref. [7] as

$$\phi = \phi_o \exp\left(-E_\phi / RT\right)$$

where $\phi_o = 1.95\text{x}10^{-4} \dfrac{\text{mol H}_2}{\text{m}\cdot\text{s}\cdot\sqrt{\text{MPa}}}$ and $E_\phi = 39.3\text{kJ/mol}$.

3. Mechanical Properties: Effects of Gaseous Hydrogen

3.1 Tensile properties

3.1.1 Smooth tensile properties

Walter, Chandler and co-workers [3-5] have categorized 9Ni-4Co steel as extremely embrittled in the presence of hydrogen gas at room temperature. Tensile properties are given in Table 3.1.1.1.

3.1.2 Notched tensile properties

Notched tensile properties of 9Ni-4Co in 69 MPa gaseous hydrogen, Table 3.1.2.1, show that this steel has almost no ductility (RA = 0.2%), and its sharp-notch strength is reduced by a factor of four compared to testing in 69 MPa gaseous helium.

3.2 Fracture mechanics

No known published data in gaseous hydrogen.

3.3 Fatigue

Fatigue crack growth rates were found to be significantly greater in 0.013 MPa gaseous hydrogen compared to vacuum (10^{-6} Pa); measurements are reported at temperatures between 225 and 375 K and cyclic stress intensity in the range of 10 to 50 MPa $m^{1/2}$ [6]. The fatigue crack growth rate in this low pressure of hydrogen is a maximum at about 273K and shows the largest difference compared to vacuum at stress intensity near 25 MPa $m^{1/2}$. At room temperature and a stress intensity of 24.7 MPa $m^{1/2}$ the fatigue crack growth rate is about $5x10^{-6}$ m/cycle in hydrogen and $8x10^{-8}$ m/cycle in vacuum. Equal partial pressures (0.013 MPa) of oxygen (O_2), carbon monoxide (CO) or nitrous oxide (N_2O) added to gaseous hydrogen reduced the fatigue crack growth rates to values associated with those gases alone, about twice the rate in vacuum [6].

3.4 Creep

No known published data in gaseous hydrogen.

4. Fabrication

Special considerations for hydrogen service have not been identified since this alloy is not recommended for hydrogen service.

5. References

1. A Magnee, JM Drapier, J Dumont, D Coutsouradis and L Habraken. Cobalt-Containing High-Strength Steels. Centre d'Information du Cobalt, Brussels (1974).
2. JL Shannon. Ultra High Strength Steels: Fe-9Ni-4Co-Cr-Mo-V (code 1221). in: WF Brown, H Mindlin and CY Ho, editors. Aerospace Structural Metals Handbook. West Lafayette: CINDAS/UASF CRDA Handbooks Operation, Purdue University (1987).
3. RJ Walter and WT Chandler. Effects of High-Pressure Hydrogen on Metals at Ambient Temperature: Final Report (NASA CR-102425). Rocketdyne (report no. R-7780-1) for the National Aeronautics and Space Administration, Canoga Park CA (February 1969).
4. RJ Walter, RP Jewitt and WT Chandler. On the Mechanism of Hydrogen-Environment Embrittlement of Iron- and Nickel-base Alloys. Mater Sci Eng 5 (1970) 99-110.
5. RP Jewitt, RJ Walter, WT Chandler and RP Frohmberg. Hydrogen Environment Embrittlement of Metals (NASA CR-2163). Rocketdyne for the National Aeronautics and Space Administration, Canoga Park CA (March 1973).
6. JD Frandsen and HL Marcus. Environmentally Assisted Fatigue Crack Propagation in Steel. Metall Trans 8A (1977) 265-272.
7. MR Louthan, RG Derrick, JA Donovan and GR Caskey. Hydrogen Transport in Iron and Steel. in: AW Thompson and IM Bernstein, editor. Effect of Hydrogen on Behavior of Materials. Metallurgical Society of the AIME (1975) p. 337-347.
8. MR Louthan and G Caskey. Hydrogen Transport and Embrittlement in Structural Metals. International Journal of Hydrogen Energy 1 (1976) 291-305.

9. ASTM. Metals and Alloys in the UNIFIED NUMBERING SYSTEM (SAE HS-1086 OCT01; ASTM DS-56H). Society of Automotive Engineers; American Society for Testing and Materials, (2001).

Table 1.1.1. Compositional ranges of 9Ni-4Co according to UNS K91472.

Heat	Fe	Ni	Co	Cr	Mn	Mo	Si	C	Other	Ref.
UNS K91472	Bal	8.50 9.50	4.25 4.75	0.65 0.85	0.20 0.40	0.90 1.10	0.20 max	0.17 0.23	0.010 max S; 0.010 max P; 0.35 max Cu; 0.06 < V < 0.12	[9]
W69	Bal	9.10	4.45	0.78	0.27	1.01	0.02	0.17	0.005 P; 0.005 S; 0.78 V	[3]

Table 3.1.1.1. Tensile properties of 9Ni-4Co steel tested at room temperature in high-pressure helium and hydrogen gas.

Material	Thermal precharging	Test environment	Strain rate (s^{-1})	S_y (MPa)	S_u (MPa)	El_u (%)	El_t (%)	RA (%)	Ref.
W69†	None	69MPa He	0.67 x10^{-3}	1289	1372	—	15	67	[3, 5]
	None	69MPa H_2		—	1207	—	0.5	15	

† annealed at 843˚C (1550˚F) for 1 hour, oil quenched; double tempered at 538˚C (1000˚F) for 2 hours

Table 3.1.2.1. Notched tensile properties of 9Ni-4Co steel tested in high-pressure helium and hydrogen gas at room temperature.

Material	Specimen	Thermal precharging	Test environment	S_y * (MPa)	σ_s (MPa)	RA (%)	Ref.
W69†	(1)	None	69MPa He	1289	2668	6.3	[3, 5]
		None	69MPa H_2	—	614	0.2	

† annealed at 843˚C (1550˚F) for 1 hour, oil quenched; double tempered at 538˚C (1000˚F) for 2 hours

* yield strength (0.2% offset) of smooth tensile bar† did not satisfy plane strain requirements for analysis of stress intensity

(1) stress concentration factor (K_t) = 8.4; notch geometry = 60˚ included angle; minimum diameter = 3.81 mm (0.15 inch); maximum diameter = 7.77 mm (0.306 inch); notch root radius = 0.024 mm (0.00095 inch); displacement rate ≈ 4 x10^{-4} mm/s.

This page intentionally left blank.

Technical Reference on Hydrogen Compatibility of Materials

High-Alloy Ferritic Steels:

Ferritic Stainless Steels (code 1500)

1. General

There are numerous classes of stainless steels, including ferritic, martensitic, austenitic, duplex, and precipitation-hardened. The ferritic stainless steels are distinguished by the primary alloying element, chromium, which provides a stable ferritic structure at all temperatures. Due to low carbon content, the ferritic stainless steels have limited strength but can have good ductility and work harden very little. The toughness of these alloys tends to be quite low and their ductile to brittle transition is at or above room temperature. The special ferritic alloys were developed for improved toughness and may contain molybdenum, providing them with corrosion resistance superior to austenitic stainless steels in most environments [1].

Ferritic stainless steel has high diffusivity and low solubility for hydrogen compared to austenitic stainless steels. Although the properties of ferritic alloys measured in hydrogen gas (particularly at high-pressure) are scarce in the literature, the general trends emerging from the literature are that the ferritic stainless steels are at least as susceptible to hydrogen-assisted fracture as the unstable austenitic stainless steels (e.g., type 301 and 304 stainless steels). NASA reports classify type 430F stainless steel as severely embrittled by high-pressure hydrogen gas [2, 3].

1.1 Composition and microstructure

The ferritic stainless steels have anywhere from 10-30 wt% Cr, however, chromium typically ranges from 12-18 wt%. Special ferritic alloys are generally those that contain higher amounts of Cr with some containing as much as 24-30 wt%. Molybdenum is sometimes added to the ferritic stainless steels in the range 1-4 wt% and Ni, if present, is generally < 2 wt%. Carbon and nitrogen contents are generally low, as in the 300-series austenitic stainless steels. The compositional ranges of a number of ferritic stainless steels are given in Table 1.1.1. Table 1.1.2 lists the compositions of alloys used to study hydrogen effects.

1.2 Common designations

The most common grades of ferritic stainless steels are known by their AISI designation, such as type 430 and 434 ferritic stainless steels. Type 400 series alloys also include a number of martensitic stainless steels, which are generally distinguished by their high strength and low resistance to hydrogen-assisted fracture in hydrogen gas [2, 3].

Some ferritic alloy designations can be easily confused with those of austenitic stainless steels. The so-called 18-2FM and 18Cr-2Mo, for example, are special ferritic stainless steels that are distinct from 18-2-Mn, which is an austenitic stainless steel containing 11-14 wt% Mn and up to 2.5 wt% Ni.

2. Permeability, Diffusivity and Solubility

Permeation and diffusion in 29Cr-4Mo-2Ni (29-4-2) have been studied by gas phase permeation experiments [4, 5] and by electrochemical diffusion studies [6, 7]. Hydrogen permeation in annealed 29-4-2 ferritic stainless steel was found to be one to two orders of magnitude greater than in austenitic stainless steels, with greater differences at low temperatures (Figure 2.1) [4, 5]. Hydrogen diffusivity of this steel was found to be 2 to 5 orders of magnitude greater than in austenitic stainless steels (Figure 2.2). Hydrogen solubility in the ferritic stainless steels is significantly less than for austenitic stainless steels (Figure 2.3).

A discontinuity in diffusivity is apparent at about 443 K, where diffusivity values at temperatures less than 443 K are lower than values extrapolated from diffusivity measurements at higher temperatures. Similar observations have been made for iron and ferritic steels, and this has been attributed to trapping of hydrogen at microstructural defects during transport of hydrogen in the lower temperature regime [8, 9]. In addition, it has been shown that the apparent diffusivity is a function of concentration of hydrogen in the lattice and the concentration of hydrogen in trapping sites [8]. At high temperature, hydrogen is not trapped due to the available thermal energy preventing the binding of hydrogen to trapping sites. Thus, the diffusivity correlation for temperatures greater than 443 K can be interpreted as the lattice diffusivity in the absence of hydrogen trapping. The apparent solubility of hydrogen (determined from the quotient of the permeability and the diffusivity) shows the effect of the diffusion discontinuity in the annealed material as well: at temperature lower than 443 K, the hydrogen solubility is higher than extrapolation from higher temperature solubility would predict. This implies that in the lower temperature regime the hydrogen in the material is a sum of hydrogen dissolved in the lattice and trapped hydrogen, while at higher temperatures where trapping is less effective, the amount of hydrogen in the material is primarily due to dissolution in the lattice.

Cold-working the 29-4-2 reduced hydrogen diffusivity by an order of magnitude or more [5]; a much larger change than observed for cold-worked austenitic stainless steels [4, 10, 11]. Deformation in ferritic steels increases the density of hydrogen trapping sites, therefore, cold-working would be expected to have a larger impact on the apparent hydrogen diffusivity compared to annealed materials (Figure 2.2). In addition, the effect of hydrogen trapping on diffusivity is extended to higher temperatures, presumably because hydrogen is bound to traps more strongly and more thermal energy is required to overcome the trapping. Permeation was also reduced by cold-working, by almost a factor of 10 (Figure 2.1). Cold-working increases the hydrogen solubility at low temperature (less than about 573 K), but it is similar to the annealed material at higher temperature (Figure 2.3). The parameters for predicting permeability, diffusivity and solubility are given in Table 2.1.

Elastic stress was found to change hydrogen diffusivity by less than 50% in the temperature range of 303 K to 353 K [6]. It appears that the magnitude of diffusivity is nominally unaffected by applied stress (a factor of 2 can be considered small for diffusion experiments), but the activation energy for diffusion increased. The partial molar volume of hydrogen in 29-4-2 was determined to be 2.3×10^{-6} m^3 mol^{-1} (mole of H atoms) from these electrochemical measurements [6].

3. Mechanical Properties: Effects of Gaseous Hydrogen

3.1 Tensile propertie

3.1.1 Smooth tensile properties

A significant reduction in tensile ductility was reported for type 430F ferritic stainless steel (heat W69) [2, 3]. Smooth bar tensile tests were performed in 69 MPa helium and hydrogen gases respectively as summarized in Table 3.1.1.1.

3.1.2 Notched tensile properties

Notched round tensile specimens of type 430F ferritic stainless steel (heat W69) tested in high-pressure gas show ~30% loss of strength in hydrogen compared to helium gas, Table 3.1.2.1. This testing was performed as part of a large test program in which this ferritic stainless steel was classified as severely embrittled [2, 3].

Perng and Altstetter tested 29Cr-4Mo-2Ni (29-4-2, heat P87) ferritic stainless steel notched sheet specimens (where plane stress conditions prevailed) in air and 0.11 MPa hydrogen gas from 298 to 573 K [12]. These sheet specimens exhibited 17 percent reduction of notch tensile strength and a 50 percent loss of ductility. The effects were most severe at room temperature and gradually disappeared as the temperature increased above 373 K. The fracture mode changed from microvoid coalescence in air to fracture surfaces dominated by quasicleavage in hydrogen gas. For temperature above ambient, the amount of ductile features increases with temperature and at 423 K the fracture surfaces are similar to tests performed in air [12].

3.2 Fracture mechanics

3.2.1 Fracture toughness

No known published data in hydrogen gas.

3.2.2 Threshold stress-intensity factor

Perng and Altstetter determined crack growth rates and threshold stress intensity factor values in sustained load testing for 29-4-2 ferritic stainless steel (heat P87) notched sheet specimens where plane stress conditions prevailed [12]. The specimens were tested in air and 0.11 MPa hydrogen gas from 298 to 373 K [12]. The testing showed the threshold stress intensity factor increased with temperature, but the crack growth rate was generally higher at elevated temperature. This is rationalized in terms of hydrogen transport and accumulation ahead of the crack tip [12].

Huang and Altstetter also determined crack growth rates and threshold stress intensity factor values in the same 29-4-2 ferritic stainless steel (heat P87) notched sheet specimens as above, except internal hydrogen from molten salt electrolytes at 503 K was also examined as a variable [13]. Rapid outgassing of hydrogen, however, occurs at room temperature in ferritic stainless steels due to its high hydrogen diffusivity. Precharged specimens contained ~2 wppm residual hydrogen after testing in air, which is believed to have been trapped in the steel; most of the hydrogen (~12 wppm) outgassed from the specimens during testing [13]. Subcritical crack growth tests conducted in air on specimens with internal hydrogen showed modest effects of the trapped residual hydrogen, however, tests of precharged material in 0.11 MPa hydrogen gas resulted in similar response to tests in hydrogen without precharging. Fracture surfaces of

material tested in hydrogen gas at room temperature were dominated by quasicleavage in both the hydrogen precharged and uncharged conditions [13].

3.3 Fatigue

Internal hydrogen precharging by cathodic techniques was found to increase fatigue crack growth rates and decrease the threshold stress intensity factor for crack propagation in a 12Cr-1Mo ferritic stainless steel [14]. Based on fracture mechanics testing in low-pressure hydrogen, the degradation of fatigue properties in hydrogen gas can be expected to be greater than observed in this study.

3.4 Creep

No known published data in hydrogen gas.

3.5 Impact

No known published data in hydrogen gas.

3.6 Disk rupture testing

Fidelle et al. categorized type 430 stainless steel as having little or no sensitivity to hydrogen embrittlement during disk rupture testing [15]. This is at odds with the tensile data from the literature, perhaps due to the relative short-time scales associated with the disk rupture tests precluding substantial hydrogen transport in the lattice over the time scale of the test.

4. References

1. RA Lula. Stainless Steel (revised from "An Introduction to Stainless Steel" by JG Parr and A Hanson). Metals Park OH: American Society for Metals (1986).
2. RJ Walter and WT Chandler. Effects of High-Pressure Hydrogen on Metals at Ambient Temperature: Final Report (NASA CR-102425). Rocketdyne (report no. R-7780-1) for the National Aeronautics and Space Administration, Canoga Park CA (February 1969).
3. RP Jewitt, RJ Walter, WT Chandler and RP Frohmberg. Hydrogen Environment Embrittlement of Metals (NASA CR-2163). Rocketdyne for the National Aeronautics and Space Administration, Canoga Park CA (March 1973).
4. T-P Perng and CJ Altstetter. Effects of Deformation on Hydrogen Permeation in Austenitic Stainless Steels. Acta Metall 34 (1986) 1771-1781.
5. T-P Perng, M Johnson and CJ Altstetter. Influence of plastic deformation on hydrogen diffusion and permeation in stainless steels. Acta Metall 37 (1989) 3393-3397.
6. L-C Hwang and T-P Perng. Hydrogen transport in ferritic stainless steel under elastic stress. Mater Chem Phys 36 (1994) 231-235.
7. C-L Yu and T-P Perng. Surface effects on electrochemical hydrogen diffusion in stainless steel. Acta Metall Mater 39 (1991) 1091-1099.
8. RA Oriani. The diffusion and trapping of hydrogen in steel. Acta Metall 18 (1970) 147-157.
9. HG Nelson and JE Stein. Gas-phase hydrogen permeation through alpha iron, 4130 steel, and 304 stainless steel from less than 100˚C to near 600˚C (NASA TN D-7265). Ames Research Center, National Aeronautics and Space Administration, Moffett Field CA (April 1973).

10. MR Louthan and RG Derrick. Hydrogen Transport in Austenitic Stainless Steel. Corros Sci 15 (1975) 565-577.
11. XK Sun, J Xu and YY Li. Hydrogen Permeation Behaviour in Austenitic Stainless Steels. Mater Sci Eng A114 (1989) 179-187.
12. T-P Perng and CJ Altstetter. Comparison of Hydrogen Gas Embrittlement of Austenitic and Ferritic Stainless Steels. Metall Trans 18A (1987) 123-134.
13. J-H Huang and CJ Altstetter. Internal Hydrogen Embrittlement of a Ferritic Stainless Steel. Metall Mater Trans 26A (1995) 845-849.
14. GF Rodkey and RH Jones. Effect of internal hydrogen on the fatigue crack growth of a 12Cr-1Mo Steel. J Nucl Mater 155-157 (1988) 760-765.
15. J-P Fidelle, R Bernardi, R Broudeur, C Roux and M Rapin. Disk Pressure Testing of Hydrogen Environment Embrittlement. in: Hydrogen Embrittlement Testing, ASTM STP 543, American Society for Testing and Materials. (1974) p. 221-253.
16. ASTM DS-56H, Metals and Alloys in the UNIFIED NUMBERING SYSTEM (SAE HS-1086 OCT01). American Society for Testing and Materials (Society of Automotive Engineers) (2001).

Table 1.1.1. Nominal compositional ranges (wt%) of several ferritic stainless steels. [16]

UNS No.	AISI No / Common Name	Fe	Cr	Mo	Ni	Mn	Si	C	other
S40500	405	Bal	11.50 14.50	—	—	1.00 max	1.00 max	0.08 max	0.10-0.30 Al; 0.030 max S; 0.040 max P
S40900	409	Bal	10.50 11.75	—	0.50 max	1.00 max	1.00 max	0.08 max	0.75 max Ti; 0.045 max S; 0.045 max P
S42900	429	Bal	14.00 16.00	—	—	1.00 max	1.00 max	0.12 max	0.030 max S; 0.040 max P
S43000	430	Bal	16.00 18.00	—	—	1.00 max	1.00 max	0.12 max	0.030 max S; 0.040 max P
S43020	430F	Bal	16.00 18.00	0.60 max	—	1.25 max	1.00 max	0.12 max	0.15 min S; 0.060 max P
S43400	434	Bal	16.00 18.00	0.75 1.25	—	1.00 max	1.00 max	0.12 max	0.030 max S; 0.040 max P
S44800	29-4-2	Bal	28.0 30.0	3.5 4.2	2.0 2.5	0.30 max	0.20 max	0.10 max	0.020 max N; 0.020 max S; 0.025 max P

Table 1.1.2. Compositions (wt%) of several ferritic stainless steels used to study hydrogen effects.

Heat	Fe	Cr	Mo	Ni	Mn	Si	C	Other	Ref.
W69 430F†	Bal	16.33	0.40	0.24	1.07	0.63	0.096	0.07 Cu; 0.293 S; 0.015 P	[2, 3]
P87 29-4-2	Bal	29.5	3.93	2.23	0.10	0.10	0.0029	0.012 N; 0.01 P; 0.009 S	[12, 13]

† free machining grade of type 430 ferritic stainless steel with high sulfur.

Table 2.1. Permeability, diffusivity and solubility relationships for ferritic stainless steels. These relationships are plotted in Figures 2.1, 2.2 and 2.3 for permeability, diffusivity and solubility respectively.

Material	Temperature range (K)	Pressure range (MPa)	$\Phi = \Phi_o \exp(-E_\Phi / RT)$		$D = D_o \exp(-E_D / RT)$		$S = S_o \exp(-E_S / RT)$		Ref.
			Φ_o $\left(\frac{\text{mol H}_2}{\text{m}\cdot\text{s}\cdot\text{MPa}^{1/2}}\right)$	E_Φ $\left(\frac{\text{kJ}}{\text{mol}}\right)$	D_o $\left(\frac{\text{m}^2}{\text{s}}\right)$	E_D $\left(\frac{\text{kJ}}{\text{mol}}\right)$	S_o $\left(\frac{\text{mol H}_2}{\text{m}^3\cdot\text{MPa}^{1/2}}\right)$	E_S $\left(\frac{\text{kJ}}{\text{mol}}\right)$	
29-4-2 (P87) Annealed	353–443	0.001–0.026	2.20×10^{-6}	38.4	8.45×10^{-6}	33.7	1.16	4.7	[4, 5]
	443–593				6.40×10^{-9}	7.0	1534	31.4	
29-4-2 (P87) deformed 25%	383–533		2.94×10^{-6}	40.3	1.71×10^{-6}	36.7	1.72	3.6	[5]
29-4-2 (P87) deformed 50%	383–533		12.3×10^{-6}	45.4	2.34×10^{-6}	37.2	5.24	8.2	
29-4-2 (P87) deformed 75%	383–533		13.2×10^{-6}	47.3	9.03×10^{-6}	45.5	1.46	1.8	
Austenitic stainless steels	373-623	1×10^{-4} –0.03	53.5×10^{-6}	56.1	0.20×10^{-6}	49.3	266	6.86	[4]

Table 3.1.1.1. Smooth tensile properties of ferritic stainless steel tested at room temperature in high-pressure gaseous hydrogen.

Material	Thermal precharging	Test environment	Strain rate (s^{-1})	S_y (MPa)	S_u (MPa)	El_u (%)	El_t (%)	RA (%)	Ref.
Annealed 430F, heat W69	None	69 MPa He	0.67 x10^{-3}	496	552	—	22	64	[2, 3]
	None	69 MPa H_2		—	538	—	14	37	

Table 3.1.2.1. Notched tensile properties of ferritic stainless steel tested at room temperature in high-pressure gaseous hydrogen.

Material	Specimen	Thermal precharging	Test environment	Displ. rate (mm/s)	S_y (MPa)	σ_s (MPa)	RA (%)	Ref.
Annealed 430F, heat W69	(1)	None	69 MPa He	0.4 x 10^{-3}	496†	1048	1.9	[2, 3]
		None	69 MPa H_2		—	717	0.6	

† yield strength of smooth tensile bar

(1) V-notched specimen: 60˚ included angle; minimum diameter = 3.81 mm (0.15 inch); maximum diameter = 7.77 mm (0.306 inch); notch root radius = 0.024 mm (0.00095 inch). Stress concentration factor (K_t) = 8.4.

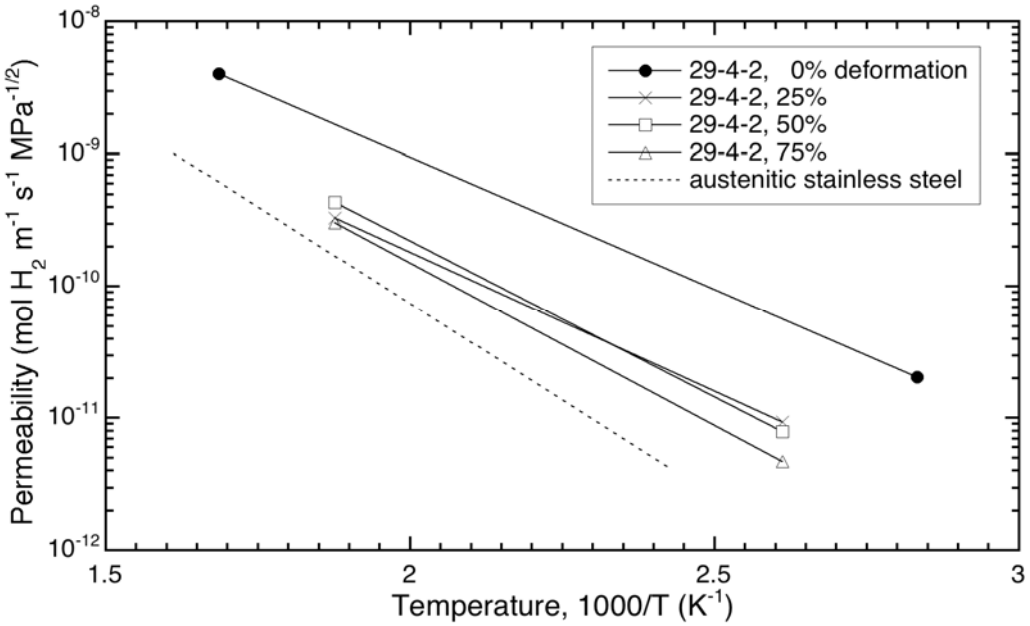

Figure 2.1. Permeability of 29-4-2 ferritic stainless steel, showing the effect of deformation on reducing permeation [5]. The dotted line represents an average permeability for several austenitic stainless alloys from Ref. [4].

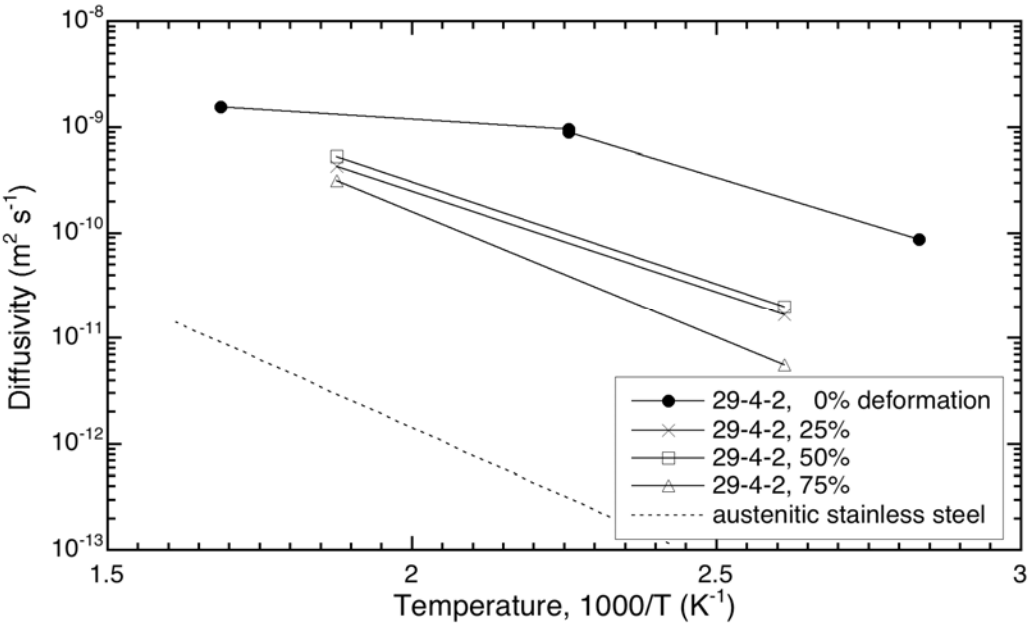

Figure 2.2. Diffusivity of 29-4-2 ferritic stainless steel, showing the effect of deformation on reducing the rate of diffusion [5]. The dotted line represents an average diffusivity for several austenitic stainless alloys from Ref. [4].

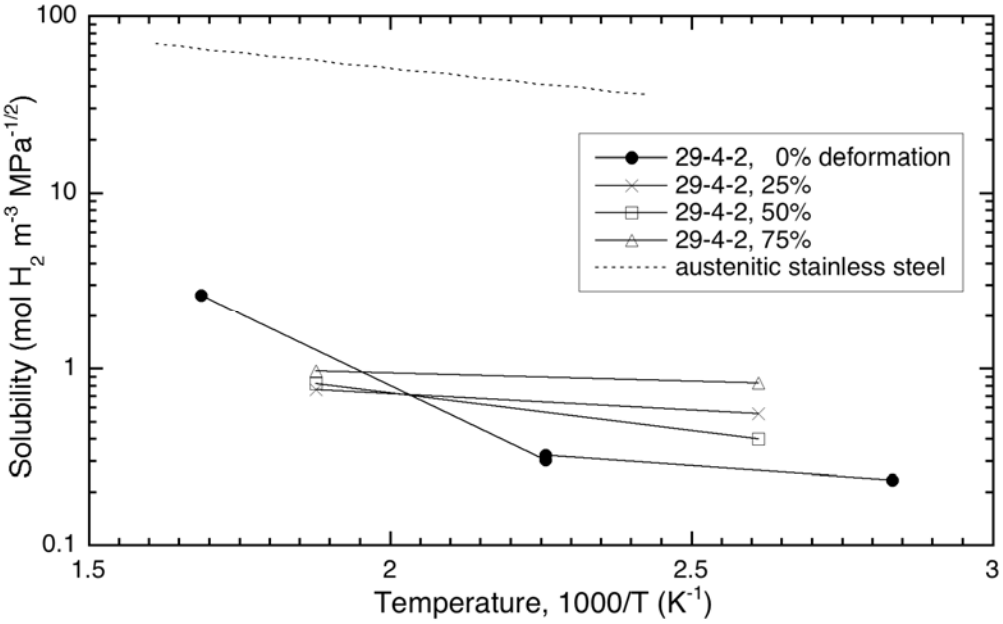

Figure 2.3. Solubility of 29-4-2 ferritic stainless steel [5]. The dotted line represents an average solubility for several austenitic stainless alloys from Ref. [4].

This page intentionally left blank.

Technical Reference on Hydrogen Compatibility of Materials

High-Alloy Ferritic Steels:

Duplex Stainless Steels (code 1600)

1. General

A duplex stainless steel is an alloy containing a two-phase microstructure of face-centered cubic austenite (γ) and body-centered cubic ferrite (α), where the phases each consist of at least 12 wt% Cr. Generally, duplex stainless steels have compositions in the range 18-26 wt% Cr, 4-7 wt% Ni, and in many cases 2-3 wt% Mo with some nitrogen. The so-called super duplex stainless steels have alloy contents at (or even slightly greater than) the high end of these ranges. Duplex stainless steels are typically used in applications that benefit from their high resistance to stress corrosion cracking, good weldability, and greater strength than other stainless steels [1].

Given this two-phase microstructure, duplex stainless steels provide a mixture of the properties of each phase so that they are tougher than the ferritic steels and stronger than the (annealed) austenitic steels by a factor of about two. This implies that their compatibility with hydrogen also reflects a combination of the phases. Ferrite is highly susceptible to hydrogen-assisted fracture and has high diffusivity and low solubility for hydrogen. Austenite is generally much less susceptible to hydrogen-assisted fracture, but has a very high solubility and very low diffusivity for hydrogen. Consequently, the resistance to hydrogen-assisted fracture increases with austenite content [2]. A further consequence of the difference in transport of hydrogen in these two primary phases is that a fully ferritic steel recovers much of its ductility in a few days when removed from a hydrogen environment, while the presence of 15% austenite results in much less recovery after removal from a hydrogen environment [2]. No detectable recovery of ductility is noted in 2205 (35% austenite) thermally precharged with hydrogen then subsequently stored at ambient temperature for 3 years [2].

In general, duplex stainless steels with internal hydrogen experience significant losses in ductility as measured by reduction of area in smooth tensile tests [2-6]. Susceptibility to hydrogen-assisted fracture appears to be greater for material that has been strain-hardened compared to annealed material [6]. Ductility losses when tested in low-pressure hydrogen gas are less severe, although quite significant considering the hydrogen fugacity at low pressure. Effects of gaseous hydrogen on fracture are also manifest in notched specimens [7, 8] and fatigue [9, 10].

1.1 Composition and microstructure

Table 1.1.1 lists the approximate compositional specification ranges for a number of duplex alloys. Table 1.1.2 provides the compositions of several heats of duplex stainless steel used to study hydrogen effects. Table 1.1.3 summarizes the nominal tensile properties and austenite content of materials from several studies on hydrogen effects.

1.2 Common designations

Duplex stainless steels are often designated with four digits: the first two digits represent the weight percent of chromium, and the second two digits represent the weight percent of nickel; thus 2205 nominally has 22% Cr and 5% Ni. However, a number of duplex stainless steels have registered trademarks and tradenames associated with them such as Uranus 50, Zeron 100, and Ferralium 255. The more common alloys and their tradenames are summarized in Table 1.1.1.

2. Permeability, Diffusivity and Solubility

Hydrogen gas permeation experiments on duplex alloys have not been found in the literature. Perng and Altstetter, however, have performed gas phase permeation experiments on highly cold-worked type 301 and type 304 stainless steels that resulted in microstructures with large fractions of α' martensite [11]; martensite and ferrite are expected to have relatively similar hydrogen transport properties since both phases are body-centered cubic (while austenite is face-centered cubic). Their results show the diffusivity of the 301 austenite-martensite composite increases with content of martensite and approaches the value measured for a ferritic stainless steel at high concentrations of martensite. The permeability of the 301 composite is also generally between the fully austenitic alloys (low permeability) and the ferritic stainless steel (high permeability), except at the highest martensite contents where the permeability in the composite is greater than the ferritic stainless steel. The hydrogen solubility is the quotient of the permeability and the diffusivity, thus the hydrogen solubility of the composite material is again between the low solubility exhibited in the ferritic stainless steel and the high solubility in the austenitic alloys.

Electrochemical and off-gassing techniques have been used to determine the diffusivity of hydrogen atoms in duplex stainless steels. Because of the two-phase structure and, generally, anisotropic microstructure, hydrogen transport in duplex steels can be a function of orientation. Hutchings et al. [12, 13] found that hydrogen diffusivity in duplex stainless steel (heat H91) was greater when the hydrogen flux was parallel to the elongated grain structure, however, this effect was relatively modest: about a factor of two. They also report that the diffusivity is not strongly affected by austenite content (γ) in the range 44% to 15%, but the diffusivity increases rapidly as the material becomes fully ferritic. The ratio of diffusivity of the duplex alloy with no austenite and with 44% austenite is about 400 [13]. This trend is consistent with the inverse rule of mixtures reported for diffusivity by Iacoviello et al. [14] of the form

$$\frac{1}{D_{eff}} = \frac{\left(1 - f_\gamma\right)}{D_\alpha} + \frac{f_\gamma}{D_\gamma} \qquad (1)$$

This is a variant of the form proposed elsewhere [15], where f_γ is the volume fraction of austenite and D_{eff} is the effective diffusivity of the alloy and D_i is the diffusivity of the individual phases. Similar to orientation effects and the effects of austenite content, cold-work was found to have only a small effect on diffusivity of 2205 duplex stainless steel [16]. The diffusivity values reported in these and several other studies are given in Figure 2.1.

Degradation of tensile ductility due to precharging with hydrogen can be precluded if the materials are removed from the hydrogen environment and heated [3]. However, it may take an extraordinarily long time to recover properties without heating [2, 14]. Significant degradation in

tensile ductility was found to remain in thermally precharged 2205 (~35% austenite) after 55 days [3] and 3 years [2] at room temperature, but nearly full recovery of ductility was achieved by heating at 573 K for 4 hours [3]. As described above, the hydrogen diffusivity is relatively insensitive to phase distribution for expected ranges (γ content from 25 to 50% or greater), thus recovery of properties is not expected to be a strong function of the relative amounts of austenite and ferrite or their morphology.

The concentration of hydrogen in a 2205 duplex stainless steel with about 35% austenite content (heat Z91A) was found to be about 20 wppm after precharging in 22 MPa H_2 gas at 623 K for 48h [2, 5]. Thermal precharging at the same temperature but a slightly lower pressure (17 MPa) resulted in hydrogen content of 15 wppm [4]. These conditions are reported to be sufficient to reach uniform saturation in tensile bars with a gauge diameter of 3.2 mm [2, 4, 5].

3. Mechanical Properties: Effects of Gaseous Hydrogen

3.1 Tensile Properties

3.1.1 Smooth Tensile Properties

Room temperature testing of smooth tensile specimens with internal hydrogen (by thermal precharging in hydrogen gas) shows significant loss in ductility [2-5] as shown in Figure 3.1.1.1 as a function of strain rate. This plot shows the general trend that susceptibility to hydrogen-assisted fracture is enhanced at low strain rates due to more time for hydrogen redistribution to susceptible features in the microstructure. In addition, both annealed and strain-hardened 2507 show a significant degradation of tensile ductility: RA as low as 25% for the hydrogen-precharged material in the strain-hardened condition (Table 3.1.1.1) [6].

Smooth tensile specimens strained in hydrogen gas (external hydrogen) generally show (Figure 3.1.1.2) an increased susceptibility to hydrogen-assisted fracture as the hydrogen pressure is increased [3, 5]. Figure 3.1.1.3 compares the absolute RA for a single heat of 2205, showing that the ductility loss is a function of hydrogen pressure. The higher susceptibility to hydrogen-assisted fracture at low strain rate in these figures is attributed to the effect of deformation rate on both hydrogen transport and martensitic transformations [5]: more hydrogen can be transported in longer tests. The role of martensitic transformations on hydrogen-assisted fracture in austenitic steels has not been fully resolved, but it appears that martensitic transformations, while perhaps not necessary for degradation of stainless steels in hydrogen environments [17], certainly exacerbate hydrogen-assisted fracture when they form [18].

Although it is expected that orientation of the microstructure in duplex stainless steels could play an important role in hydrogen-assisted fracture, tensile testing of 2205 pipe with internal hydrogen shows little effect of orientation [4]. Tensile specimens tested in low-pressure external hydrogen, however, do show some effect of orientation [3-5]. Moreover, banded microstructures show larger variations with orientation than comparatively isotropic microstructures [4]. For testing in environmental hydrogen without significant prior hydrogen exposure, hydrogen must be transported from the surface of the specimen into the lattice. Since hydrogen diffusivity is much greater in ferrite compared to austenite, the morphology and orientation of the ferrite with respect to the cross section of the tensile specimen should play an important role on relatively short time scales, such as those associated with tensile tests. For example, ferrite bands that are oriented perpendicular to the tensile axis will be more effective at transporting hydrogen to the

center of a tensile specimen than ferrite bands that are aligned along the tensile axis. Moreover, orientation effects will probably become more important at lower ferrite content because ferrite will be less contiguous at lower volume fractions.

3.1.2 Notched Tensile Properties

Notched tensile foils of Ferralium 255 (heat P88) suffer a significant reduction in notch tensile strength and elongation to fracture when tested in 0.11 MPa hydrogen gas compared to testing in air at ambient temperature [7]. At temperature $\geq$ 373 K, there is no difference in properties measured in air and 0.11 MPa hydrogen gas [7].

3.2 Fracture mechanics

3.2.1 Fracture toughness

A significant reduction in the fracture toughness of thermally-precharged 2507 was reported for material in the strain-hardened condition (Table 3.2.1.1) [6]. Although a fracture toughness (K_{IC}) of 48 MPa $m^{1/2}$ in the thermally precharged condition is significantly lower than the material in the absence of thermal precharging, this value is consistent with threshold stress intensity factors measured for low-alloy steels [19] that are used in high-pressure hydrogen service.

3.2.2 Threshold stress-intensity factor

Altstetter et al. determined crack growth rates and threshold stress-intensity factors in notched sheet specimens of Ferralium 255 (heat P88) where plane stress conditions prevailed [7, 20]. Specimens were tested in up to 0.22 MPa hydrogen gas [7] and precharged to uniform concentration in molten salts at temperature of 538 K (i.e., internal hydrogen) [20]. These studies found that threshold values decreased as hydrogen pressure increased. The threshold values were also greater at elevated temperature for tests performed in hydrogen gas, particularly for tests at 348 K and 373 K [7].

Classic microvoid coalescence was observed on the fracture surfaces of precharged specimens at low hydrogen contents, while the amount of flat cleavage facets was greater for specimens with greater hydrogen content [20]. Threshold stress-intensity factors with internal hydrogen were relatively unaffected by testing temperature in the range 273 and 323 K [20].

3.3 Fatigue

Fatigue testing of a 2507 super duplex stainless steel (M92) in flowing hydrogen gas (i.e. hydrogen at approximately one atmosphere pressure) resulted in crack growth rates that are almost an order of magnitude higher than in argon for $\Delta K > 25$ MPa $m^{1/2}$ with R = 0.5 (ratio of minimum to maximum K and load) [10]. The crack growth rates, however, were similar for small stress intensity range (ΔK), less than about 15 MPa $m^{1/2}$ [10]. The upper and lower bounds of crack growth rates as a function of ΔK from Ref. [10] are shown in Figure 3.3.1. Crack growth rates also tended to be faster for greater R ratios although they become similar at $\Delta K >$ 30 MPa $m^{1/2}$ [10]. Fractography in this study showed that the ferrite failed by cleavage. A subsequent study [9] found that temperature in the range 298 K to 453 K had little effect on fatigue crack growth rates in flowing hydrogen.

3.4 Creep

No known published data in hydrogen gas.

3.5 Impact

No known published data in hydrogen gas.

3.6 Disk rupture testing

Disk rupture tests have been performed on duplex alloys referred to as 326 [21] and IN744 [22]; these alloys appear to be similar to one another with nominally 26Cr-7Ni and no molybdenum. Duplex stainless steel is classified as displaying little or no sensitivity to hydrogen in these studies and particularly attractive due to its high-strength [21]. This is at odds with the tensile and fracture mechanics data outlined in previous sections, perhaps due to the relative short-time scales associated with the disk rupture tests precluding substantial hydrogen transport in the lattice.

4. Fabrication

4.1 Primary processing

The resistance to hydrogen-assisted fracture of a 2205 duplex stainless steel (heat E96) was found to increase with austenite content in tensile testing in external hydrogen (0.2 MPa hydrogen gas) and with internal hydrogen (thermal precharging in 25 MPa hydrogen gas at 633 K) [2]. The observation that austenitic phases in duplex steels are more resistant to hydrogen-assisted fracture than ferritic phases is consistent with the view that austenitic stainless steels are relatively resistant to hydrogen-assisted fracture compared to ferritic steels [23].

4.2 Heat Treatment

Heat treatment was used to produce between about 5 and 50% austenite in duplex stainless steel 2205. The RA (both with internal and external hydrogen) was found to drop from greater than 50% to less than 20% as the amount of austenite was reduced (Figure 4.1.1) [2]. The trend for strain rate effects was similar for all microstructures (see Section 3.1.1). The effect of austenite content, however, must be balanced with the fact that the yield strengths of the microstructures with high austenite contents were somewhat lower (600 MPa compared to 750 MPa) than the microstructures with low austenite content (Table 1.1.3); hydrogen effects tend to be more pronounced in higher strength alloys.

4.3 Properties of welds

Laser welded notched tensile specimens from 2205 plate (heat Y05) were tested in 0.2 MPa gaseous hydrogen and reported in Ref. [8]. The austenite content in the weld was varied by controlling the welding process and it was found that material with higher austenite content showed greater resistance to hydrogen. The notched tensile strength (σ_s) of the base material (43% austenitic) was reduced by 9% when testing in hydrogen gas, while the σ_s of a weld with only 25% austenite was reduced by 28% in hydrogen gas.

Susceptibility to hydrogen-assisted fracture of duplex stainless steel increases markedly when the delta ferrite content is increased above 50% in weld deposits produced using an Ar-10 vol%

H_2 shielding gas [24]. Hydrogen-bearing shielding gases are used to improve weld pool fluidity and prevent surface oxidation, but hydrogen is entrapped in the microstructure during the welding process, increasing hydrogen susceptibility.

5. References

1. RA Lula. Stainless Steel (revised from "An Introduction to Stainless Steel" by JG Parr and A Hanson). Metals Park OH: American Society for Metals (1986).
2. AA El-Yazgi and D Hardie. Effect of heat treatment on susceptibility of duplex stainless steel to embrittlement by hydrogen. Mater Sci Technol 16 (2000) 506-510.
3. W Zheng and D Hardie. The effect of hydrogen on the fracture of a commercial duplex stainless steel. Corros Sci 32 (1991) 23-36.
4. W Zheng and D Hardie. Effect of structural orientation on the susceptibility of commercial duplex stainless steel to hydrogen embrittelement. Corrosion 47 (1991) 792-799.
5. AA El-Yazgi and D Hardie. The embrittlement of a duplex stainless steel by hydrogen in a variety of environments. Corros Sci 38 (1996) 735-744.
6. C San Marchi, BP Somerday, J Zelinski, X Tang and GH Schiroky. Mechanical properties of super duplex stainless steel 2507 after gas phase thermal precharging with hydrogen. Metall Mater Trans 38A (2007) 2763-2775.
7. T-P Perng and CJ Altstetter. Cracking Kinetics of Two-Phase Stainless Steel Alloys in Hydrogen Gas. Metall Trans 19A (1988) 145-152.
8. MC Young, SLI Chan, LW Tsay and CS Shin. Hydrogen-enhanced cracking of 2205 duplex stainless steel welds. Mater Chem Phys 91 (2005) 21-27.
9. TJ Marrow, PJ Cotterill and JE King. Temperature effects on the mechanism of time independent hydrogen assisted fatigue crack propagation in steels. Acta Metall Mater 40 (1992) 2059-2068.
10. TJ Marrow, CA Hippsley and JE King. Effect of mean stress on hydrogen assisted fatigue crack propagation in duplex stainless steel. Acta Metall Mater 39 (1991) 1367-1376.
11. T-P Perng and CJ Altstetter. Effects of Deformation on Hydrogen Permeation in Austenitic Stainless Steels. Acta Metall 34 (1986) 1771-1781.
12. RB Hutchings, A Turnbull and AT May. Measurement of hydrogen transport in a duplex stainless steel. Scr Metall Mater 25 (1991) 2657-2662.
13. A Turnbull and RB Hutchings. Analysis of hydrogen atom transport in a two-phase alloy. Mater Sci Eng A177 (1994) 161-171.
14. F Iacoviello, M Habashi and M Cavallini. Hydrogen embrittlement in the duplex stainless steel Z2CND2205 hydrogen-charged at 200˚C. Mater Sci Eng A224 (1997) 116-124.
15. U Bernabai and R Torella. Thermal analysis of hydrogen-charged austenitic and duplex stainless steel. Int J Hydrogen Energy 18 (1993) 763-771.
16. SS Chen, TI Wu and JK Wu. Effects of deformation on hydrogen degradation in a duplex stainless steel. J Mater Sci 39 (2004) 67-71.
17. AW Thompson. Ductility Losses in Austenitic Stainless Steels Caused by Hydrogen. in: IM Bernstein and AW Thompson, editors. Proceedings of the International Conference on the Effects of Hydrogen on Materials Properties and Selection and Structural Design: Hydrogen in Metals, 1973, Champion PA. American Society of Metals (1974) p. 91-105.
18. G Han, J He, S Fukuyama and K Yokogawa. Effect of strain-induced martensite on hydrogen environment embrittlement of sensitized austenitic stainless steels at low temperatures. Acta Mater 46 (1998) 4559-4570.

19. AW Loginow and EH Phelps. Steels for Seamless Hydrogen Pressure Vessels. Corrosion 31 (1975) 404-12.
20. J-H Huang and CJ Altstetter. Cracking of Duplex Stainless Steel Due to Dissolved Hydrogen. Metall Mater Trans 26A (1995) 1079-1085.
21. PF Azou and JP Fidelle. Very low strain rate hydrogen gas embrittlement (HGE) and fractography of high-strength, mainly austenitic stainless steels. in: MR Louthan, RP McNitt and RD Sisson, editors. Environmental Degradation of Engineering Materials III, 1987, The Pennsylvania State University, University Park PA. The Pennsylvania State University, University Park PA p. 189-198.
22. J-P Fidelle, R Bernardi, R Broudeur, C Roux and M Rapin. Disk Pressure Testing of Hydrogen Environment Embrittlement. in: Hydrogen Embrittlement Testing, ASTM STP 543, American Society for Testing and Materials. (1974) p. 221-253.
23. RJ Walter and WT Chandler. Influence of Gaseous Hydrogen on Metals: Final Report. Rocketdyne for the National Aeronautics and Space Administration, Canoga Park CA (Oct 1973).
24. K Shinozaki, L Ke and TH North. Hydrogen cracking in duplex stainless steel weld metal. Welding Journal 71 (1992) S387-S396.
25. ASTM. ASTM DS-56H, Metals and Alloys in the UNIFIED NUMBERING SYSTEM (SAE HS-1086 OCT01). 2001.
26. SL Chou and WT Tsai. Effect of grain size on the hydrogen-assisted cracking in duplex stainless steels. Mater Sci Eng A270 (1999) 219-224.
27. WC Luu, PK Liu and JK Wu. Hydrogen transport and degradation of a commercial duplex stainless steel. Corros Sci 44 (2002) 1783-1791.

Table 1.1.1. Compositions (wt%) of several common commercial duplex stainless steels [25].

UNS No	AISI No / Common Name	Fe	Cr	Ni	Mo	Cu	Mn	Si	C	N	other
S32101	LDX 2101	Bal	21.0 22.0	1.35 1.7	0.1 0.8	0.1 0.8	4.0 6.0	1.0 max	0.04 max	0.20 0.25	0.04 max P; 0.3 max S
S32205	2205	Bal	22.0 23.0	4.5 6.5	3.0 3.5	—	2.0 max	1.0 max	0.03 max	0.14 0.20	0.03 max P; 0.02 max S
S32304	2304	Bal	21.5 24.5	3.0 5.5	0.05 0.60	0.05 0.6	2.5 max	1.0 max	0.03 max	0.05 0.20	0.04 max P; 0.04 max S
S32404	Uranus 50 (Uranus B50)	Bal	20.5 22.5	5.5 8.5	2.0 3.0	1.0 2.0	2.0 max	1.0 max	0.04 max	0.2 max	0.03 max P; 0.01 max S
S32520	Uranus 52N+	Bal	24.0 26.0	5.5 8.0	3.0 4.0	0.5 2.0	1.5 max	0.8 max	0.03 max	0.20 0.35	0.035 max P; 0.02 max S
S32550	Ferralium 255	Bal	24.0 27.0	4.5 6.5	2.9 3.9	1.5 2.5	1.5 max	1.0 max	0.04 max	0.10 0.25	0.04 max P; 0.03 max S
S32750	SAF 2507	Bal	24.0 26.0	6.0 8.0	3.0 5.0	—	1.2 max	0.8 max	0.03 max	0.24 0.32	0.035 max P; 0.02 max S
S32760	Zeron 100	Bal	24.0 26.0	6.0 8.0	3.0 4.0	0.5 1.0	1.0 max	1.0 max	0.03 max	0.2 0.3	0.5-1.0 W; 0.03 max P; 0.01 max S
S32900	329	Bal	23.0 28.0	2.5 5.0	1.0 2.0	—	1.0 max	0.75 max	0.08 max	—	0.04 max P; 0.03 max S

Table 1.1.2. Compositions (wt%) of several heats of duplex stainless steels used to study hydrogen effects.

Heat	Alloy	Fe	Cr	Ni	Mo	Cu	Mn	Si	C	N	Other	Ref.
P88	Ferralium 255	Bal	26	5.5	3	1.6	nr	nr	nr	0.16	nr	[7]
H91	Uranus 50	Bal	21.6	6.3	2.51	0.77	0.63	0.87	0.06	nr	<0.01 P; 0.01 S	[12, 13]
M91	Zeron 100	Bal	24.04	6.827	3.77	0.626	0.77	0.175	0.024	0.215	0.025 P; 0.002 S; 0.625 W	[9, 10]
Z91A	2205	Bal	22.3	5.7	2.9	0.06	1.62	0.35	0.027	nr	0.021 P; <0.002 S	[4]
Z91B		Bal	22.9	5.2	3.12	0.03	0.99	0.5	0.016	nr	0.019 P; 0.002S	[3, 4]
E96	2205	Bal	23.0	5.0	3.0	nr	1.0	nr	nr	0.13	nr	[2, 5]
I97	Similar to 2205	Bal	22.78	5.64	2.5	0.15	1.43	0.39	0.03	0.13	0.028 P; 0.011 S	[14]
C99A	2205	Bal	22.15	5.28	3.11	—	1.58	0.53	0.024	0.19	0.028 P; 0.002 S	[26]
C99B		Bal	22.4	5.42	3.24	0.21	1.43	0.41	0.014	0.198	0.025 P; 0.004 S	
L02	2205	Bal	22.79	5.32	3	0.04	1.53	0.37	0.03	0.2	0.03 P; 0.03 S	[27]
Y05	2205	Bal	21.1	5.8	2.7	0.02	1.42	0.45	0.052	0.165	0.025 P; 0.022 S	[8]
S07	2507	Bal	25.22	6.94	3.9	nr	0.46	0.25	0.011	0.287	0.019 P; 0.0006 S	[6]

nr = not reported

Table 1.1.3. Austenite content and tensile properties of duplex stainless steels (prior to hydrogen exposure) used to study hydrogen effects.

Material	Austenite content (%)	Strain rate (s^{-1})	S_y (MPa)	S_u (MPa)	El_t (%)	RA (%)	Ref.
Z91A - L	37	10^{-4}	651	795	42	84	[4]
Z91A - T			634	785	41	74	
Z91B - L	35		620	740	36	85	
Z91B - T			600	710	39	83	
Z91B	35	—	577	766	36	87	[3]
E96	35	—	623	744	42	78	[5]
E96 - 50	50	3.7×10^{-6}	592	758	39.1	80.5	[2]
E96 - 15	15		704	807	30.6	64.7	
E96 - 0	0		743	844	19.9	51.7	

L = Longitudinal, T = Transverse

Table 3.1.1.1. Smooth tensile properties of duplex stainless steel at room temperature; measured in air with internal hydrogen (thermal precharging in hydrogen gas).

Material	Thermal precharging	Test environment	Strain rate (s^{-1})	S_y (MPa)	S_u (MPa)	El_u (%)	El_t (%)	RA (%)	Ref.
2507, heat S07 annealed	None	Air	1.2×10^{-3}	647	879	25	48	85	[6]
	(1)	Air		745	914	24	35	46	
2507, heat S07 strain-hardened	None	Air	1.2×10^{-3}	988	1110	1.2	26	80	[6]
	(1)	Air		1208	1221	1.0	12	25	

(1) 138 MPa hydrogen, 573 K, 240 h (saturation); measured average concentration of 125 wppm hydrogen (7000 appm)

Table 3.2.1.1. Fracture toughness of duplex stainless steel at room temperature; measured in air with internal hydrogen (thermal precharging in hydrogen gas).

Material	Test method	Thermal precharging	Test environment	S_y † (MPa)	K_{IC} (MPa $m^{1/2}$)	Ref.
2507, heat S07 strain-hardened	3PB LEFM & EPFM	None	Air	988	285 ‡	[6]
		(1)	Air	1208	48	

3PB = 3-point bending specimen, LEFM = linear elastic fracture mechanics, EPFM = elastic-plastic fracture mechanics

† yield strength of smooth tensile specimen

‡ value determined from J_Q (i.e. specimen did not meet the geometrical requirements of ASTM E1820 for K_{IC} or J_{IC})

(1) 138 MPa hydrogen, 573 K, 1440 h (saturation); measured average concentration of 125 wppm hydrogen (7000 appm)

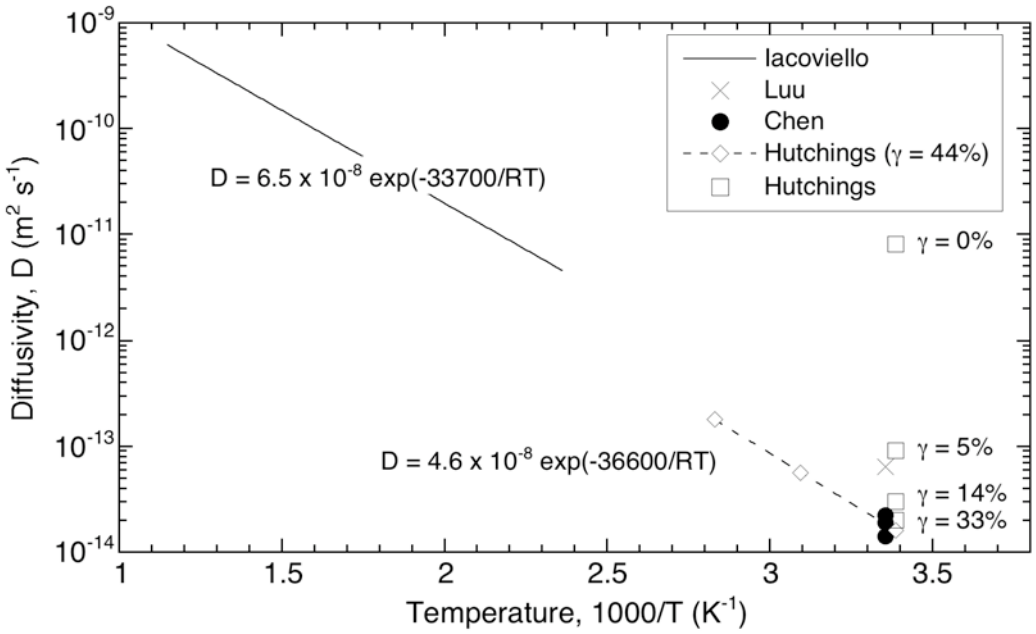

Figure 2.1. Hydrogen diffusivity as a function of temperature for several duplex alloys: Iacoviello, heat I97 [14]; Luu, heat L02 [27]; Chen, heat L02, values for annealed, cold-worked 20% and 40% respectively in increasing order of diffusivity [16]; Hutchings, heat H91 [12, 13].

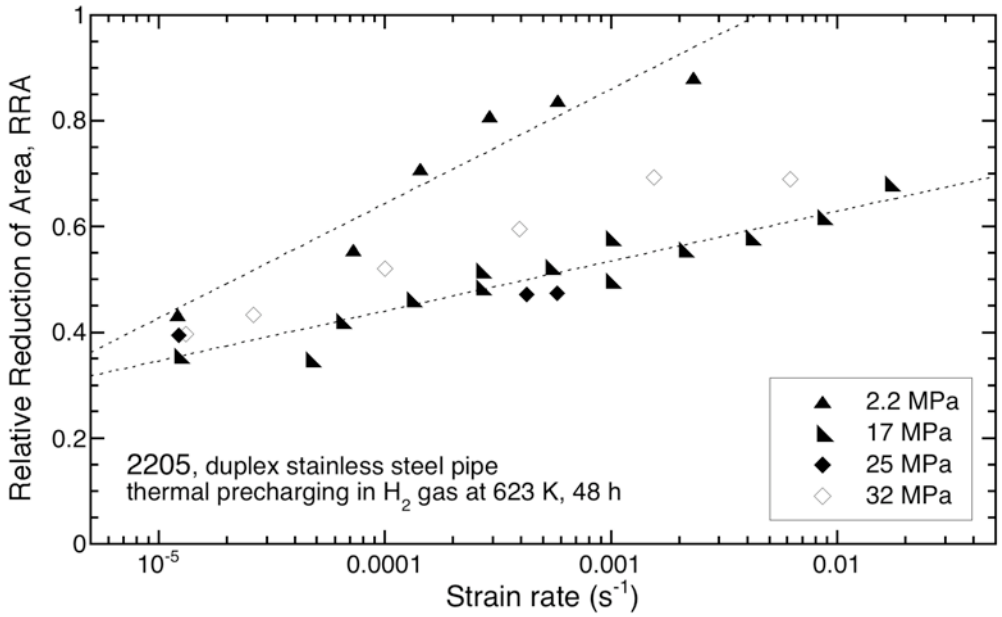

Figure 3.1.1.1. Relative reduction of area of 2205 duplex stainless steel as a function of strain rate in smooth tensile tests. The material has been thermally precharged with hydrogen at 623 K and several hydrogen gas pressures: closed symbols heat Z91B from Ref. [3]; open symbols heat E96 from Ref. [5].

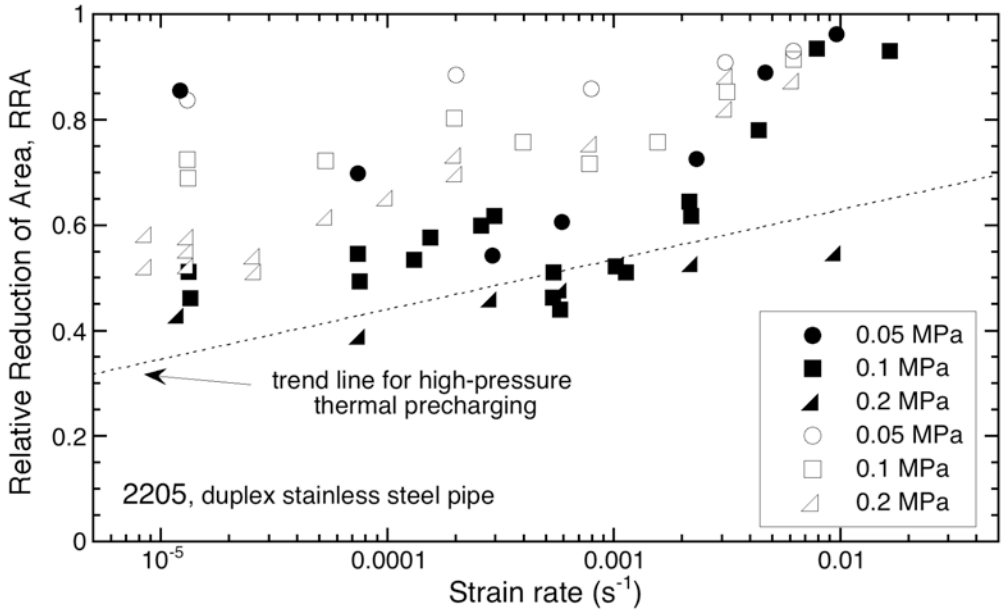

Figure 3.1.1.2. Relative reduction of area for 2205 duplex stainless steel as a function of strain rate in smooth tensile tests. Tests were conducted in hydrogen gas at room temperature and several hydrogen gas pressures: closed symbols heat Z91B from Ref. [3]; open symbols heat E96 from Ref. [5]. Trend line from Figure 3.1.1.1.

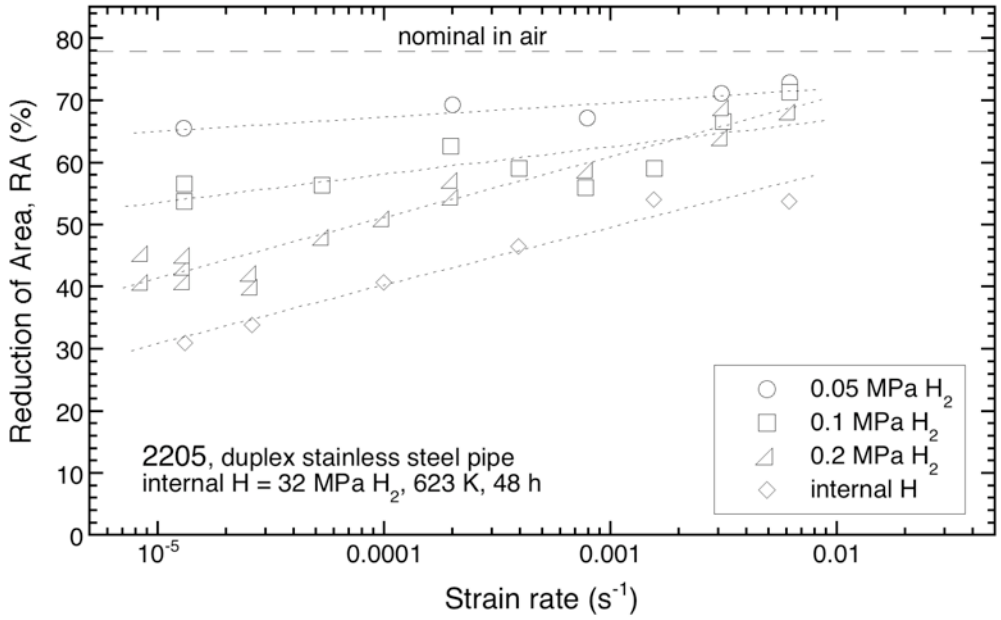

Figure 3.1.1.3. Reduction of area for 2205 duplex stainless steel (heat E96) as a function of strain rate in smooth tensile tests comparing internal and external hydrogen. Same data as from Figure 3.1.1.1 and 3.1.1.2. [5]

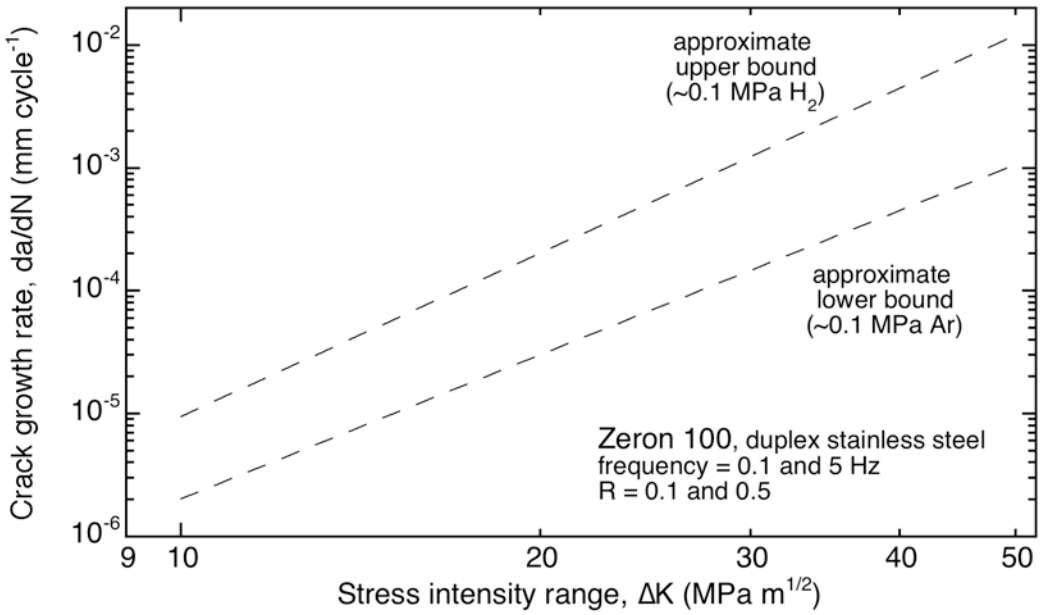

Figure 3.3.1. Approximate bounds for crack growth of compact tension specimens (heat M91) in approximately 0.1 MPa gas, R = 0.5. Crack growth rates are independent of frequency at 0.1 and 5 Hz. The crack growth rate is intermediate between these bounds for R = 0.1 in hydrogen at low ΔK, but converges to the upper bound at high ΔK. [10]

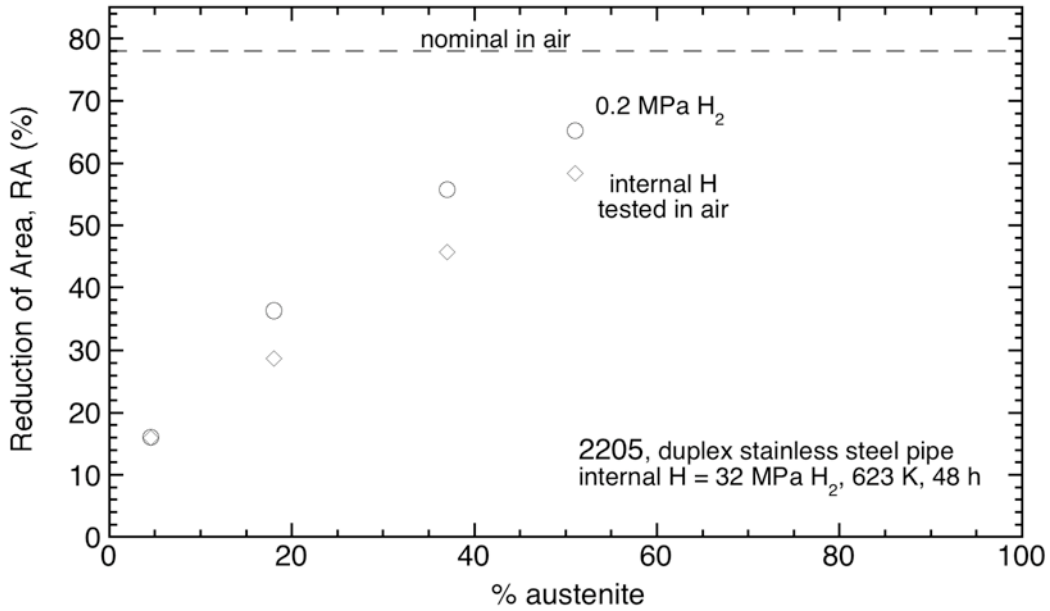

Figure 4.1.1. Reduction of area for 2205 duplex stainless steel (heat E96) as a function of austenite content with internal hydrogen and in external hydrogen. [2]

Technical Reference on Hydrogen Compatibility of Materials

High-Alloy Ferritic Steels:

Semi-Austenitic Stainless Steels (code 1700)

1. General

The semi-austenitic stainless steels are precipitation-strengthened alloys that can be heat treated to a range of mechanical properties [1, 2]. These alloys are used for their combination of high strength, high toughness, and corrosion resistance. Alloy 17-7PH is commonly used as a spring material to temperatures as high as 590 K [3]. Semi-austenitic stainless steels, however, have low fracture toughness in high strength conditions and at low (subzero) temperature.

In general, very little data exist for these alloys in gaseous hydrogen; however, the available data indicate that the fracture resistance of semi-austenitic stainless steels is very sensitive to gaseous hydrogen [4], a characteristic that is common to high-strength alloys. The data from notched tensile tests indicate that this class of alloys has essentially no resistance to fracture in hydrogen environments [4]. Indeed, the semi-austenitic stainless steels appear to be among the families of alloys that are most susceptible to hydrogen-assisted fracture. Based on the available data, these alloys are not recommended for stress-bearing components in hydrogen gas.

1.1 Composition and microstructure

The semi-austenitic stainless steels are variants of common austenitic stainless steels (the so-called 18-8 class) with additions of alloying elements not generally associated with the austenitic alloys, such as aluminum. Table 1.1.1 lists the approximate composition specification ranges for several common semi-austenitic stainless steels. Table 1.1.2 provides the composition of a semi-austenitic stainless steel used to study hydrogen-assisted fracture.

1.2 Common designations

Tradenames are commonly used for these alloys. Common names include 17-7PH (AISI Type 631), PH15-7Mo (AISI Type 632), AM-350 (AISI Type 633), AM-355 (AISI Type 634) and PH14-8Mo. The alloy designation 17-7PH refers to the nominal chromium and nickel contents (in wt %), with the addition of “PH” to indicate its status as a precipitation-hardening composition. The designation of “Mo” indicates alloying additions of molybdenum (usually about 2.5 wt%).

2. Permeability, Diffusivity and Solubility

Hydrogen permeation and diffusion data are unavailable for this class of alloys. Based on the studies of martensitic precipitation-strengthened stainless steels [5, 6], the effective hydrogen diffusivity is expected ~10^{-12} m^2/s.

3. Mechanical Properties: Effects of Gaseous Hydrogen

3.1 Tensile properties

3.1.1 Smooth tensile properties

The data in Table 3.1.1.1 show that the ductility of 17-7PH is significantly degraded when tested in high-pressure hydrogen, i.e., hydrogen reduces the ductility by 95%. This reduction in ductility is among the most severe reported for any alloy tested in hydrogen gas. Alloy AM-350 also shows severe ductility loss in the solution annealed condition [7]; degradation is expected to be more severe in high-strength conditions.

3.1.2 Notched tensile properties

The data in Table 3.1.2.1 show that the notched tensile strength of 17-7PH is extremely degraded when tested in high-pressure hydrogen. It has also been shown that partial pressures of hydrogen less than an atmosphere can significantly reduce the notched tensile strength of 17-7PH [4].

3.2 Fracture mechanics

No known published data in hydrogen gas.

3.3 Fatigue

No known published data in hydrogen gas.

3.4 Creep

No known published data in hydrogen gas.

3.5 Impact

No known published data in hydrogen gas.

3.6 Disk rupture testing

Disk rupture tests show that the fracture resistance of semi-austenitic stainless steels (AM-355) and martensitic stainless steels (17-4PH and PH13-8Mo) is extremely sensitive to gaseous hydrogen [8].

4. Fabrication

4.1 Primary processing

Compositional control is very important with these alloys [1], thus they are often produced by premium remelting processes such as vacuum-arc remelting (VAR) and electroslag remelting (ESR).

4.2 Heat treatment

These alloys typically employ complicated precipitation-strengthening treatments; more information can be found in manufacturer's data sheets and general references.

4.3 Properties of welds

The semi-austenitic stainless steels can be welded [1], although the weld properties will typically be inferior to the base metal. See also manufacturer's specifications and data sheets.

5. References

1. D Peckner and IM Bernstein. Handbook of Stainless Steels. New York: McGraw-Hill (1977).
2. RA Lula. Stainless Steel (revised from "An Introduction to Stainless Steel" by JG Parr and A Hanson). Metals Park OH: American Society for Metals (1986).
3. JR Kattus. Age Hardening Steels: Fe-17Cr-7Ni-1Al (code 1502). in: WF Brown, H Mindlin and CY Ho, editors. Aerospace Structural Metals Handbook. 2. CINDAS/UASF CRDA Handbooks Operation, Purdue University (1992).
4. RJ Walter and WT Chandler. Effects of High-Pressure Hydrogen on Metals at Ambient Temperature: Final Report. Rocketdyne (report no. R-7780-1) for the National Aeronautics and Space Administration, Canoga Park CA (February 1969).
5. LW Tsay, WC Lee, RK Shiue and JK Wu. Notch tensile properties of laser-surface-annealed 17-4 PH stainless steel in hydrogen-related environments. Corros Sci 44 (2002) 2101-2118.
6. WC Chiang, CC Pu, BL Yu and JK Wu. Hydrogen susceptibility of 17-4 PH stainless steel. Mater Lett 57 (2003) 2485-2488.
7. GR Caskey. Hydrogen Compatibility Handbook for Stainless Steels (DP-1643). EI du Pont Nemours, Savannah River Laboratory, Aiken SC (June 1983).
8. J-P Fidelle. Present status of the disk pressure test for hydrogen embrittlement. in: L Raymond, editor. Test Methods for Hydrogen Embrittlement: Prevention and Control, ASTM STP 962, American Society for Testing and Materials. (1988) p. 153-172.
9. ASTM DS-56H, Metals and Alloys in the UNIFIED NUMBERING SYSTEM (SAE HS-1086 OCT01). American Society for Testing and Materials (Society of Automotive Engineers) (2001).

Table 1.1.1. Compositions (wt%) of several common semi-austenitic (precipitation-strengthened) stainless steels [9].

UNS No	Common Name (AISI No)	Fe	Cr	Ni	Mo	Al	Mn	Si	C	other
S17700	17-7PH (Type 631)	Bal	16.00 18.00	6.50 7.75	—	0.75 1.50	1.00 max	1.00 max	0.09 max	0.040 max P; 0.040 max S
S15700	PH15-7Mo (Type 632)	Bal	14.00 16.00	6.50 7.75	2.00 3.00	0.75 1.50	1.00 max	1.00 max	0.09 max	0.04 max P; 0.03 max S
S14800	PH14-8Mo	Bal	13.75 15.00	7.75 8.75	2.00 3.00	0.75 1.50	1.00 max	1.00 max	0.05 max	0.015 max P; 0.010 max S
S35000	AM-350 (Type 633)	Bal	16.00 17.00	4.00 5.00	2.50 3.25	—	0.50 1.25	0.50 max	0.07 0.11	0.07-0.13 N; 0.040 max P; 0.030 max S
S35500	AM-355 (Type 634)	Bal	15.00 16.00	4.00 5.00	2.50 3.25	—	0.50 1.25	0.50 max	0.10 0.15	0.07-0.13 N; 0.040 max P; 0.030 max S

Table 1.1.2. Compositions (wt%) of semi-austenitic stainless steel used to study the effects of hydrogen on mechanical properties.

Heat	Alloy	Fe	Cr	Ni	Mo	Al	Mn	Si	C	Other	Ref.
W69	17-7PH	Bal	17.29	7.10	nr	0.9	0.68	0.64	0.072	0.028 P; 0.005 S	[4]

nr = not reported

Table 3.1.1.1. Smooth tensile properties of semi-austenitic stainless steel at room temperature; measured in external hydrogen gas or with internal gas.

Material	Thermal precharging	Test environment	Strain rate (s^{-1})	S_y (MPa)	S_u (MPa)	El_u (%)	El_t (%)	RA (%)	Ref.
17-7PH ‡ (heat W69)	None	air	0.67 x10^{-3}	1124	1200	—	17	45	[4]
	None	69 MPa H_2		—	1041	—	1.7	2.5	
AM-350, SA	None	air	—	420	1160	—	70	—	[7]
	None	69 MPa He		420	1240	—	55	—	
	None	0.69 MPa D_2		410	455	—	3	—	
	None	6.9 MPa D_2		345	430	—	4	—	
	None	69 MPa D_2		430	520	—	2.6	—	
	(1)	air		455	580	—	3/4	—	

SA = solution annealed (1330K)
‡ condition TH1050
(1) 69 MPa deuterium gas, 570 K, 625 h

Table 3.1.2.1. Notched tensile properties of semi-austenitic stainless steel at room temperature; measured in external hydrogen gas.

Material	Specimen	Thermal precharging	Test environment	Displ. rate (mm/s)	S_y † (MPa)	σ_s (MPa)	RA (%)	Ref.
17-7PH ‡ (heat W69)	(a)	None	Air	~0.35 x10^{-3}	1124	2151	0.6	[4]
		None	69 MPa H_2		—	483	0.4	

† yield strength of smooth tensile specimen
‡ condition TH1050
(a) V-notched specimen: 60˚ included angle; minimum diameter = 3.81 mm; maximum diameter = 7.77 mm; notch root radius = 0.024 mm. Stress concentration factor (K_t) = 8.4.

This page intentionally left blank.

Technical Reference on Hydrogen Compatibility of Materials

High-Alloy Ferritic Steels:

Martensitic Stainless Steels

Precipitation Hardening (Fe-Cr-Ni type) (code 1810)

1. General

The Fe-Cr-Ni martensitic stainless steels are precipitation-strengthened alloys that can be heat treated to a range of mechanical properties. These alloys are used for their combination of high strength, high toughness, and corrosion resistance, as well as their ability to maintain strength to somewhat elevated temperature (up to about 573 K). However, martensitic stainless steels suffer a loss in toughness at low (subzero) temperature. Additional details are available in standard references on stainless steels (e.g., Refs. [1, 2]), and from manufacturers' data sheets.

The available data indicate that Fe-Cr-Ni, precipitation-strengthened martensitic stainless steels are very sensitive to hydrogen-assisted fracture, a common characteristic of high-strength alloys, and this degradation of properties increases with increasing strength of the material. Solution annealed materials appear to be much less sensitive to hydrogen-assisted fracture, although no tests have been performed in high-pressure hydrogen gas. In general, very little data exist for these alloys in gaseous hydrogen, thus a few representative reports are cited here that present data from tests performed with electrolytic precharging.

Based on the available data, this family of alloys is not recommended for service in hydrogen environments.

1.1 Composition and microstructure

The Fe-Cr-Ni martensitic stainless steels have lower nickel contents than the semi-austenitic stainless steels with additions of alloying agents not generally associated with the (non-precipitation strengthened) austenitic alloys, such as aluminum, copper, niobium and titanium. Table 1.1.1 lists the compositional specification ranges for several common Fe-Cr-Ni martensitic stainless steels.

1.2 Common designations

Tradenames are commonly used for these alloys. Some of the common alloys are referred to by the chromium and nickel content, such as 17-4 PH (AISI type 630) and 15-5 PH (ASTM XM-12), the designation "PH" indicates its status as a precipitation-hardening composition. The Custom 4xx alloys represent another family of tradenames from this class of alloys. Stainless W (AISI type 635) is common precipitation-strengthened martensitic stainless steel.

2. Permeability, Diffusivity and Solubility

We are unaware of any permeation and diffusion measurements for this class of materials exposed to gaseous hydrogen; however, hydrogen diffusion has been measured by

electrochemical methods. The effective diffusivity is given in Table 2.1 as determined from several electrochemical studies. The effective hydrogen diffusivity in these materials is several orders of magnitude greater than the austenitic stainless steels.

3. Mechanical Properties: Effects of Gaseous Hydrogen

3.1 Tensile properties

3.1.1 Smooth tensile properties

Hydrogen precharging of 17-4 PH in 13.8 MPa hydrogen gas at 475 K for 24 hours resulted in significant loss of reduction of area for smooth tensile specimens tested in air for the solution annealed (SA) and precipitation-strengthened (H900) conditions [3].

In addition, there are data from electrochemically precharged materials for a variety of alloys from this family. These studies indicate modest changes in properties in the solution annealed condition [4, 5], and significant degradation of strength and ductility in the precipitation-strengthened conditions [3-6].

3.1.2 Notched tensile properties

The notched tensile strength of solution-annealed and precipitation-hardened 17-4 PH was not affected by testing in 2 atmospheres of hydrogen gas [7]. However, evaluation of the fracture surfaces indicated a change in fracture mode [7], which suggests that notched tensile strength may not be an adequate metric for hydrogen-assisted fracture at lower gas pressures. The notched tensile strength is likely degraded in high fugacity hydrogen.

3.2 Fracture mechanics

The fracture toughness of 17-4PH martensitic stainless steel is substantially reduced when tested in hydrogen gas, Table 3.2.1. The fracture toughness is reduced by more than 50% for the solution-annealed condition in 69 MPa hydrogen gas, and this reduction increases with strength to almost 90% for the peak-aged condition [8]. These data also show that the susceptibility to hydrogen-assisted fracture increases with gas pressure.

3.3 Fatigue

Crack growth rates in 17-4 PH were significantly increased in 2 atmospheres of hydrogen gas [9]. Fracture surfaces from these fatigue specimens show less plasticity in the fracture process compared to tests in air.

3.4 Creep

No known published data in hydrogen gas.

3.5 Impact

No known published data in hydrogen gas.

3.6 Disk rupture testing

Disk rupture tests show that martensitic stainless steels (such as 17-4PH and PH13-8Mo) are extremely sensitive to hydrogen-assisted fracture in gaseous environments [10].

4. Fabrication

Precipitation-hardening martensitic stainless steels have considerable variation in alloy composition and are available in a range of product forms; nevertheless, the limited data suggest that this class of stainless steels is very susceptible to hydrogen-assisted fracture both prior to and after aging.

4.1 Primary processing

Forming and machining operations are generally performed in the solution-annealed (SA) condition, which disrupts the oxide that forms during solution annealing in air. It has been suggested in the literature that solution-annealing finished parts of 17-4 PH prior to precipitation hardening results in a uniform oxide that prevents hydrogen uptake during electrochemical precharging [3]. This study also proposes extended precipitation-strengthening heat treatments in oxygen to achieve a robust and continuous oxide. The kinetics of hydrogen transport through the oxides on these alloys has not been reported.

4.2 Heat treatment

The material is typically distributed in the solution annealed condition (SA) and heat treated to the desired properties. Heat treatments are most commonly designated by the letter “H” and temperature in degrees Fahrenheit, such that H900 indicates precipitation strengthening at 900˚F (755 K).

4.3 Properties of welds

The martensitic stainless steels are readily weldable with filler wire that matches the base material, although austenitic stainless steel (300-series) filler wire can be used to produce joints with lower strength then the base material [1].

5. References

1. D Peckner and IM Bernstein. Handbook of Stainless Steels. New York: McGraw-Hill (1977).
2. RA Lula. Stainless Steel (revised from "An Introduction to Stainless Steel" by JG Parr and A Hanson). Metals Park OH: American Society for Metals (1986).
3. GT Murray, JP Bouffard and D Briggs. Retardation of hydrogen embrittlement of 17-4 PH stainless steels by nonmetallic surface layers. Metall Trans 18A (1987) 162-164.
4. F El Hilali, M Habashi and A Mohsine. Comportement mecanique de l'acier inoxydable martensitique 17-4 PH en corrosion sous contrainte et a la fragilisation par l'hydrogene environmetal. Ann Chim Sci Mat 24 (1999) 169-194.
5. WC Chiang, CC Pu, BL Yu and JK Wu. Hydrogen susceptibility of 17-4 PH stainless steel. Mater Lett 57 (2003) 2485-2488.

6. GT Murray. Hydrogen embrittlement of 15-5 PH stainless steels. Metall Trans 12A (1981) 2138-2141.
7. LW Tsay, WC Lee, RK Shiue and JK Wu. Notch tensile properties of laser-surface-annealed 17-4 PH stainless steel in hydrogen-related environments. Corros Sci 44 (2002) 2101-2118.
8. GR Caskey. Hydrogen Compatibility Handbook for Stainless Steels (DP-1643). EI du Pont Nemours, Savannah River Laboratory, Aiken SC (June 1983).
9. LW Tsay, TY Yang and MC Young. Embrittlement of laser surface-annealed 17-4 PH stainless steel. Mater Sci Eng A311 (2001) 64-73.
10. J-P Fidelle. Present status of the disk pressure test for hydrogen embrittlement. in: L Raymond, editor. Test Methods for Hydrogen Embrittlement: Prevention and Control, ASTM STP 962, American Society for Testing and Materials. (1988) p. 153-172.
11. ASTM DS-56H, Metals and Alloys in the UNIFIED NUMBERING SYSTEM (SAE HS-1086 OCT01). American Society for Testing and Materials (Society of Automotive Engineers) (2001).

Table 1.1.1. Compositions (wt%) of several common commercial precipitation-strengthened martensitic stainless steels of the Fe-Cr-Ni type [11].

UNS No	Common Name (AISI/ASTM)	Fe	Cr	Ni	Mo	Cu	Al	Nb	Ti	Mn	Si	C	other
S17400	17-4 PH (Type 630)	Bal	15.0 17.5	3.00 5.00	—	3.00 5.00	—	0.15 0.45	—	1.00 max	1.00 max	0.07 Max	0.040 max P; 0.030 max S
S15500	15-5 PH (XM-12)	Bal	14.00 15.50	3.50 5.50	—	2.50 4.50	—	0.15 0.45	—	1.00 max	1.0 max	0.07 max	0.040 max P; 0.030 max S
S13800	PH 13-8 Mo (XM-13)	Bal	12.25 13.25	7.50 8.50	2.00 2.50	—	0.90 1.35	—	—	0.20 max	0.10 max	0.05 max	0.01 max N; 0.01 max P; 0.008 max S
S45500	Custom 455 (XM-16)	Bal	11.00 12.50	7.50 9.50	0.50 max	1.50 2.50	—	0.10 0.50	0.80 1.40	0.50 max	0.50 max	0.05 max	0.040 max P; 0.030 max S

Table 2.1. Hydrogen diffusivity in precipitation-strengthened martensitic stainless steels (Fe-Cr-Ni type) at room temperature.

Material	Condition‡	Method	Diffusivity (m^2/s)	Ref.
17-4 PH	SA	Electrochemical	0.46×10^{-12}†	[5]
	H900		0.28×10^{-12}†	
17-4 PH	SA	Electrochemical	2.74×10^{-12}†	[7]
	H900		0.97×10^{-12}†	
	H1025		0.81×10^{-12}†	

‡ SA = solution annealed; H900 = aged at 755 K; H1050 = aged at 839 K

† effective diffusivity (D_{eff})

Table 3.2.1. Fracture toughness of precipitation-strengthened martensitic stainless steels (Fe-Cr-Ni type) at room temperature; measured in external hydrogen gas.

Material	Test method	Thermal precharging	Test environment	S_y (MPa)	K_Q ‡ (MPa)	Ref.
17-4PH SA	C-specimen	None	69 MPa He	(28)†	97	[8]
		None	3.5 MPa H_2		71	
		None	69 MPa H_2		31	
17-4PH H817	C-specimen	None	69 MPa He	(38)†	104	[8]
		None	3.5 MPa H_2		31	
		None	69 MPa H_2		20	
17-4PH H950	C-specimen	None	69 MPa He	(42)†	97	[8]
		None	3.5 MPa H_2		29	
		None	69 MPa H_2		13	
17-4PH H1100	C-specimen	None	69 MPa He	(35)†	—	[8]
		None	3.5 MPa H_2		57	
		None	69 MPa H_2		34	

SA = solution annealed (1339 K, 2 h); H817 = underaged (SA + 719 K, 1h); H950 = peak aged (SA + 783 K, 1 h); H1100 = overaged (SA + 866 K, 1 h)

† Rockwell hardness, scale C

‡ not clear if plane strain requirements are met in these studies

Technical Reference on Hydrogen Compatibility of Materials

High-Alloy Ferritic Steels:

Martensitic Stainless Steels

Heat Treatable (Fe-Cr type) (code 1820)

1. General

The martensitic stainless steels with low nickel are hardenable by heat treatment to a range of mechanical properties. These alloys are used for their combination of high strength and corrosion resistance [1]. The heat treatment process used to attain high strength in the Fe-Cr type stainless steels involves quenching and tempering.

In general, very little data exists for these alloys in gaseous hydrogen; however, the available data indicate that martensitic stainless steels are susceptible to hydrogen-assisted fracture in gaseous hydrogen, a characteristic common to high-strength alloys. The data from notched tensile tests indicate that this class of alloys is extremely susceptible to fracture in hydrogen environments. Indeed, the Fe-Cr martensitic stainless steels are among the families of alloys that are most susceptible to hydrogen-assisted fracture. Based on the available data, these alloys must be used with caution as structural materials in hydrogen gas service.

1.1 Composition and microstructure

The Fe-Cr martensitic stainless steels are distinguished from the precipitation-hardening, martensitic stainless steels by the lack of nickel as an alloying constituent. The Fe-Cr martensitic stainless steels fall into two categories: low carbon and high carbon. Table 1.1.1 lists the approximate composition specification ranges for several common Fe-Cr martensitic stainless steels. Table 1.1.2 provides the compositions of several heats of martensitic stainless steels used to study the effects of hydrogen on mechanical properties.

1.2 Common designations

The Fe-Cr martensitic stainless steels are typically referred to by their AISI designation: type 400-series alloys. The 400-series also consist of a number of non-hardenable varieties, commonly referred to as the ferritic stainless steels (which are not included in this section). There are also a group of similar alloys developed specifically for fusion reactor applications, such as MANET; these are not included.

2. Permeability, Diffusivity and Solubility

We are unaware of any permeation measurements for this class of materials exposed to gaseous hydrogen. Based on electrochemical measurements of effective diffusivity in the precipitation-hardening, martensitic stainless steels, we might expect hydrogren diffusivity to be intermediate between low-alloy steels and austenitic stainless steels: on the order of 10^{-12} m^2/s.

3. Mechanical Properties: Effects of Gaseous Hydrogen

3.1 Tensile properties

3.1.1 Smooth tensile properties

The data in Table 3.1.1.1 show that the ductility of type 410 and type 440C alloys is significantly degraded when tested in high-pressure hydrogen. Hydrogen-precharged type 440C in a low-strength condition also experiences reduced elongation at both room temperature and low temperature (200 K) [2].

3.1.2 Notched tensile properties

The data in Table 3.1.2.1 show that the notched tensile strength of type 410 and type 440C martensitic stainless steels is extremely degraded when tested in high-pressure hydrogen. It has also been shown that partial pressures of hydrogen less than an atmosphere can significantly reduce the notched tensile strength of type 410 [3].

3.2 Fracture mechanics

No known published data in hydrogen gas.

3.3 Fatigue

No known published data in hydrogen gas.

3.4 Creep

No known published data in hydrogen gas.

3.5 Impact

No known published data in hydrogen gas.

3.6 Disk rupture testing

Disk rupture tests show that type 410 stainless steel is extremely sensitive to fracture in hydrogen gas [4].

4. Fabrication

The Fe-Cr martensitic stainless steels are available in a range of product forms and a variety of compositions; however, the limited evidence suggests that 400-series alloys are generally susceptible to hydrogen-assisted fracture.

5. References

1. RA Lula. Stainless Steel (revised from "An Introduction to Stainless Steel" by JG Parr and A Hanson). Metals Park OH: American Society for Metals (1986).
2. GR Caskey. Hydrogen Compatibility Handbook for Stainless Steels (DP-1643). EI du Pont Nemours, Savannah River Laboratory, Aiken SC (June 1983).

3. RJ Walter and WT Chandler. Effects of High-Pressure Hydrogen on Metals at Ambient Temperature: Final Report. Rocketdyne (report no. R-7780-1) for the National Aeronautics and Space Administration, Canoga Park CA (February 1969).
4. J-P Fidelle, R Bernardi, R Broudeur, C Roux and M Rapin. Disk Pressure Testing of Hydrogen Environment Embrittlement. in: Hydrogen Embrittlement Testing, ASTM STP 543, American Society for Testing and Materials. (1974) p. 221-253.
5. ASTM DS-56H, Metals and Alloys in the UNIFIED NUMBERING SYSTEM (SAE HS-1086 OCT01). American Society for Testing and Materials (Society of Automotive Engineers) (2001).
6. RP Jewitt, RJ Walter, WT Chandler and RP Frohmberg. Hydrogen Environment Embrittlement of Metals. Rocketdyne for the National Aeronautics and Space Administration, Canoga Park CA (March 1973).

Table 1.1.1. Compositions (wt%) of several Fe-Cr martensitic stainless steels [5].

UNS no.	AISI no. / common name	Fe	Cr	Mn	Si	C	Other
S41000	410	Bal	11.50 13.50	1.00 max	1.00 max	0.15 max	0.040 max P; 0.030 max S
S42000	420	Bal	12.00 14.00	1.00 max	1.00 max	>0.15	0.040 max P; 0.030 max S
S44004	440C	Bal	16.00 18.00	1.00 max	1.00 max	0.95 1.20	0.75 max Mo; 0.040 max P; 0.030 max S

Table 1.1.2. Compositions (wt%) of several heats of Fe-Cr martensitic stainless steels used to study hydrogen effects on mechanical properties.

Heat	Alloy	Fe	Cr	Mn	Si	C	Other	Ref.
W69-410	410	Bal	12.26	0.71	0.60	0.145	0.016 P; 0.007 S; 0.40 Ni; 0.08 Mo; 0.11 Cu; 0.02 Al	[3]
W69-440C	440C	Bal	17.33	0.48	0.33	0.96	0.013 P; 0.024 S; 0.36 Ni; 0.48 Mo	[3]

Table 3.1.1.1. Smooth tensile properties of martensitic stainless steels at room temperature; measured with internal hydrogen or in external hydrogen gas.

Material	Thermal precharging	Test environment	Strain rate (s^{-1})	S_y (MPa)	S_u (MPa)	El_u (%)	El_t (%)	RA (%)	Ref.
410 (heat W69-410)	None	air	0.67 x10^{-3}	1324	1524	—	15	60	[3, 6]
	None	69 MPa H_2		—	1144	—	1.3	12	
440C (heat W69-440C)	None	air	0.67 x10^{-3}	1627	2075	—	3.5	3.1	[3, 6]
	None	69 MPa H_2		—	820	—	—	0	
440C	None	air	—	377	620	—	7.1	—	[2]
	(1)	air		377	575	—	4.6	—	
	None	air, 200 K		406	670	—	7.7	—	
	(1)	air, 200 K		450	570	—	4.2	—	

(1) 69 MPa deuterium, 620 K, 500 h (gauge diameter ~ 5 mm)

Table 3.1.2.1. Notched tensile properties of martensitic stainless steels at room temperature; measured in external hydrogen gas.

Material	Specimen	Thermal precharging	Test environment	Displ. rate (mm/s)	S_y † (MPa)	σ_s (MPa)	RA (%)	Ref.
410 (heat W69-410)	(a)	None	air	~0.35 x10^{-3}	1324	2730	1.4	[3, 6]
		None	69 MPa H_2		—	565	0.6	
440C (heat W69-440C)	(a)	None	air	~0.35 x10^{-3}	1627	1027	0.6	[3, 6]
		None	69 MPa H_2		—	510	0	

† yield strength of smooth tensile specimen

(a) V-notched specimen: 60˚ included angle; minimum diameter = 3.81 mm; maximum diameter = 7.77 mm; notch root radius = 0.024 mm. Stress concentration factor (K_t) = 8.4.

Technical Reference on Hydrogen Compatibility of Materials

Austenitic Steels:

300-Series Stainless Alloys

Type 304 and 304L (code 2101)

1. General

Type 304 stainless steels are austenitic alloys that have a good combination of machinability, weldability and corrosion resistance. Type 304 stainless steel is, however, susceptible to strain-induced martensitic transformations during room temperature deformation including machining operations. The role of martensite on hydrogen embrittlement in austenitic stainless steels has not been firmly established. Although generally viewed to be neither necessary nor sufficient to explain susceptibility to hydrogen embrittlement in austenitic stainless steels, α' martensite, is associated with lower resistance to hydrogen embrittlement. The trend for Fe-Cr-Ni stainless steels (300-series alloys) is that higher nickel and chromium concentrations suppress the martensitic transformation temperature and thus the strain-induced martensite [1-3].

The alloy content of type 304 stainless steel results in a relatively low stacking fault energy compared to more highly alloyed stainless steels such as type 316. Austenitic stainless steels with low stacking fault energy are more susceptible to hydrogen embrittlement, a feature generally attributed to non-uniform plastic deformation [4, 5]. Warm-working type 304 stainless steel results in shorter dislocation slip distances (due to increased dislocation density) and, in one interpretation, improved resistance to hydrogen embrittlement [4].

Type 304 stainless steel is sensitive to carbide precipitation on grain boundaries between approximately 773 K and 1073 K, this phenomenon is called sensitization. A low-carbon grade, designated 304L, is used to moderate this sensitization. Carbides themselves are believed to have little, if any, effect on susceptibility to hydrogen embrittlement [6]; however, carbide precipitation in stainless steels has been linked to chromium depletion in adjacent areas, which then become more prone to general corrosion [7]. In addition, these regions, which are depleted in both chromium and carbon, are vulnerable to strain-induced martensitic transformations resulting in greater susceptibility to hydrogen embrittlement [6].

The general trends outlined above indicate that high alloy content and warm-working enhance resistance to hydrogen embrittlement of type 304 stainless steel. Although there is no data to substantiate the benefit of high nickel and chromium in type 304, these elements are associated with two features that generally improve resistance to hydrogen embrittlement: (1) nickel and chromium stabilize the austenite matrix with respect to martensitic transformations, and (2) nickel and chromium tend to increase the stacking fault energy [8, 9]. Cold-working of type 304 stainless steels should be avoided, particularly in materials for hydrogen service, in favor of warm-working to avoid the formation of martensitic phases. Although carbon is an austenite stabilizer, low-carbon grades, such as 304L, are recommended to avoid potential sensitization and improve weldability.

1.1 Composition and microstructure

Table 1.1.1 lists specification limits for type 304 stainless steels and the compositions of several heats used to study hydrogen effects.

1.2 Common designations

UNS S30400 (304)
UNS S30403 (304L)
UNS S30451 (304N)
UNS S30453 (304LN)

2. Permeability, Diffusivity and Solubility

The permeability of stainless steel is briefly reviewed in Refs. [2, 10, 11]; diffusivity and solubility are briefly reviewed in [2, 11]. Permeability, diffusivity and solubility can be described by standard Arrhenius-type relationships. Solubility data are normally determined from the ratio of permeability and diffusivity.

Permeability appears to be nearly independent of the composition and microstructure for stable austenitic stainless steels [11, 12]. Ref. [12] shows that nitrogen additions to type 304 stainless steel (type 304N) do not significantly affect hydrogen solubility at low hydrogen pressures. Strain-induced martensite in type 304 stainless steel (e.g., as a consequence of deformation processes), however, causes an increase in permeability and diffusivity [13]. Although the solubility of hydrogen in martensitic phases is usually less than in austenitic phases, the solubility in deformed type 304 stainless steel with martensitic phases is reported to be greater than in type 304 without martensitic phases [13]. This is attributed to increased hydrogen trapping in the deformed microstructure [13].

Relationships for permeability and solubility fit to data for several austenitic stainless steel alloys are given in Table 2.1 and plotted in Figure 2.1 and 2.2 respectively. These relationships are expected to apply to types 304, 304L, and 304N stainless steels. It is important to note that these data are determined at elevated temperature and low pressure; they are extrapolated for use near room temperature and high pressure. For this reason, it is recommended that the relationships from Refs. [12, 13] be used for extrapolation to low temperature since these provide conservative estimates (high values) of permeability (Figure 2.1) and solubility (Figure 2.2).

3. Mechanical Properties: Effects of Gaseous Hydrogen

3.1 Tensile properties

3.1.1 Smooth tensile properties

Annealed type 304 stainless steel is susceptible to hydrogen embrittlement in tension, Table 3.1.1.1. The reduction in area (RA) of annealed type 304 stainless steel with either internal or external hydrogen can be as low as 30% compared to 75-80% for material in the absence of hydrogen. In one study, warm-working by high energy rate forging (HERF) has been shown to improve both strength and resistance to hydrogen embrittlement [4]; it is unclear whether other warm-working processes have a similarly beneficial effect on resistance to hydrogen

embrittlement. Hydrogen has a negligible effect on yield strength of type 304 stainless steel that is free of martensite and carbide precipitation, but slightly lowers the ultimate strength.

Strain rate does not have a large impact on hydrogen embrittlement of type 304 stainless steel with internal hydrogen at conventional rates, e.g., $<0.01\ s^{-1}$, Figure 3.1.1.1. At higher strain rates the ductility is substantially improved; this is interpreted as high velocity dislocations separating from hydrogen atmospheres [14].

Ductility, measured from smooth tensile specimens of type 304 stainless steels with internal hydrogen (thermally precharged in hydrogen gas), reaches a minimum at temperature near 200 K, Table 3.1.1.2 and Figure 3.1.1.2. At 77 K and 380 K the ductility of type 304 stainless steel with internal hydrogen is not degraded.

Sensitized type 304 stainless steel has lower ductility than annealed type 304 when tested in air; in hydrogen gas the absolute and relative reduction in area is lower for sensitized type 304 than annealed material [3]. See also section 4.2.

3.1.2 Notched tensile properties

Notched tensile specimens show substantial loss in ductility and strength when exposed to internal or external hydrogen, Table 3.1.2.1. Several notched specimens show as much as 50% loss in ductility [15] and 25% loss in strength [1-3]. Notched tensile specimens that have been tested in hydrogen gas display greater loss in strength and ductility at higher pressure, Figure 3.1.2.1 [15]. Data also show that notched specimens exposed to high pressure hydrogen gas at room temperature for 24 hours prior to testing suffer greater loss in strength than specimens tested after minutes in the high pressure hydrogen gas [15]. These data clearly demonstrate that tensile testing of stainless steel in external hydrogen gas does not provide limiting behavior for material that will be exposed to hydrogen for long periods of time.

3.2 Fracture mechanics

3.2.1 Fracture toughness

J-integral fracture toughness of high energy rate forgings has been reported to strongly depend on the orientation of the microstructure and to be significantly reduced for type 304 stainless steel measured in external hydrogen gas with internal hydrogen (or deuterium) [3, 16]. Due to the difficulty of instrumenting fracture mechanics specimens in high-pressure hydrogen gas, the J_m and tearing modulus (dJ/da) at maximum load are used in that study for comparison of orientations and testing conditions (values at maximum load do not represent a standardized fracture toughness). Nonetheless, it was observed that in most cases internal hydrogen in combination with testing in high-pressure external hydrogen gas produced a greater effect on both the fracture toughness and the tearing modulus than testing in external hydrogen gas without internal hydrogen [3, 16].

3.2.2 Threshold stress-intensity factor

Low-strength austenitic alloys (<700 MPa) have been shown to have high resistance to crack extension in external hydrogen gas under static loads [17]. Data for 304 in two microstructural conditions are shown in Table 3.2.2.1. For type 304 stainless steel, it was not possible to achieve crack propagation under plane strain conditions in 22.2 mm thick test specimens [17].

3.3 Fatigue

No known published data in hydrogen gas.

3.4 Creep

No known published data in hydrogen gas.

3.5 Impact

The impact fracture energy of type 304L stainless steel is affected by internal hydrogen, Table 3.5.1. The impact energy is more affected by hydrogen at 77 K than at 298 K; as opposed to tensile testing that shows greater loss in ductility at 298 K compared to 77 K, see section 3.1.1 and Figure 3.1.1.2. It appears that HERF microstructures are more susceptible to impact in the presence of hydrogen, however, the microstructural details of these alloys were not reported [3].

3.6 Disk rupture tests

Disk rupture tests show the same general trends as tensile tests, in particular martensitic phases due to cold deformation processes and machining exacerbate susceptibility to hydrogen embrittlement in type 304 stainless steel [18, 19].

4. Fabrication

4.1 Primary processing

Warm-working type 304 stainless steel by HERF may improve resistance to hydrogen embrittlement [4], Figure 4.1.1.

4.2 Heat treatment

Carbides form on grain boundaries in the temperature range 773 K to 1073 K in 300-series stainless steels. This temperature range should be avoided since carbide formation leads to localized depleted in chromium and carbon content adjacent to grain boundaries and susceptibility to corrosion [7]. These regions depleted in chromium and carbon have lower stability (carbon is an austenite stabilizer, and both elements lower the martensitic transformation temperature) resulting in strain-induced martensite along the grain boundaries and greater susceptibility to hydrogen embrittlement in tensile testing of type 304 stainless steel in hydrogen gas, Figure 4.2.1 [6].

4.3 Properties of welds

Refs. [20, 21] report properties of 304L gas tungsten arc (GTA) welds with 308L filler wire measured in external hydrogen gas with and without internal hydrogen. Tensile properties of GTA welded joints are provided in Table 4.3.1 for smooth tensile specimens with both internal and external hydrogen and Table 4.3.2 for notched tensile specimens tested in external hydrogen gas. The loss in ductility in these tensile tests correlates well with expected hydrogen content. Fracture of the welds in the absence of hydrogen was by microvoid coalescence. Detailed fractography shows failure to be associated with ferrite-austenite interfaces [20]; failure, however, was dominated by ductile fracture processes [21].

5. References

1. GR Caskey. Hydrogen Damage in Stainless Steel. in: MR Louthan, RP McNitt and RD Sisson, editors. Environmental Degradation of Engineering Materials in Hydrogen. Blacksburg VA: Laboratory for the Study of Environmental Degradation of Engineering Materials, Virginia Polytechnic Institute (1981) p. 283-302.
2. GR Caskey. Hydrogen Effects in Stainless Steels. in: RA Oriani, JP Hirth and M Smialowski, editors. Hydrogen Degradation of Ferrous Alloys. Park Ridge NJ: Noyes Publications (1985) p. 822-862.
3. GR Caskey. Hydrogen Compatibility Handbook for Stainless Steels (DP-1643). EI du Pont Nemours, Savannah River Laboratory, Aiken SC (June 1983).
4. MR Louthan, GR Caskey, JA Donovan and DE Rawl. Hydrogen Embrittlement of Metals. Mater Sci Eng 10 (1972) 357-368.
5. BC Odegard, JA Brooks and AJ West. The Effect of Hydrogen on Mechanical Behavior of Nitrogen-Strengthened Stainless Steel. in: AW Thompson and IM Bernstein, editors. Proceedings of an International Conference on Effect of Hydrogen on Behavior of Materials, 1975, Moran WY. The Metallurgical Society of AIME (1976) p. 116-125.
6. G Han, J He, S Fukuyama and K Yokogawa. Effect of strain-induced martensite on hydrogen environment embrittlement of sensitized austenitic stainless steels at low temperatures. Acta mater 46 (1998) 4559-4570.
7. RA Lula. Stainless Steel (revised from "An Introduction to Stainless Steel" by JG Parr and A Hanson). Metals Park OH: American Society for Metals (1986).
8. RE Schramm and RP Reed. Stacking Fault Energies of Seven Commercial Austenitic Stainless Steels. Metall Trans 6A (1975) 1345-1351.
9. CG Rhodes and AW Thompson. The Composition Dependence of Stacking Fault Energy in Austenitic Stainless Steels. Metall Trans 8A (1977) 1901-1905.
10. AD LeClaire. Permeation of Gases Through Solids: 2. An assessment of measurements of the steady-state permeability of H and its isotopes through Fe, Fe-based alloys, and some commercial steels. Diffusion and Defect Data 34 (1983) 1-35.
11. XK Sun, J Xu and YY Li. Hydrogen Permeation Behaviour in Austenitic Stainless Steels. Mater Sci Eng A114 (1989) 179-187.
12. MR Louthan and RG Derrick. Hydrogen Transport in Austenitic Stainless Steel. Corros Sci 15 (1975) 565-577.
13. T-P Perng and CJ Altstetter. Effects of Deformation on Hydrogen Permeation in Austenitic Stainless Steels. Acta metall 34 (1986) 1771-1781.
14. JH Holbrook and AJ West. The Effect of Temperature and Strain Rate on the Tensile Properties of Hydrogen Charged 304L, 21-6-9, and JBK 75. in: IM Bernstein and AW Thompson, editors. Proceedings of the International Conference on Effect of Hydrogen on Behavior of Materials: Hydrogen Effects in Metals, 1980, Moran WY. The Metallurgical Society of AIME (1980) p. 655-663.
15. RP Jewitt, RJ Walter, WT Chandler and RP Frohmberg. Hydrogen Environment Embrittlement of Metals (NASA CR-2163). Rocketdyne for the National Aeronautics and Space Administration, Canoga Park CA (March 1973).
16. MR Dietrich, GR Caskey and JA Donovan. J-Controlled Crack Growth as an Indicator of Hydrogen-Stainless Steel Compatibility. in: IM Bernstein and AW Thompson, editors. Proceedings of the International Conference on Effect of Hydrogen on Behavior of

Materials: Hydrogen Effects in Metals, 1980, Moran WY. The Metallurgical Society of AIME (1980) p. 637-643.
17. MW Perra. Sustained-Load Cracking of Austenitic Steels in Gaseous Hydrogen. in: MR Louthan, RP McNitt and RD Sisson, editors. Environmental Degradation of Engineering Materials in Hydrogen. Blacksburg VA: Laboratory for the Study of Environmental Degradation of Engineering Materials, Virginia Polytechnic Institute (1981) p. 321-333.
18. J Chene, M Aucouturier, R Arnould-Laurent, P Tison and J-P Fidelle. Hydrogen Transport by Deformation and Hydrogen Embrittlement in Selected Stainless Steels. in: IM Bernstein and AW Thompson, editors. Hydrogen Effects in Metals, 1980, Moran WY. The Metallurgical Society of AIME p. 583-595.
19. J-P Fidelle, R Bernardi, R Broudeur, C Roux and M Rapin. Disk Pressure Testing of Hydrogen Environment Embrittlement. in: Hydrogen Embrittlement Testing, ASTM STP 543, American Society for Testing and Materials. (1974) p. 221-253.
20. JA Brooks and AJ West. Hydrogen Induced Ductility Losses in Austenitic Stainless Steel Welds. Metall Trans 12A (1981) 213-223.
21. JA Brooks, AJ West and AW Thompson. Effect of Weld Composition and Microstructure on Hydrogen Assisted Fracture of Austenitic Stainless Steels. Metall Trans 14A (1983) 75-84.
22. ASTM DS-56H, Metals and Alloys in the UNIFIED NUMBERING SYSTEM (SAE HS-1086 OCT01). American Society for Testing and Materials (Society of Automotive Engineers) (2001).
23. RJ Walter, RP Jewitt and WT Chandler. On the Mechanism of Hydrogen-Environment Embrittlement of Iron- and Nickel-base Alloys. Mater Sci Eng 5 (1970) 99-110.
24. GR Caskey and RD Sisson. Hydrogen Solubility in Austenitic Stainless Steels. Scr Metall 15 (1981) 1187-1190.
25. TL Capeletti and MR Louthan. The Tensile Ductility of Austenitic Steels in Air and Hydrogen. J Eng Mater Technol 99 (1977) 153-158.
26. RE Stoltz and AJ West. Hydrogen Assisted Fracture in FCC Metals and Alloys. in: IM Bernstein and AW Thompson, editors. Proceedings of the International Conference on Effect of Hydrogen on Behavior of Materials: Hydrogen Effects in Metals, 1980, Moran WY. The Metallurgical Society of AIME (1980) p. 541-553.
27. RE Stoltz, NR Moody and MW Perra. Microfracture Model for Hydrogen Embrittlement of Austenitic Steels. Metall Trans 14A (1983) 1528-1531.

Table 1.1.1. Specification limits for type 304 stainless steels and composition of several heats of used to study hydrogen effects.

Heat	alloy	Fe	Cr	Ni	Mn	Si	C	N	other	Ref.
UNS S30400	304	Bal	18.00 20.00	8.00 10.50	2.00 max	1.00 max	0.08 max	—	0.030 max S; 0.045 max P	[22]
UNS S30403	304L	Bal	18.00 20.00	8.00 12.00	2.00 max	1.00 max	0.030 max	—	0.030 max S; 0.045 max P	[22]
UNS S30451	304N	Bal	18.00 20.00	8.00 10.50	2.00 max	1.00 max	0.08 max	0.10 0.16	0.030 max S; 0.045 max P	[22]
UNS S30453	304LN	Bal	18.00 20.00	8.00 12.00	2.00 max	1.00 max	0.030 max	0.10 0.16	0.030 max S; 0.045 max P	[22]
W69	304L	Bal	18.5	9.78	1.78	0.49	0.20	—	0.011 S; 0.014 P; 0.10 Cu; 0.09 Mo	[23]
O76	304L	Bal	19.10	9.41	1.51	0.63	0.026	—		[5]
O76N	304LN	Bal	19.75	8.35	1.73	0.39	0.031	0.25		[5]
H80	304L	Bal	19.0	11.0	1.8	0.5	0.02	0.05	0.015 S; 0.04 P	[14]
P81	304L	Bal	19.7	11.7	1.95	0.50	0.027	0.053	<0.2 Co	[17]
B83w	304L/ 308L	Bal	19.8	10.4	1.8	0.56	0.02	0.04	0.012 S; 0.017 P	
C83	304L	Bal	18.35	10.29	1.57	0.43	0.03	—	0.008 S; 0.015 P; 0.17 Mo	[3]
C83N	304N	Bal	18.37	8.43	1.66	0.19	0.06	0.25	0.025 S; 0.30 P; 0.10 Mo; 0.15 Cu	[3]
H98	304	Bal	18.33	8.35	1.01	0.59	0.060	—	0.018 P; 0.009 S	[6]

w = composition of the weld fusion zone

Table 2.1. Average permeability and solubility relationships determined for several austenitic stainless steels.

Material	Temperature range (K)	Pressure range (MPa)	$\Phi = \Phi_o \exp(-E_\Phi / RT)$		$S = S_o \exp(-E_S / RT)$		Ref.
			Φ_o $\left(\frac{\text{mol H}_2}{\text{m}\cdot\text{s}\cdot\sqrt{\text{MPa}}}\right)$	E_Φ $\left(\frac{\text{kJ}}{\text{mol}}\right)$	S_o $\left(\frac{\text{mol H}_2}{\text{m}^3\cdot\sqrt{\text{MPa}}}\right)$	E_S $\left(\frac{\text{kJ}}{\text{mol}}\right)$	
Average of several austenitic alloys †	423-700	0.1-0.3	1.2×10^{-4}	59.8	179	5.9	[12]
Based on >20 studies on 12 austenitic alloys	—	—	3.27×10^{-4}	65.7	—	—	[10]
Average of six austenitic alloys	473-703	0.1	2.81×10^{-4}	62.27	488	8.65	[11]
Average of four austenitic alloys	373-623	1×10^{-4}-0.03	5.35×10^{-5}	56.1	266	6.86	[13]

† Data from Ref. [12] is determined for deuterium: permeability has been corrected here to give permeability of hydrogen (by multiplying by the square root of the mass ratio: √2); solubility is assumed to be independent of isotope.

Table 2.2. Hydrogen solubility of type 304 stainless steel measured using hot extraction after thermal precharging in hydrogen gas.

Material	Surface condition	Thermal precharging	Hydrogen concentration †		Ref.
			wppm	appm	
304L annealed	600 grit finish	69 MPa H_2 470 K	72	4000	[24]
	Electropolished		81	4500	
304L HERF	600 grit finish		71	3900	
	Electropolished		81	4500	
304L 100% CW	600 grit finish		71	3900	
	Electropolished		79	4300	

HERF = high energy rate forging, CW = cold work

† 1 wppm ≈ 55 appm

Table 3.1.1.1. Smooth tensile properties of type 304 stainless steel at room temperature; measured in air with internal hydrogen (thermal precharging in hydrogen gas), or measured in external hydrogen gas, or measured in external hydrogen gas with internal hydrogen.

Material	Thermal precharging	Test environment	Strain rate (s^{-1})	S_y (MPa)	S_u (MPa)	El_u (%)	El_t (%)	RA (%)	Ref.
304L, heat W69 annealed	None	69 MPa He	0.67 x10^{-3}	234	531	—	86	78	[15, 23]
	None	69 MPa H_2		—	524	—	79	71	
304L	None	Air	—	—	641	—	—	60	[15]
	(1)	34 MPa H_2		—	614	—	—	46	
	(1)	69 MPa H_2		—	593	—	—	44	
304L, heat O76 annealed plate	None	Air	3 x10^{-3}	214	607	—	73	77	[5]
	(2)	69 MPa H_2		221	531	—	32	32	
304L HERF	None	Air	—	552	683	—	35	76	[4]
	(3)	Air		579	717	—	41	68	
304L	None	Air	—	207	573	—	75	82	[4]
	None	69 MPa He		186	565	—	74	81	[4, 25]
	None	69 MPa H_2		207	503	—	48	33	
304LN, heat O76N annealed plate	None	Air	3 x10^{-3}	379	765	—	62	72	[5]
	(2)	69 MPa H_2		379	765	—	65	54	
304N	None	69 MPa He	—	641	848	—	43	74	[25]
	None	69 MPa H_2		641	841	—	36	54	
304N, heat C83N	None	Air	—	760	880	—	33	71	[3]
	None	69 MPa He		630	850	—	43	74	
	None	69 MPa H_2		640	840	—	36	54	
	(4)	Air		740	830	—	31	65	
	(4)	69 MPa H_2		550	790	—	37	46	

HERF = high energy rate forging

(1) Hold at test pressure for 24 h before loading (room temperature)

(2) 24.1 MPa hydrogen, 473 K, 240 h (gauge diameter = 5 mm): calculated surface concentration of 55 wppm hydrogen (3000 appm), decreasing toward center

(3) 69 MPa hydrogen

(4) 69 MPa hydrogen, 430K, 1000 h

Table 3.1.1.2. Smooth tensile properties of type 304 stainless steel as a function of temperature; measured in air with internal hydrogen (thermal precharging in hydrogen or deuterium gas).

Material	Thermal precharging	Test environment	Strain rate (s^{-1})	S_y (MPa)	S_u (MPa)	El_u (%)	El_t (%)	RA (%)	Ref.
304L, heat C83 bar stock	None (1)	Air 380 K	—	240†	680‡	58	69	83	[3]
				260†	730‡	60	70	72	
	None (1)	Air 273 K		310†	1160‡	80	89	79	
				330†	870‡	44	44	36	
	None (1)	Air 200 K		360†	1500‡	61	70	72	
				390†	1210‡	44	44	22	
	None (1)	Liquid N_2 77 K		390†	2200‡	60	64	72	
				430†	2100‡	59	65	72	
304L HERF	None (2)	Air 380 K	—	440†	630‡	32	44	82	[3]
				440†	650‡	32	43	80	
	None (2)	Air 298 K		480†	930‡	57	68	86	
				510†	990‡	55	62	61	
	None (2)	Air 250 K		490†	1100‡	52	61	81	
				610†	1120‡	41	41	33	
	None (2)	Air 200 K		660†	1390‡	46	55	75	
				620†	1300‡	43	44	32	
304N, heat C83N	None (3) – D_2	Air 375 K	—	820	950‡	11	26	73	[3]
				820	970‡	11	22	70	
	None (3) – D_2	Air 298 K		906	1110‡	16	28	77	
				950	1185‡	16	28	61	
	None (3) – D_2	Air 245 K		975	1340‡	27	37	84	
				1063	1420‡	22	27	39	
	None (3) – D_2	Air 220 K		1026	1450‡	26	35	81	
				1093	1480‡	21	24	28	
	None (3) – D_2	Air 200 K		1096	1810‡	47	56	76	
				1160	1510‡	19	23	32	

† true stress at 5% strain
‡ true stress at maximum load
(1) 69 MPa hydrogen gas, 470 K, 35000 h
(2) 69 MPa hydrogen gas, 620 K, 500 h
(3) 69 MPa deuterium gas, 620 K, 500 h

Table 3.1.2.1. Notched tensile properties of type 304 stainless steel at room temperature; measured in air with internal hydrogen (thermal precharging in hydrogen gas), or measured in external hydrogen gas, or measured in external hydrogen gas with internal hydrogen.

Material	Specimen	Thermal precharging	Test environment	Displ. rate (mm/s)	S_y † (MPa)	σ_s (MPa)	RA (%)	Ref.
304L, heat W69 annealed	(a)	None	69 MPa He	0.7 x10^{-3}	234	703	21	[15, 23]
		None	69 MPa H_2		—	614	11	
304L	K_t = 1	None	Air	—	—	703	60	[15]
		(1)	34 MPa H_2		—	614	46	
		(1)	69 MPa H_2		—	586	44	
	K_t = 2	None	Air		—	738	60	
		(1)	34 MPa H_2		—	710	53	
		(1)	69 MPa H_2		—	680	54	
	K_t = 4	None	Air		—	807	60	
		(1)	34 MPa H_2		—	686	44	
		(1)	69 MPa H_2		—	648	41	
304L	(b)	None	Air	—	—	896	—	[3]
		None	0.1 MPa H_2		—	786	—	
		None	1.0 MPa H_2		—	703	—	
		None	6.9 MPa H_2		—	662	—	
304L	(b)	None	Air	—	600‡	770	26	[3]
		(2) – Ar	Air		600‡	710	21	
		(2) – H_2	Air		530‡	580	12	

K_t = stress concentration factor
† yield strength of smooth tensile specimen
‡ nominal strength of smooth tensile specimen
(a) V-notched specimen: 60˚ included angle; minimum diameter = 3.81 mm; maximum diameter = 7.77 mm; notch root radius = 0.024 mm. K_t = 8.4.
(b) V-notched specimen: 30˚ included angle; minimum diameter = 3.35 mm; maximum diameter = 4.80 mm; notch root radius = 0.127 mm.
(1) Hold at test pressure for 24 h before loading (room temperature)
(2) 69 MPa hydrogen or argon gas, 380 K, 4800 h

Table 3.2.2.1. Threshold stress intensity factor for type 304 stainless steel in external high-pressure hydrogen gas.

Material	S_y † (MPa)	RA † (%)	Threshold Stress Intensity (MPa $m^{1/2}$)		Ref.
			100 MPa H_2	200 MPa H_2	
304L, heat P81 HERF 840˚C, WQ	593	66	NCP 110	NCP 110	[17] ‡
304L, heat P81 HERF 980˚C, WQ	372	70	—	NCP 50	[17] ‡

HERF = high energy rate forging, WQ = water quench
† yield strength and reduction in area of smooth tensile specimen, not exposed to hydrogen
‡ same data also reported in Ref. [26, 27]

Table 3.5.1. Impact fracture energy for type 304 stainless steel; measured in air with internal hydrogen (thermal precharging in hydrogen gas).

Material	Specimen	Thermal precharging	Test environment	S_y † (MPa)	Impact Energy (J)	Ref.
304L	(a)	None	Air 78 K	—	165	[3]
		(1)		—	110	
		None	Air 298 K	—	194	
		(1)		—	185	
304L HERF	(a)	None	Air 77 K	—	160	[3]
		(2)		—	95	
		None	Air 298 K	—	199	
		(2)		—	152	

HERF = high-energy rate forging
† yield strength of smooth tensile specimen, not exposed to hydrogen
(a) modified Naval Research Laboratory dynamic tear specimen [3]
(1) 17.9 MPa hydrogen gas, 470 K, 1000 h
(2) 29.6 MPa hydrogen gas, 470 K, 1300 h

Table 4.3.1. Smooth tensile properties of type 304 composite GTA welds at room temperature; measured in external hydrogen gas with internal hydrogen (thermal precharging in hydrogen gas).

Material	Thermal precharging	Test environment	Strain rate (s^{-1})	S_y (MPa)	S_u (MPa)	El_u (%)	El_t (%)	RA (%)	Ref.
304L/308L GTA welds heat B83w‡	None	Air	0.33 x 10^{-3}	396	619	17	23	64	[20, 21]
	None	69 MPa H_2		410	622	18	23	54	
	None	172MPa H_2		457	647	16	19	48	
	(1)	Air		410	627	15	17	44	
	(1)	69 MPa H_2		426	616	12	16	41	
	(2)	Air		423	632	12	13	34	
	(2)	172MPa H_2		477	667	11	12	31	

HERF = high energy rate forging, GTA = gas tungsten arc

‡ The base material for these studies was HERF, back extrusions of 304L, machined to cylindrical shape (10 cm diameter, 1.5 cm wall thickness) with circumferential double J grooves; eight to ten weld passes were required to fill groove. The filler material was 308L. Tensile bars contain base material and heat affected zone with the fusion zone centered in the gauge length.

(1) 24 MPa hydrogen gas, 473 K, 240 h (gauge diameter = 5 mm): calculated concentration gradient of 45 to 4 wppm surface to center (2500 to 200 appm)

(2) 69 MPa hydrogen gas, 473 K, 240 h (gauge diameter = 5 mm): calculated concentration gradient of 72 to 7 wppm surface to center (4000 to 400 appm)

Table 4.3.2. Notched tensile properties of type 304 composite GTA welds with different amounts of ferrite at room temperature; measured in external hydrogen gas.

Material	Specimen	Thermal precharging	Test environment	Displ. rate (mm/s)	S_y † (MPa)	σ_s (MPa)	RA (%)	Ref.
304L/308L FN = 4.7 heat B83w‡	(a)	None	Air	—	—	729	40	[20]
		None	69 MPa H_2		—	658	14	
304L/308L FN = 8.5 heat B83w‡	(a)	None	Air		—	894	40	
		None	69 MPa H_2		—	740	17	

HERF = high energy rate forging, GTA = gas tungsten arc, FN = ferrite number

† yield strength of smooth tensile specimen

‡ The base material for these studies was HERF back extrusions of 304L, machined to cylindrical shape (10 cm diameter, 1.5 cm wall thickness) with circumferential double J grooves; eight to ten GTA weld passes were required to fill groove. The filler material was 308L. Tensile bars contain base material and heat affected zone with the fusion zone centered in the gauge length.

(a) V-notched specimen: 45˚ included angle; minimum diameter = 3.95 mm; notch root radius = 1.3 mm.

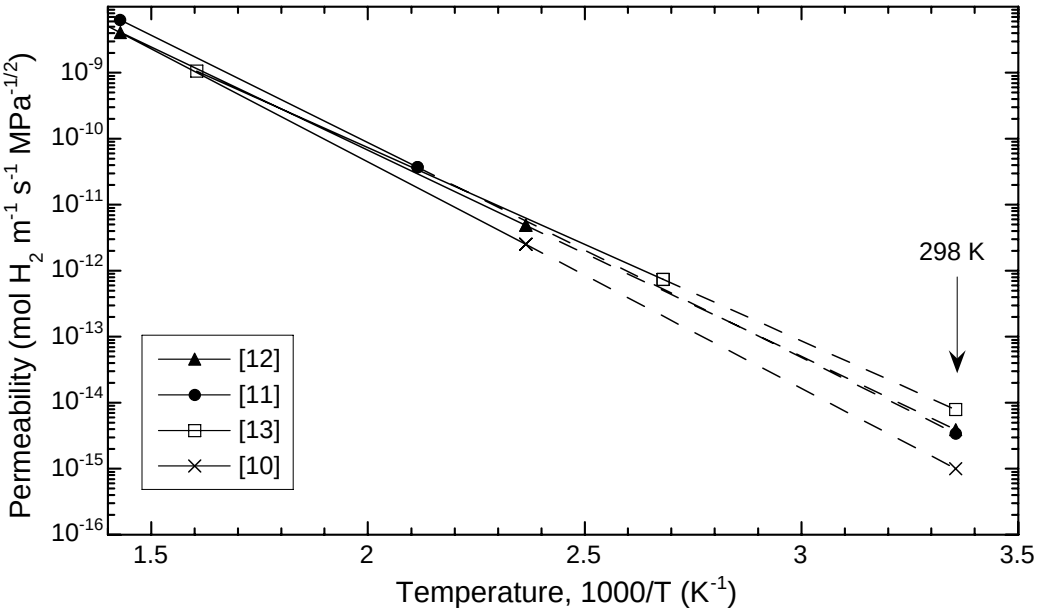

Figure 2.1. Permeability relationships (from Table 2.1) for austenitic stainless steels extrapolated (dashed lines) to 298 K. Permeability from Ref. [12] was determined for deuterium and has been corrected to give permeability of hydrogen by multiplying by the square root of the mass ratio: √2.

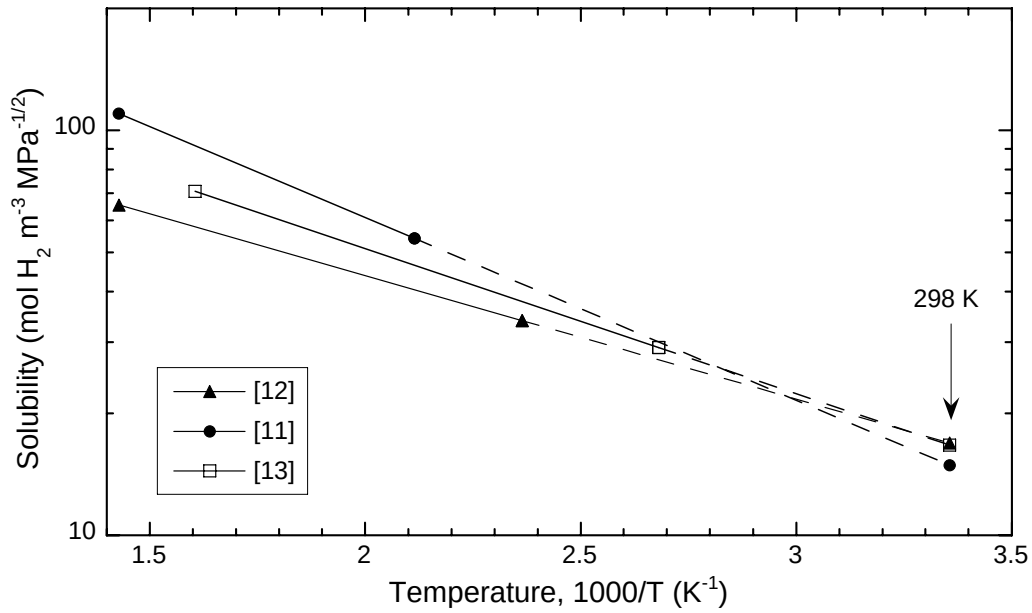

Figure 2.2. Solubility relationships (from Table 2.1) extrapolated (dashed lines) to 298 K and determined from permeability and diffusivity data for austenitic stainless steels. Data from Ref. [12] are for deuterium.

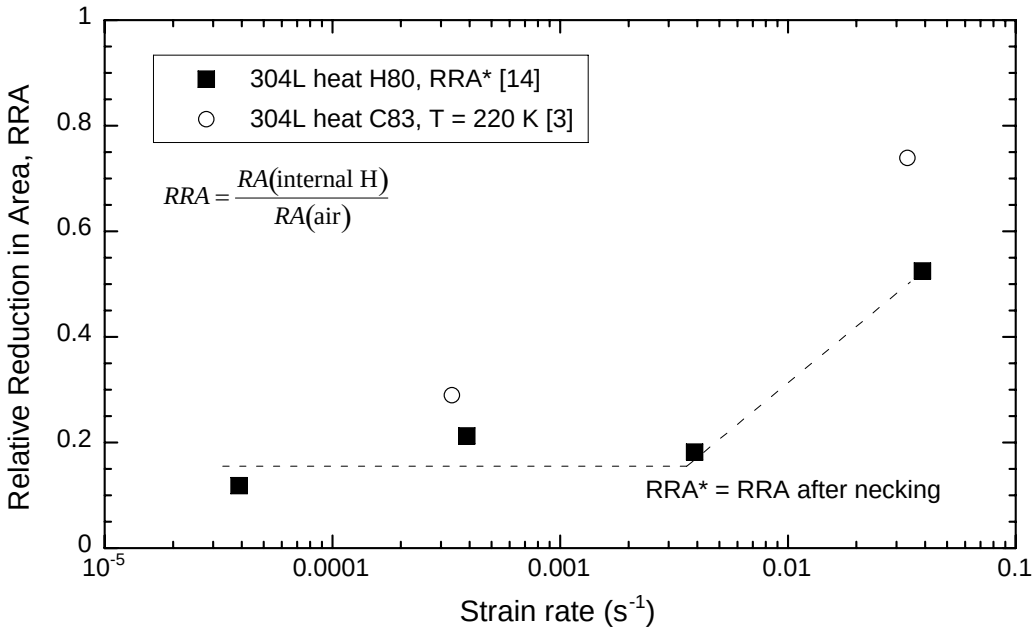

Figure 3.1.1.1. Relative reduction in area (RRA) of smooth tensile specimens of type 304 stainless steel with internal hydrogen as a function of strain rate. Precharging conditions Ref. [3]: 69 MPa H_2 at 470 K. Precharging conditions Ref. [14]: 69 MPa H_2 at 573 K (uniform).

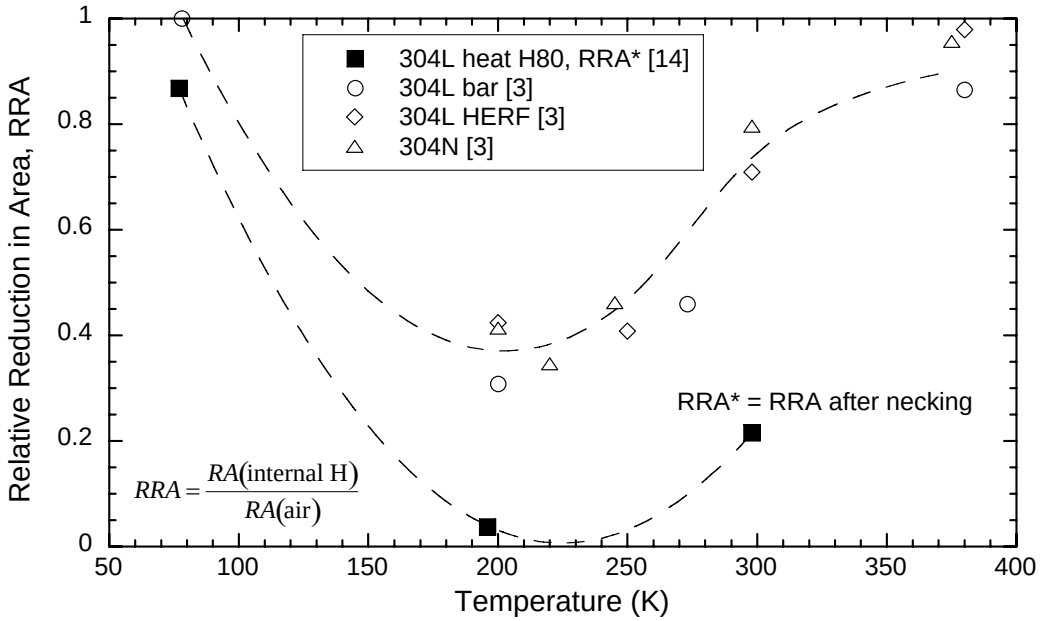

Figure 3.1.1.2. Relative reduction in area (RRA) of smooth tensile specimens of type 304 stainless steels as a function of temperature; measured in air with internal hydrogen (thermal precharging from hydrogen gas). Data from Ref. [3] also given in Table 3.1.1.2. Precharging conditions Ref. [3]: 304L bar, 69 MPa H_2 at 470 K; 304L HERF, 69 MPa H_2 at 620 K; 304N, 69 MPa D_2 at 620 K. Precharging conditions Ref. [14]: 69 MPa H_2 at 573 K (uniform).

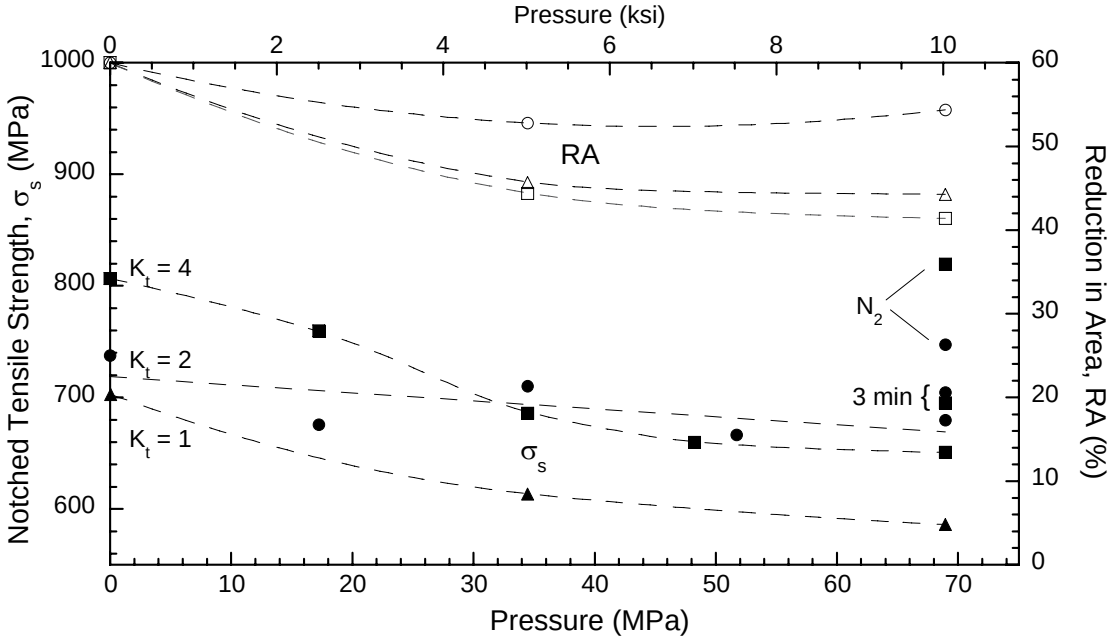

Figure 3.1.2.1. Notched tensile strength and reduction in area of type 304 stainless steel as a function of external hydrogen gas pressure and notch geometry, except where noted the exposure time in hydrogen gas at pressure is 24 hours. [15]

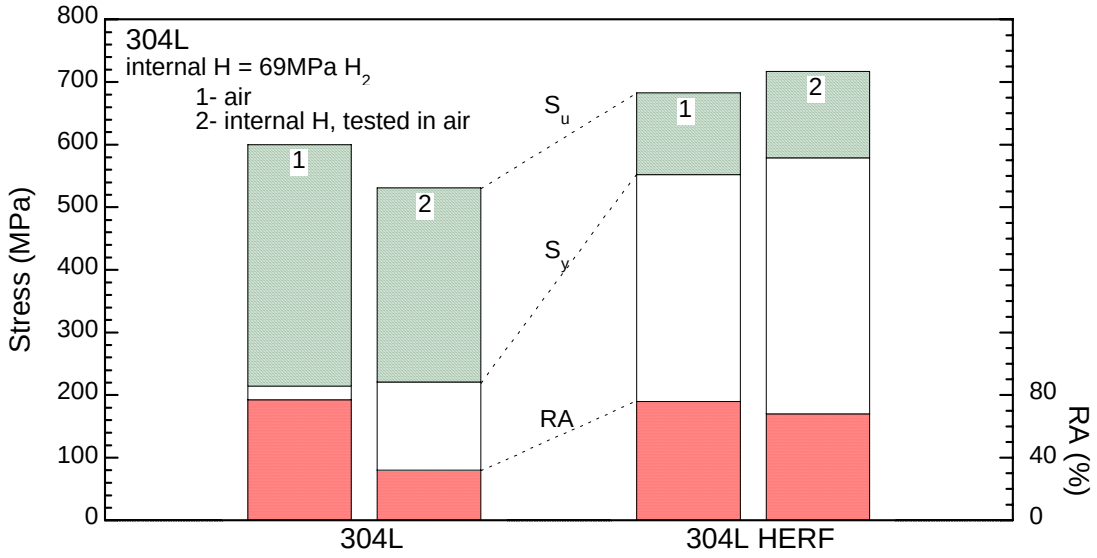

Figure 4.1.1. Smooth tensile properties of type 304L stainless steel as a function of thermomechanical processing with internal hydrogen (thermal precharging in hydrogen gas). Data also given in Table 3.1.1.1. [4]

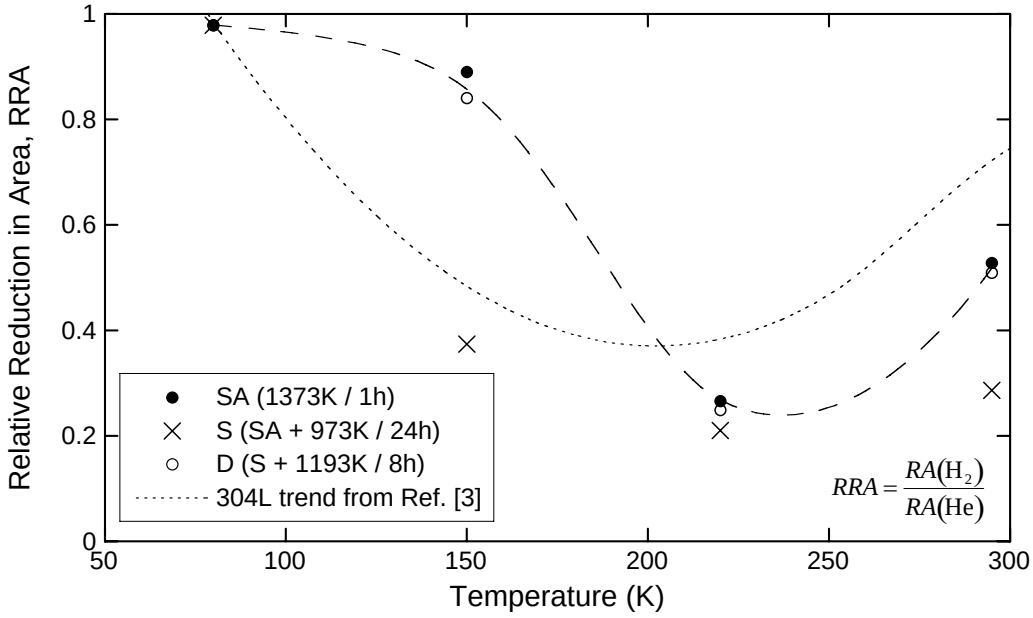

Figure 4.2.1. Relative reduction in area (RRA) of smooth tensile specimens of type 304 stainless steel (heat H98) as a function of temperature and sensitization; measured in external hydrogen gas (1 MPa) relative to external helium gas (1 MPa) [6]. Trend for 304L from Ref. [3] is from Figure 3.1.1.2 with internal hydrogen. SA = solution annealed, S = sensitized, D = desensitized

This page intentionally left blank.

Technical Reference on Hydrogen Compatibility of Materials

Austenitic Steels:

300-Series Stainless Alloys

Type 316 and 316L (code 2103)

1. General

Type 316 & 316L stainless steels are metastable austenitic alloys that have molybdenum for improved corrosion resistance and high-temperature strength. Due to their high nickel and molybdenum content, this family of alloys has high stacking fault energy; a feature that promotes cross slip and is generally associated with superior hydrogen compatibility [1, 2]. Indeed, data suggest that 316 stainless steel is more resistant to hydrogen-assisted fracture than most other austenitic stainless steels and that this resistance seems to improve with nickel concentration (within the standard compositional limits).

Type 316 stainless steel is sensitive to carbide precipitation on grain boundaries between approximately 773 K and 1073 K. A low-carbon grade, designated 316L, is used to moderate this sensitization. Carbides themselves are believed to have little, if any, effect on hydrogen-assisted fracture of austenitic stainless steels [3-5]. Carbon is an austenite stabilizer and carbide precipitation in austenitic alloys has been linked to chromium depletion in adjacent areas. Regions poor in carbon and chromium are prone to strain-induced martensitic transformations and may be active hydrogen trapping sites.

The role of martensite on hydrogen embrittlement in austenitic stainless steels has not been firmly established. Although generally viewed to be neither necessary nor sufficient to explain hydrogen-assisted fracture in austenitic stainless steels, α' martensite, in both sensitized and nonsensitized microstructures, is associated with lower resistance to hydrogen embrittlement. The trend for Fe-Cr-Ni stainless steels (300-series alloys) is that higher nickel concentration suppresses the martensitic transformation temperature and thus the strain-induced martensite [6-8]. The role of high-nickel compositions in type 316 stainless steels can then be said to improve both resistance to martensitic transformations and, it appears, resistance to hydrogen-assisted fracture.

1.1 Composition

Table 1.1.1 lists the composition of several heats of 316 used to study hydrogen effects and summarized in this report. Chinese alloy HR-1 has a composition similar to nickel-rich 316 and is reported to have superior resistance to hydrogen-assisted fracture than type 316 stainless steel [9]; specifics of this alloy and its development have not been reported in the literature.

1.2 Common designations

UNS S31600 (316)
UNS S31603 (316L)
UNS S31651 (316N)

2. Permeability, Diffusivity and Solubility

Refs. [7] and [10] provide summaries of permeability and solubility data for stainless steels. Relationships for permeability and solubility fit to data for several austenitic stainless steel alloys are given in Table 2.1. Permeability can be described by a standard Arrhenius-type relationship and appears to be nearly independent of the composition and microstructure for most austenitic stainless steels [7, 10, 11]. It is important to note that permeability data are generally extrapolated from temperatures above ambient and pressures of just a few atmospheres or less. Figure 2.1 plots relationships for permeability of type 316 stainless steels from a number of studies.

Solubility data are normally determined from the ratio of permeability and diffusivity. As a consequence of the large uncertainty typically associated with these data, in particular diffusivity, solubility data from the literature commonly vary by an order of magnitude, as shown in Figure 2.2. Ref. [10] shows that nitrogen additions to type 316 stainless steel (type 316N) do not significantly affect hydrogen solubility at low hydrogen pressures. In addition, careful comparison of diffusivity data suggests that, unlike permeability, diffusivity varies with alloy composition and/or microstructure [10], implying that solubility will also vary with alloy composition and/or microstructure. This is supported by hydrogen analysis of a number of stainless steels that have been thermally precharged with hydrogen and it isotopes, showing that hydrogen concentrations can be alloy dependent [6, 12, 13].

3. Mechanical Properties: Effects of Gaseous Hydrogen

3.1 Tensile properties

3.1.1 Smooth tensile properties

Room temperature tensile properties of 316 in gaseous hydrogen generally show little or no loss in ductility, Table 3.1.1.1. An important exception to this trend reported significant loss in ductility for high-energy rate forged material that had been thermally precharged in gaseous hydrogen and tested in high-pressure hydrogen gas, Figure 3.1.1.1; the absolute ductility determined in that study, however, remained relatively high (RA $\geq$ 50%), while the strength of the material was not reported. Ductility loss of about 10% (reduction of area in hydrogen relative to reduction of area in helium, RRA ~ 0.9) was noted in a low nickel 316 alloy (heat H98) when tested in 1 MPa gaseous hydrogen at room temperature [5]. Strain-induced α' martensite was observed to be distributed throughout the grains in that study.

Ductility loss was also reported for material that was thermally precharged, Table 3.1.1.1, however, the thermal precharging cycle was in the sensitization range of this alloy [14]. The nickel content of this heat (R84, Table 1.1.1) is at the lower limit of the UNS designation, and strain-induced martensite was observed. These data also differ in that the material was tested as thin sheet specimens, which are thought to be more sensitive to surface flaws than standard bar specimens [15]. Effects of hydrogen on the flow stress of type 316 stainless steel are discussed in detail in Refs. [14, 16].

Low temperature has been shown to have a significant effect on the hydrogen-assisted fracture of type 316 stainless steel. Smooth bar tensile properties of 316 at several temperatures between 380 K and 200 K, Table 3.1.1.2, show relatively modest changes in strength and

ductility due to thermal precharging with hydrogen [8]. Testing in 1 MPa hydrogen gas, however, shows a significant reduction in ductility (as measured by the ratio of reduction in area in hydrogen to helium) at 150 and 220 K, but essentially no ductility loss at 80K [5]. Both sets of data show the greatest ductility loss due to hydrogen near 200 K, Figure 3.1.1.2. In addition to the difference in hydrogen source (internal versus external) in these two studies, the nickel content is substantially different in the two tested alloys. The lower nickel content of heat H98 may explain the greater susceptibility to hydrogen. This view must be expressed with caution, however, since the relative yield strengths of these alloys is not known, nor is the data sufficient to address differences between testing in the presence of internal or external hydrogen.

Tensile properties at elevated temperatures show no effect of internal hydrogen (thermal precharging) except for a slight decrease in reduction of area for temperatures from ambient to ~900 K and modest solute hardening near 600 K, Figures 3.1.1.3 and 3.1.1.4. Test specimens were heated to the test temperature rapidly (about one minute) and tests were performed at rapid extension rates (0.21 mm/s) to reduce loss of hydrogen during heating and testing [17].

3.1.2 Notched tensile properties

Notched tensile specimens show no difference in properties when tested in 69 MPa helium or hydrogen, Table 3.1.2.1.

3.2 Fracture mechanics

3.2.1 Fracture toughness

J-integral fracture toughness of high-energy rate forgings (HERF) has been reported to strongly depend on the orientation of the microstructure and to be significantly reduced when thermally precharged with deuterium and tested in hydrogen gas [18]. Due to the difficulty of instrumenting fracture specimens in high-pressure hydrogen gas, the J_m and tearing modulus (dJ/da) at maximum load are used in that study for comparison of orientations and testing conditions (values at maximum load do not represent a standardized fracture toughness). In addition, the alloy used in that study had a high volume of inclusions, which is believed to have biased the results to lower values [18]. Nonetheless, it was observed that in most cases thermally precharging the material (69 MPa hydrogen at 520 K for 7 days) was necessary to produce an effect of hydrogen on both the fracture toughness and the tearing modulus.

Ref. [19] shows that both sensitization (see section 4.2) and cathodic charging with hydrogen lowered fracture toughness.

3.2.2 Threshold stress-intensity factor

Low-strength austenitic microstructures (<700 MPa) have been shown to have high resistance to cracking in high-pressure hydrogen gas environments under static loads [20]. Data for 316 in two microstructural conditions are given in Table 3.2.2.1.

3.3 Fatigue

No known published data in hydrogen gas.

3.4 Creep

No known published data in hydrogen gas.

3.5 Impact

No known published data in hydrogen gas.

3.6 Disk rupture testing

Disk rupture tests indicate that type 316 stainless steel with low carbon and high nickel (heat A87, designated 316ELC) is not susceptible to high-pressure hydrogen gas in the annealed condition or the 60% cold worked condition [21]. In comparison, type 316 alloys with lower nickel and higher carbon displayed a slightly lower rupture pressure in hydrogen than helium [21]. At low temperatures (~220 K) the rupture pressure of 316L was reduced about 30% in hydrogen compared to helium and martensitic phases were detected [22]. Welded disks of 316L stainless steel were also reported to be more susceptible to rupture in hydrogen at room temperature and lower temperatures as compared to the base metal [22], see also section 4.3.

4. Fabrication

4.1 Primary processing

Electroslag remelting (ESR) of type 316 stainless steel improved the fracture toughness of cathodically charged material to values greater than determined for unrefined, annealed 316 of nominally the same composition [19]. Higher annealing temperatures were also found in this study to improve the fracture toughness of charged and sensitized materials.

4.2 Heat treatment

Type 316 stainless steel shows a larger susceptibility to hydrogen embrittlement (1 MPa gaseous H_2) in smooth tensile bars when sensitized (973 K for 24 h) compared to solution-annealed microstructures, Figure 3.1.1.2 [5]. Solution-annealed microstructures (of both type 304 and 316 stainless steels) featured strain-induced α' martensite distributed through the grain structure and transgranular fracture, while sensitized microstructures featured α' martensite preferentially along grain boundaries and intergranular failure [5]. The transition from transgranular failure to intergranular fracture is accompanied by loss in ductility. There is no direct evidence that the martensite contributes to fracture, however, it is speculated that α' martensite may facilitate hydrogen accumulation at the crack tip by enhancing hydrogen mobility [5], or perhaps by acting as trapping sites for hydrogen.

In another study, high-pressure hydrogen gas (70 MPa) did not affect the ductility of 316 stainless steel heat treated for 2 hours at 1323 K [23]. Both smooth (Table 4.2.1) and notched (Table 4.2.2) tensile geometries were tested. This temperature is greater than typically associated with sensitization of stainless steels, which may explain the absence of a sensitization effect. The composition of this alloy is not known, but the general lack of susceptibility observed in this study for 316 base metal and welds is shared with 316 alloys that have nickel compositions toward the higher end of the nickel specification for 316 alloys.

4.3 Properties of welds

Electron beam (EB) and gas tungsten arc (GTA) welds were found to be unaffected by high-pressure hydrogen gas in tension [23]. Flat-plate tensile specimens were tested in both smooth

(Table 4.3.1) and notched (Table 4.3.2) geometries. Segregated microstructures were observed in the welds, and the fracture surfaces displayed ductile-dimple failure.

Welded disks of type 316L stainless steel containing 8.5% ferrite ruptured at 15-20% lower pressures in hydrogen than helium in disk rupture tests [22]. The welded and base metal disks performed equally well in helium.

Laser Engineered Net Shaping (LENS™) is a process that has features analogous to fusion welding processes: powders are melted with a laser, solidified on a substrate and built-up in subsequent passes. The ductility of smooth tensile bars machined from LENS™-fabricated 316 materials has been reported in Ref. [24]. The loss of ductility due to thermal precharging with hydrogen (138 MPa gaseous hydrogen at 300˚C for 10 days) was found to be greater in LENS™ compared to a wrought 316 [24] and to data from Table 3.1.1.2. Fracture was localized near interlayer boundaries in hydrogen precharged specimens with secondary cracking near interpass boundaries normal to the fracture surface.

5. References

1. MR Louthan, GR Caskey, JA Donovan and DE Rawl. Hydrogen Embrittlement of Metals. Mater Sci Eng 10 (1972) 357-368.
2. BC Odegard, JA Brooks and AJ West. The Effect of Hydrogen on Mechanical Behavior of Nitrogen-Strengthened Stainless Steel. in: AW Thompson and IM Bernstein, editors. Effect of Hydrogen on Behavior of Materials. New York: TMS (1976) p. 116-125.
3. AW Thompson. The Behavior of Sensitized 309S Stainless Steel in Hydrogen. Mater Sci Eng 14 (1974) 253-264.
4. CL Briant. Hydrogen Assisted Cracking of Sensitized 304 Stainless Steel. Metall Trans 9A (1978) 731-733.
5. G Han, J He, S Fukuyama and K Yokogawa. Effect of strain-induced martensite on hydrogen environment embrittlement of sensitized austenitic stainless steels at low temperatures. Acta mater 46 (1998) 4559-4570.
6. GR Caskey. Hydrogen Damage in Stainless Steel. in: MR Louthan, RP McNitt and RD Sisson, editors. Environmental Degradation of Engineering Materials in Hydrogen. Blacksburg VA: Laboratory for the Study of Environmental Degradation of Engineering Materials, Virginia Polytechnic Institute (1981) p. 283-302.
7. GR Caskey. Hydrogen Effects in Stainless Steels. in: RA Oriani, JP Hirth and M Smialowski, editors. Hydrogen Degradation of Ferrous Alloys. Park Ridge NJ: Noyes Publications (1985) p. 822-862.
8. GR Caskey. Hydrogen Compatibility Handbook for Stainless Steels (DP-1643). EI du Pont Nemours, Savannah River Laboratory, Aiken SC (June 1983).
9. J Qian, J Chen, J Chen, Z Xu, W Wang and C Pan. Corrosion of austenitic stainless steel in liquid lithium. Journal of Nuclear Materials 179-181 (1991) 603-606.
10. S Xiukui, X Jian and L Yiyi. Hydrogen Permeation Behaviour in Austenitic Stainless Steels. Mater Sci Eng A114 (1989) 179-187.
11. MR Louthan and RG Derrick. Hydrogen Transport in Austenitic Stainless Steel. Corros Sci 15 (1975) 565-577.
12. GR Caskey and RD Sisson. Hydrogen Solubility in Austenitic Stainless Steels. Scr Metall 15 (1981) 1187-1190.

13. GR Caskey. Hydrogen Solution in Stainless Steels (DPST-83-425). Savannah River Laboratory, Aiken SC (May 1983).
14. Y Rosenthal, M Mark-Markowitch, A Stern and D Eliezer. Tensile Flow and Fracture Behaviour of Austenitic Stainless Steels after Thermal Aging in a Hydrogen Atmosphere. Mater Sci Eng 67 (1984) 91-107.
15. RE Stoltz. Plane Strain Tensile Testing for Measuring Environment Sensitive Fracture. Metall Trans 12A (1981) 543-545.
16. Y Rosenthal, M Mark-Markowitch, A Stern and D Eliezer. The influence of hydrogen on the plastic flow and fracture behavior of 316L stainless steel. Scr Metall 15 (1981) 861-866.
17. WC Mosley. Effects of Internal Helium on Tensile Properties of Austenitic Stainless Steels and Related Alloys at 820˚C. in: AW Thompson and NR Moody, editor. Hydrogen Effects in Materials. TMS (1996) p. 855-864.
18. MR Dietrich, GR Caskey and JA Donovan. J-Controlled Crack Growth as an Indicator of Hydrogen-Stainless Steel Compatibility. in: IM Bernstein and AW Thompson, editor. Hydrogen Effects in Metals. The Metallurgical Society of AIME (1980) p. 637-643.
19. MG Hebsur and JJ Moore. Influence of inclusions and heat treated microstructure on hydrogen assisted fracture properties of AISI 316 stainless steel. Eng Fract Mech 22 (1985) 93-100.
20. MW Perra. Sustained-Load Cracking of Austenitic Steels in Gaseous Hydrogen. in: MR Louthan, RP McNitt and RD Sisson, editors. Environmental Degradation of Engineering Materials in Hydrogen. Blacksburg VA: Laboratory for the Study of Environmental Degradation of Engineering Materials, Virginia Polytechnic Institute (1981) p. 321-333.
21. PF Azou and JP Fidelle. Very low strain rate hydrogen gas embrittlement (HGE) and fractography of high-strength, mainly austenitic stainless steels. in: MR Louthan, RP McNitt and RD Sisson, editor. Environmental Degradation of Engineering Materials III. The Pennsylvania State University, University Park PA (1987) p. 189-198.
22. J Chene, M Aucouturier, R Arnould-Laurent, P Tison and J-P Fidelle. Hydrogen Transport by Deformation and Hydrogen Embrittlement in Selected Stainless Steels. in: IM Bernstein and AW Thompson, editor. Hydrogen Effects in Metals. The Metallurgical Society of AIME (1980) p. 583-595.
23. EL Raymond and RR Vandervoort. Tensile Properties of Welded or Sensitized 316 Stainless Steel in High-Pressure Hydrogen Gas (UCRL-52128). University of California, Lawrence Livermore Laboratory, Livermore CA (Sept 1976).
24. BP Somerday, JE Smugeresky and JA Brooks. Hydrogen-assisted fracture in LENS-fabricated 316 stainless steel. in: NR Moody, AW Thompson, RE Ricker, GW Was and RH Jones, editors. Hydrogen Effects on Material Behavior and Corrosion Deformation Interactions. Warrendale PA: TMS (2003) p. 499-508.
25. ASTM. Metals and Alloys in the UNIFIED NUMBERING SYSTEM (SAE HS-1086 OCT01; ASTM DS-56H). Society of Automotive Engineers; American Society for Testing and Materials, (2001).
26. RJ Walter and WT Chandler. Effects of High-Pressure Hydrogen on Metals at Ambient Temperature: Final Report (NASA CR-102425). Rocketdyne (report no. R-7780-1) for the National Aeronautics and Space Administration, Canoga Park CA (February 1969).
27. TL Capeletti and MR Louthan. The Tensile Ductility of Austenitic Steels in Air and Hydrogen. J Eng Mater Technol 99 (1977) 153-158.

28. RP Jewitt, RJ Walter, WT Chandler and RP Frohmberg. Hydrogen Environment Embrittlement of Metals (NASA CR-2163). Rocketdyne for the National Aeronautics and Space Administration, Canoga Park CA (March 1973).
29. RE Stoltz, NR Moody and MW Perra. Microfracture Model for Hydrogen Embrittlement of Austenitic Steels. Metall Trans 14A (1983) 1528-1531.
30. AI Gromov and YK Kovneristyi. Permeability, Diffusion, and Solubility of Hydrogen in Cr-Ni and Cr-Mn Austenitic Steels. Met Sci Heat Treat 22 (1980) 321-324.
31. EHV Deventer and VA Maroni. Hydrogen Permeation Characteristics of some Austenitic and Nickel-base Alloys. J Nucl Mater 92 (1980) 103-111.
32. T Tanabe, Y Tamanishi, K Sawada and S Imoto. Hydrogen Transport in Stainless Steels. J Nucl Mater 122&123 (1984) 1568-1572.
33. E Hashimoto and T Kino. Hydrogen Permeation Through Type 316 Stainless Steels and Ferritic Steel for Fusion Reactor. J Nucl Mater 133&134 (1985) 289-291.
34. KS Forcey, DK Ross, JCB Simpson and DS Evans. Hydrogen Transport and Solubility in 316L and 1.4914 Steels for Fusion Reactor Applications. J Nucl Mater 160 (1988) 117-124.
35. DM Grant, DL Cummings and DA Blackburn. Hydrogen in 316 Steel - Diffusion, Permeation and Surface Reaction. J Nucl Mater 152 (1988) 139-145.
36. T Shiraishi, M Nishikawa, T Tamaguchi and K Kenmotsu. Permeation of mulit-component hydrogen isotopes through austenitc stainless steels. J Nucl Mater 273 (1999) 60-65.
37. AJ West and MR Louthan. Dislocation Transport and Hydrogen Embrittlement. Metall Trans 10A (1979) 1675-1682.

Table 1.1.1. Composition of several heats of 316 stainless steel used to study hydrogen effects as well as limits specified by the Unified Numbering System for 316 (UNS 31600) and 316L (UNS 31603).

Heat	Fe	Cr	Ni	Mn	Mo	Si	C	other	Ref.
UNS 31600	Bal	16.00 18.00	10.00 14.00	2.00 max	2.00 3.00	1.00 max	0.08 max	0.030 max S; 0.045 max P	[25]
UNS 31603	Bal	16.00 18.00	10.00 14.00	2.00 max	2.00 3.00	1.00 max	0.03 max	0.030 max S; 0.045 max P	[25]
W69	Bal	17.52	12.45	1.73	2.67	0.56	0.05	0.024 P; 0.022 S; 0.22 Cu	[26]
O76	Bal	17.41	13.51	1.56	2.53	0.71	0.061		[2]
P81	Bal	17.5	13.5	0.06	2.5	0.17	0.05	0.07 N	[20]
R84	Bal	17.7	10.2	1.4	1.6	0.6	0.029	Designated 316L	[14]
A87	Bal	16.9	13.9	1.42	2.5	0.38	0.008	0.003 S; 0.0114 P	[21]
H98	Bal	17.10	10.05	0.66	2.02	0.48	0.040	0.002 S; 0.010 P	[5]

Table 2.1. Permeability and solubility data, averages determined for several austenitic stainless steels. Permeability from Ref. [11] is determined for deuterium and has been corrected here to give permeability of hydrogen by multiplying by the square root of the mass ratio: $\sqrt{2}$. Solubility is assumed to be independent of isotope.

Temperature range (K)	Pressure range (MPa)	$\Phi = \Phi_o \exp(-E_\Phi / RT)$		$S = S_o \exp(-E_S / RT)$		Ref.
		Φ_o $\left(\frac{\text{mol H}_2}{\text{m}\cdot\text{s}\cdot\sqrt{\text{MPa}}}\right)$	E_Φ $\left(\frac{\text{kJ}}{\text{mol}}\right)$	S_o $\left(\frac{\text{mol H}_2}{\text{m}^3\cdot\sqrt{\text{MPa}}}\right)$	E_S $\left(\frac{\text{kJ}}{\text{mol}}\right)$	
423-700	0.1-0.3	1.2×10^{-4}	59.8	179	5.9	[11]
473-703	0.1	2.81×10^{-4}	62.27	488	8.65	[10]

Table 3.1.1.1. Tensile properties of 316 stainless steel tested at room temperature in air, in high-pressure gaseous environments (hydrogen or helium), or thermally precharged in gaseous hydrogen and tested in air.

Material	Thermal precharging	Test environment	Strain rate (s^{-1})	S_y (MPa)	S_u (MPa)	El_u (%)	El_t (%)	RA (%)	Ref.
Not specified	None	69 MPa He	—	214	496	—	68	78	[1, 27]
	None	69 MPa H_2		214	524	—	72	77	
Cold drawn rod, heat W69	None	69 MPa He	0.67 x10^{-3}	441	648	—	59	72	[26, 28]
	None	69 MPa H_2		—	683	—	56	75	
Annealed plate, heat O76	None	Air	3 x10^{-3}	262	579	—	68	78	[2]
	None	69 MPa H_2		221	524	—	72	77	
Annealed sheet	None	Air	0.6 x10^{-3}	263	568	—	90	75	[23]
	None	70 MPa He		248	565	—	85	70	
	None	70 MPa H_2		249	566	—	85	75	
Sensitized thin sheet, heat R84	(1) – Ar	Air	0.5 x10^{-3}	327*	685	62	63	—	[14]
	(1) – H_2	Air		331*	691	43	51	—	

* stress at 0.2% strain

(1) 0.5 MPa hydrogen or argon gas, 873K, 170 hours: measured concentration of ~6 wppm hydrogen (300-325 appm)

Table 3.1.1.2. Effect of internal hydrogen (thermal precharging in high-pressure hydrogen gas) on tensile properties of 316 at low temperatures tested in air, from Ref. [8]; composition and metallurgical condition not given.

Test temperature (K)	Thermal precharging	Flow stress* (MPa)	Ultimate Stress† (MPa)	El_u (%)	El_t (%)	RA (%)
380	None	810	830	7	20	80
	(1)	880	930	11	22	70
273	None	890	1040	21	33	77
	(1)	990	1160	20	32	68
250	None	900	1150	27	40	78
	(1)	1030	1280	24	35	66
200	None	960	1210	24	43	79
	(1)	1100	1410	26	37	65

* true stress at 5% strain
† true stress at maximum load
(1) 69 MPa hydrogen gas, 620 K, 3 weeks

Table 3.1.2.1. Notched tensile properties of type 316 stainless steel tested at room temperature in air and high-pressure hydrogen and helium gas.

Material	Specimen	Thermal precharging	Test environment	Displ. rate (mm/s)	S_y (MPa)	σ_s (MPa)	RA (%)	Ref.
Cold drawn rod, heat W69	(1)	None	69 MPa He	0.4×10^{-3}	441†	1110	18	[26, 28]
		None	69 MPa H_2		—	1110	19	
Annealed sheet	(2)	None	Air	8.3×10^{-3}	345	625	70	[23]
		None	70 MPa He		298	608	80	
		None	70 MPa H_2		331	618	70	

† yield strength of smooth tensile bar
(1) V-notched specimen: 60˚ included angle; minimum diameter = 3.81 mm (0.15 inch); maximum diameter = 7.77 mm (0.306 inch); notch root radius = 0.024 mm (0.00095 inch). Stress concentration factor (K_t) = 8.4.
(2) Dog-bone notched specimens. Gage: length = 13 mm; width = 5 mm; thickness = 2.3 mm. V-notch: 60˚ included angle; depth = 0.6 mm; maximum root radius = 0.05 mm.

Table 3.2.2.1. Threshold stress intensity for type 316 stainless steel in high-pressure hydrogen gas from Ref. [20], heat P81 (data also reported in Ref. [29]).

Condition	S_y (MPa)	RA (%)	Threshold Stress Intensity (MPa $m^{1/2}$)	
			100 MPa H_2	200 MPa H_2
HERF 840˚C, WQ	689	65	NCP 132	NCP 132
WR 600˚C, WQ	903	70	—	99†

HERF = high-energy rate forging, WQ = water quench, WR = warm roll , NCP = no crack propagation at given stress intensity

† did not satisfy plane strain requirements for analysis of stress intensity

Table 4.2.1. Tensile properties of “sensitized” type 316 stainless steel tested at room temperature in air and high-pressure hydrogen and helium gas.

Material	Thermal precharging	Test environment	Strain rate (s^{-1})	S_y (MPa)	S_u (MPa)	El_u (%)	El_t (%)	RA (%)	Ref.
Rolled rod; HT 1323K, 2h, WQ	None	Air	0.6 x10^{-3}	232	558	—	78	80	[23]
	None	70 MPa He		250	658	—	68	80	
	None	70 MPa H_2		230	667	—	65	75	
Rolled rod: HT 1323K, 2h, AC	None	Air	0.6 x10^{-3}	213	558	—	76	80	[23]
	None	70 MPa He		218	639	—	68	75	
	None	70 MPa H_2		248	642	—	70	75	
Rolled rod: HT 1323K, 2h, FC	None	Air	0.6 x10^{-3}	212	561	—	75	80	[23]
	None	70 MPa He		222	666	—	72	80	
	None	70 MPa H_2		240	671	—	68	80	

HT = heat treatment; WQ = water quench; AC = air cool; FC = furnace cool over 24 hours

Table 4.2.2. Notched tensile properties of "sensitized" type 316 stainless steel tested at room temperature in air and high-pressure hydrogen and helium gas.

Material	Specimen	Thermal precharging	Test environment	Displ. rate (mm/s)	S_y (MPa)	σ_s (MPa)	RA (%)	Ref.
Rolled rod; HT 1323K, 2h, WQ	(1)	None	Air	8.3×10^{-3}	411	723	60	[23]
		None	70 MPa He		429	785	65	
		None	70 MPa H_2		412	778	70	
Rolled rod; HT 1323K, 2h, AC	(1)	None	Air	8.3×10^{-3}	374	723	60	[23]
		None	70 MPa He		375	779	65	
		None	70 MPa H_2		387	785	65	
Rolled rod; HT 1323K, 2h, FC	(1)	None	Air	8.3×10^{-3}	376	717	60	[23]
		None	70 MPa He		380	790	70	
		None	70 MPa H_2		382	757	70	

HT = heat treatment; WQ = water quench; AC = air cool; FC = furnace cool over 24 hours

(1) V-notched specimen: 60˚ included angle; minimum diameter = 3.4 mm; maximum diameter = 5 mm; maximum root radius = 0.05 mm.

Table 4.3.1. Tensile properties of type 316 stainless steel welds (full penetration, butt joints) tested at room temperature in air and high-pressure hydrogen and helium gas.

Material	Thermal precharging	Test environment	Strain rate (s^{-1})	S_y (MPa)	S_u (MPa)	El_u (%)	El_t (%)	RA (%)	Ref.
EB welded sheet	None	Air	0.6×10^{-3}	269	562	—	75	70	[23]
	None	70 MPa He		260	574	—	70	70	
	None	70 MPa H_2		256	560	—	75	70	
GTA welded sheet	None	Air	0.6×10^{-3}	273	572	—	80	70	[23]
	None	70 MPa He		287	585	—	85	70	
	None	70 MPa H_2		272	575	—	85	70	

EB = electron beam; GTA = gas tungsten arc

Table 4.3.2. Notched tensile properties of type 316 stainless steel welds (full penetration, butt joints) tested at room temperature in air and high-pressure hydrogen and helium gas.

Material	Specimen	Thermal precharging	Test environment	Displ. rate (mm/s)	S_y (MPa)	σ_s (MPa)	RA (%)	Ref.
EB welded sheet	(1)	None	Air	8.3×10^{-3}	393	622	65	[23]
		None	70 MPa He		343	616	65	
		None	70 MPa H_2		351	621	60	
GTA welded sheet	(1)	None	Air	8.3×10^{-3}	387	607	65	[23]
		None	70 MPa He		342	614	70	
		None	70 MPa H_2		344	611	65	

EB = electron beam; GTA = gas tungsten arc

(1) Dog-bone notched specimens. Gage: length = 13 mm; width = 5 mm; thickness = 2.3 mm. V-notch centered on the weld bead: 60˚ included angle; depth = 0.6 mm; maximum root radius = 0.05 mm.

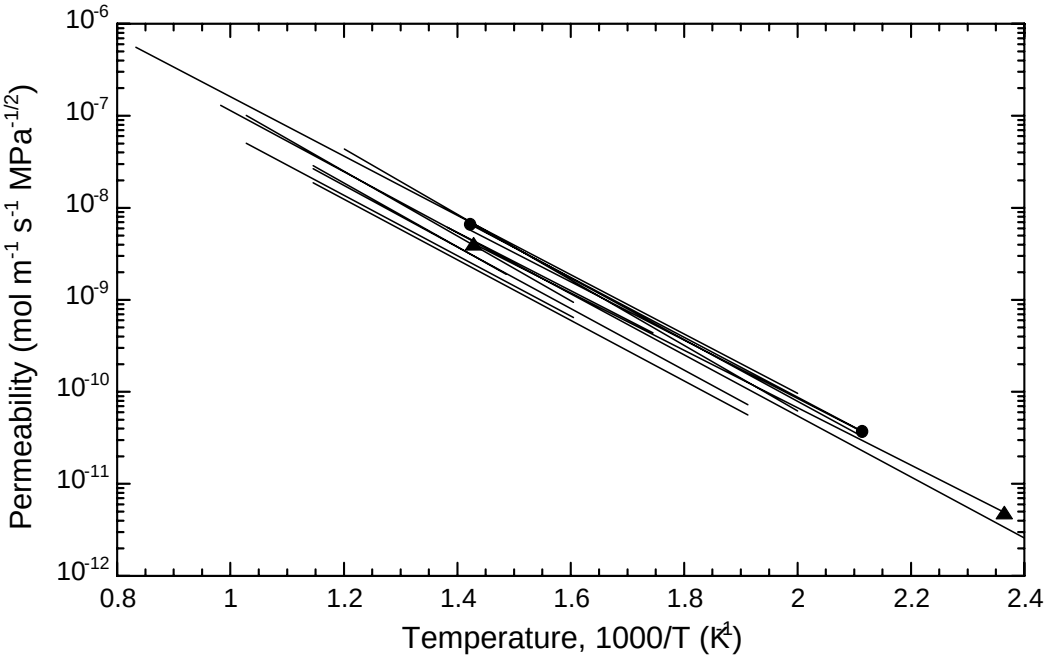

Figure 2.1. Permeability relationships for type 316 stainless steels from a number of references [10, 11, 30-36]. The relationships marked with circles [10] and triangles [11] are averages determined for several austenitic stainless steels, and are given in Table 2.1. Permeability from Ref. [11] is determined for deuterium and has been corrected to give permeability of hydrogen by multiplying by the square root of the mass ratio: $\sqrt{2}$.

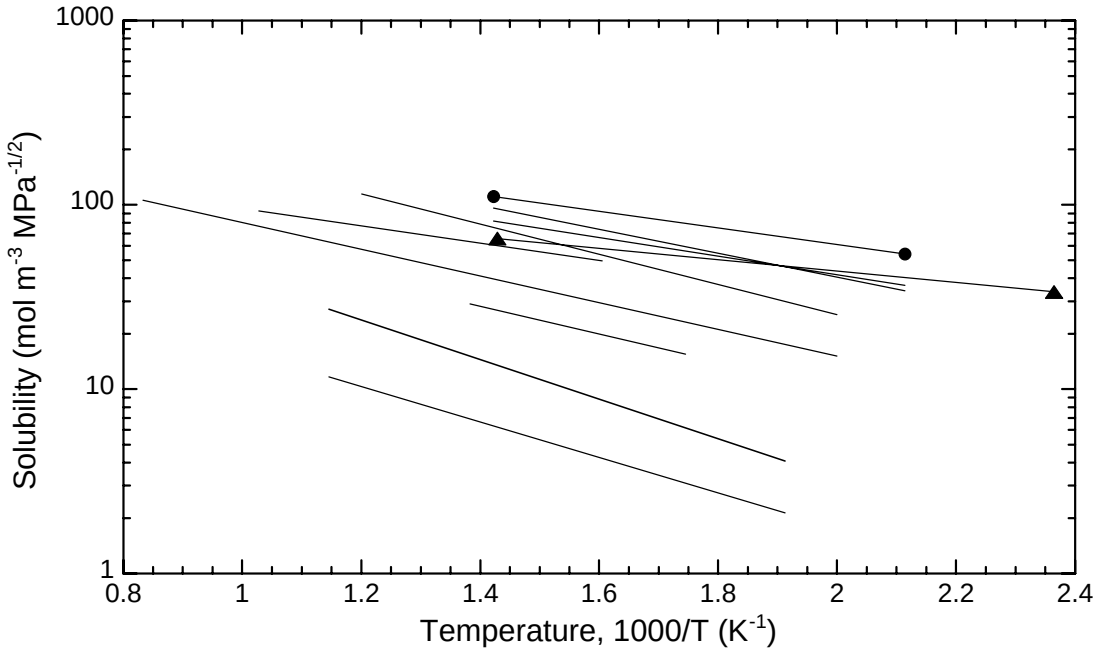

Figure 2.2. Solubility relationships determined from permeability and diffusivity data for type 316 stainless steels from a number of references [10, 11, 30, 32-35]. The relationships marked with circles [10] and triangles [11] are determined from averages for several austenitic stainless steels, and are given in Table 2.1. Data from Ref. [11] are for deuterium.

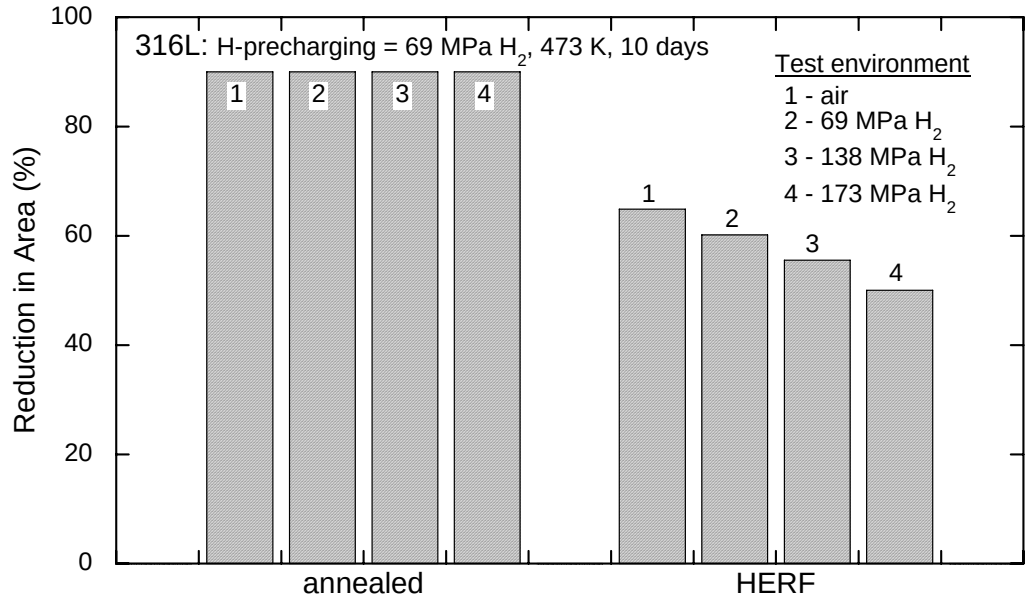

Figure 3.1.1.1. Ductility of smooth tensile specimens of annealed and forged type 316L stainless steel that have been precharged from hydrogen gas at elevated temperature and then tested in hydrogen gas at room temperature. HERF = high energy rate forging [37]

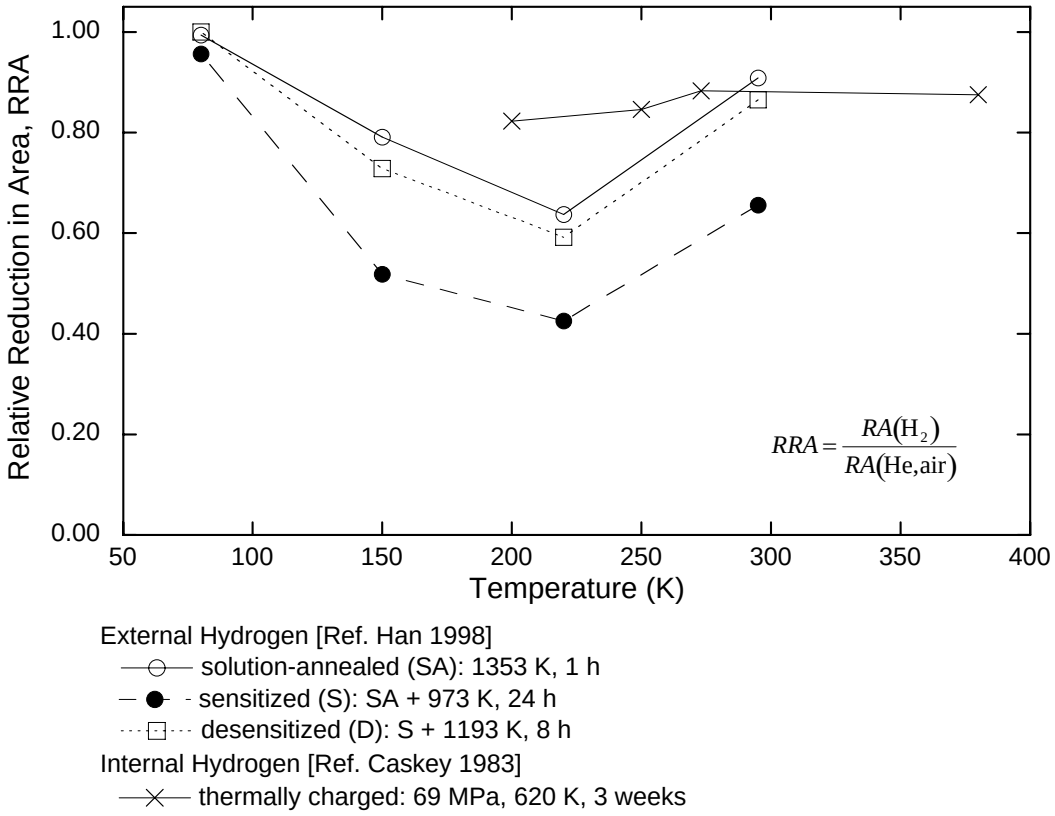

Figure 3.1.1.2. Ductility loss in smooth tensile bars due to hydrogen as a function of temperature, microstructure and hydrogen source. Ref. [5] reports reduction in area in 1 MPa hydrogen gas relative to reduction in area in 1 MPa helium gas at temperatures between 80 and 295 K for annealed and sensitized conditions. Ref. [8] reports reduction in area of thermally precharged specimens tested in air relative to uncharged specimens tested in air between 200 and 380 K (Table 3.1.1.1).

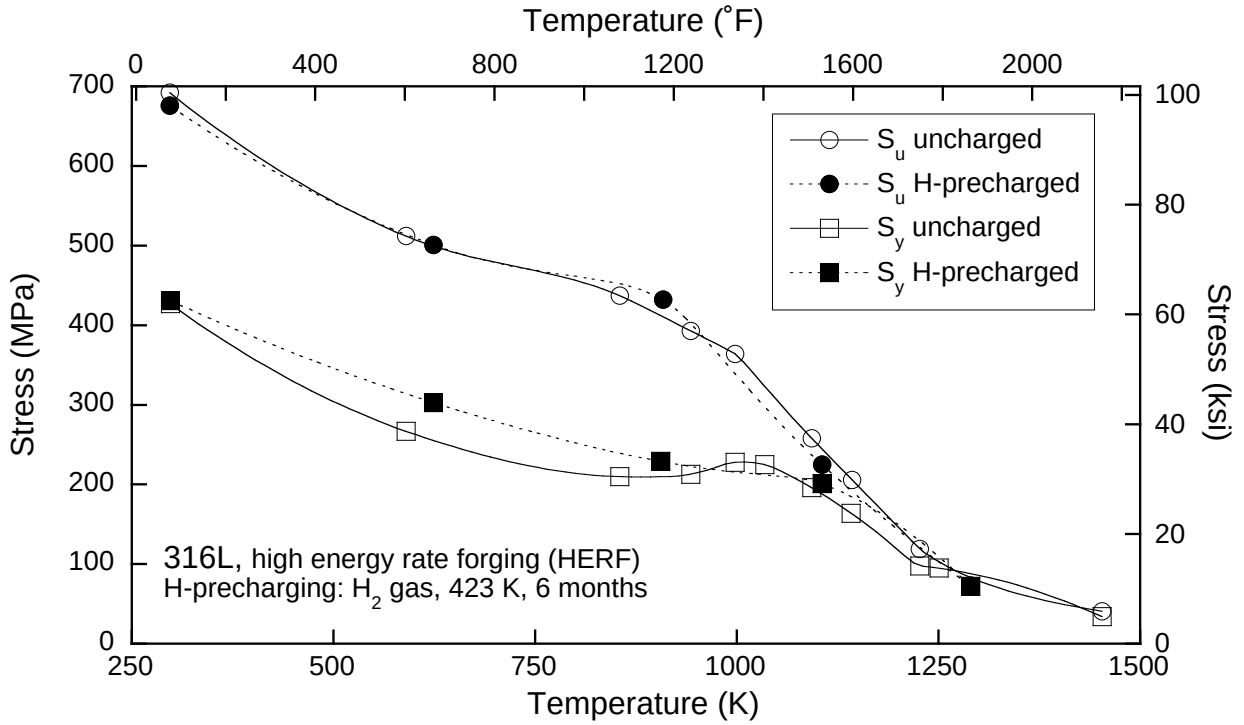

Figure 3.1.1.3. Tensile strength of type 316L stainless steel at elevated temperature in air and thermally precharged in gaseous hydrogen, tested in air. Extension rate = 0.21 mm/s. [17].

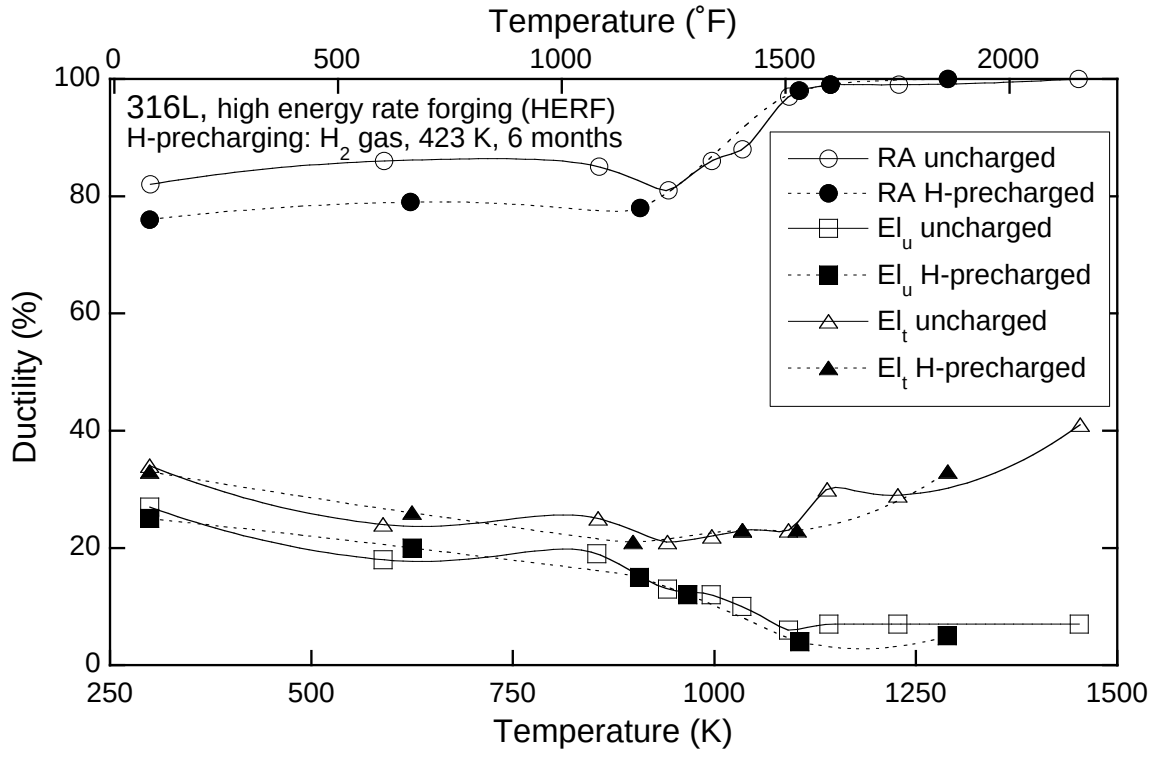

Figure 3.1.1.4. Tensile ductility of type 316L stainless steel at elevated temperature in air and thermally precharged in gaseous hydrogen, tested in air. Extension rate = 0.21 mm/s. [17]

Technical Reference on Hydrogen Compatibility of Materials

Austenitic Steels:

300-Series Stainless Steels,

Stabilized Alloys: Types 321 & 347 (code 2104)

1. General

Types 321 and 347 stainless steels are designed to be single-phase austenite having chromium and nickel contents similar to Types 304 and 316 stainless steels. The alloy chemistries of Types 321 and 347 are distinguished from the other 300-series stainless steels by the addition of titanium (Type 321) or niobium (Type 347). Titanium and niobium are strong carbide formers, and these alloying elements are added to promote the precipitation of intragranular titanium carbides or niobium carbides in preference to intergranular chromium carbides, i.e., $Cr_{23}C_6$. The formation of intergranular chromium carbides in 300-series stainless steels at elevated temperatures is the well-known sensitization phenomenon, which renders grain boundaries more susceptible to corrosion. The Types 321 and 347 stainless steels are referred to as “stabilized” grades because the precipitation of titanium carbides or niobium carbides inhibits sensitization.

The predominant metallurgical variable governing hydrogen-assisted fracture in 300-series stainless steels is alloy composition, particularly nickel content. Results consistently demonstrate that these steels become more susceptible to hydrogen-assisted fracture as nickel content decreases [1-3]. Lower nickel content promotes both strain-induced martensite formation and more severe localized deformation, and both of these metallurgical features have been associated with hydrogen-assisted fracture in 300-series stainless steels. The specifications for nickel in Types 321 and 347 stainless steels are 9-12 wt% and 9-13 wt%, respectively. Based on these specifications, the Types 321 and 347 alloys are expected to be susceptible to hydrogen-assisted fracture when exposed to hydrogen gas, particularly when nickel is at the lower end of the specification.

The limited mechanical property data presented for Types 321 and 347 stainless steels in this chapter suggest that these alloys can be susceptible to hydrogen-assisted fracture, however not all data indicate such susceptibility. The inconsistency in the hydrogen-assisted fracture response reflected by the data may be attributed to materials testing variables, such as loading rate and the method of hydrogen exposure.

1.1 Composition and microstructure

Table 1.1.1 provides the alloy composition specifications for Types 321 and 347 stainless steels. Table 1.1.2 summarizes the alloy compositions and product forms of the Types 321 and 347 stainless steels used in hydrogen compatibility studies that are cited in this chapter.

1.2 Common designations

Type 321: UNS32100 (321), UNS32109 (321H)

Type 347: UNS34700 (347), UNS34709 (347H), UNS34751 (347LN)

2. Permeability, Diffusivity and Solubility

References [1, 4, 5] provide summaries of permeability, diffusivity, and solubility data for hydrogen in austenitic stainless steels. The permeability, diffusivity, and solubility *vs* temperature relationships for 300-series stainless steels are clustered in a band, which includes relationships for Types 321 and 347 stainless steels [1, 5]. The parameters in selected permeability (Φ), diffusivity (D), and solubility (S) relationships for Types 321 and 347 stainless steels are listed in Table 2.1. Also included in Table 2.1 are parameters for relationships that are expected to provide reasonable approximations for all 300-series stainless steels.

3. Mechanical Properties: Effects of Gaseous Hydrogen

3.1 Tensile properties

3.1.1 Smooth tensile properties

Tensile fracture data from smooth specimens strained in high-pressure hydrogen gas demonstrate that Types 321 and 347 stainless steels can be susceptible to hydrogen-assisted fracture, but results are not consistent. Tensile data measured at room temperature are summarized in Table 3.1.1.1. Data for a Type 347 stainless steel (material L72) reveal that testing in 69 MPa hydrogen gas severely degrades ductility, where the reduction in area (RA) in hydrogen is less than 50% of the value in helium. Data for a Type 321 stainless steel (material W73) reveal a more moderate effect of hydrogen on ductility. In this case, the RA measured in 34.5 MPa hydrogen gas was only about 10% less than the value measured in helium. Two possible variables that could account for the difference in the effect of hydrogen on these two materials are the hydrogen gas pressures and alloy compositions; however, a possible effect of alloy composition (in particular nickel content) cannot be assessed since this information was not provided for Type 347 material L72.

A more notable discrepancy in susceptibility to hydrogen-assisted fracture is found for the two Type 347 materials in Table 3.1.1.1. While testing in hydrogen gas causes a reduction in ductility greater than 50% for material L72, hydrogen has no effect on ductility for material H73. Although the hydrogen gas pressures are different for the two materials, both pressures are high enough to cause hydrogen-assisted fracture in 300-series stainless steels. Two other possible sources for the difference in hydrogen-assisted fracture behavior are the alloy compositions and tensile strain rates. Higher strain rates are known to mitigate environment-assisted fracture when straining and environmental exposure are conducted concurrently. The strain rate used during testing of material H73 is relatively high and could mitigate hydrogen-assisted fracture, since the combination of short test duration and low hydrogen diffusivity may limit hydrogen uptake into the material.

Tensile properties measured at low and elevated temperatures are summarized in Tables 3.1.1.2 and 3.1.1.3. A general trend for austenitic stainless steels is that hydrogen effects on

ductility are minimized at low temperature (i.e., < 150 K) and elevated temperature (i.e., > 300 K) and are greatest at a temperature near 200 K [1, 6]. The effect of hydrogen on ductility for the Type 321 steel is similar at room temperature and 144 K; in both cases, the RA measured in hydrogen is about 10-15% less than the value measured in helium. It is possible that hydrogen-assisted fracture would be more pronounced at a temperature near 200 K. For the Type 347 material H73, ductility is not affected by hydrogen gas at 111 K or 950 K. Although these trends for the Type 347 steel may be consistent with expected temperature effects, the high tensile strain rate must be considered in this case.

3.1.2 Notched tensile properties

Results from tests in high-pressure hydrogen gas indicate that hydrogen-assisted fracture may be more severe in notched tensile specimens. The data for Type 321 material W73 strained in 34.5 MPa hydrogen gas at room temperature (Table 3.1.2.1) show that RA is severely degraded (>60% loss in RA) and strength is also reduced (>10% loss in σ_s). These effects of hydrogen on tensile properties are more pronounced compared to results from smooth specimens of Type 321 material W73 (Table 3.1.1.1). The tensile properties for Type 347 material H73 are not affected by hydrogen at room temperature; however, the displacement rate for these tests was relatively high and could have mitigated hydrogen-assisted fracture.

Properties measured from notched tensile specimens at low and elevated temperatures are summarized in Tables 3.1.2.2 and 3.1.2.3. Hydrogen did not affect the tensile properties of Type 321 material W73 at 144 K. This tensile behavior at 144 K is generally consistent with the expectation that hydrogen has a diminished effect on ductility for austenitic stainless steels in the temperature range 100-150 K. The tensile properties of Type 347 material H73 were not significantly affected by hydrogen at either 111 K or 950 K. This trend is consistent with expected temperature effects, but the high displacement rates that were employed in the study of Type 347 [7] must also be considered.

3.2 Fracture mechanics

3.2.1 Fracture toughness

Fracture toughness tests were conducted on Types 321 and 347 stainless steels in 34.5 MPa hydrogen gas [7, 8]. The measurements were conducted using linear elastic fracture mechanics methods; however, these test methods are not appropriate for low-strength, high-toughness materials such as the austenitic stainless steels. Consequently, the test methods and material property data are considered to be not reliable.

3.2.2 Threshold stress intensity factor

Tests to measure the threshold stress intensity factor were conducted for Type 321 stainless steel in 34.5 MPa hydrogen gas [8]. The reported test methods and material property data are considered to be not reliable.

3.3 Fatigue

3.3.1 Low-cycle fatigue

Low-cycle fatigue tests conducted on a Type 347 stainless steel did not reveal a detrimental effect of hydrogen. Smooth, uniaxial specimens from the Type 347 material H73 (Table 1.1.2)

were subjected to tension-compression loading (constant total strain range, where the minimum strain was zero) at a frequency of about 0.06 Hz while exposed to 34.5 MPa hydrogen gas. The strain range *vs* number of cycles to failure data are presented in Figure 3.3.1.1. The strain range *vs* number of cycles to failure data from tests in hydrogen gas and helium gas fall on the same trend line.

3.3.2 High-cycle fatigue

The high-cycle fatigue response of Type 347 stainless steel (material H73) was not affected by hydrogen. Stress-controlled, tension-tension tests were conducted in 34.5 MPa hydrogen gas at a frequency of 20 Hz and a load ratio of 0.1 using smooth, uniaxial specimens. The maximum applied tensile stress *vs* number of cycles to failure data are presented in Figure 3.3.2.1. The tensile stress *vs* number of cycles to failure data from tests in hydrogen gas and helium gas follow the same trend line, but, as discussed in previous sections, the high frequency (i.e., rate) must be considered when interpreting these results.

3.4 Creep

Tests on Type 347 stainless steel did not reveal an effect of hydrogen on creep rupture life. However, the strain to failure during creep was significantly reduced by hydrogen. Smooth specimens of Type 347 material H73 (Table 1.1.2) were subjected to constant applied load in 34.5 MPa hydrogen gas at 950 K. The time to reach various creep strain levels, time to rupture, and strain to failure were measured as a function of applied stress. These data are summarized in Table 3.4.1, and the stress *vs* time to rupture data are plotted in Figure 3.4.1. The limited data show that at a fixed stress level of about 140 MPa the time to rupture was not affected by hydrogen, but the RA measured after testing in hydrogen gas was about 70% lower than the value measured after testing in helium gas.

3.5 Impact

No known published data in hydrogen gas.

3.6 Disk rupture testing

No known published data in hydrogen gas.

4. Fabrication

4.1 Properties of welds

No known published data in hydrogen gas.

5. References

1. GR Caskey. Hydrogen Effects in Stainless Steels. in: RA Oriani, JP Hirth and M Smialowski, editors. Hydrogen Degradation of Ferrous Alloys. Park Ridge NJ: Noyes Publications (1985) p. 822-862.
2. S Fukuyama, M Imade and K Yokogawa. Development of New Material Testing Apparatus in High-Pressure Hydrogen and Evaluation of Hydrogen Gas Embrittlement of Metals. 2007.

3. C SanMarchi, BP Somerday, X Tang and GH Schiroky. Effects of Alloy Composition and Strain Hardening on Tensile Fracture of Hydrogen-Precharged Type 316 Stainless Steels. International Journal of Hydrogen Energy 33 (2008) 889-904.
4. C San Marchi, BP Somerday and SL Robinson. Permeability, Solubility and Diffusivity of Hydrogen Isotopes in Stainless Steels at High Gas Pressure. Int J Hydrogen Energy 32 (2007) 100-116.
5. XK Sun, J Xu and YY Li. Hydrogen Permeation Behaviour in Austenitic Stainless Steels. Mater Sci Eng A114 (1989) 179-187.
6. L Zhang, M Wen, M Imade, S Fukuyama and K Yokogawa. Effect of Nickel Equivalent on Hydrogen Gas Embrittlement of Austenitic Stainless Steels Based on Type 316 at Low Temperatures. Acta Materialia 56 (2008) 3414-3421.
7. JA Harris and MC VanWanderham. Properties of Materials in High Pressure Hydrogen at Cryogenic, Room, and Elevated Temperatures: Annual Report. Pratt & Whitney Aircraft (NASA contract NAS8-26191), West Palm Beach, FL (1971).
8. RJ Walter and WT Chandler. Influence of Gaseous Hydrogen on Metals: Final Report. Rocketdyne (NASA contract NAS8-25579), Canoga Park, CA (1973).
9. ASTM. ASTM DS-56H, Metals and Alloys in the UNIFIED NUMBERING SYSTEM (SAE HS-1086 OCT01). 2001.
10. JA Harris and MC VanWanderham. Properties of Materials in High Pressure Hydrogen at Cryogenic, Room, and Elevated Temperatures: Final Report. Pratt & Whitney Aircraft (NASA contract NAS8-26191), West Palm Beach, FL (1973).
11. XK Sun, J Xu and YY Li. Hydrogen permeation behavior in metastable austenitic stainless steels 321 and 304. Acta Metall 37 (1989) 2171-2176.
12. EH Van Deventer and VA Maroni. Hydrogen Permeation Characteristics of some Austenitic and Nickel-base Alloys. J Nucl Mater 92 (1980) 103-111.
13. MR Louthan and G Caskey. Hydrogen Transport and Embrittlement in Structural Metals. Int J Hydrogen Energy 1 (1976) 291-305.
14. MR Louthan, GR Caskey, JA Donovan and DE Rawl. Hydrogen Embrittlement of Metals. Mater Sci Eng 10 (1972) 357-368.

Table 1.1.1. Allowable composition ranges (wt%) for Types 321 and 347 stainless steels [9].

UNS No.	AISI No.	Fe	Cr	Ni	Mn	Nb	Ti	Si	C	other
S32100	321	Bal	17.00 19.00	9.00 12.00	2.00 max	—	5xC min	1.00 max	0.08 max	0.030 max S; 0.045 max P
S34700	347	Bal	17.00 19.00	9.00 13.00	2.00 max	10xC min	—	1.00 max	0.08 max	0.030 max S; 0.045 max P

Table 1.1.2. Compositions (wt%) of Types 321 and 347 stainless steels in hydrogen compatibility studies.

Heat	Product Form	Fe	Cr	Ni	Mn	Nb	Ti	Si	C	other	Ref.
S89 321	sheet (A 1223 K/4 h + FC)	Bal	17.96	8.08	0.49	—	0.51	0.84	0.053	0.010 S; 0.032 P	[5]
W73 321	32 mm plate (HR + A)	Bal	17.80	10.45	1.46	—	0.51	0.58	0.06	0.015 S; 0.026 P	[8]
H73 347	19 mm D bar (A 1297 K/1 h + AC + CF)	Bal	18.4	10.10	2.0	0.83*	—	0.94	0.06	0.010 S; P nr	[10]

nr = not reported; A = anneal; AC = air cool; CF = cold finished; D = diameter; FC = furnace cool; HR = hot rolled

* Nb+Ta

Table 2.1. Parameters in permeability, diffusivity and solubility relationships for hydrogen in Types 321 and 347 austenitic stainless steels.

Material	Temperature Range (K)	Pressure Range (MPa)	$\Phi = \Phi_o \exp(-E_\Phi / RT)$		$D = D_o \exp(-E_D / RT)$		$S = S_o \exp(-E_S / RT)$		Ref.
			Φ_o $\left(\frac{\text{mol H}_2}{\text{m}\cdot\text{s}\cdot\text{MPa}^{1/2}}\right)$	E_Φ $\left(\frac{\text{kJ}}{\text{mol}}\right)$	D_o $\left(\frac{\text{m}^2}{\text{s}}\right)$	E_D $\left(\frac{\text{kJ}}{\text{mol}}\right)$	S_o $\left(\frac{\text{mol H}_2}{\text{m}^3\cdot\text{MPa}^{1/2}}\right)$	E_S $\left(\frac{\text{kJ}}{\text{mol}}\right)$	
S89 321	473-703	0.1	$2.44\text{x}10^{-4}$	62.70	$4.61 \text{ x } 10^{-7}$	53.79	529	8.91	[5, 11]
321 *	497-933	$0.6 \text{ x } 10^{-6}$ - $1.2 \text{ x } 10^{-2}$	$8.53\text{x}10^{-5}$	59.4	—	—	—	—	[12]
347 *	823-973	—	$3.59\text{x}10^{-4}$	69.0	$2.55\text{x}10^{-6}$	61.9	141	7.1	[1]
300-series stainless steels	—	—	$1.2\text{x}10^{-4}$	59.8	$8.9 \text{ x } 10^{-7}$	53.9	135	5.9	[4]

* Alloy composition not reported.

Table 3.1.1.1. Smooth tensile properties of Types 321 and 347 stainless steels tested at room temperature in hydrogen gas. Properties in air and/or helium gas are included for comparison.

Material	Thermal precharging	Test environment	Strain rate (s^{-1})	S_y (MPa)	S_u (MPa)	El_u (%)	El_t (%)	RA (%)	Ref.
W73 321	None	Air	0.067 x10^{-3} *	221	600	—	77	71	[8]
		34.5 MPa He		200	579	—	63	66	
		34.5 MPa H_2		255	593	—	64	60	
H73 347	None	34.5 MPa He	0.67 x10^{-3} *,†	461	695	—	37	70	[7]
		34.5 MPa H_2		455	752	—	40	71	
L72‡ 347	None	69 MPa He	—	206	572	—	60	80	[13, 14]
		69 MPa H_2		200	510	—	38	37	

* Estimated from displacement rate and specimen gauge length.
† Strain rate up to S_y. Strain rate increased to 1.3x10^{-3} s^{-1} between S_y and S_u.
‡ Alloy composition not reported.

Table 3.1.1.2. Smooth tensile properties of Types 321 and 347 stainless steels tested at low temperature in hydrogen gas. Properties in helium gas are included for comparison.

Material	Thermal precharging	Test environment	Temp (K)	Strain rate (s^{-1})	S_y (MPa)	S_u (MPa)	El_u (%)	El_t (%)	RA (%)	Ref.
W73 321	None	34.5 MPa He	144	0.067 x10^{-3} *	—	855	—	48	67	[8]
		34.5 MPa H_2			—	841	—	43	56	
H73 347	None	34.5 MPa He	111	0.67 x10^{-3} *,†	720	1378	—	43	64	[7]
		34.5 MPa H_2			664	1267	—	43	64	

* Estimated from displacement rate and specimen gauge length.
† Strain rate up to S_y. Strain rate increased to 1.3x10^{-3} s^{-1} between S_y and S_u.

Table 3.1.1.3. Smooth tensile properties of Type 347 stainless steel tested at elevated temperature in hydrogen gas. Properties in helium gas are included for comparison.

Material	Thermal precharging	Test environment	Temp. (K)	Strain rate (s^{-1})	S_y (MPa)	S_u (MPa)	El_u (%)	El_t (%)	RA (%)	Ref.
H73 347	None	34.5 MPa He	950	0.67 x10^{-3} *,†	397	414	—	25	67	[7]
		34.5 MPa H_2			397	424	—	25	67	

* Estimated from displacement rate and specimen gauge length.
† Strain rate up to S_y. Strain rate increased to 1.3x10^{-3} s^{-1} between S_y and S_u.

Table 3.1.2.1. Notched tensile properties of Types 321 and 347 stainless steels tested at room temperature in hydrogen gas. Properties in helium gas are included for comparison.

Material	Specimen	Thermal precharging	Test environment	Displ. rate (mm/s)	S_y † (MPa)	σ_s (MPa)	RA (%)	Ref.
W73 321	(a)	None	34.5 MPa He	~0.4 x10^{-3}	200	779	6.4	[8]
		None	34.5 MPa H_2		255	683	2.3	
H73 347	(b)	None	34.5 MPa He	42 x10^{-3}	461	1184	20	[7]
		None	34.5 MPa H_2		455	1169	18	

† yield strength of smooth tensile bar

(a) V-notched specimen: 60˚ included angle; minimum diameter = 3.81 mm; maximum diameter = 7.77 mm; notch root radius = 0.024 mm. Elastic stress concentration factor, K_t = 8.4.

(b) V-notched specimen: 60˚ included angle; minimum diameter = 8.00 mm; maximum diameter = 12.70 mm; notch root radius = 0.051 mm. Elastic stress concentration factor, K_t = 8.4.

Table 3.1.2.2. Notched tensile properties of Types 321 and 347 stainless steels tested at low temperature in hydrogen gas. Properties in helium gas are included for comparison.

Material	Specimen	Thermal precharging	Test environment	Temp. (K)	Displ. rate (mm/s)	S_y † (MPa)	σ_s (MPa)	RA (%)	Ref.
W73 321	(a)	None	34.5 MPa He	144	~0.4 x10^{-3}	—	986	12	[8]
		None	34.5 MPa H_2			—	972	12	
H73 347	(b)	None	34.5 MPa He	111	42 x10^{-3}	720	1579	12	[7]
		None	34.5 MPa H_2			664	1540	12	

† yield strength of smooth tensile bar

(a) V-notched specimen: 60˚ included angle; minimum diameter = 3.81 mm; maximum diameter = 7.77 mm; notch root radius = 0.024 mm. Elastic stress concentration factor, K_t = 8.4.

(b) V-notched specimen: 60˚ included angle; minimum diameter = 8.00 mm; maximum diameter = 12.70 mm; notch root radius = 0.051 mm. Elastic stress concentration factor, K_t = 8.4.

Table 3.1.2.3. Notched tensile properties of Type 347 stainless steel tested at elevated temperature in hydrogen gas. Properties in helium gas are included for comparison.

Material	Specimen	Thermal precharging	Test environment	Temp. (K)	Displ. rate (mm/s)	S_y † (MPa)	σ_s (MPa)	RA (%)	Ref.
H73 347	(b)	None	34.5 MPa He	950	42 x10^{-3}	397	713	19	[7]
		None	34.5 MPa H_2			397	693	16	

† yield strength of smooth tensile bar.

(b) V-notched specimen: 60˚ included angle; minimum diameter = 8.00 mm; maximum diameter = 12.70 mm; notch root radius = 0.051 mm. Elastic stress concentration factor, K_t = 8.4.

Table 3.4.1. Creep properties of Type 347 stainless steel tested at 950 K in hydrogen gas. Properties in helium gas are included for comparison.

Material	Stress (MPa)	Test environment	Time to creep (hr)			Time to rupture (hr)	El (%)	RA (%)	Ref.
			0.5%	1.0%	2.0%				
H73 347	279	34.5 MPa He	<0.1	0.15	0.2	0.3	8.7	48	[7]
	134	34.5 MPa He	3.0	9.0	16.5	24.5	8.5	44	
	137	34.5 MPa H_2	8.0	14.0	21.0	23.9	2.6	14	
	81	34.5 MPa H_2	60.0	115.0	187.0	>187.0	NCR	NCR	

NCR = no creep rupture

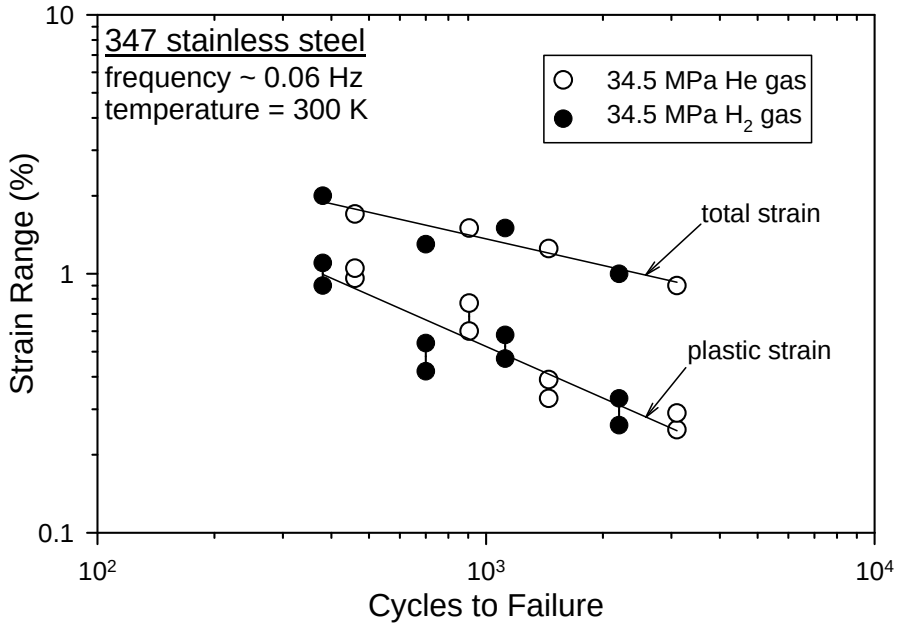

Figure 3.3.1.1. Applied strain range *vs* number of cycles to failure data for Type 347 stainless steel (material H73) [7]. Two plots are presented for one set of results: the data are plotted using the plastic strain range as well as the total strain (elastic + plastic) range. Two symbols are plotted for each data point on the plastic strain range plot, where the symbols indicate the variation in plastic strain during the test. Data are shown for tests conducted in both hydrogen gas and helium gas.

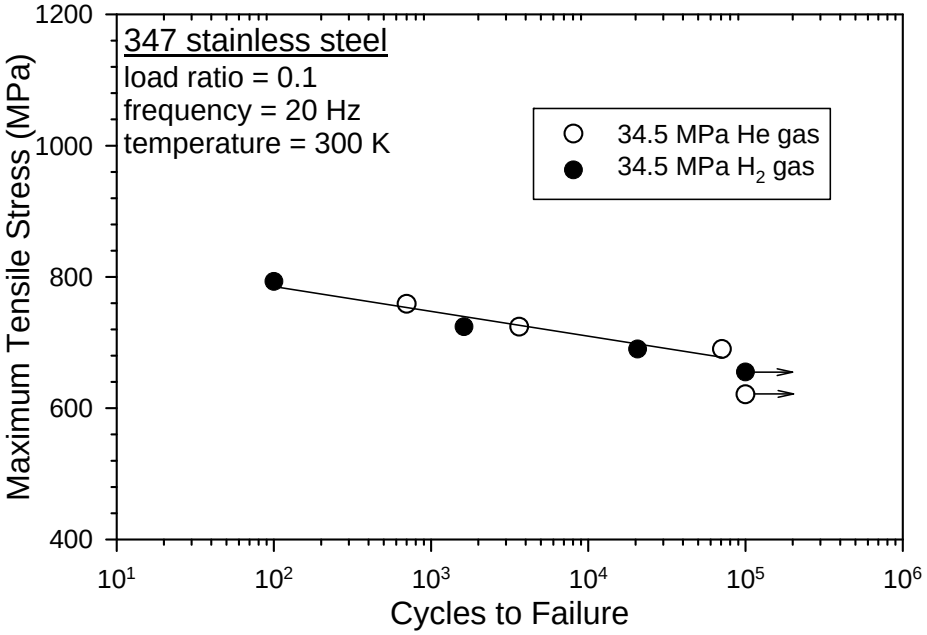

Figure 3.3.2.1. Maximum tensile stress *vs* number of cycles to failure data for Type 347 stainless steel (material H73) [7]. Data are shown for tests conducted in both hydrogen gas and helium gas. The test specimens at the two lowest stress levels did not fail and tests were terminated at 10^5 cycles.

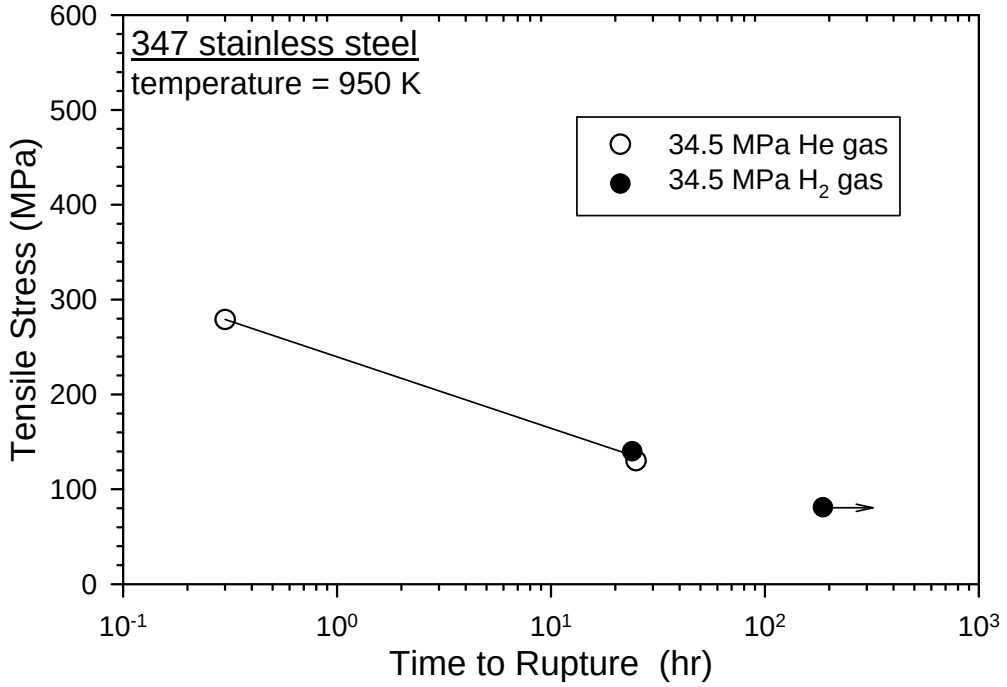

Figure 3.4.1. Tensile stress *vs* time to rupture data for Type 347 stainless steel (material H73) [7]. Data are shown for tests conducted in both hydrogen gas and helium gas. The test specimen at the lowest stress level did not fail and the test was terminated at about 200 hr.

Technical Reference on Hydrogen Compatibility of Materials

Nitrogen-Strengthened Stainless Alloys:

22-13-5 (code 2201)

1. General

Alloy 22-13-5 is a nitrogen-strengthened austenitic stainless steel that combines excellent corrosion resistance with high yield strength, ductility and fracture toughness at room temperature and cryogenic temperatures. Yield strengths greater than 1000 MPa can be achieved in this alloy by warm-working. Although ferrite is typically not observed in bar stock, solidification of primary ferrite is thought to be important for high quality fusion welds and is observed in welded joints.

Although very little data exist for 22-13-5 in gaseous hydrogen environments, published tensile data indicate that this alloy is not strongly affected by hydrogen gas environments even at cryogenic temperatures. This is attributed to the relatively high stacking fault energy in this alloy [1, 2], which promotes cross slip and homogeneous deformation.

1.1 Composition and microstructure

Table 1.1.1 lists the UNS composition for 22-13-5 and the compositions of several heats of 22-13-5 used to study hydrogen effects.

1.2 Common designations

Nitronic 50, XM-19, UNS S20910

2. Permeability, Diffusivity and Solubility

Ref. [3] provides a summary of data for other stainless steels. It is important to note that permeability and solubility data are generally extrapolated from temperatures above ambient and pressures of a few atmospheres or less; as a consequence, there is a significant amount of scatter amongst the data. The temperature dependent permeability is typically expressed as

$$\phi = \phi_o \exp\left(-E_\phi / RT\right) \tag{1}$$

Louthan and Derrick found that a single set of constants described the permeability of deuterium in a number of austenitic stainless steels [4]; these constants are:

$$\phi_o = 1.19\text{x}10^{-4} \frac{\text{mol H}_2}{\text{m} \cdot \text{s} \cdot \sqrt{\text{MPa}}} \text{ and } E_\phi = 59.8 \text{ kJ/mol}. \tag{2}$$

The pre-exponential factor has been corrected to account for the difference between deuterium and hydrogen by multiplying by $\sqrt{2}$. Although the permeability of hydrogen in 22-13-5 has not been measured, these relationships provide an estimate.

The solubility of hydrogen in steels is assumed to follow Sievert's Law: hydrogen concentration in the steel is proportional to the square root of the fugacity of the hydrogen gas. The proportionality constant, Sievert's parameter (S) has the standard Arrhenius form:

$$S = S_o \exp\left(-E_S / RT\right) \tag{3}$$

The solubility in nitrogen-strengthened austenitic stainless steel appears to be about 50 to 100% higher than the 300-series stainless steels [5, 6]. Thus, the solubility in 22-13-5 is estimated here by taking the temperature dependence proposed by Louthan and Derrick [4] for a variety of austenitic stainless steels and a pre-exponential factor based on measured uniform hydrogen concentrations in 22-13-5 that have been reported in the literature [2, 6, 7]:

$$S_o = 214 \frac{\text{mol H}_2}{\text{m}^3 \cdot \sqrt{\text{MPa}}} \text{ and } E_S = 5.8 \text{ kJ/mol} \tag{4}$$

These values are offered as a general indicator of solubility and may not be accurate for all conditions; hydrogen concentrations quoted elsewhere in this document are values that have been reported in the respective reference. A thorough study of solubility in this alloy is needed, including analysis of the effect of composition on solubility, in particular the effect of nitrogen.

3. Mechanical Properties: Effects of Gaseous Hydrogen

3.1 Tensile properties

3.1.1 Smooth tensile properties

This alloy generally shows low degradation of tensile ductility due to hydrogen for temperatures from 77 K to 380 K. In some cases, hydrogen increased yield strength, although this effect is small. Modest decreases in strength have also been reported, although not more than 10% loss. Basic tensile properties of hydrogen-exposed 22-13-5 from a number of studies at room temperature are summarized in Table 3.1.1.1. Figure 3.1.1.1 shows the effects of both internal and external sources of hydrogen on the tensile properties of two forgings (these data are also in Table 3.1.1.1). An important exception to the trends in Table 3.1.1.1 is shown in Figure 3.1.1.2: significant ductility losses were reported for high energy rate forging (HERF) samples that were thermally precharged in hydrogen gas and then tested in high pressure hydrogen gas at room temperature. The fracture mode remained ductile, dominated by microvoid coalescence, at pressures of hydrogen up to 173 MPa, with the lowest measured RA of 35% [8]. Details of the microstructure and mechanical properties are not provided in that study.

The effect of cryogenic temperature is shown in Figure 3.1.1.3 and 3.1.1.4 for 22-13-5 thermally charged with hydrogen.

3.1.2 Notched tensile properties

This alloy shows some ductility loss due to hydrogen in notched tensile specimens precharged with high concentrations of hydrogen. The reduction of area measured in notched tensile specimens is shown in Fig. 3.1.2.1 for two heats of 22-13-5 subjected to two heat treatments in the uncharged and thermally precharged conditions. These data also demonstrate the importance of microstructural control as the loss in ductility due to heat treating at 1073 K is

greater than the loss due to hydrogen exposure in material heat treated at 1273 K, see section 4.2. The fracture mode, microvoid coalescence, was not noticeably affected by precharging with hydrogen in these specimens.

Notched tensile data for cryogenic temperatures are shown in Figure 3.1.2.2; these data show less ductility loss, possibly due to lower hydrogen concentrations.

3.2 Fracture mechanics

3.2.1 Fracture toughness

The effect of hydrogen on fracture properties was found to vary substantially in forged materials depending on orientation of the propagating crack relative to the microstructure [9]. The J-integral fracture toughness at maximum load J_m and the tearing modulus at maximum load dJ/da (change in J with crack length) are more susceptible to hydrogen effects when the crack is propagating perpendicular to forging flow lines in forged bar as compared to propagating parallel to forging flow lines, Table 3.2.1.1. Even though the values of J_m and dJ/da are affected by hydrogen for cracks propagating across flow lines, the hydrogen-affected values remain greater than the values for cracks propagating along flow lines in material not exposed to hydrogen.

3.2.2 Threshold stress- intensity factor

No crack propagation was observed in wedge-opening load (WOL) testing in hydrogen gas at a stress intensity of 132 MPa $m^{1/2}$ [10]. The material, P81 Table 1.1.1, was high-energy rate forged at 980˚C, and had a yield strength of 724 MPa. Crack propagation was nominally parallel to the flow lines of the forging. The WOL specimen was loaded in 200 MPa hydrogen gas at ambient temperature for 5000 hours. The testing procedure generally followed the requirements of ASTM E 1681-99 [11].

3.3 Fatigue

No known published data in hydrogen gas.

3.4 Creep

No known published data in hydrogen gas.

3.5 Impact

Charpy impact toughness was not affected by thermally precharging 22-13-5 (68 wppm uniform hydrogen) at room temperature and 77 K [7]. The tensile properties of the material tested in impact are given in Figure 3.1.1.4.

3.6 Disk Rupture Tests

Disk rupture tests of 22-13-5, heat A87, and other nitrogen-strengthened stainless steels display slight to moderate reductions in rupture pressure when pressurized with hydrogen compared to helium [12].

4. Fabrication

4.1 Primary processing

Microstructural features such as flow lines can have a significant effect on fracture toughness in air and in a hydrogen environment; therefore, microstructural orientation is an important design consideration.

4.2 Heat treatment

Control of processing temperatures is important, as there is some evidence that brittle second phases can form at temperatures less than 1123 K [2]. In similar alloys such as 21-6-9, ferrite may rapidly transform to brittle σ-phase in the temperature range of about 923 K to 1173 K [13]. These microstructural issues are independent of hydrogen exposure, but could exacerbate hydrogen-assisted fracture.

4.3 Properties of welds

Detailed microstructural investigation of 22-13-5 gas tungsten arc (GTA) welds tested in hydrogen gas are presented in Ref. [14, 15]. Fracture of the welds was by microvoid coalescence and hydrogen precharging did not significantly alter the morphology of the fracture surfaces. The tensile properties are listed in Table 4.1.1.

5. References

1. BC Odegard, JA Brooks and AJ West. The Effect of Hydrogen on Mechanical Behavior of Nitrogen-Strengthened Stainless Steel. in: AW Thompson and IM Bernstein, editors. Effect of Hydrogen on Behavior of Materials. New York: TMS (1976) p. 116-125.
2. BP Somerday and SL Robinson. H- and Tritium-Assisted Fracture in N-Strengthened, Austentitic Stainless Steel. JOM - J Min Met Mater Soc 55 (2003) 51-55.
3. GR Caskey. Hydrogen Effects in Stainless Steels. in: RA Oriani, JP Hirth and M Smialowski, editors. Hydrogen Degradation of Ferrous Alloys. Park Ridge NJ: Noyes Publications (1985) p. 822-862.
4. MR Louthan and RG Derrick. Hydrogen Transport in Austenitic Stainless Steel. Corrosion Science 15 (1975) 565-577.
5. GR Caskey and RD Sisson. Hydrogen Solubility in Austenitic Stainless Steels. Scr Metall 15 (1981) 1187-1190.
6. GR Caskey. Hydrogen Damage in Stainless Steel. in: MR Louthan, RP McNitt and RD Sisson, editors. Environmental Degradation of Engineering Materials in Hydrogen. Blacksburg VA: Laboratory for the Study of Environmental Degradation of Engineering Materials, Virginia Polytechnic Institute (1981) p. 283-302.
7. L Ma, G Liang, J Tan, L Rong and Y Li. Effect of Hydrogen on Cryogenic Mechanical Properties of Cr-Ni-Mn-N Austenitic Steels. J Mater Sci Technol 15 (1999) 67-70.
8. AJ West and MR Louthan. Dislocation Transport and Hydrogen Embrittlement. Metall Trans 10A (1979) 1675-1682.
9. GR Caskey. Hydrogen Compatibility Handbook for Stainless Steels (DP-1643). EI du Pont Nemours, Savannah River Laboratory, Aiken SC (June 1983).
10. MW Perra. Sustained-Load Cracking of Austenitic Steels in Gaseous Hydrogen. in: MR Louthan, RP McNitt and RD Sisson, editors. Environmental Degradation of Engineering

Materials in Hydrogen. Blacksburg VA: Laboratory for the Study of Environmental Degradation of Engineering Materials, Virginia Polytechnic Institute (1981) p. 321-333.
11. ASTM E 1681-99, Standard Test Method for Determining Threshold Stress Intensity Factor for Environment-Assisted Cracking of Metallic Materials. American Society for Testing and Materials (1999).
12. PF Azou and JP Fidelle. Very low strain rate hydrogen gas embrittlement (HGE) and fractography of high-strength, mainly austenitic stainless steels. in: MR Louthan, RP McNitt and RD Sisson, editor. Environmental Degradation of Engineering Materials III. The Pennsylvania State University, University Park PA (1987) p. 189-198.
13. CL Ferrera. The Formation and Effects of Sigma Phase in 21-6-9 Stainless Steel (PMT-87-0017). Rockwell International, Rocky Flats Plant, Golden CO (November 1987).
14. JA Brooks and AJ West. Hydrogen Induced Ductility Losses in Austenitic Stainless Steel Welds. Metall Trans 12A (1981) 213-223.
15. JA Brooks, AJ West and AW Thompson. Effect of Weld Composition and Microstructure on Hydrogen Assisted Fracture of Austenitic Stainless Steels. Metall Trans 14A (1983) 75-84.
16. ASTM. Metals and Alloys in the UNIFIED NUMBERING SYSTEM (SAE HS-1086 OCT01; ASTM DS-56H). Society of Automotive Engineers; American Society for Testing and Materials, (2001).
17. BC Odegard and AJ West. On the Thermo-Mechanical Behavior and Hydrogen Compatibility of 22-13-5 Stainless Steel. Mater Sci Eng 19 (1975) 261-270.
18. TL Capeletti and MR Louthan. The Tensile Ductility of Austenitic Steels in Air and Hydrogen. J Eng Mater Technol 99 (1977) 153-158.

Table 1.1.1. Composition of several heats of 22-13-5 used to study hydrogen effects as well as specification limits.

heat	Fe	Cr	Ni	Mn	Mo	Si	C	N		Ref.
UNS S20910	Bal	20.50 23.50	11.50 13.50	4.00 6.00	1.50 3.00	1.00 max	0.06 max	0.20 0.40	0.10-0.30 Nb; 0.10-0.30 V; 0.030 max S; 0.060 max P	[16]
O75	Bal	22.15	12.74	5.26	2.20	0.50	0.050	0.34	0.23 Nb; 0.26 V; 0.006 S; 0.019 P	[17]
O76	Bal	23.00	12.98	4.68	1.75	0.36	0.050	0.38		[1]
P81	Bal	23.11	12.91	4.76	1.75	0.38	0.05	0.39	0.18 Nb	[10]
C83	Bal	21.48	12.36	5.44	2.12	0.42	0.05	0.25	0.19 Nb; 0.2 V; 0.010 S; 0.015 P	[9]
B83*	Bal	22.9	12.9	4.6	1.8	0.42	0.05	0.35	0.008 S; 0.012 P	[15]
A87	Bal	21.6	12.2	5.1	2.1	0.38	0.051	0.27	0.007 S; 0.02 P	[12]
S03a	Bal	21.26	11.87	4.67	2.20	—	0.036	0.276		[2]
S03b	Bal	21.32	13.11	5.02	2.04	—	0.013	0.30		[2]

* composition in GTA weld fusion zone

Table 3.1.1.1. Tensile properties of 22-13-5 thermally precharged and tested in hydrogen gas at room temperature.

Material	Thermal precharging	Test environment	Strain rate (s^{-1})	S_y (MPa)	S_u (MPa)	El_u (%)	El_t (%)	RA (%)	Ref.
Bar, as-received, heat C83	None	Air	—	440	710	—	43	72	[6, 9, 18]
	None	69 MPa He		400	680	—	47	74	
	None	69 MPa H_2		400	680	—	45	73	
Bar, as-received	None	Air	—	800*	1190†	32	41	69	[9]
	(1)	Air		820*	1240†	33	44	65	
Annealed plate, heat O76	None	Air	3 x10^{-3}	586	938	—	51	67	[1]
	(2)	69 MPa H_2		579	951	—	54	68	
Warm-worked bar, heat O75	None	Air	0.3 x10^{-3}	841	958	30	—	66	[17]
	None	69 MPa H_2		841	986	27	—	67	
	(2)	Air		855	1007	27	—	64	
	(2)	69 MPa H_2		924	1082	23	—	62	
High energy rate forging (HERF), heat O75	None	Air	0.3 x10^{-3}	1269	1317	9	—	20	[17]
	None	69 MPa H_2		1202	1276	7	—	29.5	
	(2)	Air		1262	1310	10	—	15.5	
	(2)	69 MPa H_2		1310	1365	10	—	20	

* true stress at 5% strain

† true stress at maximum load

(1) 69 MPa hydrogen gas, 620 K, 3 weeks

(2) 24 MPa hydrogen gas, 473 K, 10.5 days: calculated surface concentration of ~50 wppm hydrogen (~2500 appm)

Table 3.2.1.1. Fracture toughness parameters for 22-13-5 tested in high-pressure hydrogen gas. Note: thermal precharging was performed with deuterium gas.

Material	Thermal precharging	Test environment	J_m (kJ/m^2)	dJ/da (MPa)	Ref.
High energy rate forging (HERF) bar, parallel†	None	69 MPa He	32	176	[9]
	None	69 MPa H_2	23	137	
	(1)	69 MPa H_2	33	211	
HERF bar, perpendicular†	None	69 MPa He	936	360	[9]
	None	69 MPa H_2	107	209	
	(1)	69 MPa H_2	181	264	

† Precracked C-shaped specimens were machined from forged bar in an orientation such that the crack propagated nominally parallel to flow lines in the bar cross section, and 90˚ from this orientation such that the crack propagated nominally across (or perpendicular to) the forging flow lines.

(1) 69 MPa deuterium gas, 620K, 3 weeks

Table 4.1.1. Smooth tensile properties of 22-13-5 composite GTA weld specimens† thermally precharged with hydrogen and tested in gaseous hydrogen at room temperature. All data are provided for completeness, but it should be emphasized that these data may not reflect the properties of any of the specific microstructures within the gauge length. [15]

Thermal precharging	Test environment	Strain rate (s^{-1})	S_y (MPa)	S_u (MPa)	El_u (%)	El_t (%)	RA (%)
None	Air	0.33 x10^{-3}	495	782	11.2	14.4	49
	69MPa H_2		511	778	13.0	16.3	48
	172MPa H_2		528	798	11.8	16.0	50
(1)	Air		510	789	9.6	10.9	38
	69MPa H_2		531	776	10.2	12.0	45
(2)	Air		514	789	9.9	10.7	35
	172MPa H_2		516	780	11.6	13.5	35

† The base material for these studies was HERF (high energy rate forging), back extrusions of 22-13-5, machined to hollow cylindrical shape (10 cm diameter, 1.5 cm wall thickness) with circumferential double J grooves. The filler material was also 22-13-5 matched to the composition of the base metal. Eight to ten weld passes were required and the composition of the weld fusion zone, heat B83, is given in Table 1.1.1. The tensile specimens contain base material and heat affected zone with the fusion zone centered in the gauge length.

(1) 24 MPa H_2 473K, 10 days: hydrogen concentration was calculated to vary from 45 to 4 wppm (2500 to 200 appm) surface to center.

(2) 69 MPa H_2 473K, 10 days: hydrogen concentration was calculated to vary from 73 to 7 wppm (4000 to 400 appm) surface to center.

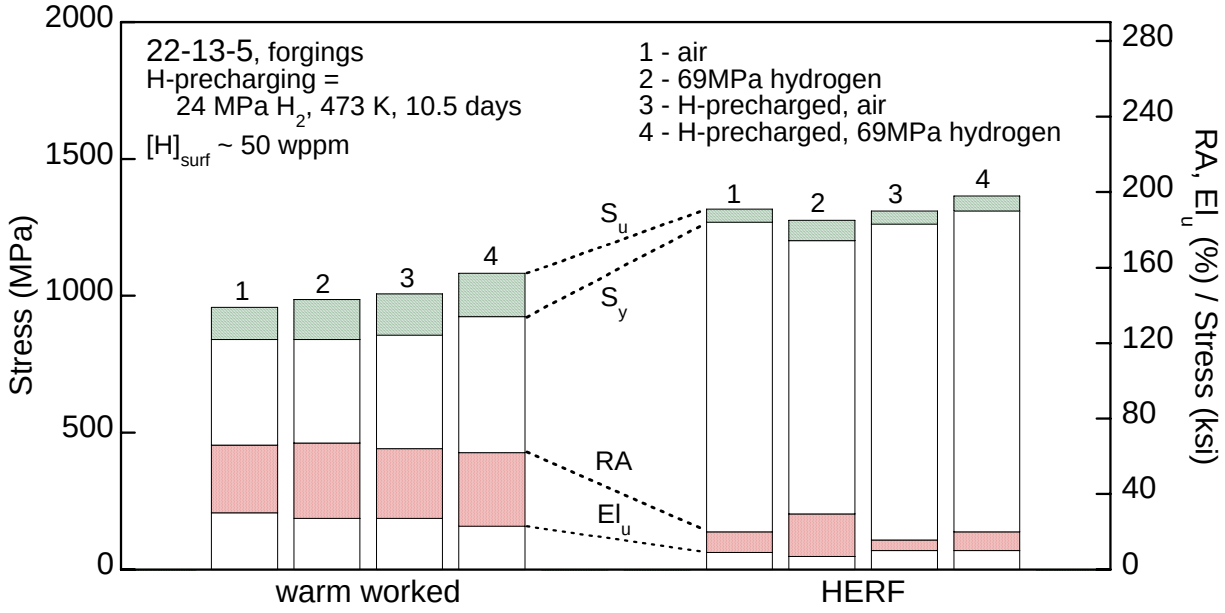

Figure 3.1.1.1. Effect of internal and external hydrogen on the tensile properties of 22-13-5 forgings (heat O75); same data is contained in Table 3.1.1.1. Strain rate = 3 x 10^{-4} s^{-1}. HERF = high energy rate forging. [17]

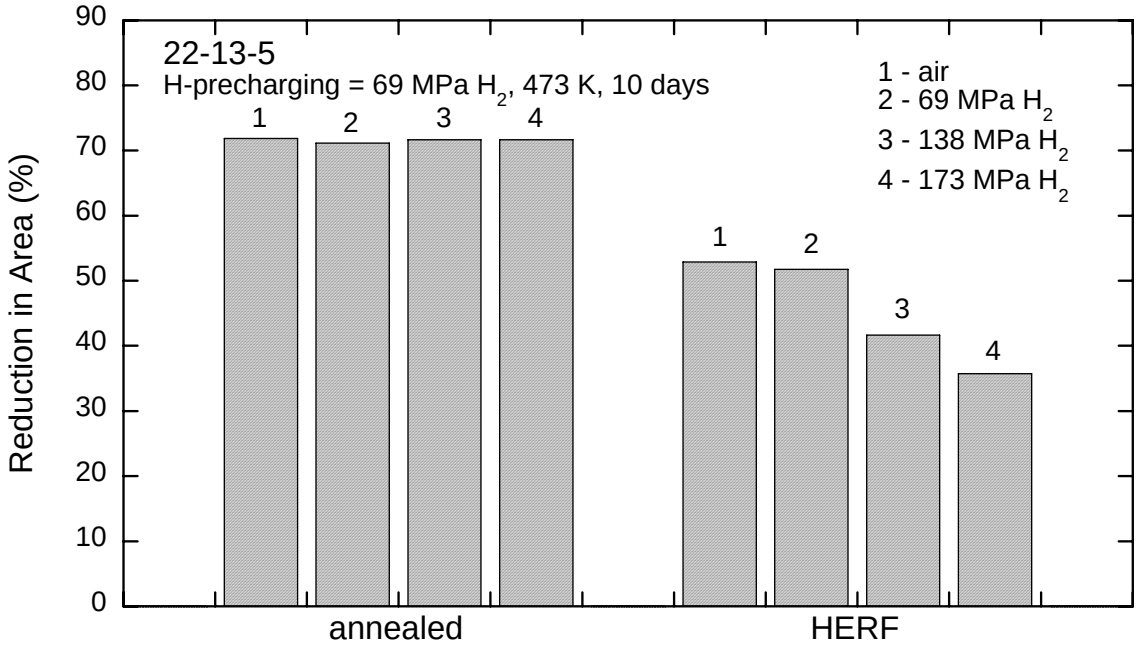

Figure 3.1.1.2. Ductility of smooth tensile specimens of annealed and forged 22-13-5 that have been precharged from hydrogen gas at elevated temperature and then tested in hydrogen gas at room temperature. HERF = high energy rate forging. [8]

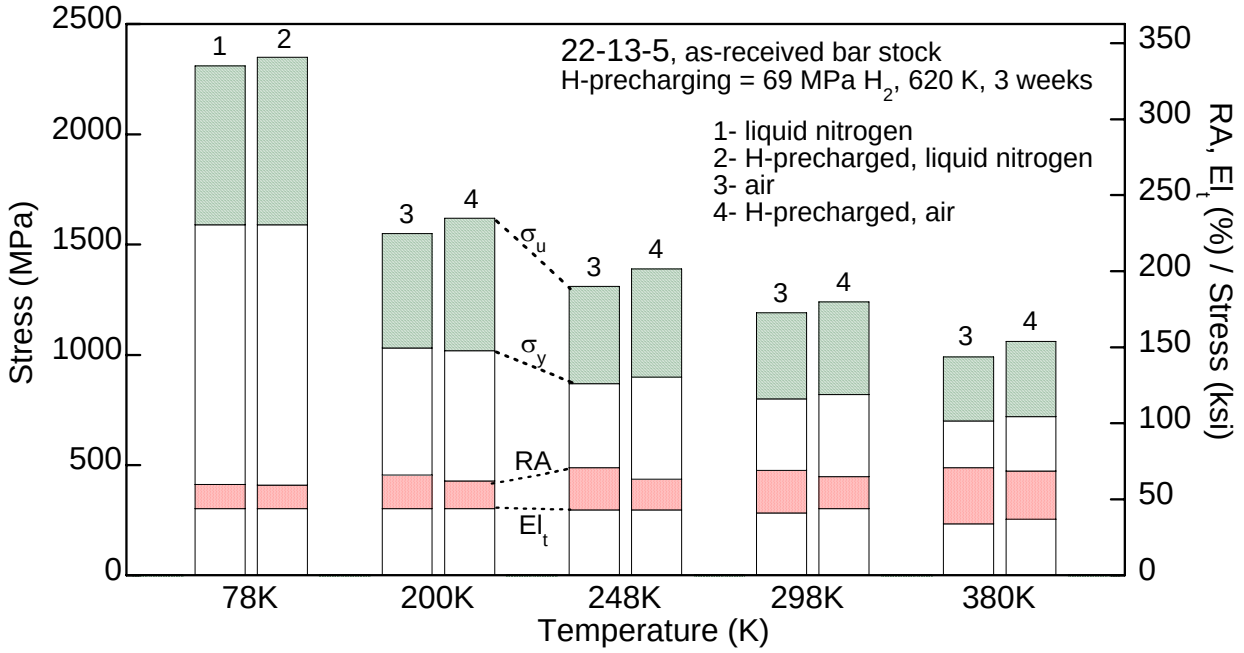

Figure 3.1.1.3. Effect of temperature on the hydrogen compatibility of 22-13-5 bar stock. Yield strength in this plot is defined as the true stress at 5% strain, ultimate strength is quoted as true stress at maximum load. [9]

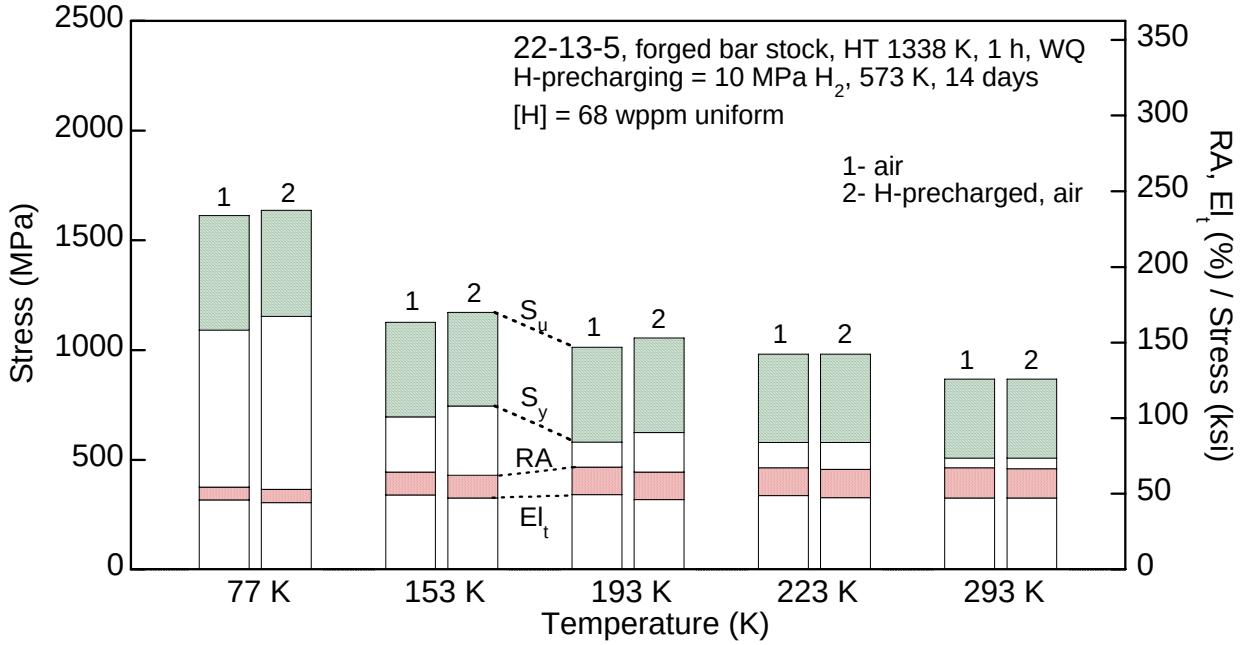

Figure 3.1.1.4. Effect of temperature on the hydrogen compatibility of 22-13-5 heat-treated bar stock. Specimen diameter = 5 mm; crosshead rate = 4.2×10^{-2} mm/s. HT = heat treatment, WQ = water quench. [7]

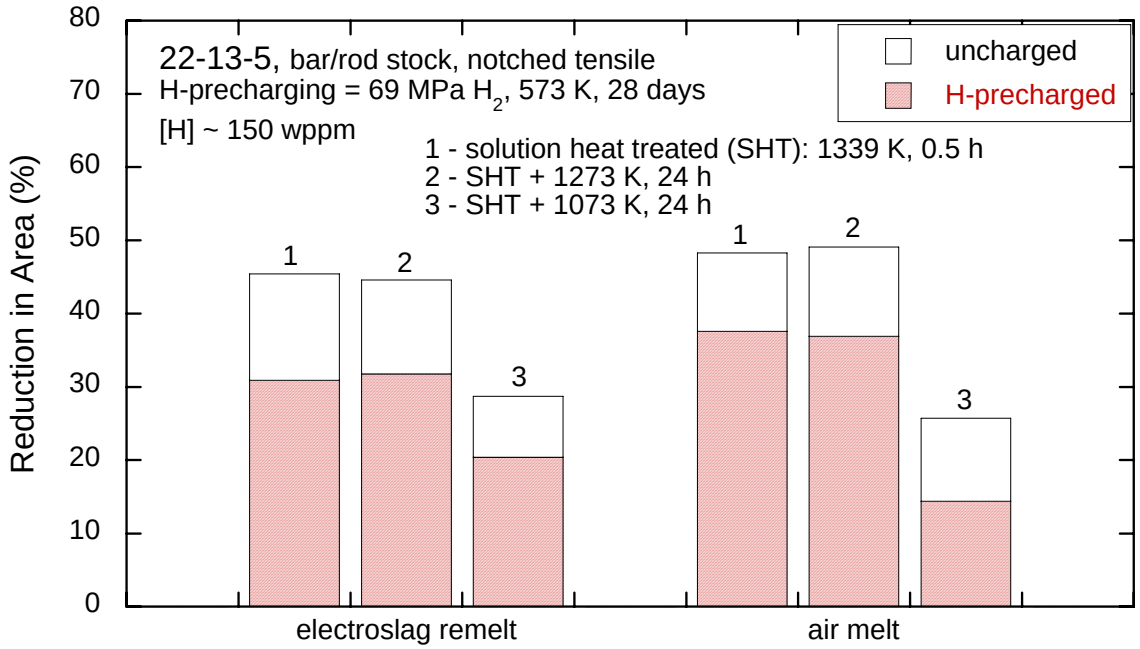

Figure 3.1.2.1. Reduction in area of notch tensile bars from two heats of 22-13-5 (electroslag remelted, heat S03b; air-melted, heat S03a). Notched specimen: semicircular notch; minimum diameter = 3.9 mm; maximum diameter = 7.9 mm; notch root radius = 0.79 mm; constant rate of displacement = $6x10^{-3}$ mm/s. [2]

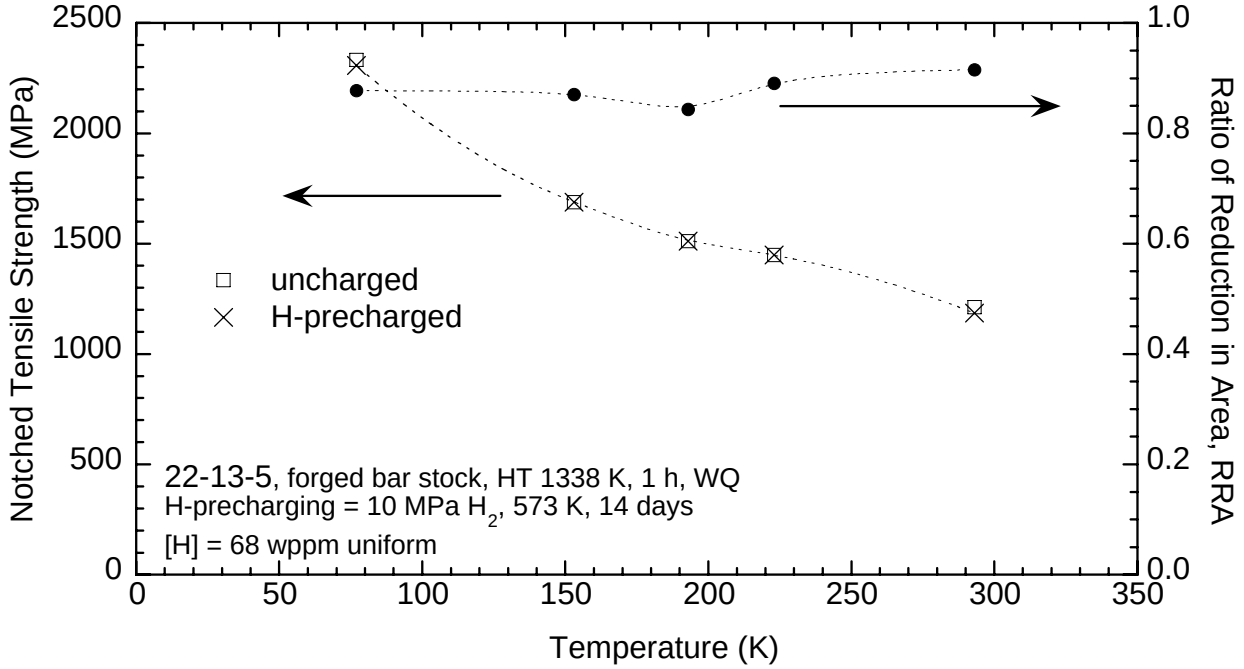

Figure 3.1.2.2. Notch tensile properties of 22-13-5 heat-treated bar stock. Notched specimen: stress concentration factor (K_t) = 4.55; notch geometry = 60˚ included angle; minimum diameter = 4 mm; maximum diameter = 5 mm; notch root radius = 0.1 mm; crosshead rate = $4.2x10^{-2}$ mm/s. HT = heat treatment, WQ = water quench. [7]

Technical Reference on Hydrogen Compatibility of Materials

Nitrogen-Strengthened Stainless Alloys:

21-6-9 (code 2202)

1. General

21Cr-6Ni-9Mn (21-6-9) is a stable austenitic stainless steel that is alloyed with nitrogen to provide superior strength compared to the standard 300-series stainless steels. The Cr+Ni content of 21-6-9 results in a relatively low stacking fault energy compared to more highly alloyed austenitic stainless steels such as type 316 stainless steel and 22Cr-13Ni-5Mn (22-13-5) [1-3]. Austenitic stainless steels with low stacking fault energy are more susceptible to hydrogen embrittlement, a feature generally attributed to non-uniform plastic deformation [1, 4]. Thermomechanical processing of 21-6-9 stainless steel results in shorter dislocation slip distances (due to increased dislocation density) and has been reported to improve ductility of material with internal hydrogen [4]. Other studies, however, show no clear benefit of worked microstructures with respect to hydrogen embrittlement and the general trend is that resistance to hydrogen embrittlement is less for higher yield strength [5-8].

The nitrogen content of 21-6-9 stainless steel is an important variable for hydrogen compatibility as high nitrogen contents are reported to significantly lower the resistance to hydrogen embrittlement [1]. Tensile testing shows that heats of 21-6-9 with nitrogen content >0.3 wt% have substantially lower ductility in the presence of hydrogen than heats with <0.3 wt% nitrogen [1]. This trend may be related to the effect of nitrogen on the stacking fault energy and associated plastic deformation behavior [1, 9].

The effect of hydrogen on 21-6-9 stainless steel appears to be very sensitive to microstructural and compositional variables; consequently, compositional variations from heat-to-heat result in the wide range of reported hydrogen-effects on tensile properties [6].The general trends outlined above indicate that high nitrogen content (>0.3 wt%) reduces resistance to hydrogen embrittlement. Other data suggest that nickel is generally important for resistance to hydrogen embrittlement in austenitic stainless steels [7, 10, 11]. Considering that nickel and chromium increase stacking fault energy [2, 3], high nickel and chromium content in 21-6-9 stainless steel is expected to be beneficial for resistance to hydrogen embrittlement. Finally, 21-6-9 in low strength conditions will generally have greater resistance to hydrogen effects.

1.1 Composition and microstructure

Table 1.1.1 lists specified compositional ranges for 21-6-9 stainless steel as well as compositions of several heats of 21-6-9 used to study hydrogen effects.

1.2 Common designations

Nitronic 40, UNS S21900 (ASTM XM-10)
21-6-9LC, UNS S21904 (ASTM XM-11)
Nitronic 40W, UNS 21980 (filler wire ER219)
Similar alloy: 21-7-9

2. Permeability, Diffusivity and Solubility

The permeability of stainless steel is briefly reviewed in Refs. [11-13]; diffusivity and solubility are briefly reviewed in Refs. [11, 13]. Permeability, diffusivity and solubility can be described by standard Arrhenius-type relationships. Solubility data are normally determined from the ratio of permeability and diffusivity.

Permeability appears to be nearly independent of the composition and microstructure for stable austenitic stainless steels [13, 14]. Nitrogen additions to type 304 [14] and type 316 [13] stainless steels do not significantly affect the permeability and solubility of these alloys. The nitrogen-strengthened stainless steels 21-6-9 and 22-13-5, on the other hand, have a significantly higher measured hydrogen concentration compared to 304L when exposed to identical high pressure and temperature [15]. This higher hydrogen concentration should translate into higher solubility. Ref. [11] proposes a solubility relationship based on hydrogen concentration measurements from hot extraction of 21-6-9 with internal hydrogen (thermally precharged from hydrogen gas), Table 2.1. Hydrogen concentrations measured by hot extraction methods are summarized in Table 2.2.

Relationships for permeability (Figure 2.1) and solubility (Figure 2.2) fit to data for several austenitic stainless steel alloys from several studies are given in Table 2.1. It is important to note that these data are determined at elevated temperature and low pressure; they are extrapolated for use near room temperature and high pressure. For this reason, it is recommended that the relationships from Refs. [14, 16], Table 2.1, be used for extrapolation to low temperature since these provide conservative estimates (high values) of permeability and solubility when extrapolated. At elevated temperature, the solubility relationships from Refs. [11, 16] are recommended.

3. Mechanical Properties: Effects of Gaseous Hydrogen

3.1 Tensile properties

3.1.1 Smooth tensile properties

In general, smooth tensile properties of 21-6-9 stainless steel are only modestly affected by external hydrogen gas. High-pressure external hydrogen gas slightly increases (or has negligible effect upon) the yield and ultimate strength of 21-6-9 stainless steel, Table 3.1.1.1. Ductility, on the other hand, is slightly reduced when measured in external hydrogen gas. These trends are amplified for 21-6-9 stainless steel with internal hydrogen (tested in air or external hydrogen gas after thermal precharging in hydrogen gas): yield strength may be significantly increased with somewhat lower increases in ultimate strength, while ductility can be substantially reduced compared to material not exposed to hydrogen, Table 3.1.1.2. These effects can be attributed to the high concentration of internal hydrogen that is obtained by thermal precharging, since hydrogen concentration increases exponentially with temperature. The effect of high internal hydrogen concentrations from thermal precharging is clearly demonstrated for smooth tensile properties in Figure 3.1.1.1: the strength increases and the ductility decreases as the external pressure of hydrogen gas is increased and these effects are further magnified with internal hydrogen.

The effect of hydrogen on tensile ductility strongly depends on the microstructural condition and composition of 21-6-9 stainless steel. Annealed microstructures tend to be less susceptible to hydrogen embrittlement than worked microstructures [5, 8]: the RRA of 21-6-9 stainless steel with internal hydrogen is generally greater for annealed than for worked microstructures as shown in Figure 3.1.1.2. Warm-working by high energy rate forging (HERF) has been reported to improve both strength and resistance to hydrogen embrittlement [4]; however, a full characterization of the materials tested in those studies was not provided and the results should be viewed as the exception rather than the rule. The data in Figure 3.1.1.2 rather show a general trend of greater susceptibility to hydrogen embrittlement as the yield strength is increased as by warm-working. There is significant uncertainty in these basic trends, however, as exemplified by the data shown in Table 3.1.1.3 for a single heat of 21-6-9 stainless steel processed to several different microstructural conditions [6]; also plotted in Figure 3.1.1.2. For this data the ductility loss of 21-6-9 with internal hydrogen and tested in external hydrogen gas indeed decreases as yield strength increases, however, cold-worked plate has the highest yield strength and is almost unaffected by hydrogen. Similarly, as show in Figure 3.1.1.2, materials with yield strength over 800 MPa have RRA that range from about 0.20 to 0.95. The broad range of response for material exposed to hydrogen can be partly explained by compositional variations.

West and Louthan performed tensile testing on a large number of heats of 21-6-9 stainless steels (data in Tables 3.1.1.1, 3.1.1.3 and 4.2.1) and found that susceptibility to hydrogen embrittlement could vary significantly depending on test variables and microstructure [6]. Although the nominal compositions of all the heats of 21-6-9 stainless steel that were tested in that study were similar, one heat differed from the others in having less nickel. This low-nickel heat of 21-6-9 also suffered the greatest loss in ductility when exposed to internal hydrogen; the lowest three points in Figure 3.1.1.2 represent this relatively low-nickel grade, heat W82a [6]. Higher nickel and chromium are known to strongly increase the stacking fault energy of stainless steels [2, 3] enhancing uniform deformation, a feature that is generally associated with greater resistance to hydrogen embrittlement [1, 4, 7].

High nitrogen content in 21-6-9 stainless steel significantly increases susceptibility to hydrogen embrittlement in smooth tensile specimens. Smooth tensile properties are plotted in Figure 3.1.1.3 for several heats of annealed 21-6-9 stainless steel that differ primarily in nitrogen content; data is also given in Table 3.1.1.4. Heats of 21-6-9 stainless steel with nitrogen levels >0.3 wt% suffer ductility (RA) losses greater than 50%, while heats with nitrogen <0.3 wt% experience a reduction in ductility of about 20% [1]. In addition, deformation mode and fracture mode were found to correlate with nitrogen content: heats with low nitrogen (<0.25 wt% N) exhibited uniform deformation and exhibit ductile fracture processes in the presence of both internal and external hydrogen, while heats with high nitrogen (>0.35 wt% N) exhibited non-uniform deformation and, when exposed to hydrogen, intergranular fracture [1]. While nitrogen appears to have an important effect on hydrogen embrittlement it should not be considered without regard to other alloying elements, such as nickel and chromium.

The magnitude of temperature effects on hydrogen embrittlement in tensile testing certainly depends on compositional and microstructural variables. The scatter in the temperature effects shown in Figure 3.1.1.4 and Table 3.1.1.5 might be explained by differences in composition or microstructure if that information were known. The trend for ductility loss measured from smooth tensile specimens of 21-6-9 stainless steels appears to be a minimum at a temperature between 200 K and 250 K, Figure 3.1.1.4. The ductility of 21-6-9 stainless steel with internal

hydrogen at low (77 K) and elevated (380 K) temperature is similar to that at room temperature. The effect of temperature on smooth tensile properties of a heat of 21-6-9 stainless steel that is relatively unaffected by internal hydrogen is shown in Figure 3.1.1.5.

Strain rate does not have a large impact on the loss of ductility of 21-6-9 stainless steel with internal hydrogen at conventional rates, e.g., $<0.001\ s^{-1}$, Figure 3.1.1.6. At higher strain rates the ductility is substantially improved; this is interpreted as a consequence of high velocity dislocations separating from hydrogen atmospheres [17].

3.1.2 Notched tensile properties

Notched tensile specimens with internal hydrogen (thermal precharging in hydrogen gas) show small decreases in ductility and no loss in strength, Figure 3.1.2.1. The modest hydrogen embrittlement for this particular alloy is expected since the nitrogen content is relatively low (about 0.25 wt%) and the strength is also low (yield strength of about 400 MPa). The basic trends outlined above for smooth tensile properties (susceptibility to hydrogen embrittlement increasing with nitrogen content and yield strength, but decreasing with nickel and chromium content) are expected in more comprehensive testing of notched specimens.

3.2 Fracture mechanics

3.2.1 Fracture toughness

Fracture toughness of 21-6-9, measured in high-pressure (external) hydrogen gas, exhibits a modest decrease of about 20% compared to tests in air, Table 3.2.1.1. Details of these tests were not provided other than the C-specimen geometry.

J-integral fracture toughness of high-energy-rate forgings (HERF) has been reported to strongly depend on the orientation of the microstructure and to be significantly reduced when measured in external hydrogen gas with internal hydrogen (or deuterium, thermally precharged in gas) [7, 18]. Due to the difficulty of instrumenting fracture mechanics specimens in high-pressure hydrogen gas, the J_m and tearing modulus (dJ/da) at maximum load are used in that study for comparison of orientations and testing conditions (values at maximum load do not represent a standardized fracture toughness). Nonetheless, it was observed that in most cases testing in external hydrogen gas with internal hydrogen produced a greater effect on both the fracture toughness and the tearing modulus than testing in hydrogen gas without internal hydrogen.

3.2.2 Threshold stress-intensity factor

Low-strength austenitic alloys (<700 MPa) have high resistance to crack extension in external hydrogen gas under static loads [19]. Data for 21-6-9 stainless steel are given in Table 3.2.2.1. For the one material tested, however, the forging temperature was in the range of rapid σ-phase transformation (see section 4.2), which may explain the low ductility reported for this material.

3.3 Fatigue

No known data in hydrogen gas.

3.4 Creep

No known data in hydrogen gas.

3.5 Impact

Impact fracture data show a modest effect of internal hydrogen for 21-6-9, Table 3.5.1. The fracture energy at liquid nitrogen temperature is not strongly affected by the presence of internal hydrogen and is about one-third of the fracture energy at room temperature. Compositional and microstructural details of the materials tested are not reported.

3.6 Disk rupture tests

Disk rupture tests of 21-6-9 stainless steel display slight to moderate reductions in rupture pressure when pressurized with hydrogen compared to helium, even in heats with high nitrogen content, heat A87 [20].

4. Fabrication

4.1 Primary processing

Microstructural features such as flow lines can have a significant effect on fracture toughness in air and on material with internal hydrogen; therefore, microstructural orientation is an important design consideration. As discussed in the section 3.1.1, 21-6-9 stainless steel in low-strength conditions generally appears to be less susceptible to hydrogen embrittlement.

4.2 Heat treatment

Processing temperatures for 21-6-9 stainless steel need to be controlled, particularly heating through the temperature range 773 K to 1173 K. Stainless steels are said to be sensitized when extensive carbide precipitation occurs in the microstructure [21]. Carbides form particularly on grain boundaries at elevated temperature (roughly 773 K to 1073 K), as a result, for example, of improper heat treatment, of heating slowly through this temperature range during annealing, and of welding processes. Sensitization compromises fracture properties of stainless steel as well as significantly reducing corrosion resistance. Figure 4.2.1 shows that sensitization reduces the ductility of 21-6-9 stainless steel; the ductility of sensitized microstructures is further reduced only slightly by the combination of internal and external hydrogen. Data from Figure 4.2.1 are also given in Table 4.2.1.

In addition to carbide formation, ferrite in 21-6-9 stainless steel may rapidly transform to brittle σ-phase in the temperature range of about 923 K to 1173 K [22]. This transformation occurs rapidly in deformed microstructures thus heat input during welding should be carefully controlled. The σ-phase degrades the ductility of the material independently of hydrogen exposure.

4.3 Properties of welds

Refs. [23, 24] report properties of gas tungsten arc (GTA) welds of 21-6-9 stainless steel with 308L and 21-6-9 filler wires measured in external hydrogen gas with and without internal hydrogen; smooth tensile properties are provided in Table 4.3.1. The loss in ductility in these tensile tests correlates well with expected hydrogen content, i.e., the ductility decreases as

hydrogen content increases due to higher hydrogen pressure. Fracture of the welds in the absence of hydrogen was by microvoid coalescence (ductile fracture processes). Detailed fractography shows failure to be associated with ferrite-austenite interfaces; fracture, however, remained primarily ductile[23, 24].

In a separate study [25], smooth and notched tensile testing of GTA and EB (electron beam) welds in 21-6-9 stainless steel revealed significantly lower ductility and slightly lower strength of the weld material compared to the base material (heat V72). Tests in high-pressure (external) hydrogen gas (69 MPa), however, revealed no effect on the smooth and notched tensile strength and ductility. Static loading of both notched and smooth tensile specimens in 69 MPa hydrogen gas to the yield point for 300 hours and subsequent testing in air also showed no change in properties of the base metal and the welds. Plane *stress* fracture toughness similarly showed no evidence of hydrogen effects. In all cases fracture surfaces revealed only ductile fracture processes and no evidence of secondary cracking or changes in fracture morphology due to testing in hydrogen. This study shows remarkably little effect of hydrogen compared to other studies.

5. References

1. BC Odegard, JA Brooks and AJ West. The Effect of Hydrogen on Mechanical Behavior of Nitrogen-Strengthened Stainless Steel. in: AW Thompson and IM Bernstein, editors. Proceedings of an International Conference on Effect of Hydrogen on Behavior of Materials, 1975, Moran WY. The Metallurgical Society of AIME (1976) p. 116-125.
2. RE Schramm and RP Reed. Stacking Fault Energies of Seven Commercial Austenitic Stainless Steels. Metall Trans 6A (1975) 1345-1351.
3. CG Rhodes and AW Thompson. The Composition Dependence of Stacking Fault Energy in Austenitic Stainless Steels. Metall Trans 8A (1977) 1901-1905.
4. MR Louthan, GR Caskey, JA Donovan and DE Rawl. Hydrogen Embrittlement of Metals. Mater Sci Eng 10 (1972) 357-368.
5. AJ West and MR Louthan. Dislocation Transport and Hydrogen Embrittlement. Metall Trans 10A (1979) 1675-1682.
6. AJ West and MR Louthan. Hydrogen Effects on the Tensile Properties of 21-6-9 Stainless Steel. Metall Trans 13A (1982) 2049-2058.
7. GR Caskey. Hydrogen Compatibility Handbook for Stainless Steels (DP-1643). EI du Pont Nemours, Savannah River Laboratory, Aiken SC (June 1983).
8. MJ Morgan. The Effects of Hydrogen Isotoptes and Helium on the Flow and Fracture Properties of 21-6-9 Stainless Steel. in: PK Liaw, JR Weertman, HL Marcus and JS Santner, editors. Proceedings of the Morris E. Fine Symposium. Warrendale PA: TMS (1991).
9. RE Stoltz and JB VanderSande. The Effect of Nitrogen on Stacking Fault Energy of Fe-Ni-Cr-Mn Steels. Metall Trans 11A (1980) 1033-1037.
10. GR Caskey. Hydrogen Damage in Stainless Steel. in: MR Louthan, RP McNitt and RD Sisson, editors. Environmental Degradation of Engineering Materials in Hydrogen. Blacksburg VA: Laboratory for the Study of Environmental Degradation of Engineering Materials, Virginia Polytechnic Institute (1981) p. 283-302.
11. GR Caskey. Hydrogen Effects in Stainless Steels. in: RA Oriani, JP Hirth and M Smialowski, editors. Hydrogen Degradation of Ferrous Alloys. Park Ridge NJ: Noyes Publications (1985) p. 822-862.

12. AD LeClaire. Permeation of Gases Through Solids: 2. An assessment of measurements of the steady-state permeability of H and its isotopes through Fe, Fe-based alloys, and some commercial steels. Diffusion and Defect Data 34 (1983) 1-35.
13. XK Sun, J Xu and YY Li. Hydrogen Permeation Behaviour in Austenitic Stainless Steels. Mater Sci Eng A114 (1989) 179-187.
14. MR Louthan and RG Derrick. Hydrogen Transport in Austenitic Stainless Steel. Corros Sci 15 (1975) 565-577.
15. GR Caskey and RD Sisson. Hydrogen Solubility in Austenitic Stainless Steels. Scr Metall 15 (1981) 1187-1190.
16. T-P Perng and CJ Altstetter. Effects of Deformation on Hydrogen Permeation in Austenitic Stainless Steels. Acta metall 34 (1986) 1771-1781.
17. JH Holbrook and AJ West. The Effect of Temperature and Strain Rate on the Tensile Properties of Hydrogen Charged 304L, 21-6-9, and JBK 75. in: IM Bernstein and AW Thompson, editors. Proceedings of the International Conference on Effect of Hydrogen on Behavior of Materials: Hydrogen Effects in Metals, 1980, Moran WY. The Metallurgical Society of AIME (1980) p. 655-663.
18. MR Dietrich, GR Caskey and JA Donovan. J-Controlled Crack Growth as an Indicator of Hydrogen-Stainless Steel Compatibility. in: IM Bernstein and AW Thompson, editors. Proceedings of the International Conference on Effect of Hydrogen on Behavior of Materials: Hydrogen Effects in Metals, 1980, Moran WY. The Metallurgical Society of AIME (1980) p. 637-643.
19. MW Perra. Sustained-Load Cracking of Austenitic Steels in Gaseous Hydrogen. in: MR Louthan, RP McNitt and RD Sisson, editors. Environmental Degradation of Engineering Materials in Hydrogen. Blacksburg VA: Laboratory for the Study of Environmental Degradation of Engineering Materials, Virginia Polytechnic Institute (1981) p. 321-333.
20. PF Azou and JP Fidelle. Very low strain rate hydrogen gas embrittlement (HGE) and fractography of high-strength, mainly austenitic stainless steels. in: MR Louthan, RP McNitt and RD Sisson, editors. Environmental Degradation of Engineering Materials III, 1987, The Pennsylvania State University, University Park PA. The Pennsylvania State University, University Park PA p. 189-198.
21. RA Lula. Stainless Steel (revised from "An Introduction to Stainless Steel" by JG Parr and A Hanson). Metals Park OH: American Society for Metals (1986).
22. CL Ferrera. The Formation and Effects of Sigma Phase in 21-6-9 Stainless Steel (PMT-87-0017). Rockwell International, Rocky Flats Plant, Golden CO (November 1987).
23. JA Brooks and AJ West. Hydrogen Induced Ductility Losses in Austenitic Stainless Steel Welds. Metall Trans 12A (1981) 213-223.
24. JA Brooks, AJ West and AW Thompson. Effect of Weld Composition and Microstructure on Hydrogen Assisted Fracture of Austenitic Stainless Steels. Metall Trans 14A (1983) 75-84.
25. RA Vandervoort. Tensile and Fracture Properties of Austenitic Stainless Steel 21-6-9 in High-Pressure Hydrogen Gas. Metals Engineering Quarterly 12 (1972) 10-16.
26. ASTM DS-56H, Metals and Alloys in the UNIFIED NUMBERING SYSTEM (SAE HS-1086 OCT01). American Society for Testing and Materials (Society of Automotive Engineers) (2001).
27. L Ma, G Liang, J Tan, L Rong and Y Li. Effect of Hydrogen on Cryogenic Mechanical Properties of Cr-Ni-Mn-N Austenitic Steels. J Mater Sci Technol 15 (1999) 67-70.

28. RE Stoltz and AJ West. Hydrogen Assisted Fracture in FCC Metals and Alloys. in: IM Bernstein and AW Thompson, editors. Proceedings of the International Conference on Effect of Hydrogen on Behavior of Materials: Hydrogen Effects in Metals, 1980, Moran WY. The Metallurgical Society of AIME (1980) p. 541-553.
29. RE Stoltz, NR Moody and MW Perra. Microfracture Model for Hydrogen Embrittlement of Austenitic Steels. Metall Trans 14A (1983) 1528-1531.

Table 1.1.1. Specification limits for 21-6-9 stainless steels and composition of several heats used to study hydrogen effects.

heat	Fe	Cr	Ni	Mn	Si	C	N	other	Ref.
UNS S21900	Bal	19.00 21.50	5.50 7.50	8.00 10.00	1.00 max	0.08 max	0.15 0.40	0.030 max S; 0.060 max P	[26]
UNS S21904	Bal	19.00 21.50	5.50 7.50	8.00 10.00	1.00 max	0.04 max	0.15 0.40	0.030 max S; 0.060 max P	[26]
UNS S21980	Bal	19.0 21.5	5.50 7.50	8.00 10.00	1.00 max	0.05 max	0.10 0.30	0.03 max S; 0.03 max P; 0.75 max Cu; 0.75 max Mo	[26]
V72	Bal	21.0	7.1	8.8	0.4	0.03	0.3	0.003 S; 0.01 P	[25]
O76a	Bal	19.90	7.53	8.70	0.17	0.033	0.12	—	[1]
O76b	Bal	19.70	7.60	8.63	0.19	0.040	0.24	—	
O76c	Bal	19.60	6.70	8.90	0.16	0.030	0.31	—	
O76d	Bal	20.10	7.12	8.55	0.19	0.035	0.43	—	
O76e	Bal	19.90	7.53	8.70	0.17	0.035	0.47	—	
H80	Bal	20.2	6.2	9.0	0.5	0.03	0.25	0.015 S; 0.02 P	[17]
P81	Bal	19.92	6.69	9.17	0.37	0.032	0.219	—	[19]
W82a	Bal	20.1	6.20	9.14	0.41	0.040	0.30	<0.01 S; <0.02 P	[6]
W82b	Bal	19.7	7.29	8.63	0.23	0.023	0.28		
W82c	Bal	19.6	7.08	9.07	0.48	0.026	0.30		
W82d	Bal	19.5	7.36	8.73	0.25	0.018	0.28		
W82e	Bal	19.8	7.10	9.21	0.15	0.014	0.24		
B83aw	Bal	20.8	8.8	8.1	0.61	0.03	0.17	0.010 S; 0.019 P	[24]
B83bw	Bal	20.7	7.8	9.3	0.60	0.03	0.27	0.006 S; 0.017 P	[24]
C83	Bal	20.32	6.71	9.01	0.24	0.015	0.35	0.016 S; 0.018 P	[7]
A87	Bal	20.9	7.1	8.8	0.44	0.035	0.37	0.005 S; 0.010 P	[20]
M91a	Bal	19.2	7.22	9.23	0.41	0.032	0.28	0.003 S; 0.014 P	[8]
M91b	Bal	19.4	6.40	8.50	0.33	0.040	0.28	<0.001 S; 0.021 P	
M91c	Bal	20.1	6.50	9.10	0.59	0.037	0.29	<0.001 S; 0.019 P	

w = composition of the weld fusion zone

Table 2.1. Average permeability and solubility relationships determined for several austenitic stainless steels, except Ref. [11] which is determined from hydrogen concentration measurements using hot extraction from 21-6-9 stainless steel thermally precharged from hydrogen gas.

Material	Temperature range (K)	Pressure range (MPa)	$\Phi = \Phi_o \exp(-E_\Phi / RT)$		$S = S_o \exp(-E_S / RT)$		Ref.
			Φ_o $\left(\frac{\text{mol H}_2}{\text{m} \cdot \text{s} \cdot \sqrt{\text{MPa}}}\right)$	E_Φ $\left(\frac{\text{kJ}}{\text{mol}}\right)$	S_o $\left(\frac{\text{mol H}_2}{\text{m}^3 \cdot \sqrt{\text{MPa}}}\right)$	E_S $\left(\frac{\text{kJ}}{\text{mol}}\right)$	
Average of several austenitic alloys †	423-700	0.1-0.3	1.2×10^{-4}	59.8	179	5.9	[14]
Based on >20 studies on 12 austenitic alloys	—	—	3.27×10^{-4}	65.7	—	—	[12]
From hot extraction measurements on 21-6-9	—	—	—	—	346	8	[11]
Average of four austenitic alloys	373-623	1×10^{-4}-0.03	5.35×10^{-5}	56.1	266	6.86	[16]
Average of six austenitic alloys	473-703	0.1	2.81×10^{-4}	62.27	488	8.65	[13]

† Data from Ref. [14] is determined for deuterium: permeability has been corrected here to give permeability of hydrogen (by multiplying by the square root of the mass ratio: $\sqrt{2}$); solubility is assumed to be independent of isotope.

Table 2.2. Hydrogen solubility of 21-6-9 stainless steels measured from hot extraction after thermal precharging in hydrogen gas.

Material	Surface condition	Thermal precharging	Hydrogen concentration†		Ref.
			wppm	appm	
21-6-9, heat H80	—	69 MPa H_2 573 K	109	6000	[17]
21-6-9 annealed	600 grit finish	69 MPa H_2 470 K	118	6500	[15]
	Electropolished		126	6900	
21-6-9 HERF	600 grit finish		126	6900	
	Electropolished		127	7000	
21-6-9 CW	600 grit finish		119	6500	
	Electropolished		126	6900	
21-6-9 annealed	—	10 MPa H_2 573 K	65	3600	[27]

HERF = high energy rate forging, CW = cold-work

† 1 wppm ≈ 55 appm

Table 3.1.1.1. Smooth tensile properties of 21-6-9 stainless steel at room temperature; measured in external hydrogen gas, or measured in air with internal hydrogen (thermal precharging in hydrogen gas), or measured in external hydrogen gas with internal hydrogen.

Material	Thermal precharging	Test environment	Strain rate (s^{-1})	S_y (MPa)	S_u (MPa)	El_u (%)	El_t (%)	RA (%)	Ref.
21-6-9, heat W82a HERF	None	Air	0.54×10^{-3}	889	993	20	46	68	[6]
	(1)	172 MPa H_2		917	993	8	11	14	
21-6-9, heat W82b HERF	None	Air		654	882	38	52	74	
	None	172 MPa H_2		703	924	30	43	67	
	(1)	172 MPa H_2		731	917	30	40	48	
21-6-9, heat W82c HERF	None	Air		848	965	26	37	75	
	(1)	172 MPa H_2		924	1062	21	31	64	
21-6-9, heat W82c HERF	None	Air		938	1000	12	30	62	
	(1)	172 MPa H_2		951	993	16	28	53	
21-6-9, heat W82e HERF	None	Air		862	958	17	35	73	
	(1)	172 MPa H_2		924	979	14	22	40	
21-6-9	None	Air	—	400†	670‡	—	58	78	[7]
	None	69 MPa He		350†	700‡	—	59	77	
	None	69 MPa H_2		360†	700‡	—	61	76	
21-6-9 CW 30%	None	Air	—	1240†	1290‡	—	26	53	[7]
	None	69 MPa He		1010†	1050‡	—	26	63	
	None	69 MPa H_2		980†	1100‡	—	26	64	
	30 MPa H_2	Air		1075†	1150‡	—	32	35	
	30 MPa H_2	69 MPa H_2		1060†	1130‡	—	36	36	
21-6-9 HERF	None	Air	—	610†	790‡	—	34	74	[7]
	None	69 MPa He		570†	780‡	—	34	75	
	None	69 MPa H_2		570†	790‡	—	30	73	
	30 MPa H_2	Air		660†	820‡	—	31	59	
	30 MPa H_2	69 MPa H_2		630†	830‡	—	31	54	

HERF = high energy rate forging, CW = cold work

† true stress at 5% strain

‡ true stress at maximum load

(1) 69 MPa hydrogen gas, 473 K, 240 h (gauge diameter = 5 mm); hydrogen concentration predicted to vary surface to center

Table 3.1.1.2. Smooth tensile properties of 21-6-9 stainless steel at room temperature; measured in air with internal hydrogen (thermal precharging in hydrogen gas).

Material	Thermal precharging	Test environment	Strain rate † (s^{-1})	S_y (MPa)	S_u (MPa)	El_u (%)	El_t (%)	RA (%)	Ref.
21-6-9	None	Air	—	434	689	—	56	56	[4]
	(1)	Air		441	724	—	30	28	
21-6-9 HERF	None	Air	—	607	793	—	32	74	[4]
	(2)	Air		655	820	—	31	59	
21-6-9, heat M91c annealed	None	Air	8.5 x 10^{-3} mm/s†	500	811	—	80	75	[8]
	(3)	Air		555	839	—	83	60	
21-6-9, heat M91a HERF	None	Air		712	932	—	40	71	
	(3)	Air		776	974	—	34	43	
21-6-9, heat M91a/b HERF	None	Air		819	969	—	26	56	
	(3)	Air		1005	1093	—	28	33	
21-6-9, heat M91b HERF	None	Air		825	1029	—	33	64	
	(3)	Air		836	948	—	—	—	
21-6-9, heat M91c HERF	None	Air		918	1032	—	46	63	
	(3)	Air		965	1073	—	46	39	

HERF = high energy rate forging

† when strain rate is not known, displacement rates are quoted if reported

(1) 69 MPa hydrogen gas, 473 K, 340 h; hydrogen concentration of 86 wppm (4700 appm)

(2) 28 MPa hydrogen gas, temperature not specified, time specified as “prolonged”

(3) 69 MPa hydrogen gas, 623 K, 1000 h (gauge diameter = 4.8 mm); calculated uniform hydrogen concentration of 170 wppm (9500 appm)

Table 3.1.1.3. Smooth tensile properties of a single heat of 21-6-9 stainless steel in different microstructural conditions at room temperature; measured in external hydrogen gas, or measured in external hydrogen gas with internal hydrogen (thermal precharging in hydrogen gas).

Material	Thermal precharging	Test environment	Strain rate (s^{-1})	S_y (MPa)	S_u (MPa)	El_u (%)	El_t (%)	RA (%)	Ref.
21-6-9, heat W82d annealed	None	Air	0.54 x 10^{-3}	414	765	45	51	63	[6]
	(1)	172 MPa H_2		496	827	40	49	59	
21-6-9, heat W82d bar stock	None	Air		758	951	21	38	54	
	None	120 MPa H_2		765	931	19	29	51	
	None	172 MPa H_2		800	938	14	18	42	
	(1)	172 MPa H_2		834	965	10	11	22	
21-6-9, heat W82d HERF	None	Air		800	896	15	28	68	
	None	172 MPa H_2		827	903	12	34	66	
	(1)	172 MPa H_2		862	931	8	11	26	
21-6-9, heat W82d CW plate	None	Air		834	917	12	23	69	
	(1)	172 MPa H_2		869	931	17	27	65	

HERF = high energy rate forging, CW = cold work

(1) 69 MPa hydrogen gas, 473 K, 240 h (gauge diameter = 5 mm); hydrogen concentration predicted to vary surface to center

Table 3.1.1.4. Smooth tensile properties of 21-6-9 stainless steel at room temperature with varying nitrogen content (given in wt%); measured in external hydrogen gas with internal hydrogen (thermal precharging in hydrogen gas).

Material	Thermal precharging	Test environment	Strain rate (s^{-1})	S_y (MPa)	S_u (MPa)	El_u (%)	El_t (%)	RA (%)	Ref.
21-6-9, heat O76a (0.12N) annealed plate	None	Air	3 x 10^{-3}	296	683	—	65	74	[1]
	(1)	69 MPa H_2		296	683	—	58	59	
21-6-9, heat O76b (0.24N) annealed plate	None	Air		386	745	—	58	72	
	(1)	69 MPa H_2		401	732	—	62	57	
21-6-9, heat O76c (0.31N) annealed plate	None	Air		434	745	—	56	56	
	(1)	43 MPa H_2		441	724	—	30	28	
21-6-9, heat O76d (0.43N) annealed plate	None	Air		490	780	—	55	67	
	(1)	69 MPa H_2		503	785	—	21	29	
21-6-9, heat O76e (0.47N) annealed plate	None	Air		510	790	—	56	67	
	(1)	69 MPa H_2		509	796	—	18	28	

(1) 24.1 MPa hydrogen gas, 473 K, 240 h (gauge diameter = 5 mm); surface concentration calculated to be 55 wppm (3000 appm)

Table 3.1.1.5. Smooth tensile properties of 21-6-9 stainless steel as a function of test temperature, measured in air with internal hydrogen (thermal precharging in hydrogen gas).

Material	Thermal precharging	Test environment	Strain rate (s^{-1})	S_y (MPa)	S_u (MPa)	El_u (%)	El_t (%)	RA (%)	Ref.
21-6-9, heat C83 bar stock	None (1)	Air 380 K	—	680†	940‡	30	39	81	[7]
				690†	1020‡	36	46	64	
	None (1)	Air 298 K		770†	1170‡	41	51	80	
				800†	1270‡	46	56	60	
	None (1)	Air 250 K		860†	1360‡	46	57	78	
				—	1380‡	41	46	36	
	None (1)	Air 200 K		970†	1550‡	48	58	79	
				1060†	1650‡	44	48	48	
	None (1)	Liquid N_2 77 K		1580†	2140‡	45	49	47	
				1600†	2060‡	36	36	32	
21-6-9 HERF	None (2)	Air 380 K	—	780†	970‡	21	31	69	[7]
				690†	930‡	26	33	49	
	None (2)	Air 298 K		780†	1140‡	32	44	71	
				890†	1220‡	30	42	62	
	None (2)	Air 220 K		900†	1320‡	33	45	73	
				960†	1420‡	37	47	55	
	None (2)	Air 200 K		1020†	1610‡	42	54	72	
				990†	1740‡	53	60	48	
21-6-9 HERF	None (3)	Air 380 K	—	540†	1040‡	47	59	84	[7]
				570†	1070‡	50	68	72	
	None (3)	Air 273 K		640†	1300‡	57	69	84	
				690†	1430‡	67	78	65	
	None (3)	Air 200 K		930†	1700‡	51	59	72	
				1050†	1830‡	49	54	59	
	None (3)	Liquid N_2 78 K		1450†	2840‡	46	56	56	
				1400†	2600‡	46	46	41	

† true stress at 5% strain
‡ true stress at maximum load
(1) 69 MPa deuterium gas, 620 K, 500 h
(2) 69 MPa hydrogen gas, 620 K, 500 h
(3) 69 MPa hydrogen gas, 470 K, 35000 h

Table 3.2.1.1. Fracture toughness of 21-6-9 stainless steel at room temperature; measured in external hydrogen gas, or measured in external hydrogen gas after exposure to hydrogen gas.

Material	Test method	Thermal precharging	Test environment	S_y † (MPa)	K_Q ‡ (MPa)	Ref.
21-6-9 HERF, Longitudinal	C-specimen	None	69 MPa He	—	79	[7]
		None	69 MPa H_2	—	81	
		0.6 MPa H_2	69 MPa H_2	—	76	
21-6-9 HERF, Transverse	C-specimen	None	69 MPa He	—	74	[7]
		None	69 MPa H_2	—	68	
		0.6 MPa H_2	69 MPa H_2	—	62	

HERF = high energy rate forging
† yield strength of smooth tensile specimen
‡ not clear if plane strain requirements are met in these studies

Table 3.2.2.1. Threshold stress intensity factor of 21-6-9 stainless steel; measured in external hydrogen gas.

Material	S_y † (MPa)	RA † (%)	Threshold Stress Intensity Factor (MPa $m^{1/2}$)		Ref.
			100 MPa H_2	200 MPa H_2	
21-6-9, heat P81 HERF (1113 K, WQ)	827	36	103	99*	[19] ‡

HERF = high-energy rate forging, WQ = water quench
† yield strength and reduction in area of smooth tensile specimen, not exposed to hydrogen
* did not satisfy plane strain requirements for analysis of linear elastic fracture mechanics
‡ data also reported in Ref. [28, 29]

Table 3.5.1. Impact fracture data for 21-6-9 stainless steel with internal hydrogen (thermal precharging in hydrogen gas).

Material	Specimen	Thermal precharging	Test environment	S_y † (MPa)	Impact Energy (J)	Ref.
21-6-9 HERF	(a)	None	Liquid N_2 77 K	—	37	[7]
		(1)		—	35	
		None	Air 298 K	—	110	
		(1)		—	91	

HERF = high-energy rate forging
† yield strength of smooth tensile specimen, not exposed to hydrogen
(a) modified Naval Research Laboratory dynamic tear specimen [7]
(1) 29.6 MPa hydrogen gas, 470 K, 1300 h

Table 4.2.1. Smooth tensile properties of sensitized 21-6-9 stainless steel at room temperature, measured in external hydrogen gas with internal hydrogen (thermal precharging in hydrogen gas).

Material	Thermal precharging	Test environment	Strain rate (s^{-1})	S_y (MPa)	S_u (MPa)	El_u (%)	El_t (%)	RA (%)	Ref.
21-6-9, heat W82a HERF	None	Air	0.54 x 10^{-3}	834	965	18	39	73	[6]
	(1)	70 MPa H_2		882	986	17	32	57	
	(1)	120 MPa H_2		882	1007	15	20	35	
	(1)	172 MPa H_2		882	993	11	15	28	
21-6-9, heat W82a HERF + S	None	Air		813	951	10	29	68	
	None	172 MPa H_2		800	944	13	28	73	
	(1)	70 MPa H_2		869	986	9	25	50	
	(1)	120 MPa H_2		882	1007	6	10	23	
	(1)	172 MPa H_2		869	972	5	10	21	

HERF = high energy rate forging, S = sensitized
(1) 69 MPa hydrogen gas, 473 K, 240 h (gauge diameter = 5 mm); hydrogen concentration predicted to vary surface to center

Table 4.3.1. Smooth tensile properties of 21-6-9 stainless steel composite GTA weld specimens at room temperature; measured in external hydrogen gas, or measured in air with internal hydrogen (thermal precharging in hydrogen gas), or measured in external hydrogen gas with internal hydrogen.

Material	Thermal precharging	Test environment	Strain rate (s^{-1})	S_y (MPa)	S_u (MPa)	El_u (%)	El_t (%)	RA (%)	Ref.
21-6-9 HERF/ 308L filler wire GTA welds, heat B83aw ‡	None	Air	0.33 x 10^{-3}	539	746	9.7	14	54	[24]
	None	69 MPa H_2		534	738	10	14	57	
	None	172 MPa H_2		573	786	11	15	61	
	(1)	Air		553	757	8.8	12	49	
	(1)	69 MPa H_2		—	756	—	—	43	
	(2)	Air		579	776	10	12	44	
	(2)	172 MPa H_2		607	849	9.7	10	44	
21-6-9 HERF/ 21-6-9 filler wire GTA welds, heat B83bw ‡	None	Air	0.33 x 10^{-3}	530	773	12	19	60	[24]
	None	69 MPa H_2		498	754	14	22	75	
	None	172 MPa H_2		543	795	12	20	69	
	(1)	Air		514	769	13	18	56	
	(1)	69 MPa H_2		612	827	—	—	50	
	(2)	Air		543	789	12	16	50	
	(2)	172 MPa H_2		589	842	14	17	49	

HERF = high energy rate forging, GTA = gas tungsten arc

‡ The base material for these studies was HERF, back extrusions of 21-6-9, machined to cylindrical shape (10 cm diameter, 1.5 cm wall thickness) with circumferential double J grooves; eight to ten GTA weld passes were required to fill groove. The filler wire material was either 308L or 21-6-9. Tensile bars contain base material and heat affected zone with the fusion zone centered in the gauge length.

(1) 24 MPa hydrogen gas, 473 K, 240 h: calculated concentration gradient of 45 to 4 wppm surface to center (2500 to 200 appm)

(2) 69 MPa hydrogen gas, 473 K, 240 h: calculated concentration gradient of 72 to 7 wppm surface to center (4000 to 400 appm)

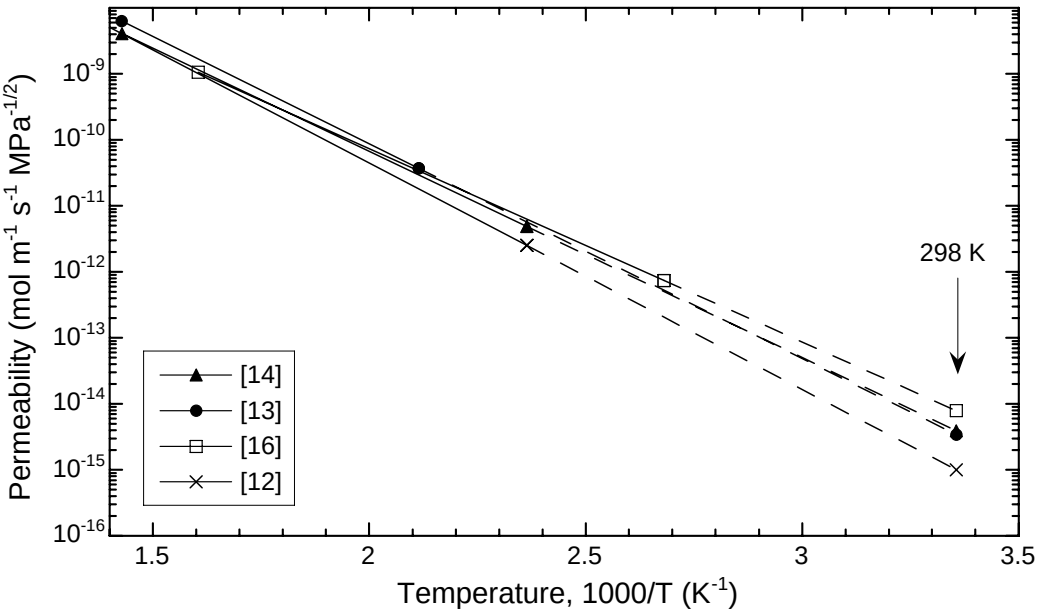

Figure 2.1. Permeability relationships (from Table 2.1) for austenitic stainless steels extrapolated (dashed lines) to 298 K. Permeability from Ref. [14] was determined for deuterium and has been corrected to give permeability of hydrogen by multiplying by the square root of the mass ratio: √2.

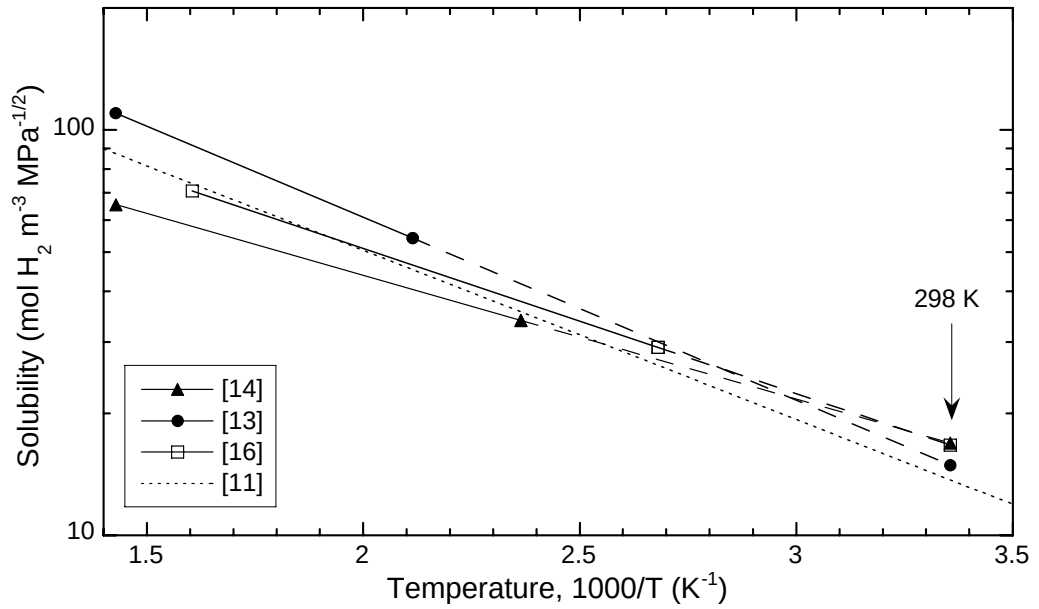

Figure 2.2. Solubility relationships (from Table 2.1) extrapolated (dashed lines) to 298 K and determined from permeability and diffusivity data for austenitic stainless steels. Data from Ref. [14] are for deuterium.

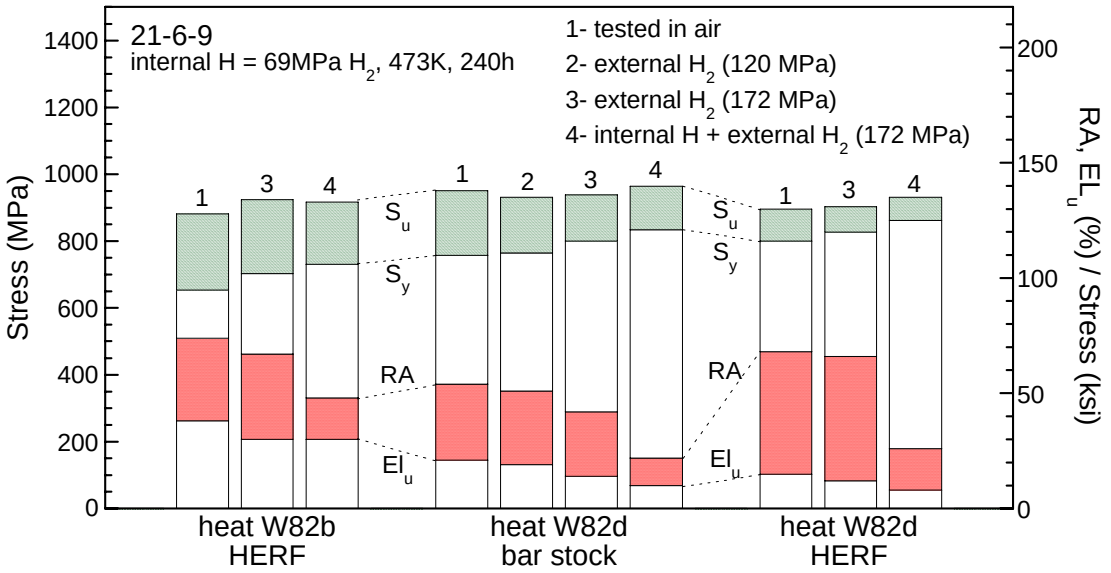

Figure 3.1.1.1. Smooth tensile properties of 21-6-9 stainless steel: (1) tested in air; (2, 3) tested in external hydrogen gas; and (4) tested in external hydrogen gas with internal hydrogen. [6]

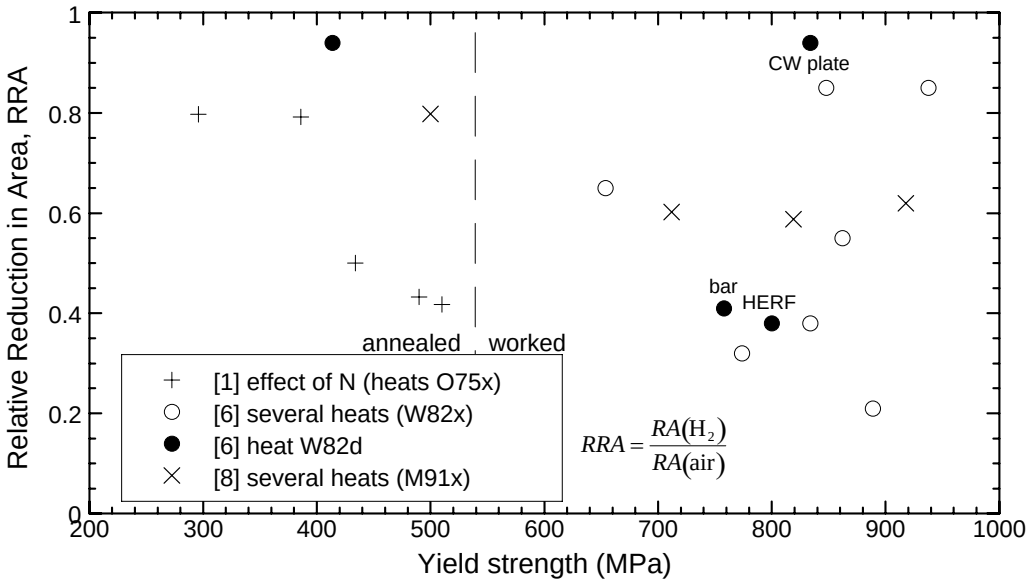

Figure 3.1.1.2. Relative reduction in area (smooth tensile) of 21-6-9 stainless steels as a function of yield strength. Ref. [1]: tested in external hydrogen gas (69 MPa) with internal hydrogen (24 MPa hydrogen gas at 473 K: non-uniform). Ref. [6]: tested in external hydrogen gas (172 MPa) with internal hydrogen (69 MPa hydrogen gas at 473 K: non-uniform). Ref. [8]: tested in air with internal hydrogen (69 MPa hydrogen gas at 623 K: uniform).

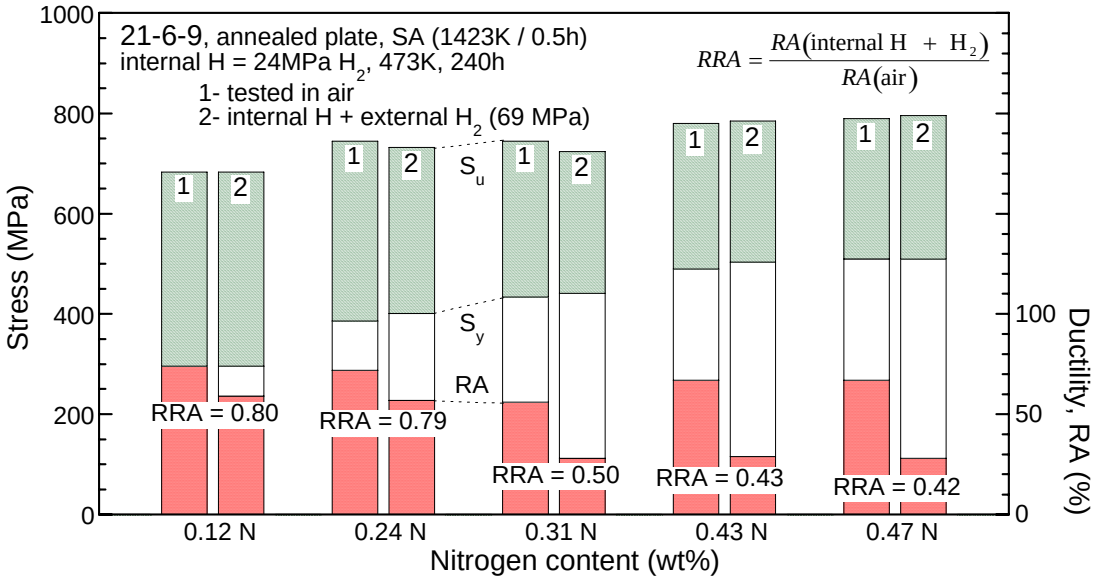

Figure 3.1.1.3. Smooth tensile properties of solution-annealed (SA) 21-6-9 stainless steel with varying nitrogen content, heats 075a-e; measured in external hydrogen gas with internal hydrogen (thermal precharging in hydrogen gas). [1]

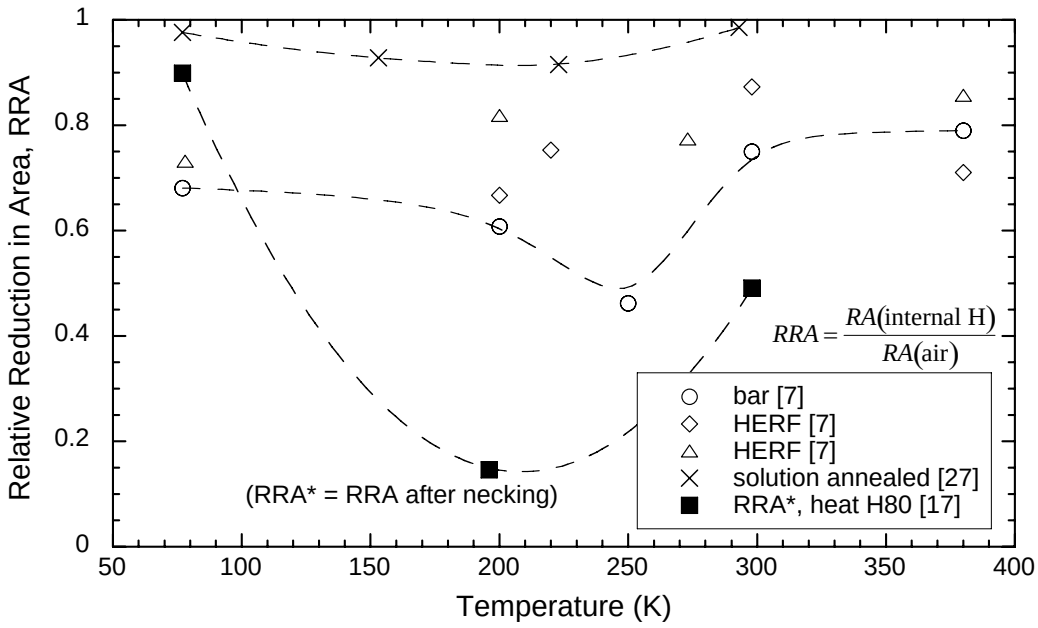

Figure 3.1.1.4. Relative reduction in area (smooth tensile) of several heats of 21-6-9 stainless steel as a function of test temperature; with internal hydrogen. Data from Ref. [7] also given in Table 3.1.1.2. Precharging conditions: Ref. [7], 21-6-9 bar, 69 MPa D_2 at 620 K; 21-6-9 HERF, 69 MPa H_2 at 620 K ; 21-6-9 HERF, 69 MPa H_2 at 470 K; Ref. [27], 10 MPa H_2 at 573 K (uniform); Ref. [17], 69 MPa H_2 at 573 K (uniform).

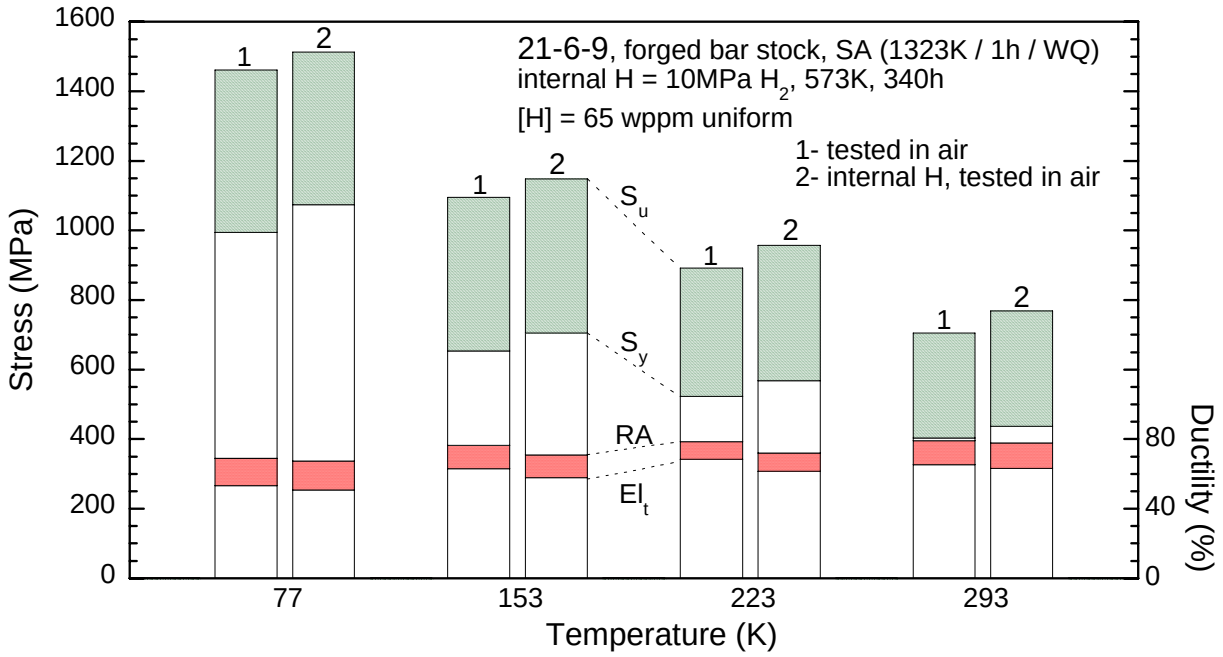

Figure 3.1.1.5. Smooth tensile properties of solution-annealed (SA) 21-6-9 stainless steel as a function of test temperature; measured in air with internal hydrogen (thermal precharging in hydrogen gas). [27]

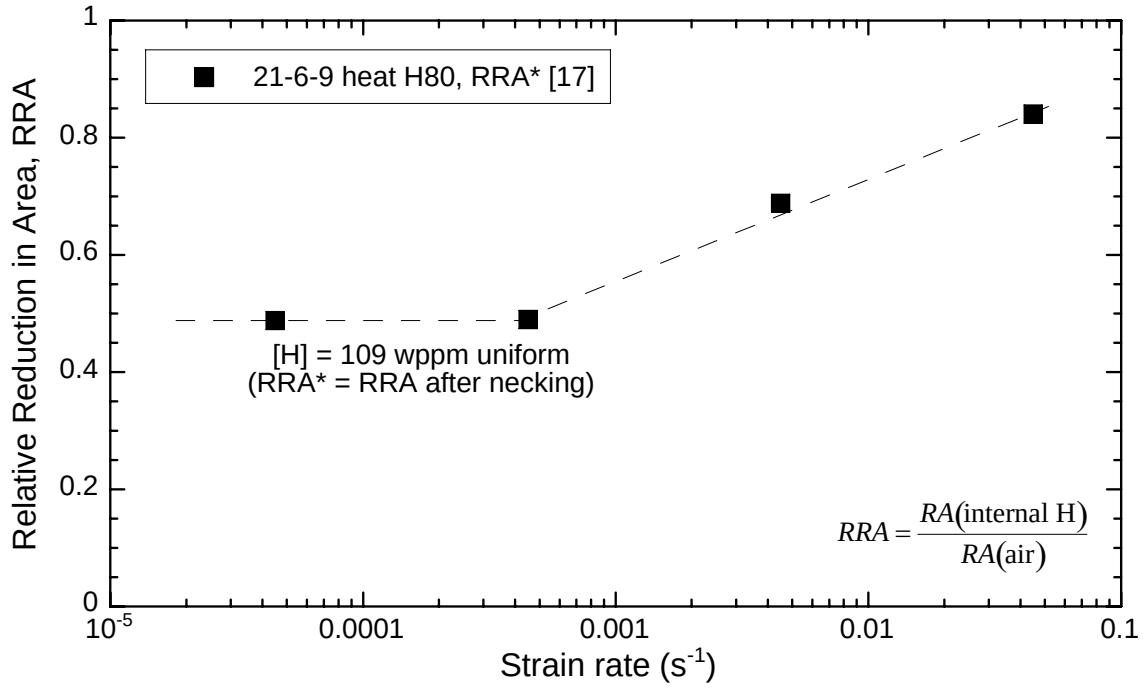

Figure 3.1.1.6. Relative reduction in area (smooth tensile) of 21-6-9 stainless steel (heat H80) as a function of strain rate; measured in air with internal hydrogen (thermal precharging in hydrogen gas). Precharging conditions: Ref. [17], 69 MPa H_2 at 573 K (uniform).

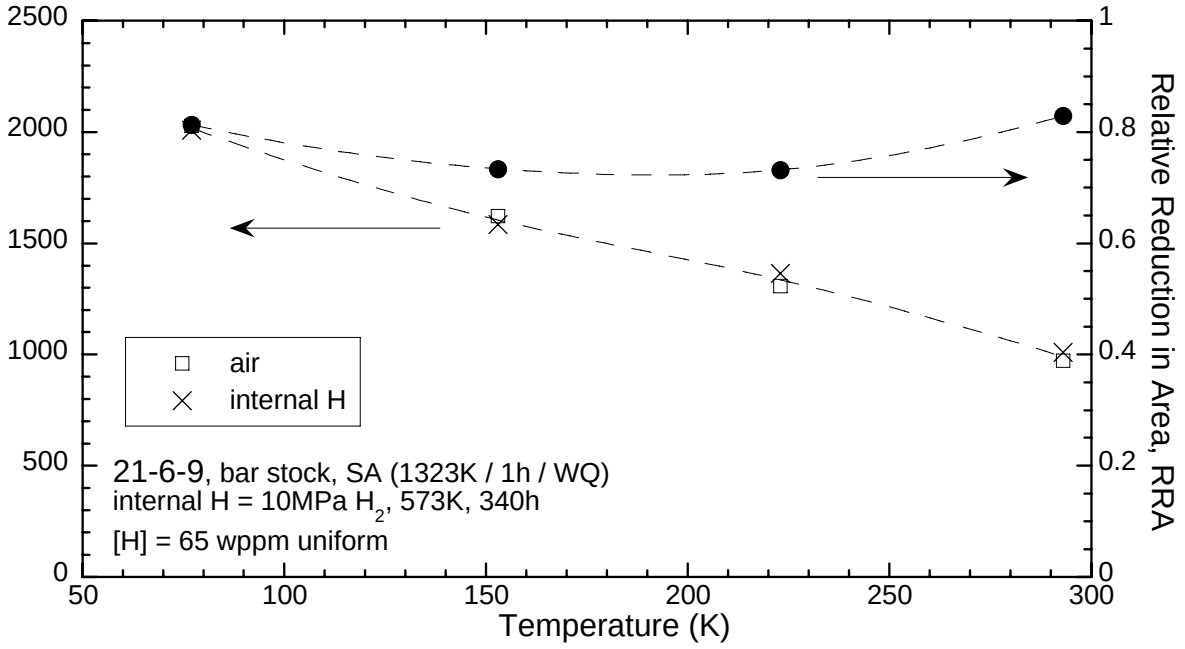

Figure 3.1.2.1. Notched tensile properties of 21-6-9 SA bar stock. Notched specimen: stress concentration factor (K_t) = 4.55; notch geometry = 60˚ included angle; minimum diameter = 4 mm; maximum diameter = 5 mm; notch root radius = 0.1 mm; crosshead rate = 4.2×10^{-2} mm/s. SA = solution annealed, WQ = water quench. [27]

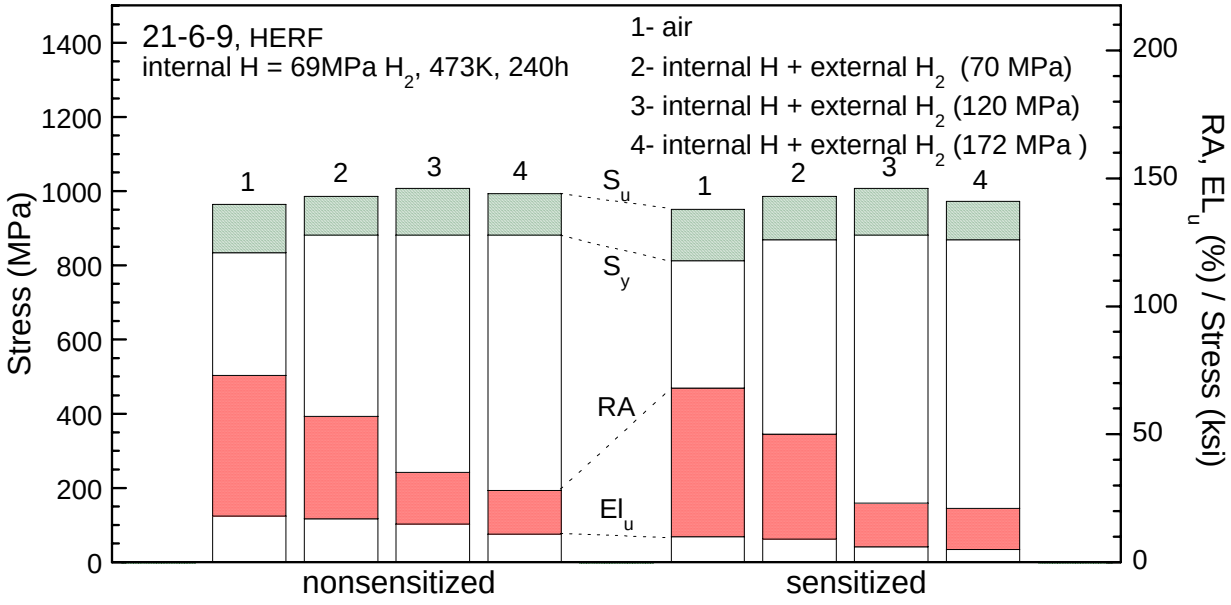

Figure 4.2.1. Smooth tensile properties of 21-6-9 stainless steel that has been sensitized; sensitization conditions are not known; measured in hydrogen gas with internal hydrogen (thermal precharging in hydrogen gas). [6]

Technical Reference on Hydrogen Compatibility of Materials

Precipitation-Strengthened Stainless Alloys:

A-286 (code 2301)

1. General

A-286 is an iron-base superalloy commonly used for its combination of high-strength and good corrosion resistance at intermediate temperatures. The high-nickel content of A-286 and its sister alloys make them resistant to strain-induced phase transformations. Although also referred to as stainless steel, A-286 is considerably different from the 300-series alloys in that it is strengthened by precipitation of the γ' phase, $Ni_3(Al,Ti)$ [1]. Although A-286 can be welded (material specifications exist for welding grades of A-286, e.g. [2]), a modified version of the alloy, called JBK-75, was developed to improve its weldability as well as improve hydrogen compatibility [3]. NASA has developed an alloy called NASA-HR-1, which is based on JBK-75, to improve strength as well as resistance to hydrogen embrittlement, oxidation and corrosion [4]. NASA-HR-1 should not be confused with the Chinese alloy HR-1, which is similar to type 316 stainless steel [5].

The high-nickel and chromium content of the A-286 family of alloys implies high stacking fault energy [6], a characteristic associated with uniform plastic deformation and consequently resistance to hydrogen embrittlement in austenitic stainless steels [7, 8]. The coherent interface of the γ' precipitates in A-286 and JBK-75, on the hand, tends to enable non-uniform plastic deformation, a feature in austenitic steels that is often used to explain comparatively poor resistance to hydrogen embrittlement [6, 9]. The uniformity of plastic deformation in precipitation strengthened austenitic alloys, however, may be less important in governing hydrogen embrittlement compared to other metallurgical features, such as internal interfaces and second phases that can interact with internal hydrogen.

Two general observations distinguish hydrogen-assisted fracture in the A-286 family of alloys from the single-phase austenitic stainless alloys: (i) A-286 that has been tested in tension in external hydrogen gas is not embrittled [6, 10-14], while A-286 with internal hydrogen (by thermal precharging in hydrogen gas) features a significant reduction in tensile ductility [3, 6, 9, 15], and (ii) JBK-75 (internal hydrogen) and A-286 (external hydrogen) that have been tested at elevated strain rates in tension do not show an increase in ductility compared to low strain rates [14, 16]. These observations could be explained by the tenacious oxide that forms upon aging A-286 (even when aged in reducing environment), which acts as a permeation barrier during the relatively short exposure of tensile tests, if these tensile specimens were machined prior to aging. The presence of an oxide, however, cannot explain the strain rate experiments of Holbrook and West on thermally precharged JBK-75, which showed no strain rate effect. Holbrook and West suggested that interactions between hydrogen and dislocations may be different in JBK-75 compared to single-phase austenitic alloys [16].

The mechanisms that contribute to hydrogen embrittlement in the A-286 family of superalloys have not been firmly established. It has been speculated that loss of matrix-γ' precipitate coherency during deformation allows hydrogen to accumulate at these incoherent interfaces leading to hydrogen-assisted fracture [6]. Observations of smaller dimple size in the

presence of internal hydrogen [6] support the view that hydrogen assists nucleation of microvoids, perhaps at newly incoherent interfaces. Ductile microvoid coalescence, however, competes with intergranular fracture in these alloys in the presence of hydrogen. Intergranular fracture is more prevalent and features less evidence of ductile fracture processes in materials aged for longer times as the number and size of grain-boundary precipitates increases with time [3, 17]. Intergranular fracture is generally attributed to the presence of η-phase (Ni_3Ti), which precipitates primarily on or near grain boundaries during aging. Heat treatments (and compositional gradients as in welds), for example, that promote precipitation of the η-phase result in higher crack growth rates and lower threshold stress intensity factors in sustained-loading fracture specimens that have been tested in high-pressure gaseous hydrogen [18, 19]. Ductility losses, as determined from tensile tests, however, do not show a dependence on the volume fraction of the η-phase, nor on the degree of intergranular fracture [3, 17]. It has been surmised that failure of tensile specimens in the presence of hydrogen is dominated by crack nucleation in these alloys, and once a crack forms it propagates rapidly along susceptible features such as grain boundaries [17]. For example, precracked tensile specimens of JBK-75 tested in hydrogen gas failed entirely by intergranular fracture, while smooth tensile specimens of the same material in the same conditions failed by microvoid coalescence [13].

While the nature of interactions between hydrogen, dislocations, and the various precipitates in the A-286 family of alloys are not unequivocally known, the data suggest that shorter aging times and lower aging temperatures result in microstructures that are less susceptible to hydrogen effects [3, 17-20]. Fusion weld microstructures may be particularly susceptible to hydrogen because titanium and nickel segregation in the weld may facilitate precipitation of the η-phase [18, 21].

1.1 Composition and microstructure

Table 1.1.1 lists the compositions of several heats of A-286 used to study hydrogen effects. Welding grades of A-286 specify low silicon and manganese, e.g. [2]. A modified version of A-286, called JBK-75, was developed to improve weldability and hydrogen compatibility [3]; the compositions of several heats of JBK-75 are listed in Table 1.1.2. More recently, JBK-75 has been modified by researchers at NASA to improve strength as well as resistance to hydrogen embrittlement, oxidation and corrosion; this alloy, NASA-HR-1, has additions of tungsten and cobalt in addition to increased nickel and molybdenum content [4].

1.2 Common designations

AISI Type 660, UNS S66286
related alloys: JBK-75 (UNS S66285), V-57, NASA-HR-1

2. Permeability, Diffusivity and Solubility

The permeation and solubility of hydrogen in JBK-75 was found to be independent of heat treatment for conventional solution heat treating and aging cycles [22]. Permeability and solubility generally follow an Arrhenius-type relationship with temperature; Table 2.1 provides these relationships for JBK-75 as well as relationships averaged for several austenitic alloys. Plotting these relationships shows that the superalloys have nominally the same permeability and solubility as the single-phase austenitic stainless alloys, Figure 2.1 and Figure 2.2.

Hydrogen concentration measurements by hot extraction techniques show somewhat different trends from permeation studies. The hydrogen concentration was found to strongly depend on processing conditions for modified A-286 (presumably JBK-75) with internal hydrogen (thermally precharged in hydrogen gas), Table 2.2 [23]. Microstructural details that might account for the measured difference were not reported or discussed in that study. In another study [15], hydrogen concentration measurements in JBK-75 by hot extraction were reported to be 20% higher than concentrations calculated based on data for austenitic alloys. The source of these discrepancies is not clear, but may be related to additional hydrogen trapped at specific microstructural features, such as precipitate interfaces. Trapping of hydrogen is generally considered to be low in single-phase austenitic alloys, however, further study is necessary to determine if hydrogen trapping is significant in precipitation-hardened stainless steels such as the A-286 family of alloys. While hot extraction techniques determine the total hydrogen in the material, i.e., both trapped hydrogen and mobile hydrogen, the solubility and permeability only depend on lattice or mobile hydrogen, which should not be strongly affected by precipitation in A-286 based alloys [22]. Therefore, the relationships provided in Ref. [24] (when corrected to hydrogen), Table 2.1, should be considered the best conservative (high value) estimate for permeability and solubility when extrapolated to room temperature. Based on available data, an upper bound to the equilibrium concentration of hydrogen in the A-286 family of alloys can be approximated from the recommended solubility relationship.

3. Mechanical Properties: Effects of Gaseous Hydrogen

3.1 Tensile properties

3.1.1 Smooth tensile properties

Room temperature tensile testing of A-286 and JBK-75 show little or no loss in ductility during straining in hydrogen gas at pressures up to 172 MPa. Tensile specimens with internal hydrogen (by thermal precharging in hydrogen gas), however, show a significant loss in ductility, typically 50 to 60% loss in reduction in area, Tables 3.1.1.1 and 3.1.1.2. As for most austenitic stainless steels, strength of A-286 and JBK-75 is relatively unaffected by both internal and external hydrogen.

Tensile ductility of JBK-75 with internal hydrogen is reduced at room temperature but is relatively little affected at lower temperature, tensile properties are provided in Table 3.1.1.3 and Figure 3.1.1.1 from room temperature to 77 K. Near room temperature JBK-75 with internal hydrogen exhibits very little ductility after necking begins, but ductility is greater at both lower temperature and elevated temperature. This is shown in Figure 3.1.1.2 for two sets of data, the lower curve represents the relative reduction in area after necking (RRA*) [16], while the upper curve is the RRA as typically reported from total plastic strain for data from Table 3.1.1.3. In all cases the ductility and evidence of ductile fracture processes increase at lower temperature [16, 20].

Unlike other stainless steels in the presence of hydrogen, ductility in JBK-75 is not recovered at elevated strain rate up to $0.06\ s^{-1}$, Figure 3.1.1.3; the data from Ref. [16] is given as the relative reduction in area after necking (RRA*).

Aging tensile specimens after machining results in enhanced precipitation of the η phase due to surface deformation and a microstructure that is more sensitive to hydrogen, Table 3.1.1.4 [15], see also section 4.2.

3.1.2 Notched tensile properties

Notched tensile specimens show essentially no difference in properties when tested in helium or hydrogen at pressures up to 69 MPa, Table 3.1.2.1. The strength of notched tensile specimens of JBK-75 is unaffected by internal hydrogen for temperatures from 77 K to room temperature; the reduction in area of notched tensile specimens, however, is reduced somewhat at room temperature but relatively unaffected at low temperature, Figure 3.1.2.1.

In a separate study, A-286 was electrolytically precharged with internal hydrogen from a molten salt bath to various uniform hydrogen concentrations up to 40 wppm [25]. The notched tensile properties were then measured on single-edge-notched specimens. At a hydrogen concentration of 40 wppm, the notched tensile strength decreased by about 20% and the reduction in area decreased by 50%. The reported ductility loss near 25 wppm [25] is similar to that reported at room temperature for JBK-75 with internal hydrogen incorporated by thermal precharging from hydrogen gas as reported in Ref [20] (and shown in Figure 3.1.2.1).

3.2 Fracture mechanics

3.2.1 Fracture toughness

The fracture toughness of JBK-75 decreased by about half for material with high concentrations of internal hydrogen (>100 wppm), Table 3.2.1.1. Both ductile features and intergranular separation were observed on JBK-75 fracture surfaces [26]; however, uncharged materials primarily featured fracture modes consistent with ductile processes, while intergranular failure was more prevalent in specimens with internal hydrogen. Void nucleation was observed at grain boundaries, but evidence of ductile void formation was less in materials with greater volumes of grain boundary η-phase [26]. The η-phase was present on grain boundaries for all conditions tested, but the longer heat treatments resulted in greater volumes of η-phase, especially at the grain boundaries, and lower fracture toughness for materials with and without internal hydrogen [26].

Fracture toughness was determined [27] from 25.4 mm (1 in) thick, wedge open loading (WOL) specimens in constant displacement tests that did not meet plane strain requirements of standardized testing procedures [28]. These data are provided only as qualitative indicators since there is no other data reported in the literature for fracture toughness of A-286 or JBK-75 in external hydrogen gas. In 34.5 MPa gaseous helium, fracture toughness values (K_Q) of 145 and 138 MPa $m^{1/2}$ are reported at 295 K and 144 K respectively, while in 34.5 MPa gaseous hydrogen values of 100 and 152 MPa $m^{1/2}$ are reported. The material for these tests was forged plate, heat W73 (Table 1.1.1), solution heat treated at 1255 K for 1 hour, oil-quenched and aged at 991 K for 16 hours followed by air-cooling.

3.2.2 Threshold stress-intensity factor

Data from a number of austenitic stainless steels and iron-based (precipitation-strengthened) superalloys show that higher resistance to cracking under static loads in hydrogen generally corresponds to lower yield strength and similar values can be expected for a wide range of

austenitic alloys [19]. Austenitic alloys with yield strengths less than about 700 MPa, in particular, have high resistance to cracking in high-pressure hydrogen gas environments under static loads [19]. Threshold stress intensity factor (K_{TH}) data for JBK-75 in high-pressure hydrogen gas, however, indicate that some microstructures are more susceptible than others, Table 3.2.2.1. Microstructure is especially important in two-phase alloy systems such as A-286, JBK-75 and other precipitation-strengthened alloys. In all cases, intergranular separation as well as ductile fracture processes were apparent from the fracture surfaces, with the fraction of ductile features scaling with threshold stress intensity factor. In addition, greater precipitation of η-phase in the grain boundary correlated with lower threshold [18]. The relatively low threshold stress intensity factor of the solution heat treated JBK-75 aged at the highest temperature is attributed to precipitation of η-phase at grain boundaries [18]. Compositional segregation in fusion-welded material also contributes to increased hydrogen susceptibility in these K_{TH} measurements [18, 19, 21].

In an earlier study, measurements of K_{TH} were attempted on 25.4 mm thick wedge open loading (WOL) specimens of A-286 that were not precracked and were loaded beyond the yield point [27]. None of the testing conditions satisfied the plane strain requirement of standardized testing procedures [28]. These data are provided for qualitative comparison. In 34.5 MPa gaseous hydrogen at room temperature, threshold stress intensity factor was found to be <113 MPa $m^{1/2}$. At 144 K, no crack propagation was observed at an applied stress intensity factor of 198 MPa $m^{1/2}$ in 34.5 MPa gaseous hydrogen. The material for these tests was forged plate, heat W73 (Table 1.1.1), solution heat treated at 1255 K for 1 hour, oil-quenched and aged at 991 K for 16 hours followed by air cooling.

The effect of external hydrogen on crack growth in sustained loading of surface-flawed thin dog-bone-like specimens of A-286 is reported to be negligible in 6.9 MPa gaseous hydrogen [29].

The threshold stress intensity factor for crack propagation of fatigue precracked A-286, with internal hydrogen from electrolytic precharging in molten salt, was measured as a function of hydrogen concentrations up to 30 wppm [30]. For these specimens, however, plane-stress conditions dominated thus the data cannot be compared to standardized plane-strain values of the stress intensity factor. Nevertheless, the relative K_{TH} (internal hydrogen relative to uncharged) was found to be about 0.75 for 30 wppm hydrogen [30]. In addition, the A-286 was less affected by hydrogen than most of the tested alloys including type 301 and 304 stainless steels and nickel-base superalloys (IN625 and IN718) [30].

3.3 Fatigue

Low-cycle fatigue experiments on A-286 show essentially no effect of hydrogen gas [31]. Hollow specimens pressurized to 34 MPa hydrogen and helium gas were tested in 1% total strain range and failed at approximately 2800 cycles.

3.4 Creep

Stress rupture tests in hydrogen gas at 922 K and a stress of 390 MPa result in a reduction in lifetime of about 20% for A-286, from 264 hours in 3.4 MPa air to 215 hours in 3.4 MPa hydrogen gas [31]. A large variation is associated with the rupture times in hydrogen.

3.5 Impact

Charpy impact tests on EB-welded JBK-75 joints show some sensitivity to internal hydrogen (by thermal precharging from hydrogen gas) [32], see section 4.3.

3.6 Disk rupture tests

Disk rupture tests at room temperature show that A-286 is unaffected by pressurized hydrogen [33, 34]. Low-cycle fatigue in the disk rupture configuration (40 cycles to 0.5 of the rupture pressure) also did not affect the rupture pressure in hydrogen [34]. In a later report, disk rupture tests on JBK-75 and A-286 equivalent alloys showed considerable hydrogen embrittlement except in the solution heat-treated condition [35]. Rupture pressures for hydrogen were almost half of the rupture pressures in helium and evidence of intergranular failure modes were explained by η-phase precipitation at grain boundaries.

At elevated temperatures (360 to 700 K), hydrogen gas reduces the rupture pressure compared to helium gas. Exposure to hydrogen gas at 8.6 MPa for 48 hours further reduces the rupture pressure when pressurized by hydrogen gas [33]. This data underscores the importance of delayed effects due to hydrogen uptake and diffusion in metals.

4. Fabrication

4.1 Primary processing

Carbide and sulfide inclusions are believed to have a significant impact on the fracture toughness of JBK-75 in the presence of hydrogen [36]. Deformation and thermomechanical processing accelerate the aging response of A-286 and JBK-75 [15, 17].

4.2 Heat treatment

Since A-286 and alloys based on A-286 are precipitation-strengthened, the heat treatment is of primary importance for controlling microstructure and therefore, controlling strength and susceptibility to hydrogen embrittlement. Lower aging temperatures may help control precipitation kinetics and reduce the formation of undesirable phases such the η-phase [17]. The typical aging cycle for A-286 is 16 hours at 993 K. A two-step aging process is often employed for JBK-75: 8 hours at 948 K, followed by 8 hours at 873 K.

A-286 and JBK-75 in the solution heat-treated condition show little ductility loss in tensile tests with internal hydrogen, Figure 4.2.1. Aging results in a significant reduction in ductility due to η-phase precipitation and this reduction is exacerbated in the presence of internal hydrogen [3, 17]. This ductility loss is essentially independent of aging times greater than a few hours, although the volume fraction of η-phase increases substantially as does the fraction of intergranular failure [3].

Deformation induced by machining has been shown to accelerate η-phase precipitation in A-286, leading to a microstructure that is more susceptible to hydrogen embrittlement, Table 3.1.1.4 [15]. Similarly, intentional cold work accelerates the aging response of JBK-75 and results in ductility loss for aging times as short as one hour with internal hydrogen, Figure 4.2.1. These data indicate that substantially shorter aging times may offer improved hydrogen compatibility without significant compromise on strength, and that standard aging cycles (993K

for 16 hours) are not appropriate for thermomechanically processed materials for service in hydrogen. Values of fracture toughness [26], Table 3.2.1.1, and threshold stress intensity factor in gaseous hydrogen [19], Table 3.2.2.1, also support the principle that shorter aging times and lower temperatures result in improved hydrogen compatibility.

4.3 Properties of welds

Tensile testing of JBK-75 gas tungsten arc (GTA) welds with high concentrations of internal hydrogen show significant losses in ductility [21]. Interdentritic regions in these welds are rich in titanium and nickel, and thus believed to be preferential sites for precipitation of the η-phase (Ni_3Ti) and vulnerable to intergranular fracture [6, 17, 18]. Fracture of the welds was primarily by microvoid coalescence with some evidence of the underlying weld microstructure, however, localized regions of intergranular fracture were observed near the surface of specimens with internal hydrogen, i.e. in regions where the hydrogen concentration was greatest. As in base material [6], the dimple size was reduced in the presence of hydrogen, presumably due to increased activation of nucleation sites, for example in the interdentritic regions. The tensile properties of GTA welds are listed in Table 4.3.1. These data are shown for reference only as they represent the properties of a composite specimen (fusion zone, heat-affected zone and base metal), however, they do demonstrate the effect of hydrogen on the ductility of the welds.

The threshold stress intensity factor of a fusion weld of JBK-75 in hydrogen was reported to be about half that measured for similarly aged forged base metal [19], Table 3.2.2.1. The increased susceptibility is attributed to the macrosegregation inherent to fusion welding processes.

Like the single-phase austenitic stainless steels, the susceptibility to hydrogen embrittlement (as measured by tensile ductility) of JBK-75 electron-beam (EB) welded joints reaches a minimum near room temperature for material with internal hydrogen [32], Table 4.3.2 and Figure 4.3.1. Charpy impact tests, however, show the greatest susceptibility to hydrogen embrittlement at lower temperature and only a nominal effect at room temperature [32]. Overaging these welded joints (30 h at 1013 K) increases susceptibility to hydrogen embrittlement, due to η-phase precipitation [32].

5. References

1. WD Klopp. Nickel Chromium Steels: Fe-25Ni-15Cr-2Ti-1.5Mn-1.3Mo-0.3V (code 1601). in: WF Brown, H Mindlin and CY Ho, editors. Aerospace Structural Metals Handbook. West Lafayette: CINDAS/USAF CRDA Handbooks Operation, Purdue University (1987).
2. AMS 5895C, Steel, Corrosion, and Heat Resistant, Bars, Wire, Forgings, Tubing, and Rings, 15Cr - 25.5Ni - 1.2Mo - 2.1Ti - 0.006B - 0.30V, Consumable Electrode Melted, 1750˚F (954˚C) Solution Heat Treated, Welding Grade, Precipitation Hardenable (UNS S66286). Society of Automotive Engineers (2000).
3. JA Brooks and AW Thompson. Microstructure and Hydrogen Effects on Fracture in the Alloy A-286. Metall Trans 24A (1993) 1983-1991.
4. PS Chen, B Panda and BN Bhat. NASA-HR-1, a New Hydrogen-Resistant Fe-Ni Base Superalloy. in: AW Thompson and NR Moody, editors. Proceedings of the Fifth International Conference on the Effect of Hydrogen on the Behavior of Materials: Hydrogen Effects in Materials, 1994, Moran WY. TMS, Warrendale PA (1996) p. 1011-1019.

5. J Qian, J Chen, J Chen, Z Xu, W Wang and C Pan. Corrosion of austenitic stainless steel in liquid lithium. J Nucl Mater 179-181 (1991) 603-606.
6. AW Thompson and JA Brooks. Hydrogen Performance of Precipitation-Strengthened Stainless Steels Based on A-286. Metall Trans 6A (1975) 1431-1442.
7. MR Louthan, GR Caskey, JA Donovan and DE Rawl. Hydrogen Embrittlement of Metals. Mater Sci Eng 10 (1972) 357-368.
8. BC Odegard, JA Brooks and AJ West. The Effect of Hydrogen on Mechanical Behavior of Nitrogen-Strengthened Stainless Steel. in: AW Thompson and IM Bernstein, editors. Proceedings of an International Conference on Effect of Hydrogen on Behavior of Materials, 1975, Moran WY. The Metallurgical Society of AIME (1976) p. 116-125.
9. AW Thompson. Ductility Losses in Austenitic Stainless Steels Caused by Hydrogen. in: IM Bernstein and AW Thompson, editors. Proceedings of the International Conference on the Effects of Hydrogen on Materials Properties and Selection and Structural Design: Hydrogen in Metals, 1973, Champion PA. American Society of Metals (1974) p. 91-105.
10. RJ Walter and WT Chandler. Effects of High-Pressure Hydrogen on Metals at Ambient Temperature: Final Report (NASA CR-102425). Rocketdyne (report no. R-7780-1) for the National Aeronautics and Space Administration, Canoga Park CA (February 1969).
11. AW Thompson. Hydrogen-Induced Ductility Loss in Commercial Precipitation-Strengthened Stainless Steels. Metall Trans 7A (1976) 315-318.
12. TL Capeletti and MR Louthan. The Tensile Ductility of Austenitic Steels in Air and Hydrogen. J Eng Mater Technol 99 (1977) 153-158.
13. RE Stoltz and AJ West. Hydrogen Assisted Fracture in FCC Metals and Alloys. in: IM Bernstein and AW Thompson, editors. Proceedings of the International Conference on Effect of Hydrogen on Behavior of Materials: Hydrogen Effects in Metals, 1980, Moran WY. The Metallurgical Society of AIME (1980) p. 541-553.
14. EJ Vesely, RK Jacobs, MC Watwood and WB McPherson. Influence of Strain Rate on Tensile Properties in High-Pressure Hydrogen. in: AW Thompson and NR Moody, editors. Proceedings of the Fifth International Conference on the Effect of Hydrogen on the Behavior of Materials: Hydrogen Effects in Materials, 1994, Moran WY. TMS, Warrendale PA (1996) p. 363-374.
15. JA Brooks and MR Louthan. Surface Preparation and Hydrogen Compatibility of an Iron Base Superalloy. Metall Trans 11A (1980) 1981-1986.
16. JH Holbrook and AJ West. The Effect of Temperature and Strain Rate on the Tensile Properties of Hydrogen Charged 304L, 21-6-9, and JBK 75. in: IM Bernstein and AW Thompson, editors. Proceedings of the International Conference on Effect of Hydrogen on Behavior of Materials: Hydrogen Effects in Metals, 1980, Moran WY. The Metallurgical Society of AIME (1980) p. 655-663.
17. BC Odegard and AJ West. The Effect of eta-phase on the Hydrogen Compatibility of a Modified A-286 Superalloy: Microstructural and Mechanical Properties Observations. in: IM Bernstein and AW Thompson, editors. Proceedings of the International Conference on Effect of Hydrogen on Behavior of Materials: Hydrogen Effects in Metals, 1980, Moran WY. The Metallurgical Society of AIME (1980) p. 597-606.
18. MW Perra and RE Stoltz. Sustained-Load Cracking of a Precipitation-Strengthened Austenitic Steel in High-Pressure Hydrogen. in: IM Bernstein and AW Thompson, editors. Proceedings of the International Conference on Effect of Hydrogen on Behavior of

Materials: Hydrogen Effects in Metals, 1980, Moran WY. The Metallurgical Society of AIME (1980) p. 645-653.
19. MW Perra. Sustained-Load Cracking of Austenitic Steels in Gaseous Hydrogen. in: MR Louthan, RP McNitt and RD Sisson, editors. Environmental Degradation of Engineering Materials in Hydrogen. Blacksburg VA: Laboratory for the Study of Environmental Degradation of Engineering Materials, Virginia Polytechnic Institute (1981) p. 321-333.
20. LM Ma, GJ Liang and YY Li. Effect of Hydrogen Charging on Ambient and Cryogenic Mechanical Properties of a Precipitate-Strengthened Austenitic Steel. in: FR Fickett and RP Reed, editors. Proceedings of the International Cryogenic Materials Conference, 1991, Huntsville AL. Advances in Cryogenic Engineering, vol. 38A. Plenum Press, NY (1992) p. 77-84.
21. JA Brooks, AJ West and AW Thompson. Effect of Weld Composition and Microstructure on Hydrogen Assisted Fracture of Austenitic Stainless Steels. Metall Trans 14A (1983) 75-84.
22. J Xu, XK Sun, WX Chen and YY Li. Hydrogen Permeation and Diffusion in Iron-base Superalloys. Acta metall mater 41 (1993) 1455-1459.
23. GR Caskey and RD Sisson. Hydrogen Solubility in Austenitic Stainless Steels. Scr Metall 15 (1981) 1187-1190.
24. MR Louthan and RG Derrick. Hydrogen Transport in Austenitic Stainless Steel. Corros Sci 15 (1975) 565-577.
25. PD Hicks and CJ Altstetter. Internal Hydrogen Effects on Tensile Properties of Iron- and Nickel-Base Superalloys. Metall Trans 21A (1990) 365-372.
26. BC Odegard, SL Robinson and NR Moody. Effects of Internal Hydrogen on the Toughness and Fracture of Forged JBK-75 Stainless Steel. in: AW Thompson and NR Moody, editors. Proceedings of the Fifth International Conference on the Effect of Hydrogen on the Behavior of Materials: Hydrogen Effects in Materials, 1994, Moran WY. TMS, Warrendale PA (1996) p. 591-598.
27. RJ Walter and WT Chandler. Influence of Gaseous Hydrogen on Metals: Final Report (NASA CR-124410). Rocketdyne for the National Aeronautics and Space Administration, Canoga Park CA (Oct 1973).
28. ASTM E 1681-99, Standard Test Method for Determining Threshold Stress Intensity Factor for Environment-Assisted Cracking of Metallic Materials. American Society for Testing and Materials (1999).
29. RG Forman. Environmental Crack-Growth Behavior of High-Strength Pressure Vessel Alloys (NASA TN D-7952). Lyndon B. Johnson Space Center, National Aeronautics and Space Administration, Houston TX (Apr 1975).
30. PD Hicks and CJ Altstetter. Hydrogen-Enhanced Cracking of Superalloys. Metall Trans 23A (1992) 237-249.
31. RP Jewitt, RJ Walter, WT Chandler and RP Frohmberg. Hydrogen Environment Embrittlement of Metals (NASA CR-2163). Rocketdyne for the National Aeronautics and Space Administration, Canoga Park CA (March 1973).
32. YY Li, LM Ma, GJ Liang, QH Gui and ZK Li. Effect of Hydrogen on Mechanical Properties of EB-Welded Joints of JBK-75 Steel from Ambient to Cryogenic Temperatures. in: RP Reed, FR Fickett, LT Summers and M Stieg, editors. Proceedings of the International Cryogenic Materials Conference, 1993, Albuquerque NM. Advances in Cryogenic Engineering, vol. 40B. Plenum Press, NY (1994) p. 1283-1289.

33. J Papp, RF Hehemann and AR Troiano. Hydrogen Embrittlement of High Strength FCC Alloys. in: IM Bernstein and AW Thompson, editors. Proceedings of the International Conference on the Effects of Hydrogen on Materials Properties and Selection and Structural Design: Hydrogen in Metals, 1973, Champion PA. American Society for Metals (1974) p. 657-669.
34. J-P Fidelle, R Bernardi, R Broudeur, C Roux and M Rapin. Disk Pressure Testing of Hydrogen Environment Embrittlement. in: Hydrogen Embrittlement Testing, ASTM STP 543, American Society for Testing and Materials. (1974) p. 221-253.
35. PF Azou and JP Fidelle. Very low strain rate hydrogen gas embrittlement (HGE) and fractography of high-strength, mainly austenitic stainless steels. in: MR Louthan, RP McNitt and RD Sisson, editors. Environmental Degradation of Engineering Materials III, 1987, The Pennsylvania State University, University Park PA. The Pennsylvania State University, University Park PA p. 189-198.
36. NR Moody, SL Robinson and WM Garrison. Austenitic Superalloy Selection and Development for Hydrogen Service from a Microstructure Perspective. in: HJ Cialoni, ME Blum, GWE Johnson and GF VanderVoort, editors. Proceedings of the Twentieth Annual Technical Meeting of the International Metallographic Society: Metallography of Advanced Materials, 1987, Monterey CA. Microstructural Science, vol. 16. ASM, Metals Park OH (1988) p. 177-192.
37. ASTM DS-56H, Metals and Alloys in the UNIFIED NUMBERING SYSTEM (SAE HS-1086 OCT01). American Society for Testing and Materials (Society of Automotive Engineers) (2001).
38. XK Sun, J Xu and YY Li. Hydrogen Permeation Behaviour in Austenitic Stainless Steels. Mater Sci Eng A114 (1989) 179-187.
39. T-P Perng and CJ Altstetter. Effects of Deformation on Hydrogen Permeation in Austenitic Stainless Steels. Acta metall 34 (1986) 1771-1781.
40. SL Robinson and NR Moody. The Effect of Hydrogen, Tritium and Decay Helium on the Fracture Toughness of a Stainless Steel Superalloy. J Nucl Mater 140 (1986) 245-251.
41. RE Stoltz, NR Moody and MW Perra. Microfracture Model for Hydrogen Embrittlement of Austenitic Steels. Metall Trans 14A (1983) 1528-1531.

Table 1.1.1. Specification limits for A-286 and composition of several heats of A-286 stainless steel used to study hydrogen effects.

heat	Fe	Cr	Ni	Ti	Mn	Mo	V	Al	Si	C	B	other	Ref.
UNS S66286	Bal	13.50 16.00	24.0 27.0	1.90 2.35	2.00 max	1.00 1.50	0.10 0.50	0.35 max	1.00 max	0.08 max	0.0010 0.010	0.40 max P 0.030 max S	[37]
W69	Bal	15.07	25.58	1.93	1.47	1.35	0.30	0.13	0.61	0.052	0.0055	0.019 P 0.010 S	[10]
W73	Bal	14.15	24.88	2.21	1.20	1.25	0.22	0.16	0.63	0.048	0.47	0.010 S 0.016 P 0.01 Zr	[27]
P81	Bal	14.0	24.33	2.15	0.13	1.16	—	—	0.16	0.054	—	—	[19]
B93	Bal	14.90	24.93	2.15	1.32	1.25	0.21	0.19	0.63	0.068	0.004	0.003 S 0.018 P	[3]
V96	Bal	14.02	24.38	2.09	0.28	1.37	0.2	0.13	0.22	0.024	0.0046	0.1 Cu 0.08 Co 0.001 S 0.001 P	[14]
V-57	Bal	14.8	26.0	3.0	0.3	1.25	0.3	0.25	0.6	0.05	0.01	Nominal values for alloy V-57	[11]

Table 1.1.2. Specification limits for JBK-75 and composition of several heats of JBK-75 stainless steel used to study hydrogen effects.

heat	Fe	Cr	Ni	Ti	Mn	Mo	V	Al	Si	C	B	other	Ref.
UNS S66286	Bal	13.50 16.00	29.00 31.00	2.0 2.3	0.20 max	1.00 1.50	0.10 0.50	0.15 0.35	0.10 max	0.01 0.03	0.002 max	0.006 max S 0.010 max P	
T75	Bal	14.48	30.46	2.07	0.11	1.22	0.25	0.27	0.15	0.020	0.0010		[6]
B80	Bal	14.02	29.58	2.10	<0.01	1.28	0.35	0.16	<0.01	0.019	<0.001		[15]
O80	Bal	15.3	29.8	2.1	0.011	1.2	0.42	0.3	0.075	0.012	0.0011	0.004 S 0.01 P	[17]
P80	Bal	15.5	30.7	2.1	0.053	1.2	0.26	0.2	0.032	0.017	<0.0005	0.0013 S <0.002 P	[19]
B83w	Bal	15.0	30.0	2.2	0.1	1.2	—	0.2	0.1	0.03	0.001	0.01 S 0.01 P	[21]
X93	Bal	15.22	29.48	1.85	0.19	1.53	0.26	0.20	0.17	0.024	0.0019	0.004 S 0.011 P	[22]

w = composition of the weld fusion zone

Table 2.1. Permeability and solubility relationships for JBK-75 and average relationships determined for several austenitic stainless steels.

Material	Temperature range (K)	Pressure range (MPa)	$\Phi = \Phi_o \exp(-E_\Phi / RT)$		$S = S_o \exp(-E_S / RT)$		Ref.
			Φ_o $\left(\frac{\text{mol H}_2}{\text{m} \cdot \text{s} \cdot \sqrt{\text{MPa}}}\right)$	E_Φ $\left(\frac{\text{kJ}}{\text{mol}}\right)$	S_o $\left(\frac{\text{mol H}_2}{\text{m}^3 \cdot \sqrt{\text{MPa}}}\right)$	E_S $\left(\frac{\text{kJ}}{\text{mol}}\right)$	
JBK-75, heat X93	483-703	0.1	4.36×10^{-4}	62.10	145	13.58	[22]
Average of several austenitic alloys †	423-700	0.1-0.3	1.2×10^{-4}	59.8	179	5.9	[24]
Average of six austenitic alloys	473-703	0.1	2.81×10^{-4}	62.27	488	8.65	[38]
Average of four austenitic alloys	373-623	1×10^{-4}-0.03	5.35×10^{-5}	56.1	266	6.86	[39]

† Data from Ref. [24] is determined for deuterium: permeability has been corrected here to give permeability of hydrogen (by multiplying by the square root of the mass ratio: $\sqrt{2}$); solubility is assumed to be independent of isotope.

Table 2.2. Hydrogen concentration of modified A-286 alloys measured using hot extraction after thermal precharging in hydrogen gas.

Material	Surface condition	Thermal precharging	Hydrogen concentration		Ref.
			wppm	appm	
JBK-75 ST + A	—	69 MPa H_2 573 K	54	3000	[16]
"modified A-286" Annealed	600 grit finish	69 MPa H_2 470 K	80	4500	[23]
	Electropolished		81	4500	
"modified A-286" HERF	600 grit finish		51	2900	
	Electropolished		55	3100	
JBK-75 ST + A	—	10 MPa H_2 573 K	25	1400	[20]

HERF = high energy rate forging, ST = solution treatment, A = age

Table 3.1.1.1. Smooth tensile properties of A-286 stainless steel at room temperature; measured in external hydrogen gas or with internal hydrogen (measured in air after thermal precharging in hydrogen gas).

Material	Thermal precharging	Test environment	Strain rate (s^{-1})	S_y (MPa)	S_u (MPa)	El_u (%)	El_t (%)	RA (%)	Ref.
A-286	None	69 MPa He	—	724	1117	—	26	47	[12]
	None	69 MPa H_2		710	1131	—	34	49	
A-286, heat W69 ST + A (1173K/2h + 993K/16h)	None	69 MPa He	0.67 x 10^{-3}	848	1089	—	26	44	[10, 31]
	None	69 MPa H_2		—	1117	—	29	43	
A-286 A (990K/16h)	None	Air	—	760†	1065	—	21	32	[6, 9]
	None	69 MPa H_2		—	—	(RRA ~ 1)			
	(1)	Air		—	—	(RRA ~ 0.5)			
A-286 HERF + A (990K/16h)	None	Air	—	850†	1105	—	—	(30)	[9]
	None	69 MPa H_2		—	—	(RRA ~ 1)			
	(1)	Air		—	—	(RRA ~ 0.5)			
A-286 HERF	None	Air	—	440†	750	—	—	(58)	[9]
	(1)	Air		—	—	(RRA ~ 1)			
A-286, heat V96 ST + A (1266K/1h/WQ+ 994K/16h/AC)	None	34 MPa He	8.3 x 10^{-6}	843	1166	24	—	50	[14]
	None	34 MPa H_2		839	1159	24	—	51	
V-57, heat V-57 ST + A (1255K/2h/OQ+ 990K/16h/AC)	None	Air	—	690	1145		32	50	[11]
	None	69 MPa H_2		—	—	(RRA ~ 0.95)			
	(2)	Air		—	—	(RRA ~ 0.25)			

HERF = high energy rate forging, ST = solution treatment, A = age, WQ = water quench, OQ = oil quench, AC = air cool

Values in parenthesis are determined from plots.

† stress at 0.2% strain

(1) 69 MPa hydrogen, 475 K, 1500 h

(2) 24 MPa hydrogen, 475 K, 400 h (gauge diameter = 6.5 mm diameter)

Table 3.1.1.2. Smooth tensile properties of JBK-75 stainless steel at room temperature; measured in external hydrogen gas, or with internal hydrogen (measured in air after thermal precharging in hydrogen gas).

Material	Thermal precharging	Test environment	Strain rate† (s^{-1})	S_y (MPa)	S_u (MPa)	El_u (%)	El_t (%)	RA (%)	Ref.
JBK-75, heat T75 ST + A (1200K/2h + 990K/16h/AC)	None	Air	—	875	1305		21	55	[6]
	None	69 MPa H_2		—	—	RRA ~ 1			
	(1)	air		—	—	RRA ~ 0.9			
JBK-75, heat P80 A (993K/16h)	None	Air	0.021 mm/s†	717	1131	—	28	51	[13]
	None	172 MPa H_2		—	—	—	—	47	
JBK-75, heat B80 A (993K/16h)	None	Air	0.33 x 10^{-3}	702	1105	18	23	45	[15]
	(2)	Air		703	1100	16	17	20	
JBK-75, heat O80 ST + A (1253K/1h/WQ + 993K/16h)	None	Air	0.83 x10^{-3}	716	1130	22	—	51	[17]
	(3)	172 MPa H_2		723	1137	16	—	24	
JBK-75, heat O80 8% CW + A (948K/8h)	None	Air	0.83 x10^{-3}	1083	1302	11	—	45	[17]
	(3)	172 MPa H_2		1089	1295	12	—	18	
JBK-75 ST + A (1253K/1h/WQ + 1013K/8 h)	None	Air	0.017 mm/s†	763	1109	—	29	58	[20]
	(4)	Air		763	1110	—	26	43	
JBK-75 A (1013 K/8 h)	None	Air	0.017 mm/s†	759	1090	—	32	59	[32]
	(5)	Air		745	1071	—	31	40	

ST = solution treatment, A = age, WQ = water quench, CW = cold work (diameter reduction)

† when strain rate is not known, displacement rates are quoted if reported

(1) 24 MPa hydrogen gas, 475 K, 100 h (gauge diameter = 3 mm); calculated concentration gradient of 45 to 4 wppm hydrogen surface to center (2500 to 250 appm)

(2) 69 MPa hydrogen gas, 473 K, 158 h (gauge diameter = 5 mm); calculated concentration gradient of 45 to 9 wppm hydrogen surface to center (2500 to 500 appm); however vacuum extraction indicated hydrogen concentration of about 20% higher

(3) 69 MPa hydrogen gas, 473 K, 240 h (gauge diameter = 5 mm); calculated concentration gradient of 99 to 2 wppm hydrogen surface to center (5500 to 100 appm)

(4) 10 MPa hydrogen gas, 573 K, 340 h (gauge diameter = 5 mm); 25 wppm hydrogen (1400 appm) measured by ion-microprobe sectional hydrogen analysis

(5) 10 MPa hydrogen gas, 573 K, 340 h (gauge thickness = 2 mm); 25 wppm hydrogen (1400 appm) measured by ion-microprobe sectional hydrogen analysis

Table 3.1.1.3. Smooth tensile properties of JBK-75 stainless steel as a function of temperature; with internal hydrogen (measured in air after thermal precharging in hydrogen gas).

Material	Thermal precharging	Test environment	Strain rate† (s^{-1})	S_y (MPa)	S_u (MPa)	El_u (%)	El_t (%)	RA (%)	Ref.
JBK-75 ST + A (1253K/1h/WQ + 1013K/8h)	None	Air 293 K	0.17 mm/s†	763	1109	—	28.9	58.1	[20]
	(1)			763	1110	—	26.1	43.4	
	None	Air 223 K		778	1152	—	30.2	57.7	
	(1)			775	1153	—	29.6	51.4	
	None	Air 153 K		806	1190	—	31.3	57.3	
	(1)			793	1207	—	33.1	56.3	
	None	Air 77 K		876	1412	—	41.6	60	
	(1)			868	1417	—	41.6	59.2	

† when strain rate is not known, displacement rates are quoted if reported

(1) 10 MPa hydrogen gas, 573 K, 340 h (gauge diameter = 5 mm); 25 wppm uniform hydrogen (1400 appm)

Table 3.1.1.4. Smooth tensile properties of JBK-75 stainless steel at room temperature as function of surface deformation due to machining; with internal hydrogen (measured in air after thermal precharging in hydrogen gas).

Material	Thermal precharging	Test environment	Strain rate (s^{-1})	S_y (MPa)	S_u (MPa)	El_u (%)	El_t (%)	RA (%)	Ref.
JKB-75, heat B80 Age† + machine	None	Air	0.33×10^{-3}	702	1105	18.2	23.4	45.3	[15]
	(1)	Air		703	1100	16.5	16.7	20.2	
JBK-75, heat B80 Age† + machine + grind	None	Air		702	1121	18.6	23.6	49.0	
	(1)	Air		716	1106	15.8	16.2	23.8	
JBK-75, heat B80 Machine + age† + grind	None	Air		806	1124	18.6	23.7	46.5	
	(1)	Air		805	1090	11.7	12.0	14.7	

† 993K/16h

(1) 69 MPa hydrogen gas, 473 K, 158 h (gauge diameter = 5 mm); calculated concentration gradient of 45 to 9 wppm hydrogen surface to center (2500 to 500 appm); however vacuum extraction indicated hydrogen concentration about 20% higher.

Table 3.1.2.1. Notched tensile properties of A-286 stainless steel at room temperature; measured in external hydrogen gas.

Material	Specimen	Thermal precharging	Test environment	Displ. rate (mm/s)	S_y † (MPa)	σ_s (MPa)	RA (%)	Ref.
A-286, heat W69 ST + A (1173K/2h/WQ+ 993K/16h/AC)	(a)	None	69 MPa He	0.7 x10^{-3}	848	1606	5.6	[10, 31]
		None	69 MPa H_2		—	1565	6.2	
A-286, heat V96 ST + A (1266K/1h/WQ+ 994K/16h/AC)	(b)	None	34 MPa He	0.21 x10^{-3}	843	1826	—	[14]
		None	34 MPa H_2		839	1756	—	

ST = solution treatment, A = age, WQ = water quench, AC = air cool

† yield strength of smooth tensile specimen

(a) V-notched specimen: 60˚ included angle; minimum diameter = 3.81 mm; maximum diameter = 7.77 mm; notch root radius = 0.024 mm. Stress concentration factor (K_t) = 8.4.

(b) Notch (minimum) diameter = 6.35 mm. Stress concentration factor (K_t) = 6.0.

Table 3.2.1.1. Fracture toughness of JBK-75 stainless steel at room temperature; measured in air with internal hydrogen (thermal precharging in hydrogen gas).

Material	Test method	Thermal precharging	Test environment	S_y (MPa)	K_Q† (MPa $m^{1/2}$)	Ref.
JBK-75, heat B80 ST + A (1253K/1h/WQ + 993K/16h)	WOL J-integral	None	Air	717	139	[36, 40]
	3PB J-integral	(1)	Air	723	77	
JBK-75, heat O80 HERF + A (1253K; 948K/8h + 873K/8h)	3PB J-integral	None	Air	937	99	[26]
		(1)	Air	—	44	
JBK-75, heat O80 HERF + A (1253K; 948K/32h)	3PB J-integral	None	Air	960	89	[26]
		(1)	Air	—	41	
JBK-75, heat O80 HERF + A (1253K; 948K/96h)	3PB LEFM	None	Air	964	87	[26]
		(1)	Air	—	35	

HERF = high energy rate forging, A = age, ST = solution treatment, WQ = water quench, WOL = wedge open loading specimen, 3PB = 3-point bending specimen, LEFM = linear elastic fracture mechanics

† not clear if plane strain requirements are met in these studies

(1) 138 MPa hydrogen, 573 K, 1500 h; estimated uniform hydrogen concentration of 120-140 wppm (6700 - 8000 appm) [36, 40]

Table 3.2.2.1. Threshold stress intensity factor for A-286 and JBK-75; measured in external hydrogen gas. The testing procedure is believed to have satisfied the requirements of ASTM E 1681-99 [28].

Material	S_y † (MPa)	RA † (%)	Threshold Stress Intensity Factor (MPa $m^{1/2}$)		Ref.
			100 MPa H_2	200 MPa H_2	
A-286, heat P81 ST +A (1253K/1h/WQ + 993K/16h)	779	46	—	94*	[19] ‡
JBK-75, heat P80 ST + A (1253K/1h/WQ + 993K/16h)	717	51	44	47	[19] ‡
JBK-75, heat P80 HERF + A (1243K/WQ + 948K/8h + 873K/8h)	855	37	109*	116*	[19] ‡
JBK-75, heat P80 HERF + A (1243K/WQ + 948K/32h)	923	38	69	66	[19] ‡
JBK-75, heat P80 Fusion weld + A (948K/8h + 873K/8h)	~700	—	~50 (H_2 pressure not reported)		[19] ‡

HERF = high-energy rate forging, ST = solution treatment, A = age, WQ = water quench

* did not satisfy plane strain requirements for analysis of linear elastic fracture mechanics

† yield strength and reduction in area of smooth tensile specimen, not exposed to hydrogen

‡ data also reported in Ref. [13, 18, 41]

Table 4.2.1. Smooth tensile properties of JBK-75 stainless steel at room temperature as a function of aging time and cold-work; measured in external hydrogen gas with internal hydrogen (thermal precharging in hydrogen gas).

Condition	Aging time	Thermal precharging	Test environment	Strain rate	S_y (MPa)	S_u (MPa)	El_u (%)	El_t (%)	RA (%)	Ref.
JBK-75, heat O80 ST + A (1253K/ 1h/WQ; 993K)	ST	None	Air	0.83×10^{-3} s^{-1}	241	620	35	—	70	[17]
		(1)	172 MPa H_2		245	618	34	—	67	
	4 h	None	Air		565	1058	26	—	61	
		(1)	172 MPa H_2		560	1012	18	—	24	
	8 h	None	Air		632	1091	24	—	57	
		(1)	172 MPa H_2		640	1063	16	—	23	
	12 h	None	Air		672	1131	22	—	51	
		(1)	172 MPa H_2		683	1092	16	—	21	
	16 h	None	Air		716	1130	22	—	51	
		(1)	172 MPa H_2		723	1137	16	—	24	
JBK-75, heat O80 8% CW + A (948 K)	1 h	None	Air		987	1169	13	—	60	
		(1)	172 MPa H_2		1054	1216	12	—	25	
	4 h	None	Air		1100	1288	11	—	52	
		(1)	172 MPa H_2		1136	1282	10	—	23	
	8 h	None	Air		1083	1302	11	—	45	
		(1)	172 MPa H_2		1089	1295	12	—	18	
JBK-75, heat O80 20% CW + A (948K)	1 h	None	Air		1196	1306	6.9	—	54	
		(1)	172 MPa H_2		1226	1325	7.8	—	31	
	4 h	None	Air		1178	1340	8.5	—	45	
		(1)	172 MPa H_2		1192	1326	9.2	—	22	
	8 h	None	Air		1085	1304	9.5	—	40	
		(1)	172 MPa H_2		1123	1295	9.6	—	19	
JBK-75, heat O80 36% CW + A (948K)	1 h	None	Air		1212	1337	5.8	—	50	
		(1)	172 MPa H_2		1240	1350	7.2	—	21	
	4 h	None	Air		1029	1269	10	—	44	
		(1)	172 MPa H_2		1075	1268	9.5	—	19	
	8 h	None	Air		785	1169	15	—	48	
		(1)	172 MPa H_2		878	1152	12	—	20	

ST = solution treatment, A = age, WQ = water quench; CW = cold work (diameter reduction)

(1) 69 MPa hydrogen gas, 473K, 240 h (gauge diameter = 5 mm): calculated concentration gradient of approximately 99 to 2 wppm hydrogen surface to center (5500 to 100 appm)

Table 4.3.1. Smooth tensile properties of JBK-75 composite GTA weld specimens at room temperature; with internal hydrogen (measured in air after thermal precharging in hydrogen gas), or measured in external hydrogen gas with internal hydrogen (thermal precharging in hydrogen gas).

Material	Thermal precharging	Test environment	Strain rate (s^{-1})	S_y (MPa)	S_u (MPa)	El_u (%)	El_t (%)	RA (%)	Ref.
JBK-75, heat B83w†	None	Air	0.33 x 10^{-3}	781	1014	6.0	8.2	38	[21]
	(1)	Air		749	980	4.6	4.8	24	
Aged (948K/8h + 873K/8h)	(2)	Air		796	993	4.2	4.4	22	
	(2)	172MPa H_2		760	953	4.6	5.0	23	

† The base material for these studies was HERF (high energy rate forging), back extrusions of JBK-75, machined to cylindrical shape (10 cm diameter, 1.5 cm wall thickness) with circumferential double J grooves; eight to ten weld passes were required to fill groove. The filler material was also JBK-75 matched to the composition of the base metal. Tensile bars contain base material and heat affected zone with the fusion zone centered in the gauge length, and were aged after machining.

(1) 24 MPa hydrogen gas, 473 K, 240 h (gauge diameter = 5 mm): calculated concentration gradient of 45 to 4 wppm surface to center (2500 to 200 appm)

(2) 69 MPa hydrogen gas, 473 K, 240 h (gauge diameter = 5 mm): calculated concentration gradient of 72 to 7 wppm surface to center (4000 to 400 appm)

Table 4.3.2. Smooth tensile properties of JBK-75 EB-weld specimens at low temperatures; with internal hydrogen (measured in air after thermal precharging in hydrogen gas).

Material	Thermal precharging	Test temperature (K)	Strain rate† (s^{-1})	S_y (MPa)	S_u (MPa)	El_u (%)	El_t (%)	RA (%)	Ref.
JBK-75 Aged (1013K/8h)	None	293	0.017 mm/s†	759	1090	—	32	59	[32]
	(1)			745	1071	—	31	40	
JBK-75 EB welds Aged (1013K/8h)	None	293		800	1041	—	18	52	
	(1)			784	1032	—	16	33	
	None	193		826	1096	—	19	51	
	(1)			832	1121	—	20	44	
	None	77		909	1306	—	25	50	
	(1)			921	1318	—	24	41	

EB = electron beam

† when strain rate is not known, displacement rates are quoted if reported

(1) 10 MPa hydrogen gas, 573 K, 340 h (gauge thickness = 2 mm); 25 wppm hydrogen (1400 appm) in the base metal and 16 wppm (920 appm) in the weld metal, measured by ion-microprobe sectional hydrogen analysis

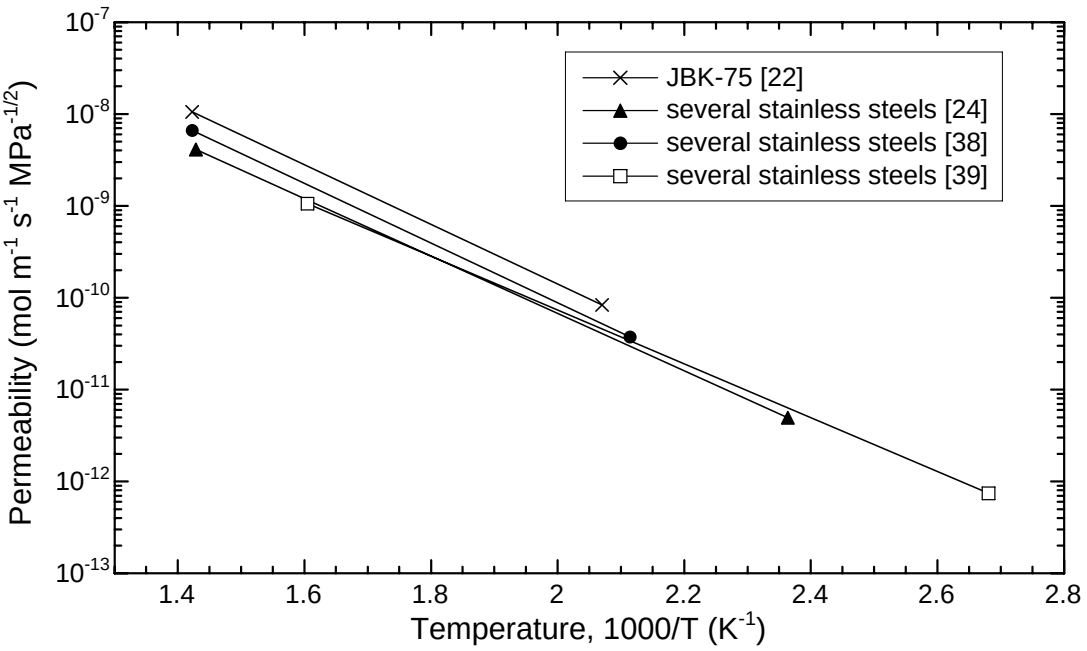

Figure 2.1. Permeability in JBK-75 and average relationships determined for several austenitic stainless steels. Data from Ref. [24] is determined for deuterium: permeability has been corrected here to give permeability of hydrogen by multiplying by the square root of the mass ratio ($\sqrt{2}$).

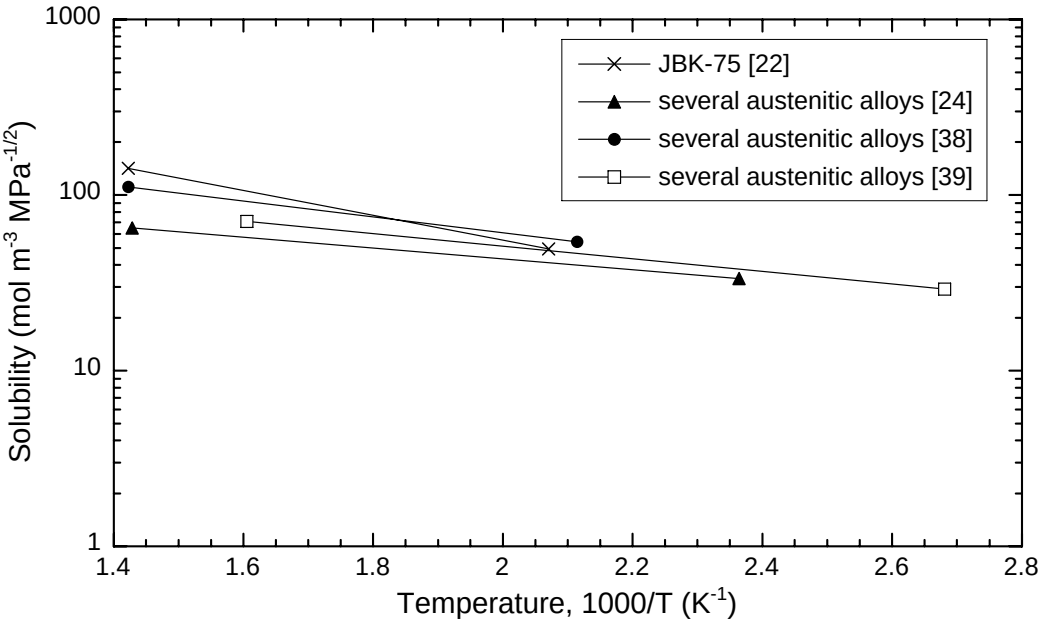

Figure 2.2. Solubility in JBK-75 and average relationships determined for several austenitic stainless steels. Data from Ref. [24] is determined for deuterium; however, solubility is assumed to be independent of hydrogen isotope.

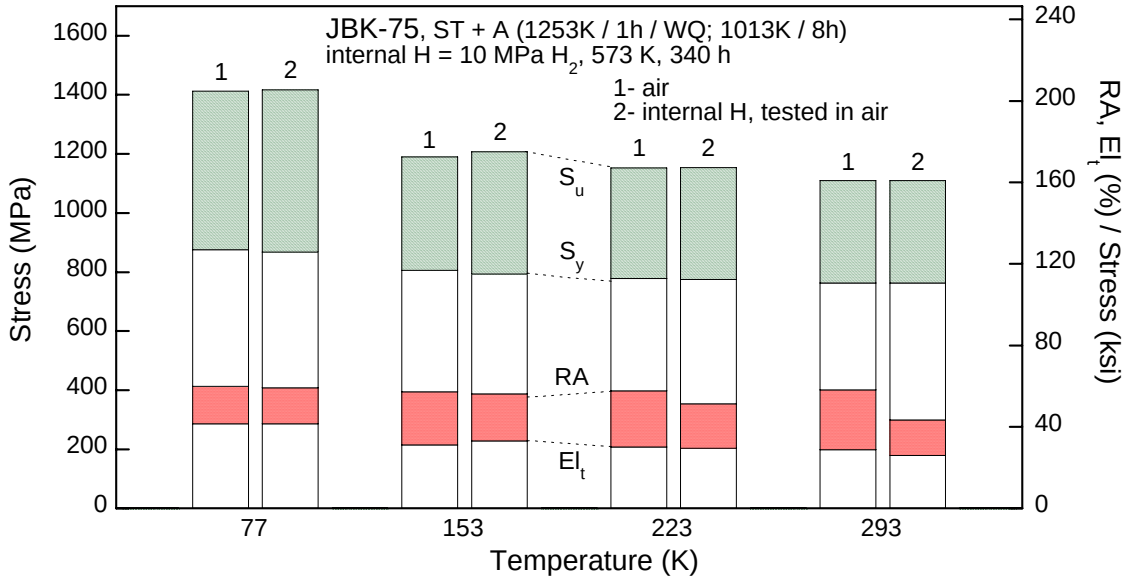

Figure 3.1.1.1. Smooth tensile properties of JBK-75 stainless steel as a function of temperature; with internal hydrogen (measured in air after thermal precharging in hydrogen gas). Data also presented in Table 3.1.1.3. [20]

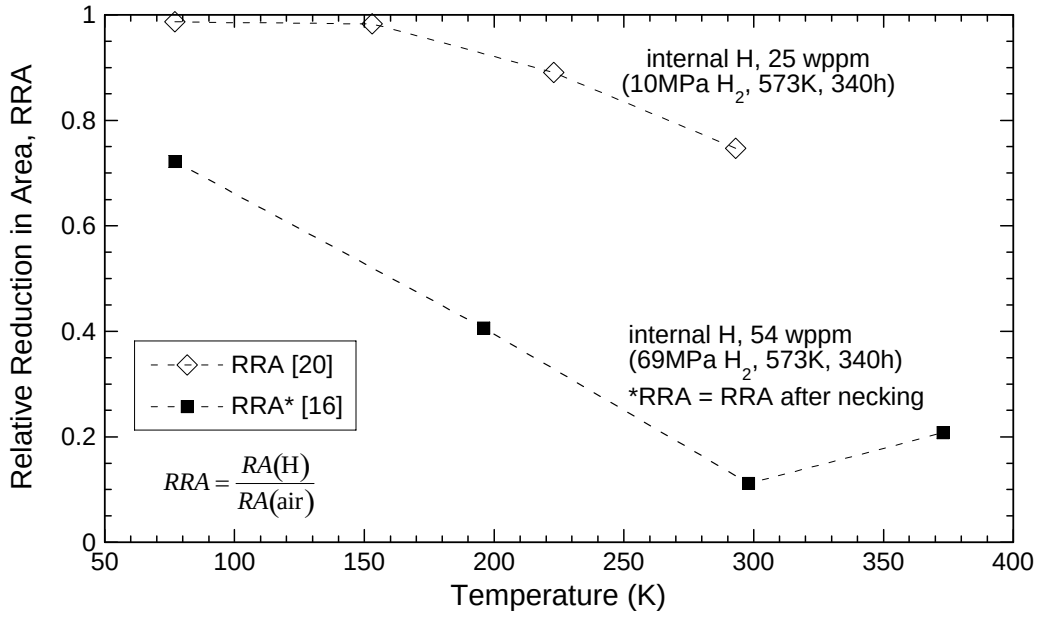

Figure 3.1.1.2. Relative reduction of area (RRA) of smooth tensile specimens of JBK-75 stainless steel as a function of temperature; with internal hydrogen (measured in air after thermal precharging in hydrogen gas). Data from Ref. [20] is also presented in Table 3.1.1.3 and Figure 3.1.1.1.

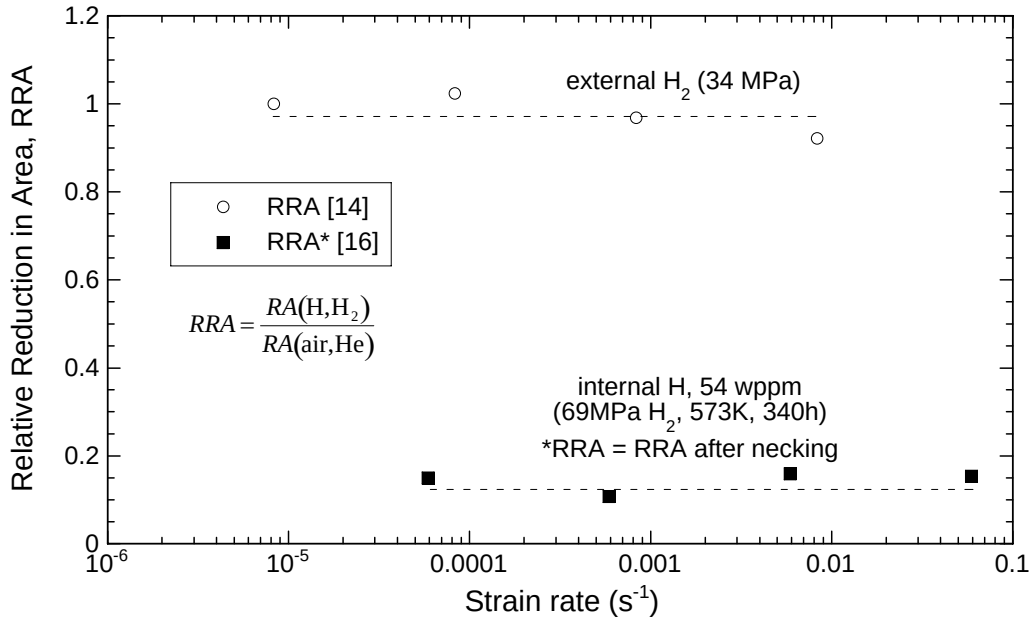

Figure 3.1.1.3. Relative reduction in area of smooth tensile specimens of JBK-75 stainless steel at room temperature as a function of strain rate.

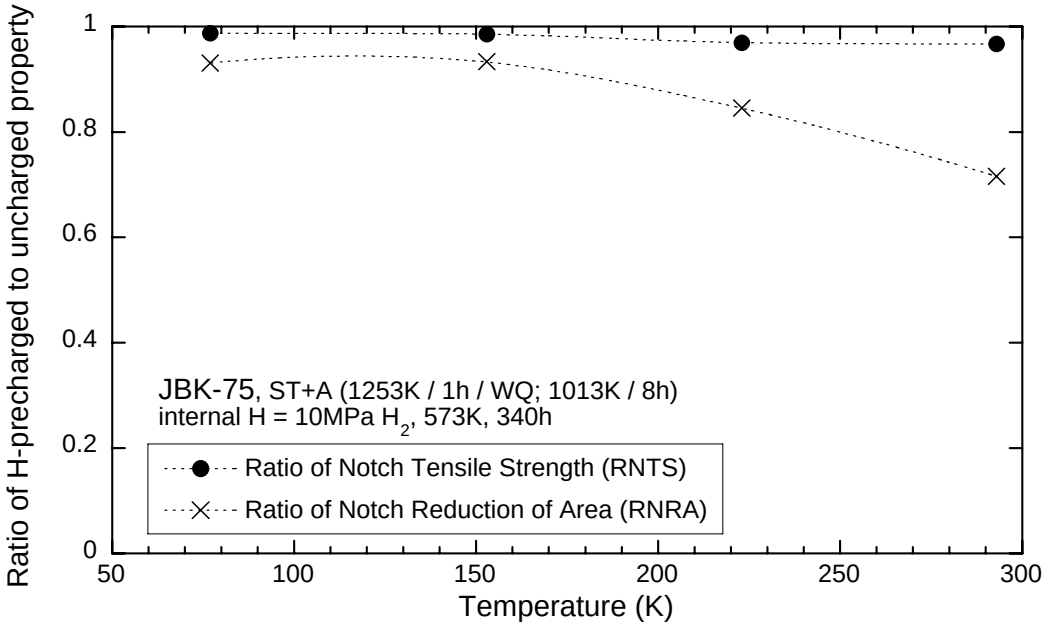

Figure 3.1.2.1. Notched tensile properties of JBK-75 stainless steel as a function of test temperature; measured in air with internal hydrogen (thermal precharging in hydrogen gas). [20]

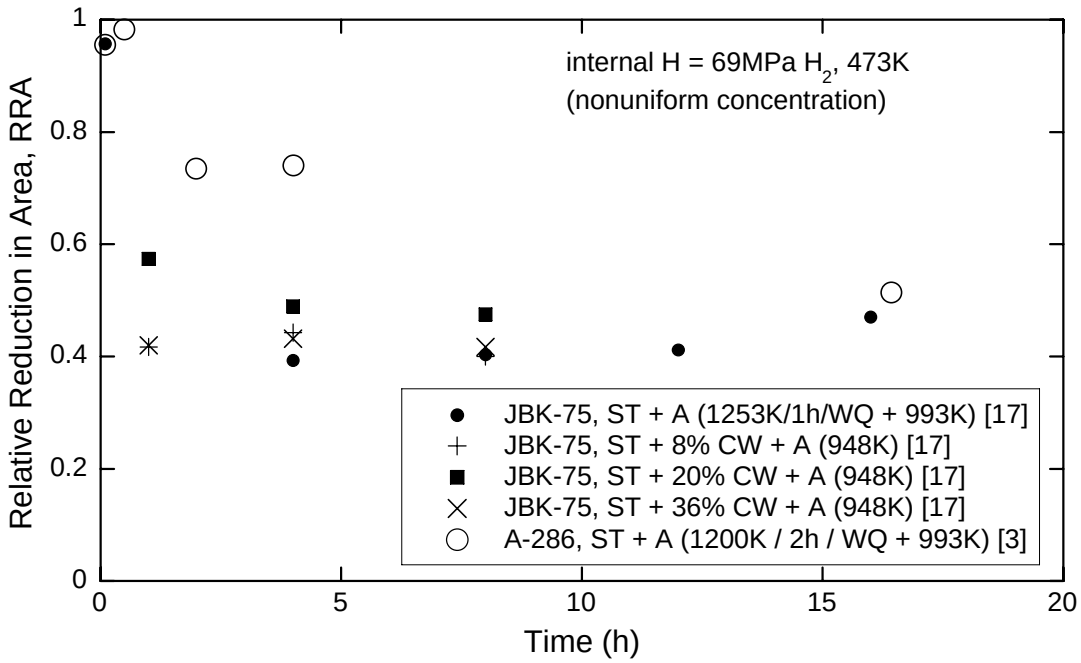

Figure 4.2.1. Relative reduction of area (RRA) as a function of aging time for several microstructural conditions of JBK-75; measured in external (172 MPa) H_2 gas with internal hydrogen (heat O80), data also reported in Table 4.2.1, and for A-286 with internal hydrogen (heat B93). ST = solution treatment, A = age, WQ = water quench, CW = cold work

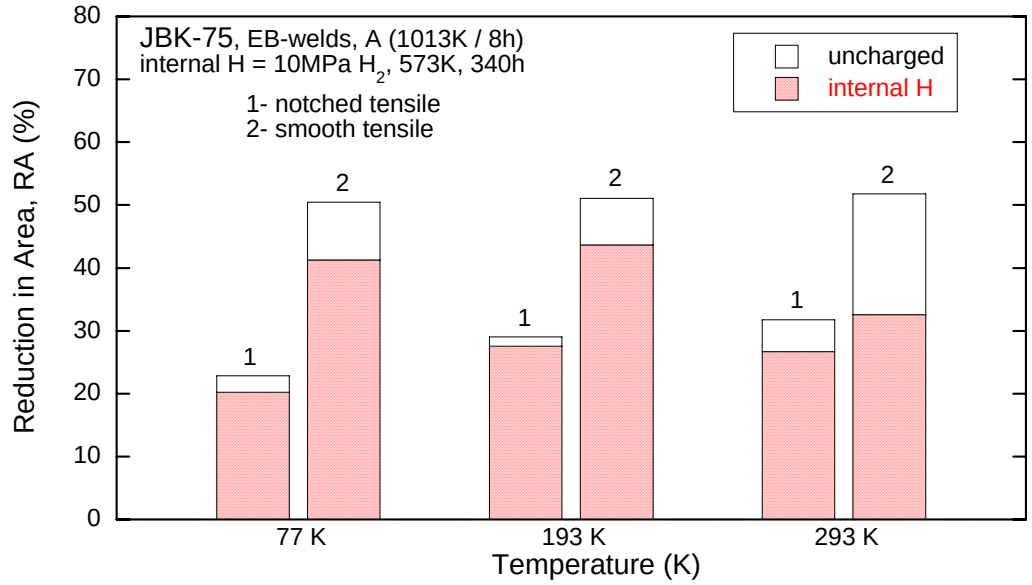

Figure 4.3.1. Reduction in area of JBK-75 stainless steel EB-welded joints as a function of test temperature; measured in air with internal hydrogen (thermal precharging in hydrogen gas). [32] EB = electron beam, A = age

Technical Reference on Hydrogen Compatibility of Materials

Specialty Alloys:

Fe-Ni-Co Sealing Alloys (code 2401)

1. General

The Fe-Ni-Co alloys under consideration here were developed as metal-ceramic (or metal-glass) seals and designed to match the coefficient of thermal expansion of the ceramic (or glass) phase. Two of the more common alloys have composition of Fe-29Ni-17Co for borosilicate glass and Fe-27Ni-25Co for alumina [1]. These alloys are single-phase austenite with relatively low strength (<700 MPa).

There is very little published information on hydrogen embrittlement for these alloys [1]. The available information shows that in the annealed condition the fracture behavior of Fe-29Ni-17Co is unaffected by high concentrations of internal hydrogen and Fe-27Ni-25Co is unaffected by external high-pressure (69 MPa) hydrogen gas. Limited tensile testing of cold-worked Fe-27Ni-25Co also indicates no susceptibility to hydrogen embrittlement for the higher strength condition.

Permeability of hydrogen in the single-phase Fe-Ni-Co alloys appears to be similar to the austenitic (300-series) stainless steels such as 304 and 316. Diffusivity, however, is higher than other austenitic alloys and solubility somewhat lower.

1.1 Composition and microstructure

Table 1.1.1 lists nominal compositions for two specialty steels used for making metal-ceramic and metal-glass joints, as well as standard designations and common tradenames.

1.2 Common designations

These alloys have a large number of trade names, which differ from region to region. Table 1.1.1 provides a partial list of the more common designations. In this document the different alloys are referred to by their nominal composition.

2. Permeability, Diffusivity and Solubility

There is limited data on permeability, diffusivity and solubility of hydrogen in Fe-Ni-Co specialty sealing alloys. The available data show the permeability to be very similar to austenitic stainless steels such as 304 and 316, Figure 2.1. The apparent diffusivity, however, is a factor of five to ten greater for Fe-29Ni-17Co and Fe-27Ni-25Co than for austenitic stainless steel, Figure 2.2. Thus, the solubility (determined from the ratio of permeability to diffusivity) is a factor of five to ten lower for the Fe-29Ni-17Co and Fe-27Ni-25Co than for the austenitic stainless steels, Figure 2.3. The relationships reported in the Figures 2.1-2.3 are given in Table 2.1 for permeability and diffusivity and in Table 2.2 for solubility. Diffusion measurements tend to have a much greater variation between studies than permeability, possibly due to differences in surface preparation of the permeation membranes. Consequently, due to the limited number of

studies, the diffusivity and solubility reported for Fe-29Ni-17Co and Fe-27Ni-25Co should be viewed critically, particularly with regard to the activation energy term.

3. Mechanical Properties: Effects of Gaseous Hydrogen

3.1 Tensile properties

3.1.1 Smooth tensile properties

The tensile properties of Fe-29Ni-17Co and Fe-27Ni-25Co show no significant effect of hydrogen; this statement is based on a single report from the literature [1]. Fe-27Ni-25Co was tested in both the cold-worked and annealed conditions in high-pressure (external) hydrogen gas at 69 MPa. Fe-29Ni-17Co was tested in the annealed condition with internal hydrogen (thermally precharged: 69 MPa hydrogen gas at 430 K for 6500 h). All specimens were tested at an initial strain rate of 1.67×10^{-4} s^{-1}. Gauge diameter was either 2.9 mm or 6.3 mm with a gauge length of 25 mm.

In addition, tubular specimens of Fe-29Ni-17Co were pressurized with 69 MPa hydrogen gas, sealed and heated at 345 K or 430 K for 2900 h or 17500 h. These specimens (9.5 mm outer diameter, 6.4 mm inner diameter) where subsequently tested in tension. The reduction of area of these thermally-precharged, tubular specimens was unchanged compared to specimens tested without exposure to hydrogen [1].

3.1.2 Notched tensile properties

Testing of notched tensile specimens of Fe-29Ni-17Co with internal hydrogen show essentially no change in reduction of area compared to unexposed specimens [1]. Thermal precharging was performed in 69 MPa hydrogen gas at 430 K for 6500 h. The maximum and minimum diameters of the notched tensile specimens were 7.1 and 5.1 mm respectively with a 60˚ included angle ($K_t \approx 5$). Testing was conducted at a rate of approximately 4×10^{-3} mm s^{-1}.

3.2 Fracture mechanics

No known data in hydrogen gas.

3.3 Fatigue

No known data in hydrogen gas.

3.4 Creep

No known data in hydrogen gas.

3.5 Impact

Internal hydrogen does not significantly affect the notched impact energy of annealed Fe-29Ni-17Co: the impact energy of thermally precharged specimens (69 MPa, 430 K, 6500 h) was 14.1 J compared to 14.3 J for the annealed material not exposed to hydrogen [1]. Impact velocity was 3.4 m/s, and $K_t \approx 5$ (maximum and minimum diameters were 5.7 and 3.8 mm respectively with a 45˚ notch).

3.6 Disk rupture tests

No known data in hydrogen gas.

4. Fabrication

4.1 Primary processing

Effects of processing on the hydrogen-assisted fracture of these alloys are unknown. As long as the alloy remains single-phase austenite, it is expected that the material will remain resistant to hydrogen embrittlement. Based on data for stable austenitic stainless steel (see other chapters of this resource), it can be expected that increasing strength by warm or cold working will have a negligible to modest effect on hydrogen embrittlement as long as the yield strength remains lower than about 700 MPa (and the alloy remains single-phase).

4.2 Heat treatment

These alloys are typically not heat-treated, which is generally expected to improve resistance to hydrogen-assisted fracture.

4.3 Properties of welds

No known data in hydrogen gas.

5. References

1. AW Thompson and WN Posey. Effect of Hydrogen on Iron-Nickel-Cobalt Sealing Alloys. J Test Eval 2 (1974) 240-242.
2. RH Collins and JC Turnbull. Degassing and Permeation of Gases in Tube Materials. Vacuum 11 (1961).
3. JK Gorman and WR Nardella. Hydrogen Permeation through Metals. Vacuum 12 (1962) 19-24.
4. DJ Mitchell and EM Edge. Permeation characteristics of some iron and nickel based alloys. J Appl Phys 57 (1985) 5226-5235.
5. DR Begeal. The permeation and diffusion of hydrogen and deuterium through Rodar, tin-coated Rodar, and solder-coated Rodar. J Vac Sci Technol 12 (1975) 405-409.
6. MR Louthan and RG Derrick. Hydrogen Transport in Austenitic Stainless Steel. Corros Sci 15 (1975) 565-577.

Table 1.1.1. Nominal composition and common designations for specialty austenitic Fe-Ni-Co sealing alloys.

Nominal composition	UNS designation	Specifications	Common names and Tradenames
Fe-29Ni-17Co	K94610 K94630	ASTM F-15 ASTM F-1466	Kovar Alloy F15 Nilo K Therlo Lock-Invar Rodar
Fe-27Ni-25Co	K94620	ASTM F-1466	Ceramvar

Table 2.1. Permeability and diffusivity relationships for Fe-Ni-Co alloys.

Material	Temperature range (K)	Pressure range (MPa)	$\Phi = \Phi_o \exp(-E_\Phi / RT)$		$D = D_o \exp(-E_D / RT)$		Ref.
			Φ_o $\left(\frac{\text{mol H}_2}{\text{m}\cdot\text{s}\cdot\sqrt{\text{MPa}}}\right)$	E_Φ $\left(\frac{\text{kJ}}{\text{mol}}\right)$	D_o $\left(\frac{\text{m}^2}{s}\right)$	E_D $\left(\frac{\text{kJ}}{\text{mol}}\right)$	
Fe-28Ni-18Co	~373~673	0.1	0.0044×10^{-3}	44.8	—	—	[2]
Fe-29Ni-17Co	773-1223	0.1	0.24×10^{-3}	66.9	—	—	[3]
Fe-29Ni-17Co †	473-673	0.1	9.8×10^{-5}	57.9	3.6×10^{-7}	43.4	[4]
Fe-29Ni-17Co	453-823	0.001-0.1	6.9×10^{-5}	56.5	6.3×10^{-7}	46.4	[5]
Fe-29Ni-17Co †	503-823	0.001-0.1	9.5×10^{-5}	58.2	3.7×10^{-7}	43.1	[5]
Fe-27Ni-25Co †	473-673	0.1	0.13×10^{-3}	57.9	7.2×10^{-7}	45.3	[4]
Fe-27Ni-25Co	453-743	0.001-0.1	0.11×10^{-3}	58.6	6.1×10^{-7}	46.0	[5]

† Measurements made with deuterium: permeability and diffusivity have been corrected here to give permeability of hydrogen (by multiplying by the square root of the mass ratio: $\sqrt{2}$).

Table 2.2. Solubility relationships for Fe-Ni-Co sealing alloys determined from the ratio of permeability and diffusivity (Table 2.1).

Material	Temperature range (K)	Pressure range (MPa)	$S = S_o \exp(-E_S/RT)$		Ref.
			S_o $\left(\frac{\text{mol H}_2}{\text{m}^3 \cdot \sqrt{\text{MPa}}}\right)$	E_S $\left(\frac{\text{kJ}}{\text{mol}}\right)$	
Fe-29Ni-17Co †	473-673	0.1	269	14.5	[4]
Fe-29Ni-17Co	453-823	0.001-0.1	109	10.0	[5]
Fe-29Ni-17Co †	503-823	0.001-0.1	259	15.1	[5]
Fe-27Ni-25Co †	473-673	0.1	178	12.5	[4]
Fe-27Ni-25Co	453-743	0.001-0.1	177	12.6	[5]

† Measurements made with deuterium: solubility is assumed to be independent of isotope.

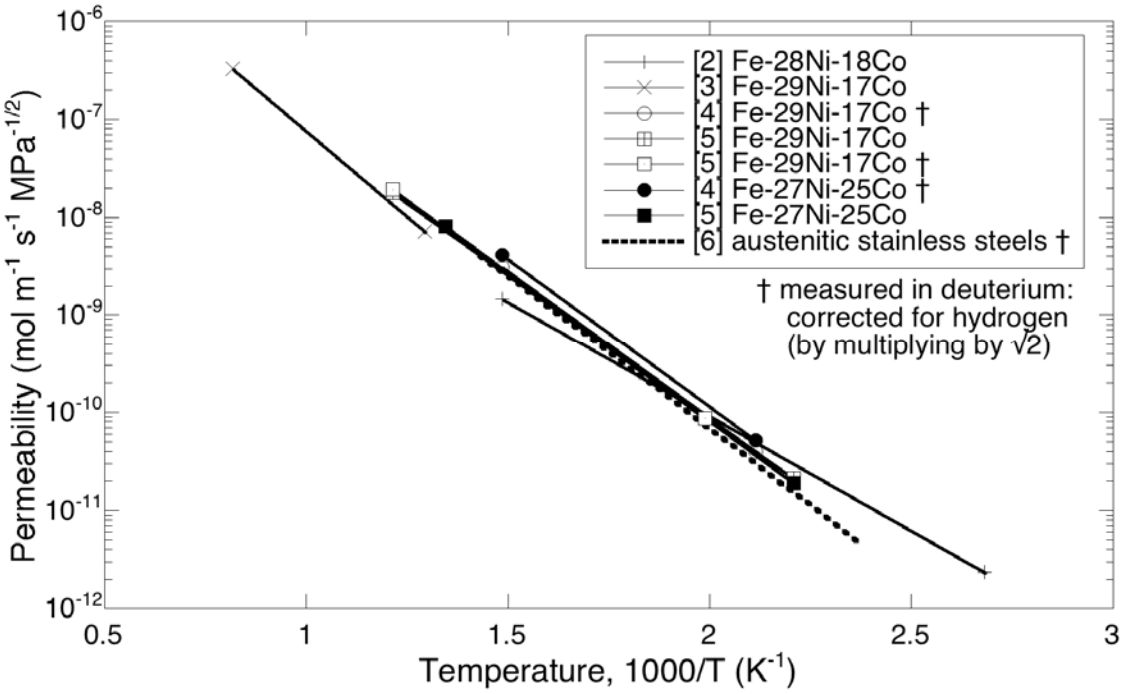

Figure 2.1. Permeability as a function of temperature (Table 2.1) for Fe-Ni-Co sealing alloys. Also plotted (dashed line) relationship for austenitic stainless steels from Ref. [6].

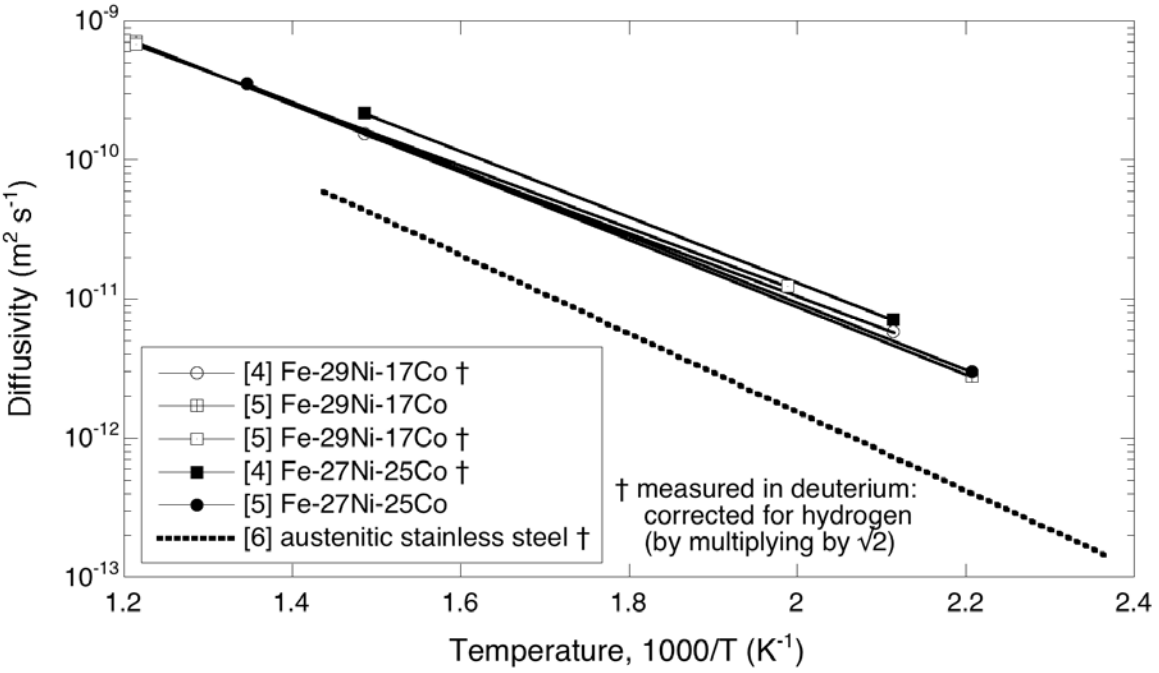

Figure 2.2. Diffusivity as a function of temperature (Table 2.1) for Fe-Ni-Co sealing alloys. Also plotted (dashed line) relationship for austenitic stainless steels from Ref. [6].

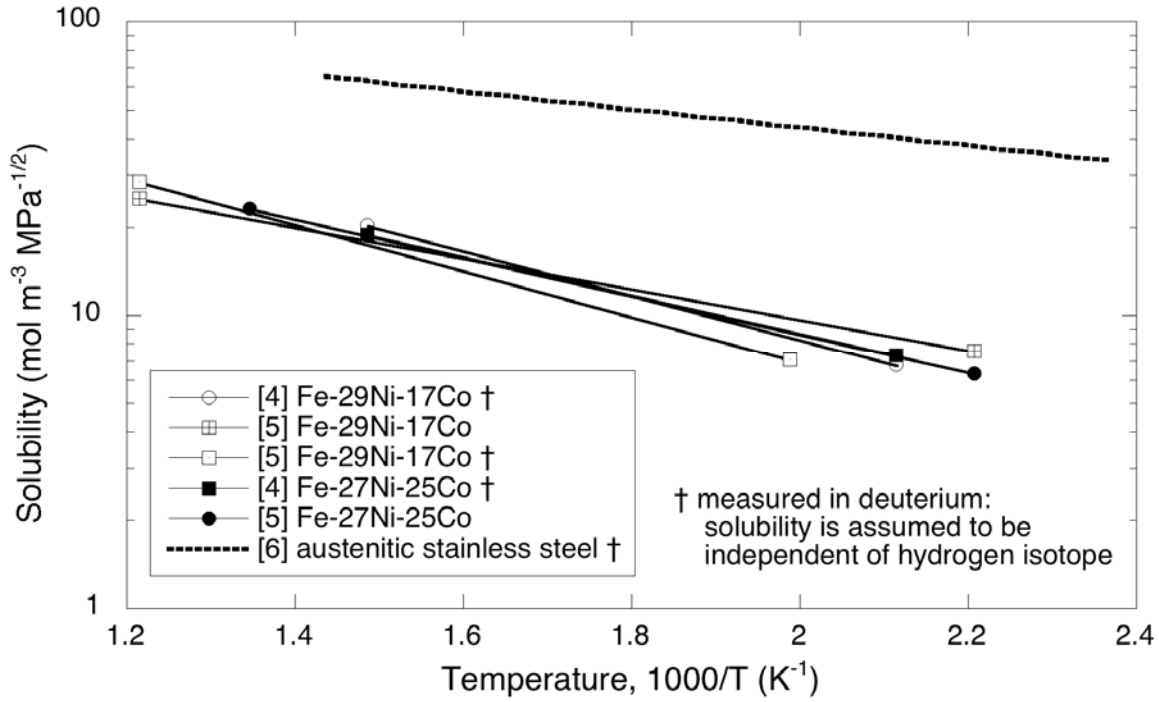

Figure 2.3. Solubility as a function of temperature (ratio of permeability and diffusivity, Table 2.2) for Fe-Ni-Co sealing alloys. Also plotted (dashed line) relationship for austenitic stainless steels from Ref. [6].

Technical Reference on Hydrogen Compatibility of Materials

Aluminum Alloys:

Non-Heat Treatable Alloys (code 3101)

1. General

The effects of hydrogen on aluminum alloys are not well understood; indeed, there is much conflicting information. Despite the perception that aluminum alloys are immune to gaseous hydrogen [1, 2], the micromechanics of deformation in aluminum are strongly affected by hydrogen [3, 4]. Aluminum alloys can be susceptible to stress corrosion cracking [5], particularly high-strength alloys for which hydrogen-assisted fracture is one mechanistic interpretation of property degradation [1, 6]. The literature on stress corrosion cracking of aluminum alloys is extensive, although testing is generally performed in aqueous or "wet" environments where hydrogen concentrations that develop in aluminum are many orders of magnitude greater than hydrogen concentrations that develop from dry hydrogen gas. Based on the available experimental data obtained during relatively short-term exposure to hydrogen gas [7-9], aluminum alloys appear to have good resistance to hydrogen-assisted fracture in dry environments.

Thermodynamically, aluminum has a low equilibrium solubility for hydrogen [10]. Moreover, the native oxide acts as a kinetic barrier to hydrogen uptake since the kinetics of formation of atomic hydrogen (a necessary step to hydrogen uptake and hydrogen-assisted fracture) is limited on the oxide surface. In the presence of electrochemical environments and wet hydrogen, however, atomic hydrogen can be readily produced and enter the aluminum lattice [1]. Under these conditions, the concentration of hydrogen in aluminum can be very high, equivalent to concentrations developed from many millions of atmospheres of dry hydrogen gas [11, 12]. Significant degradation of fracture properties of high-strength aluminum alloys has been reported in "wet" gases [1].

Hydrogen-assisted fracture in all materials depends on the characteristics of hydrogen transport [13, 14]; therefore, interpretation of testing results for aluminum alloys in hydrogen gas must be made with consideration of potential kinetic limitations on hydrogen transport. However, there are large variations in the literature data on hydrogen solubility and diffusivity [10, 15]. Studies of hydrogen transport in aluminum are complicated by the low solubility of hydrogen [10], the kinetic effects associated with the native oxide and hydrogen trapping, such as the interactions of hydrogen atoms with vacancies [15, 16] or other microstructural features [10, 15].

1.1 Composition and microstructure

The Aluminum Association (AA) designations have been widely adopted for aluminum alloys. The nominally pure aluminum alloys are designated 1XX for cast alloys and 1XXX for wrought alloys. Common designations of commercially pure wrought aluminum include 1060 (99.6%) and 1100 (99%), while 1199 (99.99%) is a common super purity grade.

1.2 Common designations

UNS A91060 (1060)
UNS A91100 (1100)
UNS A91199 (1199)
UNS A91350 (1350)

2. Permeability, Diffusivity and Solubility

The solubility and diffusivity of hydrogen in aluminum alloys are reviewed in Refs. [10, 15], showing significant scatter in the data. Reported values for hydrogen solubility in pure aluminum vary by six orders of magnitude when extrapolated to room temperature [10], with the largest reported value at room temperature being about 2.5×10^{-6} mol H_2 m^{-3} $MPa^{-1/2}$. The low solubility of hydrogen in aluminum makes it particularly difficult to quantify lattice hydrogen concentrations (and thus infer solubility) by gas extraction techniques, which do not distinguish between hydrogen dissolved in the metal and hydrogen trapped by specific metallurgical features [10]. Thus, care should be extended to the extrapolation of hydrogen solubility trends from high-temperature to ambient temperature [15]. Gas permeation experiments allow for determination of the rate of hydrogen transport through a metal at steady state (i.e., permeation), as well as the diffusivity of hydrogen through the metal by analysis of transport transients. Solubility is the ratio of permeability and diffusivity (Ref. [17] provides some background on the thermodynamic origin of the relationships between permeation, diffusion and equilibrium dissolution), thus hydrogen solubility can be determined accordingly.

Reported values of hydrogen diffusivity for pure aluminum vary by at least two orders of magnitude at elevated temperature, and by many orders of magnitude at ambient temperature. In particular, diffusivity values extrapolated to ambient temperature from elevated temperature data appear to predict values at the low end of this spectrum. Several studies near ambient temperature, however, report consistent values for hydrogen diffusivity of about 10^{-11} m^2/s [10, 15, 16], significantly higher than extrapolated values. The discontinuity between hydrogen diffusivity extrapolated from high temperature and hydrogen diffusivity measured directly at low temperature is interpreted to be due to hydrogen trapping, especially the trapping by vacancies at elevated temperature [15, 16]. At low temperature, the equilibrium vacancy concentration is sufficiently low that hydrogen transport should not be limited by interactions with vacancies (unless the material is supersaturated with vacancies, i.e. contains high concentration of non-equilibrium vacancies due to the characteristics of materials processing).

Aluminum is often considered to be a barrier to hydrogen permeation. Indeed, the native oxide on aluminum metal is an effective kinetic barrier to hydrogen permeation, thus as long as the oxide maintains its integrity the effective permeation of hydrogen through aluminum appears to be kinetically limited by surface processes. Using the apparent upper bounds for solubility and diffusivity that are quoted above, the hydrogen permeability through the aluminum lattice at ambient temperature would be about 2.5×10^{-17} mol H_2 m^{-1} s^{-1} $MPa^{-1/2}$. This value is many orders of magnitude greater than values extrapolated from elevated temperature and several orders of magnitude lower than estimates for stainless steels. The effective permeability of aluminum with native oxide, however, will be much lower since the kinetics of formation of atomic hydrogen on the oxide is very low.

3. Mechanical Properties: Effects of Gaseous Hydrogen

3.1 Tensile properties

3.1.1 Smooth tensile properties

The tensile properties of commercially pure aluminum (99.0%; alloy 1100) are unaffected by testing in high-pressure gaseous hydrogen, Table 3.1.1.1. Similarly, the tensile properties of high-purity aluminum (99.993% annealed bar, S_u = 103 MPa) were found to be unaffected by hydrogen pressure up to 52 MPa [7].

3.1.2 Notched tensile properties

Notched tensile properties of commercially pure aluminum are not degraded by testing in high-pressure gaseous hydrogen, Table 3.1.2.1.

3.2 Fracture mechanics

No known published data in hydrogen gas for pure aluminum. Fracture mechanics data on high-strength aluminum alloys tested in hydrogen gas can be found in Refs. [1, 18]. The literature on the effects of hydrogen from environments (stress-corrosion cracking) is extensive and beyond the scope of this review; however, these effects have been shown to be substantial for highly alloyed aluminum.

4. Fabrication

Hydrogen trapping appears to play an important role on the hydrogen transport in aluminum and its alloys [10, 15], if not the micromechanisms of hydrogen-assisted fracture. Therefore, test results need to be interpreted in the context of the specifics of the microstructural condition of the tested alloy. In the case of pure aluminum, the vacancy concentration is a critical concern for hydrogen transport, particularly since aluminum can have artificially high concentrations of vacancies due to quenching processes.

Relatively large hydrogen contents in aluminum alloys can result from casting processes due to the high solubility of hydrogen in liquid aluminum [19]. There is a significant body of literature that addresses this issue for castings [20], which is beyond the scope of applications for high-pressure hydrogen gas infrastructure.

5. References

1. MO Speidel. Hydrogen Embrittlement and Stress Corrosion Cracking of Aluminum Alloys. in: R Gibala and RF Hehemann, editors. Hydrogen Embrittlement and Stress Corrosion Cracking. Metals Park OH: American Society for Metals (1984) p. 271-296.
2. PM Ordin. Safety Standard for Hydrogen and Hydrogen Systems: Guidelines for Hydrogen System Design, Materials Selection, Operations, Storage, and Transportation. Office of Safety and Mission Assurance, National Aeronautics and Space Administration, Washington DC (1997).
3. GM Bond, IM Robertson and HK Birnbaum. Effects of hydrogen on deformation and fracture processes in high-purity aluminum. Acta Metall 36 (1988) 2193-2197.

4. PJ Ferreira, IM Robertson and HK Birnbaum. Hydrogen effects on the character of dislocations in high-purity aluminum. Acta Mater 47 (1999) 2991-2998.
5. RP Gangloff. Hydrogen assisted fracture of high strength alloys. in: I Milne, RO Ritchie and B Karihaloo, editors. Comprehensive Structural Integrity. 6. New York NY: Elsevier Science (2003).
6. H Vogt and MO Speidel. Stress corrosion cracking of two aluminum alloys: a comparison between experimental observations and data based on modelling. Corros Sci 40 (1998) 251-270.
7. RM Vennett and GS Ansell. A Study of Gaseous Hydrogen Damage in Certain FCC Metals. Trans ASM 62 (1969) 1007-1013.
8. RJ Walter and WT Chandler. Effects of High-Pressure Hydrogen on Metals at Ambient Temperature: Final Report (NASA CR-102425). Rocketdyne (report no. R-7780-1) for the National Aeronautics and Space Administration, Canoga Park CA (February 1969).
9. RP Jewitt, RJ Walter, WT Chandler and RP Frohmberg. Hydrogen Environment Embrittlement of Metals (NASA CR-2163). Rocketdyne for the National Aeronautics and Space Administration, Canoga Park CA (March 1973).
10. JR Scully, GA Young and SW Smith. Hydrogen solubility, diffusion and trapping in high purity aluminum and selected Al-base alloys. Materials Science Forum 331-337 (2000) 1583-1600.
11. HK Birnbaum, C Buckley, F Zeides, E Sirois, P Rozenak, S Spooner and JS Lin. Hydrogen in aluminum. J Alloy Compd 253-254 (1997) 260-264.
12. CE Buckley and HK Birnbaum. Characterization of the charging techniques used to introduce hydrogen in aluminum. J Alloy Compd 330-332 (2002) 649-653.
13. HG Nelson. Testing for Hydrogen Environment Embrittlement: Primary and Secondary Influences. in: Hydrogen Embrittlement Testing, ASTM STP 543, American Society for Testing and Materials. Philadelphia PA (1974) p. 152-169.
14. HG Nelson. Hydrogen Embrittlement. in: CL Briant and SK Banerji, editors. Embrittlement of Engineering Alloys. Treatise on Materials Science and Technology, volume 25. New York: Academic Press (1983) p. 275-359.
15. GA Young and JR Scully. The diffusion and trapping of hydrogen in high purity aluminum. Acta Mater 46 (1998) 6337-6349.
16. E Hashimoto and T Kino. Hydrogen diffusion in aluminum at high temperatures. J Phys F: Met Phys 13 (1983) 1157-1165.
17. C San Marchi, BP Somerday and SL Robinson. Permeability, Solubility and Diffusivity of Hydrogen Isotopes in Stainless Steels at High Gas Pressure. Int J Hydrogen Energy 32 (2007) 100-116.
18. RJ Walter and WT Chandler. Influence of Gaseous Hydrogen on Metals: Final Report (NASA CR-124410). Rocketdyne for the National Aeronautics and Space Administration, Canoga Park CA (Oct 1973).
19. DEJ Talbot. Effects of hydrogen in aluminum, magnesium, copper, and their alloys. International Metallurgical Reviews 20 (1975) 166-184.
20. PN Anyalebechi. Techniques for determination of the hydrogen content in aluminum and its alloys. in: Proceedings of the 120th TMS Annual Meeting: Light Metals, 1991, New Orleans LA. TMS: Warrendale PA. p. 1025-1046.

Table 3.1.1.1. Smooth tensile properties of nominally pure aluminum tested at room temperature in high-pressure helium and hydrogen gas.

Material	Thermal precharging	Test environment	Strain rate (s^{-1})	S_y (MPa)	S_u (MPa)	El_u (%)	El_t (%)	RA (%)	Ref.
1100 O temper	None	34.5 MPa He	0.67 x10^{-3}	—	110	—	42	93	[8, 9]
	None	34.5 MPa H_2		—	110	—	39	93	

Table 3.1.2.1. Notched tensile properties of nominally pure aluminum tested at room temperature in high-pressure helium and hydrogen gas.

Material	Specimen	Thermal precharging	Test environment	Displ. rate (mm/s)	S_y (MPa)	σ_s (MPa)	RA (%)	Ref.
1100 O temper	(1)	34.5 MPa He	69 MPa He	0.4 x 10^{-3}	—	124	20	[8, 9]
		34.5 MPa H_2	69 MPa H_2		—	172	21	

† yield strength of smooth tensile bar

(1) V-notched specimen: 60˚ included angle; minimum diameter = 3.81 mm (0.15 inch); maximum diameter = 7.77 mm (0.306 inch); notch root radius = 0.024 mm (0.00095 inch). Stress concentration factor (K_t) = 8.4.

This page intentionally left blank.

Technical Reference on Hydrogen Compatibility of Materials

Aluminum Alloys:

Heat-Treatable Alloys, 2XXX-series (code 3210)

1. General

It is generally accepted that a metal must adsorb hydrogen before the hydrogen can degrade the properties of the metal. The thermodynamics and kinetics of the interactions between gaseous hydrogen and aluminum alloys are not well understood. Therefore, the effects of gaseous hydrogen on fracture in aluminum alloys has not been adequately addressed in the literature.

Despite an incomplete understanding of the fundamental thermodynamics and kinetics of hydrogen-aluminum interactions, all of the available data suggest that the structural properties of aluminum alloys are not affected by gaseous hydrogen if moisture is absent [1, 2]. Studies of the micromechanics of deformation in aluminum, on the other hand, show that deformation is strongly affected by hydrogen [3, 4], demonstrating that hydrogen may affect the mechanical properties of aluminum alloys. Indeed, aluminum alloys can be susceptible to stress corrosion cracking [5, 6], for which hydrogen-assisted fracture is one mechanistic interpretation of property degradation [1, 5, 7].

More work is necessary to determine the limiting behavior of 2XXX-series in gaseous hydrogen. Nevertheless, the available data from the stress-corrosion-cracking literature appears to provide a more conservative assessment of hydrogen-assisted fracture in aluminum alloys than gaseous hydrogen exposures.

1.1 Composition and microstructure

The Aluminum Association (AA) designations are typically used for aluminum alloys and the materials definitions are provided in the AMS specifications (Aerospace Material Specification, also called SAE-AMS). The 2XXX-series alloys are the aluminum-copper, precipitation-strengthening aluminum alloys, although engineering alloys include controlled amounts of other transition metals and silicon. Several common varieties are given in Table 1.1.1.

The alloy temper (i.e., specific heat treatment) is specified after the AA designation, such as 2014-T6. Mill tempers often include stress relief and may include several numbers, such as T6511. The T6 temper represents the peak-aged condition and is the most common for the 2XXX-series alloys. The T8 tempers are strain-hardened, then precipitation-strengthened. Common tempers for aluminum alloys are specified in AMS 2770 thru 2772.

1.2 Common designations

UNS A92014 (2014), UNS A92024 (2024), UNS A92219 (2219), UNS A92224 (2224)

2. Permeability, Diffusivity and Solubility

The solubility and diffusivity of hydrogen in pure aluminum are reviewed in Refs. [8, 9]; little data for engineering alloys is reported in the literature. The data for pure aluminum is summarized in the section of this Technical Reference on pure aluminum alloys.

3. Mechanical Properties: Effects of Gaseous Hydrogen

3.1 Tensile properties

3.1.1 Smooth tensile properties

There are few published data for 2XXX-series aluminum alloys in gaseous hydrogen. The limited data [10] show a slight increase in ductility for aluminum alloys when tested in high-pressure gas compared to tests in air, Table 3.1.1.1. The apparent improvement in ductility is likely related to removal of the environmental condition associated with atmospheric moisture.

3.1.2 Notched tensile properties

No known published data in hydrogen gas.

3.2 Fracture mechanics

The fracture toughness (K_{IC}) and threshold stress intensity factor (K_{TH}) of 2219-T87 aluminum are reported by Walter and Chandler in 34.5 MPa gaseous hydrogen and helium at room temperature and temperature of 144 K [11]. Their 2219-T87 material was obtained as plate with a yield strength of 390 MPa. They found essentially no difference in values of fracture reisstance measured in helium and hydrogen: both K_{IC} and K_{TH} values are reported to be about 30 MPa $m^{1/2}$ at room temperature, and about 40 MPa $m^{1/2}$ at 144 K.

3.3 Fatigue

No known published data in hydrogen gas.

3.4 Creep

No known published data in hydrogen gas.

3.5 Impact

No known published data in hydrogen gas.

3.6 Disk rupture testing

No known published data in hydrogen gas.

4. Fabrication

4.1 Primary processing

Relatively large hydrogen contents in aluminum alloys can result from casting processes due to the high solubility of hydrogen in liquid aluminum [12]; this residual hydrogen can be much

larger than dissolved from exposure to high-pressure gaseous hydrogen near room temperature. There is a significant body of literature that addresses this issue for castings [13].

4.2 Heat treatment

Vacancies appear to play an important role in trapping and transport of hydrogen in aluminum alloys [8, 9], therefore the high concentrations of vacancies associated with tempering are likely to have a substantial effect on hydrogen transport in precipitation-strengthened aluminum alloys. It is unclear, however, if trapped hydrogen plays a significant role on the micromechanisms of hydrogen-assisted fracture in aluminum alloy exposed to gaseous hydrogen.

5. References

1. MO Speidel. Hydrogen Embrittlement and Stress Corrosion Cracking of Aluminum Alloys. in: R Gibala and RF Hehemann, editors. Hydrogen Embrittlement and Stress Corrosion Cracking. Metals Park OH: American Society for Metals (1984) p. 271-296.
2. PM Ordin. Safety Standard for Hydrogen and Hydrogen Systems: Guidelines for Hydrogen System Design, Materials Selection, Operations, Storage, and Transportation. Office of Safety and Mission Assurance, National Aeronautics and Space Administration, Washington DC (1997).
3. GM Bond, IM Robertson and HK Birnbaum. Effects of hydrogen on deformation and fracture processes in high-purity aluminum. Acta Metall 36 (1988) 2193-2197.
4. PJ Ferreira, IM Robertson and HK Birnbaum. Hydrogen effects on the character of dislocations in high-purity aluminum. Acta Mater 47 (1999) 2991-2998.
5. GA Young and JR Scully. The effects of test temperature, temper, and alloyed copper on the hydrogen-controlled crack growth rate of an Al-Zn-Mg-(Cu) Alloy. Metall Mater Trans 33A (2002).
6. RP Gangloff. Hydrogen assisted fracture of high strength alloys. in: I Milne, RO Ritchie and B Karihaloo, editors. Comprehensive Structural Integrity. 6. New York NY: Elsevier Science (2003).
7. H Vogt and MO Speidel. Stress corrosion cracking of two aluminum alloys: a comparison between experimental observations and data based on modelling. Corros Sci 40 (1998) 251-270.
8. GA Young and JR Scully. The diffusion and trapping of hydrogen in high purity aluminum. Acta Mater 46 (1998) 6337-6349.
9. JR Scully, GA Young and SW Smith. Hydrogen solubility, diffusion and trapping in high purity aluminum and selected Al-base alloys. Materials Science Forum 331-337 (2000) 1583-1600.
10. MR Louthan and G Caskey. Hydrogen Transport and Embrittlement in Structural Metals. Int J Hydrogen Energy 1 (1976) 291-305.
11. RJ Walter and WT Chandler. Influence of Gaseous Hydrogen on Metals: Final Report. Rocketdyne for the National Aeronautics and Space Administration, Canoga Park CA (Oct 1973).
12. DEJ Talbot. Effects of hydrogen in aluminum, magnesium, copper, and their alloys. International Metallurgical Reviews 20 (1975) 166-184.

13. PN Anyalebechi. Techniques for determination of the hydrogen content in aluminum and its alloys. in: Proceedings of the 120th TMS Annual Meeting: Light Metals, 1991, New Orleans LA. TMS: Warrendale PA p. 1025-1046.
14. ASTM. ASTM DS-56H, Metals and Alloys in the UNIFIED NUMBERING SYSTEM (SAE HS-1086 OCT01). 2001.

Table 1.1.1. Compositional ranges (wt%) of several common 2XXX-series aluminum alloys [14]; additional and modified requirements are common for specific applications.

UNS No	Aluminum Association Designation	Al	Cu	Mg	Mn	Zn	Cr	Ti	V	Zr	Si	Fe
A92014	2014	Bal	5.0 3.9	0.80 0.20	1.2 0.40	0.25 max	0.10 max	0.15 max	—	—	1.2 0.50	0.70 max
A92024	2024	Bal	4.9 3.8	1.8 1.2	0.90 0.30	0.25 max	0.10 max	0.15 max	—	—	0.50 max	0.50 max
A92224	2224	Bal	4.4 3.8	1.8 1.2	0.90 0.30	0.25 max	0.10 max	0.15 max	—	—	0.12 max	0.15 max
A92219	2219	Bal	6.8 5.8	0.02 max	0.40 0.20	0.10 max	—	0.10 0.02	0.10 0.25	0.05 0.15	0.20 max	0.30 max

Table 3.1.1.1. Smooth tensile properties of 2XXX-series aluminum alloys tested at room temperature in high-pressure helium and hydrogen gas.

Material	Thermal precharging	Test environment	Strain rate (s^{-1})	S_y (MPa)	S_u (MPa)	El_u (%)	El_t (%)	RA (%)	Ref.
2011	None	Air	—	269	338	—	17	48	[10]
	None	69 MPa He		227	296	—	18	57	
	None	69 MPa H_2		220	296	—	17	58	
2024	None	Air	—	358	489	—	15	33	[10]
	None	69 MPa He		324	441	—	19	36	
	None	69 MPa H_2		310	427	—	18	35	

Technical Reference on Hydrogen Compatibility of Materials

Aluminum Alloys:

Heat-Treatable Alloys, 7XXX-series (code 3230)

1. General

The 7XXX-series aluminum alloys are attractive for structural applications, since these alloys can be strengthened through heat treatment. The 7XXX alloys have elements such as Zn, Mg, and Cu that form precipitates in the aluminum matrix when the alloys are heat treated. These precipitates are the source of strengthening in the 7XXX alloys.

It is generally accepted that atomic hydrogen must dissolve in a metal in order to degrade the mechanical properties of the metal. The thermodynamics and kinetics of the interactions between gaseous hydrogen and aluminum alloys are not well understood. Therefore, the effects of gaseous hydrogen on fracture of aluminum alloys have not been adequately explored in the literature.

Despite an incomplete understanding of the fundamental thermodynamics and kinetics of hydrogen gas-aluminum interactions, all of the available data suggest that the mechanical properties of aluminum alloys are not degraded in dry gaseous hydrogen [1, 2]. However, studies of stress-corrosion cracking of aluminum alloys have implicated environmental hydrogen in the cracking mechanism [2-4], indicating that aluminum alloys are not inherently immune to hydrogen-assisted fracture. While stress-corrosion cracking data may provide a conservative assessment of hydrogen-assisted fracture of aluminum alloys, more work is necessary to evaluate the realistic performance of 7XXX alloys in gaseous hydrogen.

1.1 Composition and microstructure

The Aluminum Association (AA) designations are typically used for aluminum alloys and the materials definitions are provided in the AMS specifications (Aerospace Material Specification, also called SAE-AMS). The alloy temper (i.e., heat treatment process) is specified after the AA designation, such as 7475-T7351. Common tempers for aluminum alloys are specified in AMS 2770 thru 2772.

Data on mechanical properties for 7XXX aluminum in gaseous hydrogen were identified for two alloys: 7039 and 7475. The alloy composition specifications for these two alloys are provided in Table 1.1.1.

1.2 Common designations

UNS A97039 (7039), UNS A97475 (7475)

2. Permeability, Diffusivity and Solubility

The solubility and diffusivity of hydrogen in pure aluminum are reviewed in Refs. [5, 6]; limited data for structural aluminum alloys are reported in the literature. The data for pure aluminum are summarized in this section of the Technical Reference (code 3101).

3. Mechanical Properties: Effects of Gaseous Hydrogen

3.1 Tensile properties

3.1.1 Smooth tensile properties

Limited data for 7XXX aluminum show that the tensile properties of these alloys are not affected by gaseous hydrogen, Table 3.1.1.1. This result was independent of how the materials were tested, i.e., concurrently strained and exposed to hydrogen gas or strained in air after long-term hydrogen exposure. It is noted that the properties in Table 3.1.1.1 are for a single alloy, 7039, but the test methods were applied to materials having different strength levels. The heat treatments for the two 7039 materials were not reported [7], but it is likely that the low-strength material was not precipitation hardened.

3.1.2 Notched tensile properties

No known published data in hydrogen gas.

3.2 Fracture mechanics

Sustained-load cracking tests conducted on 7XXX aluminum alloys in high-pressure gaseous hydrogen did not reveal any hydrogen-induced subcritical crack extension. Table 3.2.1 summarizes details of the testing on a 7475-T7351 alloy [8]. The wedge-opening load (WOL) specimens had two different orientations relative to the aluminum plate dimensions: tensile loading parallel to the longitudinal direction with cracking parallel to the transverse direction (LT orientation) and tensile loading parallel to the thickness dimension with cracking parallel to the transverse direction (ST orientation). No cracking was detected in the aluminum alloys during exposure to 207 MPa hydrogen gas for 5000 hrs at the prescribed initial stress-intensity factor levels.

3.3 Fatigue

No known published data in hydrogen gas.

3.4 Creep

No known published data in hydrogen gas.

3.5 Impact

No known published data in hydrogen gas.

3.6 Disk rupture testing

No known published data in hydrogen gas.

4. Fabrication

4.1 Primary processing

Relatively large hydrogen contents in aluminum alloys can result from casting processes due to the high solubility of hydrogen in liquid aluminum [9]; this residual hydrogen content can be

much larger than the amount dissolved from exposure to high-pressure gaseous hydrogen near room temperature. There is a significant body of literature that addresses this issue for castings [10].

4.2 Heat treatment

Vacancies appear to play an important role in trapping and transport of hydrogen in aluminum alloys [5, 6], therefore the high concentrations of excess vacancies resulting from heat treatment are likely to have a substantial effect on hydrogen transport in precipitation-strengthened aluminum alloys. It is unclear, however, if trapped hydrogen plays a significant role in enabling hydrogen-assisted fracture in aluminum alloys exposed to gaseous hydrogen.

5. References

1. P.M. Ordin, "Safety Standard for Hydrogen and Hydrogen Systems: Guidelines for Hydrogen System Design, Materials Selection, Operations, Storage, and Transportation," Office of Safety and Mission Assurance, National Aeronautics and Space Administration, Washington DC 1997.
2. M.O. Speidel: in *Hydrogen Embrittlement and Stress Corrosion Cracking*, R. Gibala and R. F. Hehemann, eds., American Society for Metals, Metals Park OH, 1984, pp. 271-296.
3. R.P. Gangloff: in *Comprehensive Structural Integrity*, vol. 6, I. Milne, R. O. Ritchie, and B. Karihaloo, eds., Elsevier Science, New York NY, 2003.
4. R.G. Song, W. Dietzel, B.J. Zhang, W.J. Liu, M.K. Tseng, and A. Atrens: *Acta Materialia*, 2004, vol. 52, pp. 4727-4743.
5. J.R. Scully, G.A. Young, and S.W. Smith: *Materials Science Forum*, 2000, vol. 331-337, pp. 1583-1600.
6. G.A. Young and J.R. Scully: *Acta materialia*, 1998, vol. 46, pp. 6337-6349.
7. M.R. Louthan and G. Caskey: *International Journal of Hydrogen Energy*, 1976, vol. 1, pp. 291-305.
8. R.E. Stoltz and A.J. West: in *Hydrogen Effects in Metals*, I. M. Bernstein and A. W. Thompson, eds., The Metallurgical Society of AIME, New York, 1981, pp. 541-553.
9. D.E.J. Talbot: *International Metallurgical Reviews*, 1975, vol. 20, pp. 166-184.
10. P.N. Anyalebechi, "Techniques for determination of the hydrogen content in aluminum and its alloys," in *Proceedings of the 120th TMS Annual Meeting: Light Metals*, New Orleans LA, 1991, pp. 1025-1046.
11. "Metals and Alloys in the UNIFIED NUMBERING SYSTEM (SAE HS-1086 OCT01)," ASTM DS-56H, American Society for Testing and Materials (Society of Automotive Engineers), 2001.

Table 1.1.1. Allowable composition ranges (wt%) for 7XXX-series aluminum alloys in hydrogen compatibility studies [11].

UNS No.	Aluminum Association Designation	Al	Cu	Mg	Mn	Zn	Cr	Ti	Si	Fe
A97039	7039	Bal	0.10 max	2.3 3.3	0.10 0.40	3.5 4.5	0.15 0.25	0.10 max	0.30 max	0.40 max
A97475	7475	Bal	1.2 1.9	1.9 2.6	0.06 max	5.2 6.2	0.18 0.25	0.06 max	0.10 max	0.12 max

Table 3.1.1.1. Smooth tensile properties of 7XXX-series aluminum alloys tested at room temperature in hydrogen gas or tested in air after long-term hydrogen exposure. Properties in air and/or helium gas are included for comparison.

Material	Thermal precharging	Test environment	Strain rate (s^{-1})	S_y (MPa)	S_u (MPa)	El_u (%)	El_t (%)	RA (%)	Ref.
7039	None	Air	—	152	179	—	14	80	[7]
	None	69 MPa He		124	138	—	14	85	
	None	69 MPa H_2		117	138	—	14	86	
7039	None	Air	—	303	379	—	13	44	[7]
	(1)	Air		310	372	—	14	45	

(1) 69 MPa H_2, 343K, 524 days

Table 3.2.1. Sustained-load cracking results for 7XXX-series aluminum alloys in high-pressure gaseous hydrogen at room temperature.

Material	S_y† (MPa)	RA† (%)	K_{Ic}† (MPa $\cdot m^{1/2}$)	Test Environment	K_{TH} (MPa $\cdot m^{1/2}$)	Ref.
7475-T7351 LT orientation	445	38	—	207 MPa H_2	NCP 40*	[8]
7475-T7351 ST orientation	432	26	—	207 MPa H_2	NCP 30*	[8]

NCP = no crack propagation at reported applied K level

†properties measured in air

*5000 hr test duration

Technical Reference on Hydrogen Compatibility of Materials

Copper Alloys:

Pure Copper (code 4001)

1. General

Nominally pure oxide-free coppers appear to be relatively unaffected by high-pressure hydrogen gas. However, mechanical testing of hydrogen-saturated copper has not been carefully investigated and it is unclear whether long-time exposure to high-pressure hydrogen gas will result in degradation of mechanical properties. The effect of high-pressure hydrogen gas on metals has been quantified in the literature by saturating metals with hydrogen at elevated temperature in high-pressure hydrogen gas [1], a process called thermal precharging. Thermal precharging of copper, however, must be considered carefully. Copper anneals at low temperatures compared to steels, and the permeability of hydrogen in copper is less than most steels; therefore, precharging conditions appropriate for steels may not be appropriate for copper. The diffusivity and solubility of hydrogen in copper is very low, thus equilibrium hydrogen saturation in copper takes exceptionally long times as in stainless steels.

Copper with oxygen inclusions is embrittled by hydrogen [2-4]. Hydrogen reduces copper oxide forming water but can also react with oxygen in solution. In particular, oxides at grain boundaries are believed to promote intergranular failure and loss of ductility. The process of hydrogen embrittlement is slow at ambient temperatures as it requires diffusion of the active species, namely oxygen and hydrogen [2-4].

The available data combined with the observation that pure coppers are relatively low strength seem to indicate that copper is not strongly affected by hydrogen, provided that the copper is oxide-free.

1.1 Composition and microstructure

There are many varieties of copper, each with compositional requirements designed to meet specific applications. OFHC copper (oxygen-free high-conductivity) is generically employed when oxygen inclusions cannot be tolerated. Hydrogen effects on alloys containing other trace elements, such as phosphorus, have not been reported in the literature with respect to gaseous hydrogen service.

2. Permeability, Diffusivity and Solubility

The permeability of hydrogen through copper (Figure 2.1) is very low, even lower than austenitic stainless steel. The low permeability is due to the combination of low diffusivity for hydrogen (Figure 2.2) and low solubility of hydrogen (Figure 2.3); permeability is the product of solubility and diffusivity. The diffusivity of hydrogen in copper, however, is not as low as in austenitic stainless steels. Table 2.1 summarizes the information plotted in Figures 2.1, 2.2 and 2.3.

3. Mechanical Properties: Effects of Gaseous Hydrogen

3.1 Tensile properties

3.1.1 Smooth tensile properties

The data for OFHC copper is not entirely consistent. Walter and Chandler report essentially no effect of hydrogen on cold drawn OFHC copper (Table 3.1.1.1) [5, 6], while Vennett and Ansell report as much as 16% loss in ultimate strength in material tested in 69 MPa hydrogen gas at constant crosshead displacement of 8.5×10^{-3} mm/s (0.02 in/min) [7]. In the latter report, the fracture surface was observed to be along a plane at 45 degrees from the loading axis in 69 MPa hydrogen compared to the double cup fracture observed when tested in air. In addition, Vennett and Ansell observed inclusions in the OFHC copper used in their study [7], perhaps indicating that these hydrogen effects could be attributed to oxides or other second phase inclusions.

Louthan et al. report the same mechanical properties (Table 3.1.1.1) for Cu with internal hydrogen [8] as for OFHC Cu tested in external hydrogen [1]; although this is presumably an error, the properties were unchanged by internal or external hydrogen. In the latter study, significant reductions in strength were reported for boron deoxidized copper with internal hydrogen [1]. These strength reductions, however, were accompanied by slight improvements in ductility, which implies that these reductions may have been due to annealing at the precharging temperature. Louthan also reports a reduction in strength for the boron-deoxidized copper when tested in high-pressure hydrogen gas; the source of this degradation is unclear, but remains suspect considering the ambiguities associated with data from Louthan et al.

3.1.2 Notched tensile properties

Notched tensile properties show the same trends as smooth tensile properties. High-pressure gaseous hydrogen is reported to have no effect on notched tensile properties of OFHC copper (Table 3.1.2.1) [5, 6]; at least for copper that showed no degradation in properties in smooth-bar tensile tests. Testing at cryogenic temperature (144 K) demonstrated no significant effect of hydrogen (at 34.5 MPa) on low-temperature notched tensile properties [6]. Details of notched tensile properties are not reported for a different heat of OFHC copper used by Vennett and Ansell, however, a loss of ultimate strength was observed in notched-bar tensile tests as in smooth-bar tensile tests (tested in high-pressure hydrogen gas) [7].

3.2 Fracture mechanics

Walter and Chandler attempted to measure threshold stress intensity factors for annealed OFHC copper at room temperature and 144 K in 34.5 MPa H_2 gas [6]. The low strength of their material and constraints on specimen geometry, however, resulted in a maximum stress intensity of about 17 MPa $m^{1/2}$ for plane strain conditions in their specimens. No crack growth was observed in static tests at room temperature for specimens loaded in the range of 16 to 20 MPa $m^{1/2}$. A small amount of crack growth was observed during tests at 144 K with plastic deformation. Although their specimens did not meet the criteria of the ASTM 399, they estimate K_{Ic} to be in the range of 16 to 20 MPa $m^{1/2}$.

3.3 Fatigue

No known published data in hydrogen gas.

3.4 Creep

No known published data in hydrogen gas.

3.5 Impact

No known published data in hydrogen gas.

3.6 Disk rupture tests

Hydrogen is reported to have no effect on copper in disk rupture tests [9]. There are no reports of extended hydrogen exposures prior to disk rupture tests.

4. Fabrication

Despite the paucity of data for nominally pure coppers in the presence of high-pressure hydrogen gas, it appears that oxide inclusions are the most detrimental features for resistance to hydrogen-assisted fracture. The presence of oxide inclusions may explain the change in fracture morphology observed in tensile testing of copper in high-pressure air compared to high-pressure hydrogen gas [7].

5. References

1. MR Louthan and G Caskey. Hydrogen Transport and Embrittlement in Structural Metals. Int J Hydrogen Energy 1 (1976) 291-305.
2. E Mattsson and F Schueckher. An investigation of hydrogen embrittlement in copper. J Inst Metals 87 (1958-59) 241-247.
3. GR Caskey, AH Dexter, ML Holzworth, MR Louthan and RG Derrick. Hydrogen Transport in Copper (DP-MS-75-6). Savannah River Laboratory, Aiken SC (1975).
4. GR Caskey, AH Dexter, ML Holzworth, MR Louthan and RG Derrick. The Effect of Oxygen on Hydrogen Transport in Copper. Corrosion 32 (1976) 370-374.
5. RJ Walter and WT Chandler. Effects of High-Pressure Hydrogen on Metals at Ambient Temperature: Final Report (NASA CR-102425). Rocketdyne (report no. R-7780-1) for the National Aeronautics and Space Administration, Canoga Park CA (February 1969).
6. RJ Walter and WT Chandler. Influence of Gaseous Hydrogen on Metals: Final Report (NASA CR-124410). Rocketdyne for the National Aeronautics and Space Administration, Canoga Park CA (Oct 1973).
7. RM Vennett and GS Ansell. A Study of Gaseous Hydrogen Damage in Certain FCC Metals. Trans ASM 62 (1969) 1007-1013.
8. MR Louthan, GR Caskey, JA Donovan and DE Rawl. Hydrogen Embrittlement of Metals. Mater Sci Eng 10 (1972) 357-368.
9. J-P Fidelle, R Bernardi, R Broudeur, C Roux and M Rapin. Disk Pressure Testing of Hydrogen Environment Embrittlement. in: Hydrogen Embrittlement Testing, ASTM STP 543, American Society for Testing and Materials. (1974) p. 221-253.
10. DW Rudd, DW Vose and S Johnson. Permability of Copper to Hydrogen. J Phys Chem 65 (1961) 1018-1020.
11. JK Gorman and WR Nardella. Hydrogen Permeation through Metals. Vacuum 12 (1962) 19-24.

12. W Eichenauer, W Loser and H Witte. Solubility and rate of diffusion of hydrogen and deuterium in nickel and copper single crystals. Z Metallk 56 (1965) 287-293.
13. L Katz, M Guinan and RJ Borg. Diffusion of H_2, D_2, and T_2 in Single-Crystal Ni and Cu. Phys Rev B 4 (1971) 330-341.
14. DR Begeal. Hydorgen and deuterium permeation in copper alloys, copper-gold brazing alloys, gold, and the in situ growth of stable oxide permeation barriers. J Vac Sci Technol 15 (1978) 1146-1154.
15. T Tanabe, Y Tamanishi, K Sawada and S Imoto. Hydrogen Transport in Stainless Steels. J Nucl Mater 122&123 (1984) 1568-1572.
16. RP Jewitt, RJ Walter, WT Chandler and RP Frohmberg. Hydrogen Environment Embrittlement of Metals (NASA CR-2163). Rocketdyne for the National Aeronautics and Space Administration, Canoga Park CA (March 1973).

Table 2.1. Permeability, diffusivity and solubility relationships for copper.

Material	Temperature range (K)	Pressure range (MPa)	$\Phi = \Phi_o \exp(-E_\Phi / RT)$		$D = D_o \exp(-E_D / RT)$		$S = S_o \exp(-E_S / RT)$		Ref.
			Φ_o $\left(\frac{\text{mol H}_2}{\text{m} \cdot \text{s} \cdot \text{MPa}^{1/2}}\right)$	E_Φ $\left(\frac{\text{kJ}}{\text{mol}}\right)$	D_o $\left(\frac{\text{m}^2}{\text{s}}\right)$	E_D $\left(\frac{\text{kJ}}{\text{mol}}\right)$	S_o $\left(\frac{\text{mol H}_2}{\text{m}^3 \cdot \text{MPa}^{1/2}}\right)$	E_S $\left(\frac{\text{kJ}}{\text{mol}}\right)$	
Pure Cu	623–773	0.15 –0.2	263×10^{-4}	52.3	—	—	—	—	[10]
OFHC Cu	623–973	0.1	4.46×10^{-4}	75.3	—	—	—	—	[11]
Single crystal Cu	700–925	0.013–0.093	5.26×10^{-4}	78.7	11.5×10^{-6}	40.8	458	37.9	[12]
			3.31×10^{-4} (D)	77.8 (D)	6.2×10^{-6} (D)	37.8 (D)	534 (D)	40.0 (D)	
Single crystal Cu	723–1198	—	—	—	11.3×10^{-6}	38.9	—	—	[13]
			—	—	7.30×10^{-6} (D)	36.8 (D)	—	—	
			—	—	6.12×10^{-6} (T)	36.5 (T)	—	—	
Several low oxygen coppers †	350–750	0.1–0.5	0.821×10^{-4}	71.7	8.6×10^{-6}	52.4	9.5	19.3	[3, 4]
OFHC Cu	493–713	0.0013 –0.13	8.40×10^{-4}	77.4	1.06×10^{-6}	38.5	792	38.9	[14]
Cu	500–1200	0.001 –0.1	0.366×10^{-4}	60.5	0.226×10^{-6}	29.3	162	31.2	[15]

(D) and (T) denote values as measured for deuterium and tritium respectively.

† Data from Refs. [3, 4] are determined for deuterium: permeability and diffusivity have been corrected here to give permeability and diffusivity of hydrogen (by multiplying by the square root of the mass ratio: $\sqrt{2}$); solubility is assumed to be independent of isotope. Diffusivity is estimated from Figure 6 in Refs. [3, 4]; solubility is calculated $(S = \Phi / D)$.

Table 3.1.1.1. Smooth tensile properties of copper at room temperature: measured in external hydrogen gas.

Material	Thermal precharging	Test environment	Strain rate (s^{-1})	S_y (MPa)	S_u (MPa)	El_u (%)	El_t (%)	RA (%)	Ref.
Cold drawn, OFHC Cu	None	69 MPa He	—	269	290	—	20	94	[5, 16]
	None	69 MPa H_2		—	283	—	20	94	
Cu	None	Air	—	96	234	—	44	71	[8]
	(1)	Air		96	228	—	45	71	
Annealed, OFHC Cu	None	Air	2.1×10^{-6} m s^{-1}	117	193	—	57	84	[6]
	None	34.5 MPa He		83	193	—	63	85	
	None	34.5 MPa H_2		76	186	—	63	84	
OFHC Cu	None	Air	—	96.5	234	—	44	71	[1]
	None	69 MPa H_2		96.5	228	—	45	71	
Boron deoxidized Cu	None	Air	—	96.5	234	—	40	92	[1]
	(2)	Air		55.2	200	—	49	92	
	None	69 MPa H_2		68.9	214	—	46	94	
	(2)	69 MPa H_2		41.4	200	—	51	96	

(1) 69 MPa hydrogen, 428 K, 720 h: ~0.03 wppm hydrogen (<1 appm)
(2) 300 MPa hydrogen, 473 K, 1344 h

Table 3.1.2.1. Notch tensile properties of copper at room temperature (except where noted): measured in external hydrogen gas.

Material	Specimen	Thermal precharging	Test environment	Displ. rate (mm/s)	S_y † (MPa)	σ_s (MPa)	RA (%)	Ref.
Cold drawn, OFHC Cu	(a) $K_t \approx 8.4$	None	69MPa He	4×10^{-4}	269	600	20	[5, 16]
		None	69MPa H_2		—	593	24	
Annealed, OFHC Cu	(a) $K_t \approx 8.4$	None	34.5 MPa He	1.2×10^{-5} s^{-1} (load-paced)	83	296	23	[6]
		None	34.5 MPa H_2		76	290	23	
		None	144 K 34.5 MPa He		—	283	29	
		None	144 K 34.5 MPa H_2		—	303	24	

K_t = stress concentration factor

† yield strength of smooth tensile specimen

(a) V-notched specimen: 60˚ included angle; minimum diameter = 3.81 mm; maximum diameter = 7.77 mm; notch root radius = 0.024 mm.

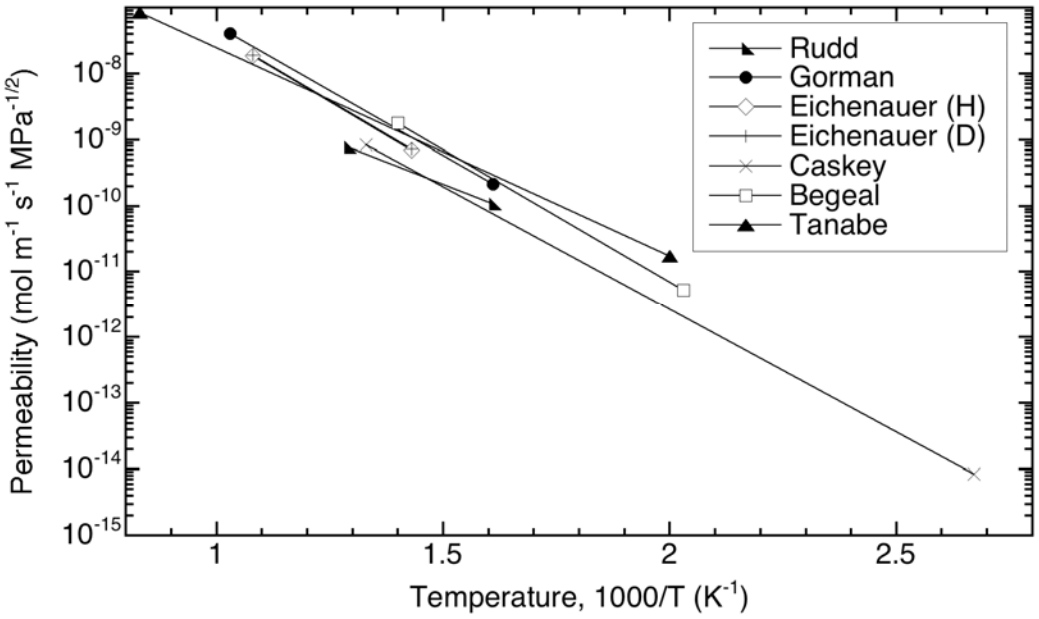

Figure 2.1. Permeability relationships (Table 2.1) for copper: Rudd [10]; Gorman [11]; Eichenauer [12]; Caskey [3, 4]; Begeal [14]; Tanabe [15]. Deuterium (D) data have been corrected to hydrogen (by multiplying by the square root of the mass ratio: √2).

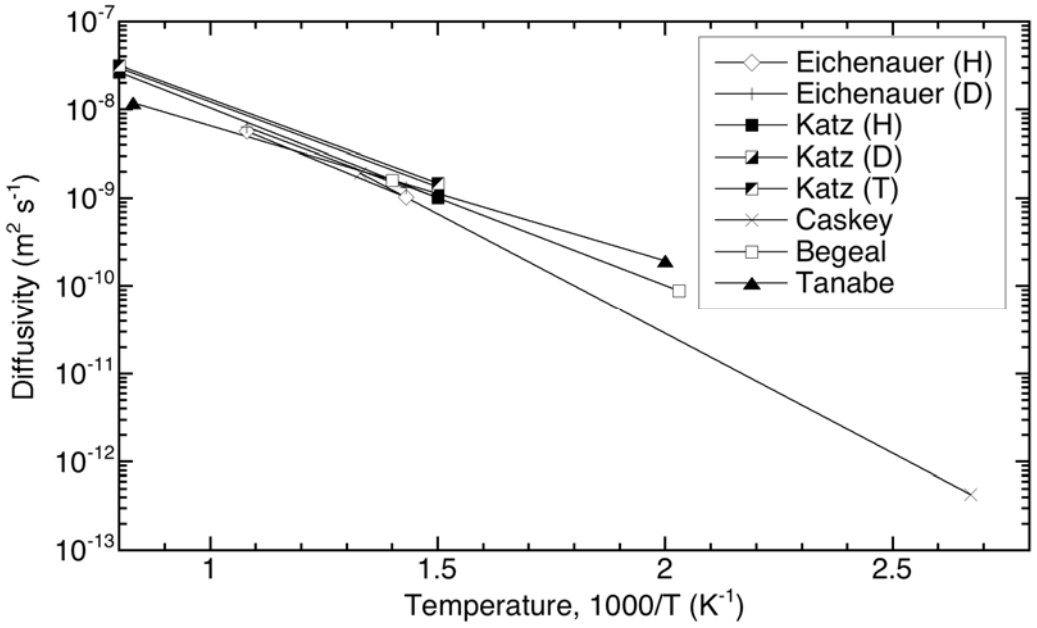

Figure 2.2. Diffusivity relationships (Table 2.1) for copper: Eichenauer [12]; Katz [13]; Caskey [3, 4]; Begeal [14]; Tanabe [15]. Deuterium (D) and tritium (T) data have been corrected to hydrogen (by multiplying by the square root of the mass ratio: √2 and √3 respectively).

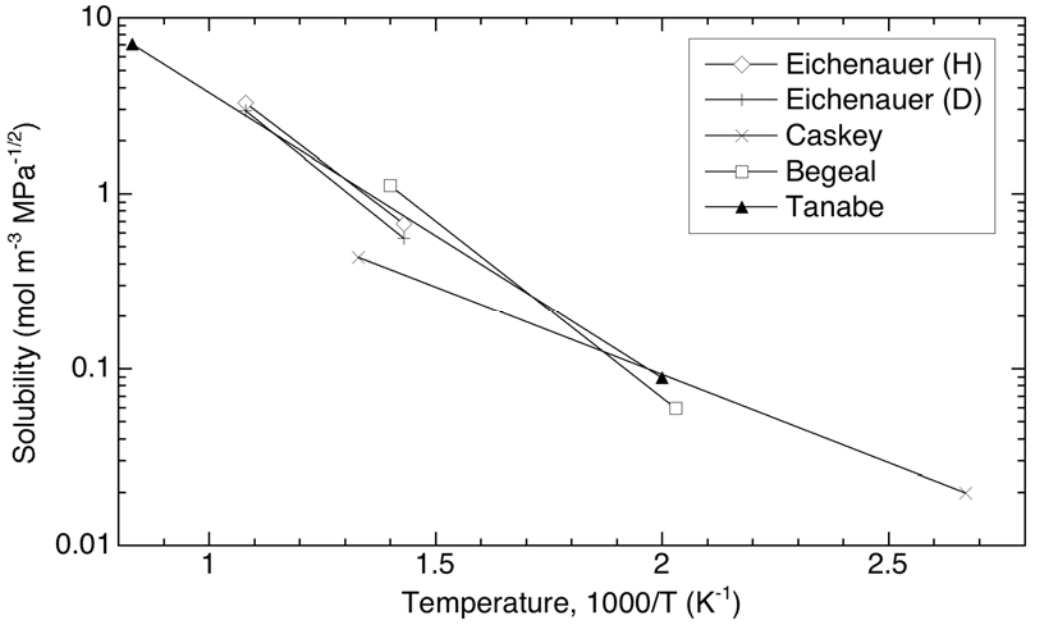

Figure 2.3. Solubility relationships (Table 2.1) for copper: Eichenauer [12]; Caskey [3, 4]; Begeal [14]; Tanabe [15]. Solubility is assumed to be independent of isotope effect, thus solubility of deuterium is nominally the same as for hydrogen.

Technical Reference on Hydrogen Compatibility of Materials

Nickel Alloys:

Solid-Solution Ni-Cr Alloys (code 5110)

1. General

Solid-solution Ni-Cr alloys are used in specialty applications for their combination of strength and high-corrosion resistance, especially at elevated temperature. For the purposes of this discussion, all non-precipitation-hardening, nickel-base alloys with chromium greater than about 10 wt% are considered to be solid-solution Ni-Cr alloys. This represents a wide range of alloy compositions, which makes it difficult to generalize the effects of materials variables on hydrogen-assisted fracture. On the other hand, given the relatively limited data available to assess the effects of gaseous hydrogen on these alloys, this is a convenient classification. The nominally single-phase microstructure of the solid-solution Ni-Cr alloys also suggests a single classification for the purposes of discussing the effects of hydrogen on material properties.

The solid-solution Ni-Cr alloys have similar (single-phase) microstructure as the austenitic stainless steels, which provides an analogy for understanding hydrogen interactions, since the latter have been more extensively studied in gaseous hydrogen environments. A number of studies have drawn this parallel, hypothesizing that hydrogen enhances localization of deformation in solid-solution Ni-Cr alloys and that the relative resistance to hydrogen-assisted fracture can be related to the intrinsic character of deformation in the materials [1, 2]. Alloys with greater stacking fault energy show better resistance to hydrogen-assisted fracture in tensile tests; for example, relatively low-chromium content in the solid-solution Ni-Cr-Fe alloys increases stacking fault energy (for constant iron content) and resistance to hydrogen-assisted fracture [1], while in austenitic stainless steels high-nickel content increases stacking fault energy and resistance to hydrogen-assisted fracture [3, 4]. Carbide precipitation, especially on grain boundaries, similarly enhances hydrogen-assisted fracture in solid-solution Ni-Cr alloys [2, 5] as in austenitic stainless steels [6, 7]. There are also important differences between solid-solution Ni-Cr alloys and austenitic stainless steels. Although generally absent from the austenitic stainless steels (with the possible exception of high-nitrogen stainless steel alloys), short-range ordering is an important phenomenon in Ni-Cr alloys that enhances hydrogen-assisted fracture [8-12]. Impurity segregation to grain boundaries (particularly phosphorus) is also implicated in hydrogen-assisted fracture of solid-solution Ni-Cr alloys [10-13] to a greater extent than in austenitic stainless steels.

Environmental variables also are expected to have similar effects on hydrogen-assisted fracture in both solid-solution Ni-Cr alloys and the austenitic stainless steels. For example, low temperature enhances localized deformation and exacerbates hydrogen-assisted fracture.

In summary, materials characteristics (such as ordering and low stacking fault energy) as well as environmental variables (such as temperature) that promote slip localization in solid-solution Ni-Cr alloys promote hydrogen-assisted fracture. In addition, carbide precipitation and grain boundary segregation also exacerbate hydrogen-assisted fracture, since their influence is enhanced by the role of hydrogen in localizing deformation [2].

1.1 Composition and microstructure

The solid-solution Ni-Cr alloys are highly alloyed, typically containing chromium in the range of 15 to 30 wt% (depending on the specifics of the alloy). These alloys generally contain 2 to 20 wt% iron, as well as significant amounts of molybdenum and cobalt in some alloys (as much as 18 and 15 wt% respectively). Tungsten and niobium are also present in modest amounts in some alloy variations. The elements that promote γ' precipitation (aluminum and titanium in particular) are generally limited to significantly less than 1 wt% each. Table 1.1.1 lists compositional ranges for several common solid-solution Ni-Cr alloys.

The solid-solution Ni-Cr alloys are nominally single phase with the FCC crystal structure, which endows them with characteristics similar to the austenitic stainless steels. Carbon contents are generally low, although the alloys can still be susceptible to precipitation of carbides at elevated temperature, particularly on grain boundaries. In addition, Ni-Cr alloys can be susceptible to ordering, which impacts deformation and the transport of hydrogen.

1.2 Common designations

Tradenames are commonly used for these alloys, including Inconel, Hastelloy, Nimonic, and many others. These same tradenames are also applied to precipitation-strengthened alloys. The tradename is occasionally dropped, such as alloy 600 and Alloy 22 in reference to Inconel 600 and Hastelloy C-22, respectively. For the purposes of this document, the Incoloy alloys (e.g., Incoloy 800 and 900 alloys) are considered iron alloys and included in the appropriate chapters.

2. Permeability, Diffusivity and Solubility

There are a number of gas-permeation studies that report the transport properties of hydrogen in the nickel-base alloys. The permeation, diffusion and solubility parameters from these studies are given in Table 2.1. The magnitude and temperature dependence of the hydrogen transport parameters are similar to those reported for austenitic stainless steels (Figures 2.1, 2.2 and 2.3). In addition, thermal precharging with hydrogen to equilibrium saturation can be used to determine the solubility at a specific temperature (provided that the precharging temperature is sufficiently high that hydrogen is not trapped and that hydrogen diffusivity is sufficiently low to prevent hydrogen loss after precharging). Figure 2.2 summarizes the solubility that is calculated from studies reporting the hydrogen content of specimens that were saturated in gaseous hydrogen at elevated temperature.

The magnitude and temperature dependence of hydrogen permeability is very consistent between studies on various solid-solution Ni-Cr alloys and values reported for austenitic stainless steels (Figure 2.1). The diffusivity of hydrogen in the solid-solution Ni-Cr alloys appears to be slightly greater than for austenitic stainless steels. Diffusion studies using isothermal desorption [14] and electrochemical [15] methods give relationships that are consistent with the higher temperature, gas-permeation measurements. In addition, these diffusion studies suggest that diffusivity depends on composition of the Ni-Cr alloys: for example, diffusivity of hydrogen in Inconel 600 is greater than in Inconel 690 by a factor of about five [14, 15]. Alloys with high chromium content (such as Inconel 690) have greater solubility for hydrogen than alloys with comparatively lower chromium content (such as Inconel 600); this is shown in Figure 2.4. Thus, alloys with comparatively high chromium content have relatively low hydrogen diffusivity (since the permeability is nominally constant and the transport properties are related: $\Phi = DS$). The

calculated values of solubility given in Table 2.2 are also shown on the plot of solubility in Figure 2.3, further demonstrating the range of solubility that can be expected for solid-solution Ni-Cr alloys with different composition. Other alloying elements may also have a significant impact, particularly those that can vary over a wide range such as iron, molybdenum, and cobalt, but their effect on transport properties has not been studied.

Strain-hardening appears to have essentially no effect on the apparent diffusivity for some alloys (such as, Inconel 690 [14, 15] and Hastelloy C-276 [16, 17]), but can have modest effects on the apparent diffusivity in other alloys (such as, Inconel 600 [14, 15] and Hastelloy G [17]). Ordering has been invoked to explain small reductions of hydrogen diffusivity in Hastelloy C-276 subjected to low-temperature aging (473K to 773K) [16], although no reduction of hydrogen diffusivity is observed for Hastelloy G subjected to the same aging treatments [17]. In general, however, the role of strain-hardening and ordering on hydrogen transport in solid-solution Ni-Cr alloys is not well understood.

Hydrogen trapping in solid-solution Ni-Cr alloys is generally attributed to carbides [14, 17], as well as dislocations [15]. In alloys with very low carbon content (such as Hastelloy C-276), hydrogen trapping is reported to be absent [16, 17] or attributed to phosphorus segregation to grain boundaries [18].

3. Mechanical Properties: Effects of Gaseous Hydrogen

3.1 Tensile properties

3.1.1 Smooth tensile properties

The effects of hydrogen on the tensile properties of solid-solution Ni-Cr alloys can be significant. In general, the tensile ductility is reduced when these alloys are tested in high-pressure gaseous hydrogen [7, 19], with the exception of Hastelloy X, which shows no effects of gaseous hydrogen at room temperature [20]. The magnitude of the reported reduction in tensile ductility can vary significantly: Hastelloy C-22 displays grain boundary fracture and relatively low tensile ductility in gaseous hydrogen at pressure of 70 MPa [7, 19], while Inconel 600 displays transgranular fracture and significantly greater tensile ductility in gaseous hydrogen at pressure of 70 MPa [7]. While the absolute values of the tensile properties are not reported in these studies, the properties of Inconel 625 and Hastelloy X in gaseous hydrogen at 34.5 MPa are reported, Table 3.1.1.1. Tensile tests have also been performed on Hastelloy X at elevated temperature in gaseous hydrogen (34.5 MPa), and for Inconel 625 at both cryogenic and elevated temperature in gaseous hydrogen, Table 3.1.1.2. The effects of hydrogen on Inconel 625 are significantly reduced at both temperature extremes.

Testing of hydrogen-precharged materials [1, 21-23] also shows reduction of tensile ductility. Inconel 600 appears to display less reduction of ductility when hydrogen precharged than other solid-solution Ni-Cr alloys, Table 3.1.1.1. In a separate study, Hastelloy X shows significantly less reduction of tensile elongation than Inconel 600 [5]. Fracture surfaces tend to be rather complicated with the most affected alloys showing evidence of intergranular fracture and strong slip localization [1, 2, 23].

The range of tensile ductility that is observed for solid-solution Ni-Cr alloys in the presence of hydrogen is generally attributed to microstructural characteristics that affect deformation.

Symons, for example, studied the effect of Cr content on laboratory heats similar to Inconel 600 (Ni-15Cr-8Fe) and Inconel 690 (Ni-30Cr-8Fe) [1], showing that chromium content is an important materials variable (all else being equal), Table 3.1.1.3. Symons related chromium content to the stacking fault energy: alloys with greater resistance to hydrogen-assisted fracture have higher stacking fault energy, which correlates with lower chromium content in the alloys studied by Symons [1]. This is analogous to the role attributed to nickel in austenitic stainless steels [24] (although stacking fault energy increases as nickel increases), as well as nitrogen in 21Cr-6Ni-9Mn austenitic stainless steel [25]. Other microstructural influences that reduce tensile ductility include carbide precipitation [5, 22], impurity segregation [13] and ordering [8, 9, 11], all of which can generally be a concern for solid-solution Ni-Cr alloys.

The effects of temperature and strain rate were explored by Chene and Brass for Inconel 600 using cathodic precharging in molten salts to about 35 wppm hydrogen and testing in air (uniform saturation of hydrogen in 5 mm thick flat tensile specimens) [26]. They found the elongation to show a minimum at temperature near 240K for hydrogen-precharged specimens and no effect of temperature on elongation in the absence of hydrogen in the temperature range from 240K to 470K. At very low temperature (77K), there was essentially no change in elongation due to hydrogen. At temperature of 513K, the elongation was also unchanged by hydrogen although significant hydrogen desorbed from the specimen during testing. In addition, Chene and Brass observed little effect of strain rate near room temperature for strain rates less than about 10^{-3} s^{-1}, in contrast to another study where the tensile elongation due to thermally precharged hydrogen was found to be decrease with strain rate to lower strain rates [5].

3.1.2 Notched tensile properties

Strength and ductility (RA) of notched tensile specimens of Inconel 625 are reduced in gaseous hydrogen compared to gaseous helium, Table 3.1.2.1. The reduction of ductility is significantly greater than the reduction of notched tensile strength. Hastelloy X displays about a 10% reduction of notched strength and ductility in gaseous hydrogen, in contrast to the smooth tensile tests where no effects of hydrogen are observed for the same testing conditions. At elevated temperature (951 K), gaseous hydrogen at pressure of 34.5 MPa has no effect on tensile properties of Inconel 625 and Hastelloy X, Table 3.1.2.2. Also at cryogenic temperature (144 K) in gaseous hydrogen at pressure of 34.5 MPa, the RA of Inconel 625 is only modestly affected (Table 3.1.2.2) compared to the reduction observed at room temperature (Table 3.1.2.1).

Tensile elongation was found to depend on the stress concentration factor in hydrogen-precharged Inconel 600 and Hastelloy X [5]. The relative decrease of tensile elongation for notched Inconel 600 ($K_t = 5.5$) was found to approximately double relative to smooth tensile specimens. For Hastelloy X, tensile elongation was relatively unaffected by hydrogen for smooth tensile specimens, compared to approximately 25% reduction in tensile elongation with a notch ($K_t = 5.5$).

3.2 Fracture mechanics

The fracture toughness of Inconel 690 is significantly reduced when the material is hydrogen precharged, Table 3.2.1 [22], while the fracture toughness of Inconel 625 in gaseous hydrogen is essentially unchanged compared to tests in gaseous helium [20, 27, 28]. The relative fracture toughness of the two alloys, however, is substantially different: the fracture toughness of the Inconel 690 is almost five times greater than the fracture toughness of Inconel 625. These

differences may reflect the difference in strength of the tested alloys (the Inconel 625 was not fully annealed), or may reflect 30 years of improvements in materials processing (the study on Inconel 625 was performed in the early 1970s, while the study on Inconel 690 is from the late 1990s). The fracture toughness of currently available and properly annealed Inconel 625 is likely consistent with the values reported here for Inconel 690. In any case, the hydrogen-affected fracture toughness of Inconel 690 remains relatively large compared to values of fracture toughness from Refs. [20, 27, 28] on Inconel 625 in an inert environment and other structural metals, such as aluminum alloys. The fracture toughness at cryogenic temperature (144 K) is greater than at room temperature and unaffected by gaseous hydrogen, Table 3.2.2.

Carbide precipitation at grain boundaries (i.e., sensitization due to thermal exposure) does not impact the fracture toughness of Inconel 690 in air, but reduces the fracture toughness in the hydrogen-precharged condition by a factor of more than 2, compared to non-sensitized material [22].

3.3 Fatigue

Low-cycle fatigue of Inconel 625 and Hastelloy X in gaseous hydrogen at pressure of 34.5 MPa is reported in several reports for NASA [20, 27]. The data is reproduced in Figure 3.3.1, showing a significant reduction in number of cycles to failure for a given value of total strain. This reduction is greater for Inconel 625 than for Hastelloy X, which is consistent with results from tensile testing.

3.4 Creep

A limited set of creep rupture data are available for Inconel 625 in Refs [20, 27] at temperature of 951 K. Rupture occurred in less than 50 hours at stress of 286 MPa in gaseous hydrogen at pressure of 34.5 MPa. Specimens in gaseous hydrogen failed during loading at stresses as low as 310 MPa. In comparison, rupture took greater than 20 hours for substantially higher stresses (430 MPa) in gaseous helium. In short, gaseous hydrogen significantly enhances creep in Inconel 625.

3.5 Impact

No known published data in gaseous hydrogen.

3.6 Disk rupture testing

Disk rupture tests show that nickel-base alloys are extremely sensitive to hydrogen-assisted fracture in gaseous environments [29].

4. Fabrication

4.1 Primary processing

Impurity segregation, as well as alloy segregation, is important issues during the production of nickel alloys. One study suggests that impurity segregation at grain boundaries in Inconel 600 enhances resistance to hydrogen-assisted fracture [13], while most studies implicate impurity segregation in exacerbating hydrogen-assisted fracture. Macrosegregation may promote

hydrogen-assisted fracture in Ni-Cr alloys in the same way that macrosegregation enhances hydrogen-assisted fracture in austenitic stainless steels [30].

4.2 Heat treatment

Proper heat treating and appropriate thermal exposure is an important consideration for some solid-solution Ni-Cr alloys, due to ordering and sensitization (carbide precipitation at grain boundaries). The effects of ordering and sensitization may not be apparent at ambient conditions, but when combined with hydrogen these effects can be substantial [22].

4.3 Properties of welds

Alloys with niobium or titanium additions (such as Inconel 625) are designed to control sensitization during welding as in type 321 and 347 austenitic stainless steels. The smooth tensile properties (Table 4.3.1), notched tensile properties (Table 4.3.2) and fracture toughness (Table 4.3.3) of the fusion zone in welded Inconel 625 are reported in Ref. [20]. Gaseous hydrogen had significantly less effect on the properties of the welds compared to the base metal, likely due to the lower strength of the fusion zone of the weld compared to the base metal.

5. References

1. DM Symons. Hydrogen Embrittlement of Ni-Cr-Fe Alloys. Metall Mater Trans 28A (1997) 655-663.
2. DM Symons. The Effect of Carbide Precipitation on the Hydrogen-Enhanced Frature Behavior of Alloy 690. Metall Mater Trans 29A (1998) 1265-1277.
3. GR Caskey. Hydrogen Compatibility Handbook for Stainless Steels (DP-1643). EI du Pont Nemours, Savannah River Laboratory, Aiken SC (June 1983).
4. GR Caskey. Hydrogen Effects in Stainless Steels. in: RA Oriani, JP Hirth and M Smialowski, editors. Hydrogen Degradation of Ferrous Alloys. Park Ridge NJ: Noyes Publications (1985) p. 822-862.
5. M Hasegawa and M Osawa. Hydrogen damage of nickel-base heat resistant alloys. Transactions ISIJ 21 (1981) 25-31.
6. G Han, J He, S Fukuyama and K Yokogawa. Effect of strain-induced martensite on hydrogen environment embrittlement of sensitized austenitic stainless steels at low temperatures. Acta Mater 46 (1998) 4559-4570.
7. S Fukuyama, M Imade and K Yokogawa. Development of new material testing appartus in high-pressure hydrogen and evaluation of hydrogen gas embrittlement of metals (PVP2007-26820). in: Proceedings of PVP-2007: ASME Pressure Vessels and Piping Division Conference, 2007, San Antonion TX. ASME (July 22-26, 2007)
8. K Miyata and M Igarashi. Effect of ordering in susceptibility to hydrogen embrittlement of a Ni-base superalloy. Metall Trans 23A (1992) 953-961.
9. RJ Coyle, JA Kargol and NF Fiore. Hydrogen-assisted ductile fracture in a Ni-base superalloy. Scr Metall 14 (1980) 939-942.
10. N Sridhar, JA Kargol and NF Fiore. Effect of low temperature aging on hydrogen-induced crack growth in a Ni-base superalloy. Scr Metall 14 (1980) 1257-1260.
11. RJ Coyle, JA Kargol and NF Fiore. The effect of aging on hydrogen embrittlement of a nickel alloy. Metall Trans 12A (1981) 653-658.

12. JA Kargol and B Ladna. The roles of ordering and impurity segregation on the hydrogen assisted crack propagation in nickel base stainless alloys. Scr Metall 16 (1982) 191-195.
13. M Cornet, C Bertrand and M Da Cunha Belo. Hydrogen embrittlement of ultrapure alloys of the Inconel 600 type: influence of the additions of elements (C, P, Sn, Sb). Metall Trans 13A (1982) 141-144.
14. DM Symons, GA Young and JR Scully. The effect of strain on the trapping of hydrogen at grain-boundary carbides in Ni-Cr-Fe alloys. Metall Mater Trans 32A (2001) 369-377.
15. M Uhlemann and BG Pound. Diffusivity, solubility and trapping behavior of hydrogen in alloys 600, 690tt and 800. Corros Sci 40 (1998) 645-662.
16. DA Mezzanotte, JA Kargol and NF Fiore. Hydrogen transport in a Ni-base superalloy. Scr Metall 14 (1980) 219-223.
17. DA Mezzanotte, JA Kargol and NF Fiore. Hydrogen transport in nickel base stainless alloys. Metall Trans 13A (1982) 1181-1186.
18. BG Pound. Hydrogen trapping in work-hardened alloys. Acta Metall Mater 39 (1991) 2099-2105.
19. S Fukuyama, M Imade, T Iijima and K Yokogawa. Development of new material testing apparatus in 230 MPa hydrogen and evaluation of hydrogen gas embrittlement of metals. in: Proceedings of PVP-2008: ASME Pressure Vessels and Piping Division Conference, 2008, Chicago IL. ASME (July 27-31, 2008)
20. JA Harris and MCV Wanderham. Properties of Materials in High Pressure Hydrogen at Cryogenic, Room, and Elevated Temperatures. Pratt and Whitney Aircraft (report no. FR-5768) for the National Aeronautics and Space Administration (Marshall Space Flight Center), West Palm Beach FL (Jul 1973).
21. AW Thompson. Hydrogen-assisted fracture in single-phase nickel alloys. Scr Metall 16 (1982) 1189-1192.
22. DM Symons. The effect of carbide precipitation on the hydrogen-enhanced fracture behavior of alloy 690. Metall Mater Trans 29A (1998) 1265-1277.
23. C San Marchi, T Zaleski, S Lee, NYC Yang and B Stuart. Effect of laser peening on the hydrogen compatibility of corrosion-resistant nickel alloy. Scr Mater 58 (2008) 782-785.
24. BC Odegard, JA Brooks and AJ West. The Effect of Hydrogen on Mechanical Behavior of Nitrogen-Strengthened Stainless Steel. in: AW Thompson and IM Bernstein, editors. Effect of Hydrogen on Behavior of Materials. Proceedings of an International Conference on Effect of Hydrogen on Behavior of Materials (Moran WY, 1975), volume New York: The Metallurgical Society of AIME (1976) p. 116-125.
25. RE Stoltz and JB VanderSande. The Effect of Nitrogen on Stacking Fault Energy of Fe-Ni-Cr-Mn Steels. Metall Trans 11A (1980) 1033-1037.
26. J Chene and AM Brass. Role of temperature and strain rate on the hydrogen-induced intergranular rupture in alloy 600. Metall Mater Trans 35A (2004) 457-464.
27. JA Harris and MCV Wanderham. Propeties of Materials in High Pressure Hydrogen at Cryogenic, Room, and Elevated Temperatures (Annual Report). Pratt and Whitney Aircraft (report no. FR-4566) for the National Aeronautics and Space Administration (Marshall Space Flight Center), West Palm Beach FL (1971).
28. RJ Walter and WT Chandler. Influence of Gaseous Hydrogen on Metals: Final Report. Rocketdyne for the National Aeronautics and Space Administration, Canoga Park CA (Oct 1973).

29. J-P Fidelle. Present status of the disk pressure test for hydrogen embrittlement. in: L Raymond, editor. Test Methods for Hydrogen Embrittlement: Prevention and Control, ASTM STP 962, American Society for Testing and Materials. (1988) p. 153-172.
30. T Michler, Y Lee, RP Gangloff and J Naumann. Influence of macro segregation on hydrogen environment embrittlement of SUS 316L stainless steel. Int J Hydrogen Energy 34 (2009) 3201-3209.
31. ASTM. ASTM DS-56H, Metals and Alloys in the UNIFIED NUMBERING SYSTEM (SAE HS-1086 OCT01). 2001.
32. T Tanabe, Y Tamanishi, K Sawada and S Imoto. Hydrogen Transport in Stainless Steels. J Nucl Mater 122&123 (1984) 1568-1572.
33. N Kishimoto, T Tanabe, T Suzuki and H Yoshida. Hydrogen diffusion and solution at high temperatures in 316L stainless steel and nickel-base heat-resistant alloys. J Nucl Mater 127 (1985) 1-9.
34. AS Schmidt, F Verfuss and E Wicke. Studies on the permeation of hydrogen and tritium through heat resistant alloys. J Nucl Mater 131 (1985) 247-260.
35. E Rota, F Waelbroeck, P Weinhold and J Winter. Measurements of surface and bulk properties for the interaction of hydrogen with Inconel 600. J Nucl Mater 111 & 112 (1982) 233-239.
36. C San Marchi, BP Somerday and SL Robinson. Permeability, Solubility and Diffusivity of Hydrogen Isotopes in Stainless Steels at High Gas Pressure. Int J Hydrogen Energy 32 (2007) 100-116.

Table 1.1.1. Compositions (wt%) of common commercial solid-solution Ni-Cr alloys [31].

UNS No	Common Name	Ni	Cr	Fe	Mo	Co	W	Al	Ti	Mn	Si	C	other
N06002	Hastelloy X (Ni–22Cr–18Fe–8Mo)	Bal	20.5 23.0	17.0 20.0	8.0 10.0	0.5 2.5	0.20 1.0	—	—	1.00 max	1.00 max	0.05 0.15	0.040 max P; 0.030 max S
N06007	Hastelloy G (Ni–23Cr–19Fe–6Mo)	Bal	21.0 23.5	18.0 21.0	5.5 7.5	2.5 max	1.0 max	—	—	1.0 2.0	1.0 max	0.05 max	1.75-2.5 Nb; 1.5-2.5 Cu; 0.04 max P; 0.03 max S
N06022	Hastelloy C-22 (Ni–22Cr–3Fe–13Mo)	Bal	20.0 22.5	2.0 6.0	12.5 14.5	2.5 max	2.5 3.5	—	—	0.50 max	0.08 max	0.015 max	0.35 max V; 0.02 max P; 0.02 max S
N06075	Nimonic 75 (Ni–20Cr–4Fe)	Bal	18.0 21.0	5.00 max	—	—	—	—	0.20 0.60	1.00 max	1.00 max	0.08 0.15	0.50 max Cu
N06600	Inconel 600 (Ni–15Cr–8Fe)	Bal (72 min)	14.00 17.00	6.00 10.00	—	—	—	—	—	1.00 max	0.50 max	0.15 Max	0.50 max Cu; 0.040 max P; 0.015 max S
N06617	Inconel 617 (Ni–22Cr–9Mo–12Co)	Bal (44.5 min)	20.0 24.0	3.00 max	8.0 10.0	10.0 15.0	—	0.80 1.50	0.60 max	1.00 max	1.00 max	0.05 0.15	0.50 max Cu; 0.006 max B; 0.015 max S;
N06625	Inconel 625 (Ni–22Cr–9Mo–4Nb)	Bal	20.0 23.0	5.0 max	8.0 10.0	—	—	0.40 max	0.40 max	0.50 max	0.50 max	0.10 max	3.15-4.15 Nb; 0.015 max P; 0.015 max S
N06690	Inconel 690 (Ni–29Cr–9Fe)	Bal (58 min)	27.0 31.0	7.0 11.0	—	—	—	0.50 max	—	0.50 max	0.50 max	0.05 max	0.50 max Cu; 0.015 max S
N10276	Hastelloy C-276 (Ni–16Cr–5Fe –16Mo)	Bal	14.5 16.5	4.0 7.0	15.0 17.0	2.5 max	3.0 4.5	—	—	1.0 max	0.08 max	0.02 max	0.35 max V; 0.030 max P; 0.030 max S

Table 1.1.2. Compositions (wt%) of solid-solution Ni-Cr alloys used in studies with hydrogen.

Heat	alloy	Ni	Cr	Fe	Mo	Co	W	Al	Ti	Mn	Si	C	other	Ref.
H73a	Inconel 625 Partially annealed bar (dia. 19 mm)	Bal	21.6	2.14	9.10	0.05	—	0.17	0.06	0.01	0.08	0.052	3.82 Nb; 0.005 P; 0.005 S	[20]
H73b	Inconel 625 Partially annealed bar (dia. 108 mm)	Bal	21.82	1.79	9.05	—	—	0.18	0.20	0.02	0.10	0.04	3.92 Nb; 0.004 P; 0.005 S	[20]
H73c	Hastelloy X Solutionized bar (dia. 19 mm)	Bal	22.31	18.36	8.27	1.60	0.51	—	—	0.61	0.71	0.074	0.0014 B; 0.016 P; 0.006 S	[20]
W73	Inconel 625 Partially annealed bar (32x70 mm)	Bal	21.14	2.55	8.97	0.07	—	0.20	0.11	0.05	0.20	0.047	3.73 Nb; 0.008 P; 0.003 S	[28]
T84a	Inconel 600	(72)	(16)	(8)	—	—	—	—	—	—	—	—	—	[32]
T84b	Nichrome	(77)	(20)	(2)	—	—	—	—	—	—	—	—	—	[32]
K85a	Inconel 600	Bal	15.9	7.0	—	—	—	0.32	0.41	0.45	0.25	0.047	0.20 Cu	[33]
K85b	Hastelloy X	Bal	20.7	19.7	8.9	1.6	0.48	—	—	0.15	0.14	0.10	0.01 Cu	[33]
S85	Nimonic PE 13	Bal	21.0	19.1	8.8	1.6	0.65	—	0.04	0.37	0.44	0.054	0.07 Cu	[34]
S98a	Inconel 690	Bal	27.5	8.1	—	0.26	—	0.26	0.25	—	0.1	0.02	0.004 B; 0.006 P; 0.001 S	[22]
S98b	Inconel 690	Bal	28.3	8.4	—	0.35	—	—	—	—	0.3	0.03	0.004 B 0.013 P; 0.001 S;	[22]
S08	Hastelloy C-22	Bal	21.8	3.8	13.0	—	3.0	—	—	0.34	0.08	0.002	—	[23]

Table 2.1. Permeability, diffusivity and solubility relationships for solid-solution Ni-Cr alloys. These relationships are plotted in Figures 2.1, 2.2 and 2.3 for permeability, diffusivity and solubility respectively.

Material	Temperature Range (K)	Pressure Range (MPa)	$\Phi = \Phi_o \exp(-E_\Phi / RT)$		$D = D_o \exp(-E_D / RT)$		$S = S_o \exp(-E_S / RT)$		Ref.
			Φ_o $\left(\frac{\text{mol H}_2}{\text{m} \cdot \text{s} \cdot \text{MPa}^{1/2}}\right)$	E_Φ $\left(\frac{\text{kJ}}{\text{mol}}\right)$	D_o $\left(\frac{\text{m}^2}{\text{s}}\right)$	E_D $\left(\frac{\text{kJ}}{\text{mol}}\right)$	S_o $\left(\frac{\text{mol H}_2}{\text{m}^3 \cdot \text{MPa}^{1/2}}\right)$	E_S $\left(\frac{\text{kJ}}{\text{mol}}\right)$	
Inconel 600	423–673	—	19.9×10^{-6}	55.2	1.70×10^{-6}	49.8	11.7	5.4	[35]
Inconel 600 (heat K85a)	873–1173	0.1–0.7	783×10^{-6}	63.7	0.49×10^{-6}	42.5	1600	21.2	[33]
Inconel 600 (heat T84a)	500–1200	0.001 –0.1	950×10^{-6}	66.2	0.136×10^{-6}	37.7	6990	28.5	[32]
Hastelloy X (heat K85b)	873–1173	0.1–0.7	881×10^{-6}	64.6	0.490×10^{-6}	43.4	1800	21.2	[33]
Nichrome (heat T84b)	500–1200	0.001 –0.1	220×10^{-6}	60.3	0.111×10^{-6}	37.2	1980	23.1	[32]
Nimonic PE13 (heat S85)	500–1200	0.001 –0.01	36.2×10^{-6}	52.3	0.092×10^{-6}	33.8	394	18.5	[34]
Austenitic stainless steels	—	—	120×10^{-6}	59.8	0.89×10^{-6}	53.9	135	5.9	[36]

Table 2.2. Solubility of hydrogen in several solid-solution Ni-Cr alloys, determined after thermal precharging in gaseous hydrogen at elevated temperature and pressure.

Material	Precharging temperature (K)	Precharging pressure (MPa)	Reported hydrogen concentration (wppm)	Solubility † $\left(\frac{\text{mol } H_2}{m^3 \cdot MPa^{1/2}}\right)$	Cr content (wt%)	Ref.
Inconel 600	723	30	40 cm^3/100g	25.7	15.4	[5]
Inconel 690 (heat S98a)	558	13	38	41.9	27.5	[22]
		34	59.5	39.1		
Inconel 690 (heat S98b)		13	38.5	42.5	28.3	
		34	60	39.5		
Ni-6Cr-8Fe	558	13	25	27.6	6.1	[1]
		34	37	24.4		
Ni-15Cr-8Fe		13	24	26.5	14.7	
		34	36	23.7		
Ni-26Cr-8Fe		13	34	37.5	26.5	
		34	55	36.2		
Ni-35Cr-8Fe		13	60	66.2	34.8	
		34	99	65.2		
Hastelloy C-22 (heat S08)	573	138	110	30.3	21.8	[23]
Hastelloy X	723	30	60 cm^3/100g	38.5	21.7	[5]

† calculated assuming density of 8.2 g/cm^3 for all alloys; actual density of some alloys is greater

Table 3.1.1.1. Tensile properties of solid-solution Ni-Cr alloys at room temperature: measured in air with internal hydrogen (thermal precharging in gaseous hydrogen), or measured in high-pressure gaseous helium and hydrogen; values in parenthesis are estimated.

Material	Thermal precharging	Test environment	Strain rate (s^{-1})	S_y (MPa)	S_u (MPa)	El_u (%)	El_t (%)	RA (%)	Ref.
Inconel 600	None	Air	0.67 x10^{-3}	280	710	—	—	75	[21]
	(1)	Air		(280)	(710)	—	—	66	
Inconel 625	None	Air	0.67 x10^{-3}	330	805	—	—	43	[21]
	(1)	Air		(330)	(805)	—	—	28	
Inconel 625 (heat H73a)	None	34.5 MPa He	0.17 x10^{-3}	579	1002	—	47	62	[20, 27]
	None	34.5 MPa H_2		694	975	—	23	30	
Inconel 625 (heat W73)	None	Air	—	648	993	—	50	54	[28]
	None	34.5 MPa He		634	993	—	55	50	
	None	34.5 MPa H_2		600	993	—	20	18	
Inconel 690 (heat S98a)	None	Air	0.4 x10^{-3}	289	668	46	56	70	[22]
	(2)	Air		310	627	41	48	43	
	(3)	Air		310	550	27	31	40	
Inconel 690 (heat S98b)	None	Air	0.4 x10^{-3}	282	668	45	52	67	[22]
	(2)	Air		282	550	22	25	32	
	(3)	Air		296	482	11	17	31	
Hastelloy C-22 (heat S08)	None	Air	2 x10^{-3}	383	810	58	89	72	[23]
	(4)	Air		426	793	52	56	41	
Hastelloy X (heat H73c)	None	34.5 MPa He	0.17 x10^{-3}	321	723	—	54	63	[20, 27]
	None	34.5 MPa H_2		340	727	—	53	63	

(1) 24 MPa gaseous hydrogen, 475K, 410 hours
(2) 13 MPa gaseous hydrogen, 558K, 1000 hours; 38 wppm hydrogen
(3) 34 MPa gaseous hydrogen, 558K, 1000 hours; 60 wppm hydrogen
(4) 138 MPa gaseous hydrogen, 573K, 820 hours; 110 wppm hydrogen

Table 3.1.1.2. Tensile properties of solid-solution Ni-Cr alloys at both cryogenic and elevated temperature in gaseous hydrogen and helium at pressure of 34.5 MPa.

Material	Thermal precharging	Test environment	Strain rate (s^{-1})	S_y (MPa)	S_u (MPa)	El_u (%)	El_t (%)	RA (%)	Ref.
Inconel 625 (heat W73)	None	He – 144 K	—	710	1130	—	43	52	[20, 27]
	None	H_2 – 144 K		696	1120	—	43	48	
Inconel 625 (heat H73a)	None	He – 951 K	0.17 x10^{-3}	507	819	—	61	68	[28]
	None	H_2 – 951 K		517	850	—	55	60	
Hastelloy X (heat H73c)	None	He – 951 K	0.17 x10^{-3}	235	550	—	53	58	[28]
	None	H_2 – 951 K		234	555	—	51	54	

Table 3.1.1.3. Tensile properties of Ni–Cr–Fe alloys thermally precharged in gaseous hydrogen and tested in air at room.

Material	Thermal precharging	Test environment	Strain rate (s^{-1})	S_y (MPa)	S_u (MPa)	El_u (%)	El_t (%)	RA (%)	Ref.
Ni–6Cr–8Fe	None	Air	0.4 x10^{-3}	207	462	—	35	45	[1]
	(1)	Air		200	420	—	31	47	
	(2)	Air		220	468	—	31	42	
Ni–15Cr–8Fe	None	Air	0.4 x10^{-3}	282	586	—	49	52	[1]
	(1)	Air		230	510	—	43	48	
	(2)	Air		255	565	—	42	45	
Ni–26Cr–8Fe	None	Air	0.4 x10^{-3}	289	593	—	53	57	[1]
	(1)	Air		255	410	—	22	31	
	(2)	Air		282	427	—	13.5	20	
Ni–35Cr–8Fe	None	Air	0.4 x10^{-3}	261	606	—	55	65	[1]
	(1)	Air		275	454	—	25	36	
	(2)	Air		300	475	—	18	27	

(1) 13 MPa gaseous hydrogen, 558K, 1000 hours
(2) 34 MPa gaseous hydrogen, 558K, 1000 hours

Table 3.1.2.1. Notched tensile properties of solid-solution Ni-Cr alloys at room temperature in high-pressure gaseous helium and hydrogen.

Material	Specimen	Thermal precharging	Test environment	Displ. rate (mm/s)	S_y † (MPa)	σ_s (MPa)	RA (%)	Ref.
Inconel 625 (heat H73a)	(a)	None	34.5 MPa He	2.1×10^{-3}	579	1252	15	[20, 27]
		None	34.5 MPa H_2		694	1227	6.9	
Inconel 625 (heat W73)	(b)	None	34.5 MPa He	0.4×10^{-3}	634	1430	9.4	[28]
		None	34.5 MPa H_2		600	1090	4.6	
Hastelloy X (heat H73c)	(a)	None	34.5 MPa He	2.1×10^{-3}	321	1005	18	[20, 27]
		None	34.5 MPa H_2		340	874	14	

† yield strength of smooth tensile bar

(a) V-notched specimen: 60˚ included angle; minimum diameter = 8 mm (0.315 inch); maximum diameter = 12.7 mm (0.5 inch); notch root radius = 0.051 mm (0.002 inch). Stress concentration factor (K_t) = 8.0.

(b) V-notched specimen: 60˚ included angle; minimum diameter = 3.81 mm (0.15 inch); maximum diameter = 7.77 mm (0.306 inch); notch root radius = 0.024 mm (0.00095 inch). Stress concentration factor (K_t) = 8.4.

Table 3.1.2.2. Notched tensile properties of solid-solution Ni-Cr alloys at both cryogenic and elevated temperature in gaseous hydrogen and helium at pressure of 34.5 MPa.

Material	Specimen	Thermal precharging	Test environment	Displ. rate (mm/s)	S_y † (MPa)	σ_s (MPa)	RA (%)	Ref.
Inconel 625 (heat W73)	(b)	None	He – 144 K	0.4×10^{-3}	710	1460	8.1	[28]
		None	H_2 – 144 K		696	1520	6.9	
Inconel 625 (heat H73a)	(a)	None	He – 951 K	2.1×10^{-3}	507	985	16	[20, 27]
		None	H_2 – 951 K		517	1014	16	
Hastelloy X (heat H73c)	(a)	None	He – 951 K	2.1×10^{-3}	235	625	18	[20, 27]
		None	H_2 – 951 K		234	621	19	

† yield strength of smooth tensile bar

(a) V-notched specimen: 60˚ included angle; minimum diameter = 8 mm (0.315 inch); maximum diameter = 12.7 mm (0.5 inch); notch root radius = 0.051 mm (0.002 inch). Stress concentration factor (K_t) = 8.0.

(b) V-notched specimen: 60˚ included angle; minimum diameter = 3.81 mm (0.15 inch); maximum diameter = 7.77 mm (0.306 inch); notch root radius = 0.024 mm (0.00095 inch). Stress concentration factor (K_t) = 8.4.

Table 3.2.1. Fracture toughness of solid-solution Ni-Cr alloys at room temperature: measured in air with internal hydrogen (thermal precharging in gaseous hydrogen), or measured in high-pressure gaseous helium and hydrogen.

Material	Test method	Thermal precharging	Test environment	S_y (MPa)	K_Q (MPa $m^{1/2}$)	Ref.
Inconel 625 (heat H73b)	LEFM, CT (ASTM E399-72)	None	34.5 MPa He	—	59 † (RL §) 63 † (LR §)	[20]
		None	34.5 MPa H_2	—	66 † (RL §) 60 † (LR §)	
Inconel 625 (heat W73)	LEFM, CT (ASTM E399-72)	None None	34.5 MPa He 34.5 MPa H_2	634 600	84 67	[28]
Inconel 690 (heat S98a)	J-integral, CT (ASTM E813)	None (1)	Air Air	289	330 ‡ 218 ‡†	[22]
Inconel 690 (heat S98b)	J-integral (ASTM E813)	None (1)	Air Air	282	330 ‡ 218 ‡†	[22]

LEFM = linear elastic fracture mechanics; CT = compact tensile

† valid K_{IC} or J_{IC} value according to testing standard

‡ calculated from J; assuming E = 207 GPa, ν = 0.3 and $K = \left[JE/\left(1-\nu^2\right)\right]^{1/2}$; initial loading rate of 1 MPa $m^{1/2}$ per minute

§ RL and LR refer to orientations as defined in ASTM standards for fracture testing, but are inferred from author description of longitudinal and transverse respectively

(1) 13 MPa gaseous hydrogen, 558K, 1000 hours; 38 wppm hydrogen

Table 3.2.2. Fracture toughness of Inconel 625 at temperature of 144 K in gaseous hydrogen and helium at pressure of 34.5 MPa.

Material	Test method	Thermal precharging	Test environment	S_y (MPa)	K_Q (MPa $m^{1/2}$)	Ref.
Inconel 625 (heat W73)	LEFM, CT (ASTM E399-72)	None None	He – 144 K H_2 – 144 K	710 696	110 108	[28]

LEFM = linear elastic fracture mechanics; CT = compact tensile

Table 4.3.1. Tensile properties of welded Inconel 625 at room temperature in high-pressure hydrogen and helium gas.

Material	Thermal precharging	Test environment	Strain rate (s^{-1})	S_y (MPa)	S_u (MPa)	El_u (%)	El_t (%)	RA (%)	Ref.
Welded ‡ Inconel 625 (heat H73a)	None	34.5 MPa He	0.17 x10^{-3}	370	736	—	24	38	[20, 27]
	None	34.5 MPa H_2		363	766	—	25	38	

‡ gas tungsten arc weld (GTAW), using AMS 5837 filler material

Table 4.3.2. Notched tensile properties of welded Inconel 625 at room temperature in high-pressure hydrogen and helium gas.

Material	Specimen	Thermal precharging	Test environment	Displ. rate (mm/s)	S_y † (MPa)	σ_s (MPa)	RA (%)	Ref.
Welded ‡ Inconel 625 (heat H73a)	(a)	None	34.5 MPa He	2.1 x 10^{-3}	370	980	14	[20, 27]
		None	34.5 MPa H_2		363	892	12	

‡ gas tungsten arc weld (GTAW), using AMS 5837 filler material
† yield strength of smooth tensile bar
(a) V-notched specimen: 60˚ included angle; minimum diameter = 8 mm (0.315 inch); maximum diameter = 12.7 mm (0.5 inch); notch root radius = 0.051 mm (0.002 inch). Stress concentration factor (K_t) = 8.0.

Table 4.3.3. Fracture toughness of welded Inconel 625 at room temperature.

Material	Test method	Thermal precharging	Test environment	S_y (MPa)	K_Q (MPa $m^{1/2}$)	Ref.
Welded ‡ Inconel 625 (heat H73b)	LEFM, CT (ASTM E399-72)	None	34.5 MPa He	—	57 † (RL §)	[20]
					55 † (LR §)	
		None	34.5 MPa H_2	—	61 † (RL §)	
					59 † (LR §)	

LEFM = linear elastic fracture mechanics; CT = compact tensile
‡ gas tungsten arc weld (GTAW), using AMS 5837 filler material
† valid K_{IC} or J_{IC} value according to testing standard
§ RL and LR refer to orientations as defined in ASTM standards for fracture testing, but are inferred from author description of longitudinal and transverse respectively

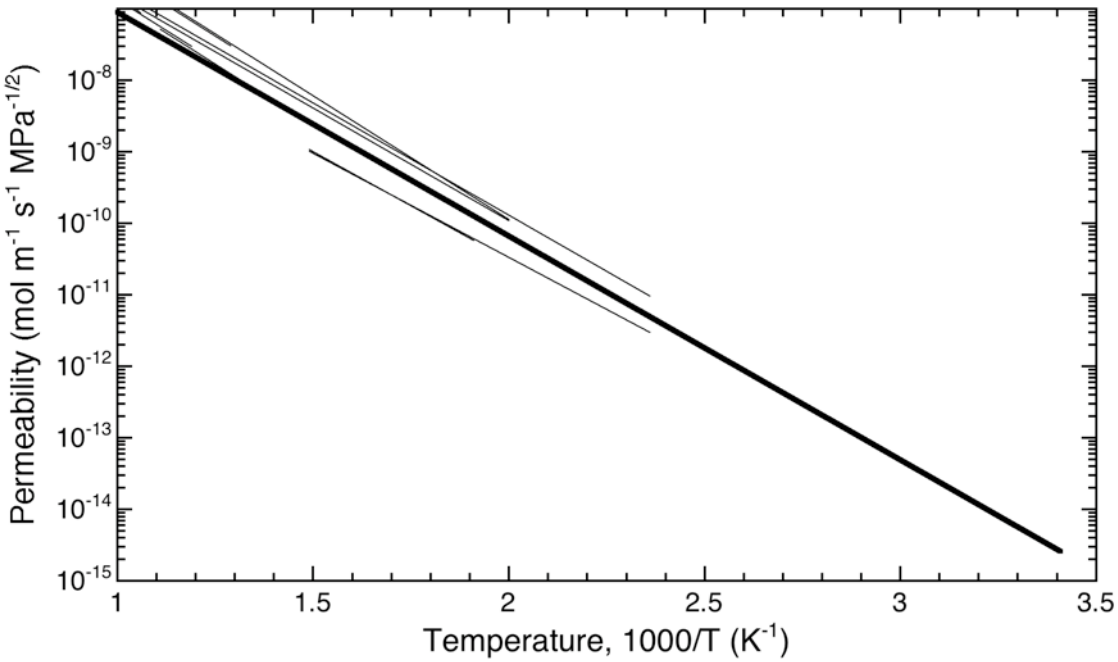

Figure 2.1. Permeability for several solid-solution Ni-Cr alloys from gas permeation experiments. All data corrected to hydrogen. The dark line represents the recommendation for austenitic stainless steels from Ref. [36].

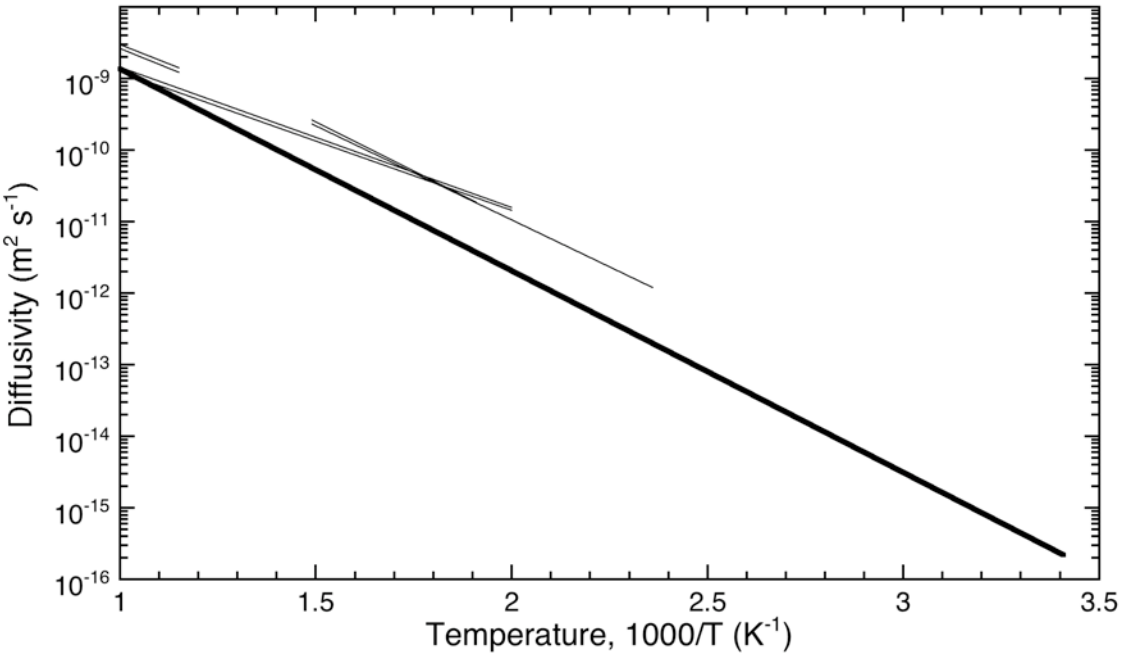

Figure 2.2. Diffusivity of several solid-solution Ni-Cr alloys from gas permeation experiments. All data corrected to hydrogen. The dark line represents the recommendation for austenitic stainless steels from Ref. [36].

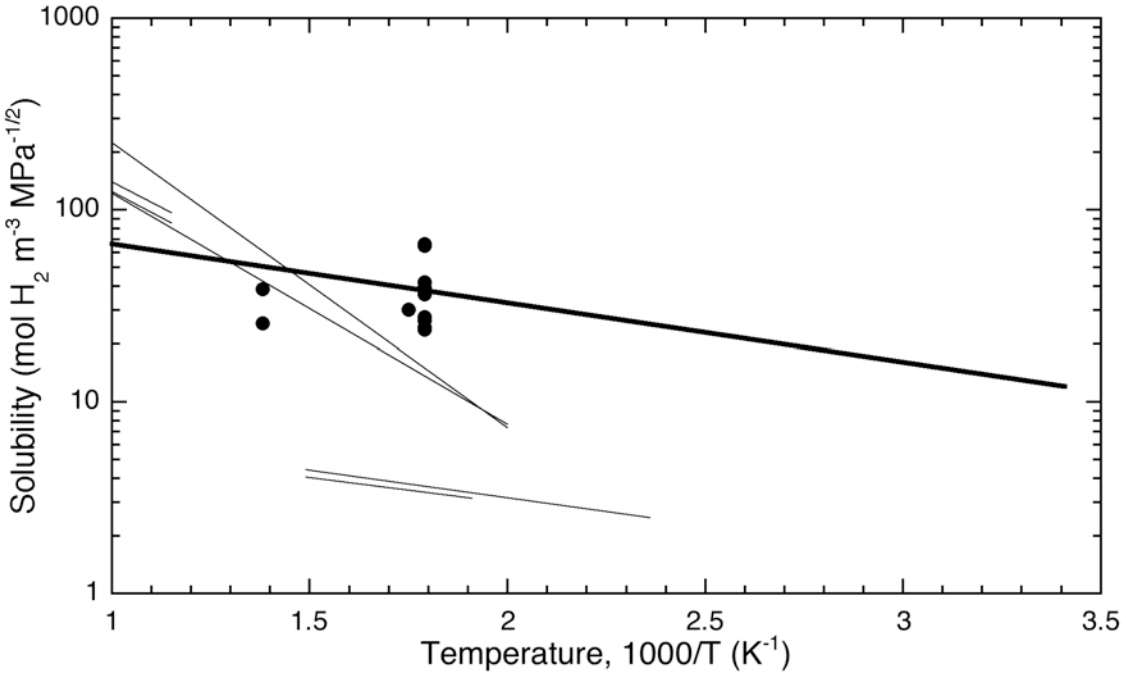

Figure 2.3. Solubility of several solid-solution Ni-Cr alloys from gas permeation experiments. All data corrected to hydrogen. The dark line represents the recommendation for austenitic stainless steels from Ref. [36]. The data points are values determined from equilibrium concentration measurements (i.e., thermal precharging) reported in Table 2.2.

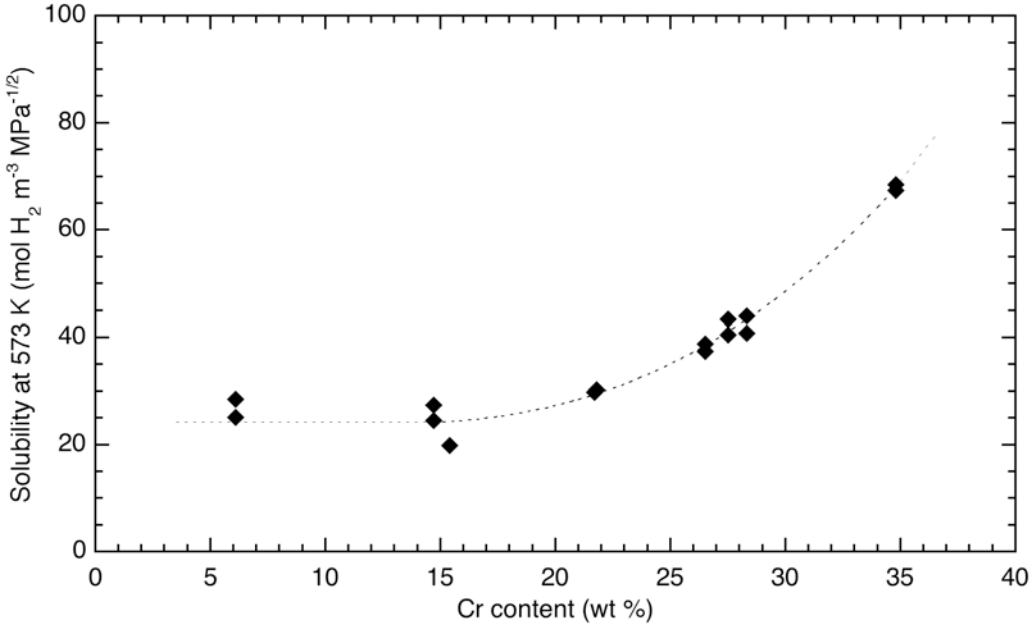

Figure 2.4. Calculated solubility from equilibrium concentration measurements plotted as a function of chromium content. Reported hydrogen concentrations are given in Table 2.2. The solubility is calculated and then corrected to temperature of 573 K assuming the temperature dependence of austenitic stainless steel (E_S = 5.9 kJ/mol) and density of 8.2 g/cm^3.

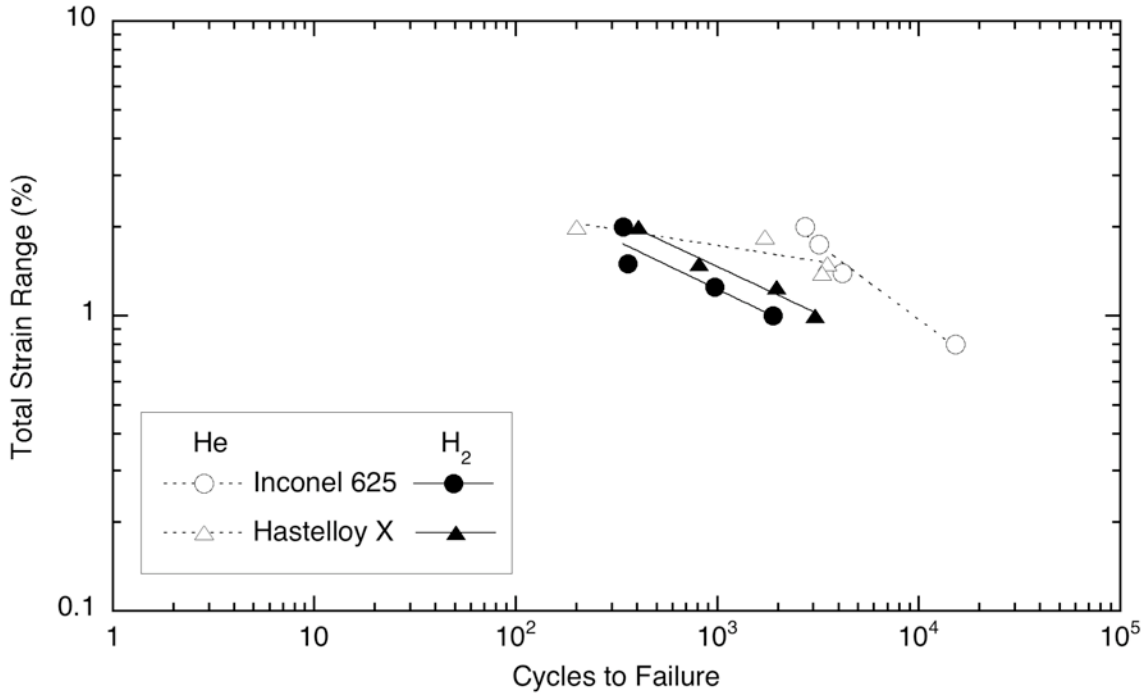

Figure 3.3.1. Low-cycle fatigue in gaseous helium and hydrogen at pressure of 34.5 MPa [20, 27].

Technical Reference on Hydrogen Compatibility of Materials

Nonmetals:

Polymers (code 8100)

1. General

Polymers are a diverse category of materials characterized by chains of covalently-bonded atoms with repeating structural units. The materials can be processed in numerous ways with almost infinite variation. The properties of polymers are determined by a number of factors including crystallinity, density, chain orientation, cross-linking, purity, phase distribution, etc.

We are unaware of hydrogen compatibility studies for common polymer materials that might be expected in gaseous hydrogen service, thus we have eliminated the sections on mechanical properties and microstructural considerations. Gas permeation through polymer materials, however, has been extensively studied; therefore we provide a non-exhaustive summary of hydrogen transport data in common polymer materials.

Relatively large amounts of hydrogen are often soluble in polymer materials; therefore, exposure to high-pressure hydrogen may cause damage (blistering or swelling) of the polymer materials. This is manifest in high-pressure applications due to depressurization of a system (or rapid temperature changes) as hydrogen expands in free volume and at interfaces within the polymers. .

1.1 Composition and microstructure

Polymers are generally characterized by the composition and molecular structure of the material. Nomenclature often evolves from common usage and generally does not incorporate structural details. We use ASTM D1418 and D1600 for guidance on naming. Table 1.1.1 includes the abbreviations used in this document.

2. Permeability, Diffusivity and Solubility

Hydrogen transport in polymers has been extensively studied, particularly for high-vacuum systems. Similar to studies of metals, studies of the hydrogen permeation in polymers have generally been performed at low pressure. Permeability, diffusivity and solubility are often assumed to be independent of pressure for metals and data generated at low-pressure are extrapolated to describe high-pressure systems. This extrapolation implies that hydrogen transport and solubility properties are independent of concentration (i.e., Fickian diffusion). While concentration-dependent transport properties (non-Fickian diffusion) are often observed in polymers, we are unaware of any studies on polymers that suggest hydrogen transport and solubility are dependent on concentration. Thus, until studies show otherwise, we assume that hydrogen permeability, diffusivity and solubility in polymers are independent of pressure. Unlike metals, hydrogen transport in polymer materials is sufficiently rapid that the permeation rates can generally be measured at or near ambient temperature.

The permeability (Φ) is determined from Fick's first law for diffusion, and represents a steady-state property of the material (assuming diffusion is independent of pressure). It is defined in the same way as for metals, such that

$$\Phi = DS \tag{1}$$

where D is the diffusivity and S is the solubility. Hydrogen transport in polymers differs from metals in one important aspect: hydrogen does not dissociate prior to dissolution in the material, thus the concentration of hydrogen dissolved in the polymer (c) is proportional to the fugacity (f, which equals the pressure in the limit of an ideal gas):

$$S = c/f \tag{2}$$

while in metals c is proportional to $\sqrt{f}$. In materials where hydrogen does not dissociate, such as polymers, it should be clear from equations 1 and 2 that the units of permeability are

$$[\Phi] = [diffusivity]\frac{[concentration]}{[pressure]} = \frac{\mathrm{m}^2}{\mathrm{s}}\frac{\mathrm{mole\ H_2}/\mathrm{m}^3}{\mathrm{MPa}} = \frac{\mathrm{mole\ H_2}}{\mathrm{m \cdot s \cdot MPa}} \tag{3}$$

Other forms of these units are, of course, possible and they can be a significant source of confusion. The units in equation 3 are commonly accepted for high-pressure hydrogen since they do not require definition of a reference state.

In tables 2.1 through 2.4, the hydrogen transport properties for a number of polymeric materials are summarized. A secondary resource [1] is used for these values and no effort was made to verify the primary references; the interested reader is also referred to Ref. [2], which contains a lists of primary sources by material. A selection of the hydrogen transport data from Ref. [1] is summarized here. Table 2.1 provides hydrogen transport properties for several common categories of plastics at approximately room temperature. Table 2.2 provides the transport properties for several commercial elastomers near room temperature, while Table 2.3 provides properties for a number of elastomers (rubbers) from a range of classes at room temperature and, when available, at elevated temperature.

Permeability, diffusivity and solubility follow a classic exponential form:

$$A = A_0 \exp\left(\frac{-E_A}{RT}\right) \tag{4}$$

where A_0 and E_A are material-dependent constants, R is are the universal gas constant (8.31447 J $\mathrm{mol^{-1}\ K^{-1}}$) and T is temperature in Kelvin. Table 2.4 provides the constants from equation 4 that summarize the temperature dependence of these properties for several of the materials from the previous tables. The temperature dependence of hydrogen transport and solubility for the materials in Table 2.4 is plotted in Figure 2.1 (permeability), Figure 2.2 (diffusivity) and Figure 2.3 (solubility); these properties are linear when plotted on a log scale as a function of $1/T$ as shown in these figures.

3. References

1. S Pauly. Permeability and Diffusion Data. in: J Brandrup, EH Immergut and EA Grulke, editors. Polymer Handbook, fourth edition. New York: John Wiley and Sons (1999).
2. SA Stern, B Krishnakumar and SM Nadakatti. Permeability of Polymers to Gases and Vapors. in: JE Mark, editor. Physical Properties of Polymers Handbook. Woodbury NY: American Institute of Physics (1996).

Table 1.1.1. Standard abbreviations (from ASTM D1418 and D1600) for common polymeric materials reported in this document.

Abbreviation	Term (AISI/ASTM)
Plastics	
LDPE	Low density polyethylene plastics
PMMA	Poly(methyl methacrylate)
PP	Polypropylene
PS	Polystyrene
PTFE	Polytetrafluorethylene
PVC	Poly(vinyl chloride)
PVF	Poly(vinyl fluoride)
Rubbers (Elastomeric Polymers)	
CIIR	Chloro-isobutene-isoprene rubber
CR	Chloroprene rubber
IIR	Isobutene-isoprene rubber
NR	Natural rubber
NBR	Acrylonitrile-butadiene rubber
NIR	Acrylonitrile-isoprene rubber
SBR	Styrene-butadiene rubber
CSM	Chloro-sulfonyl-polyethylene
EPDM	Terpolymer of ethylene, propylene, and a diene
FKM	One type of fluoro rubber
VMQ	Silicone rubber (vinyl and methyl substituents)

Table 2.1. Hydrogen transport properties for some common plastics from Ref. [1]; abbreviations from Table 1.1.1. Values in parenthesis are not given in Ref. [1], and were calculated using equation 1.

Material	Temperature (K)	$\Phi \times 10^{9}$ $\left(\frac{\text{mol } H_2}{\text{m} \cdot \text{s} \cdot \text{MPa}}\right)$	$D \times 10^{12}$ $\left(\frac{\text{m}^2}{\text{s}}\right)$	S $\left(\frac{\text{mol } H_2}{\text{m}^3 \cdot \text{MPa}}\right)$
LDPE 0.914 g/cm^3	298	3.3	47.4	70.5
PP 0.907 g/cm^3, 50% crystallinity	293	13.8	210	(65.9)
PS biaxial structure	298	7.58	—	—
PMMA	308	1.24	—	—
PVC unplasticized	298	0.58	50	12
	300	0.80	48	(16.7)
PTFE	298	3.3	—	—
	298	3.23	14.7	220
PVF	308	0.18	—	—
PVF (Kynar)	308	0.180	33.6	(5.36)

Table 2.2. Hydrogen transport properties for some common commercial elastomers from Ref. [1].

Material	Temperature (K)	$\Phi \times 10^{9}$ $\left(\frac{\text{mol } H_2}{\text{m} \cdot \text{s} \cdot \text{MPa}}\right)$	$D \times 10^{12}$ $\left(\frac{\text{m}^2}{\text{s}}\right)$	S $\left(\frac{\text{mol } H_2}{\text{m}^3 \cdot \text{MPa}}\right)$
Hypalon 40 (CSM)	308	3.68	265	14.5
Kraton FG	308	22.4	1160	19.2
Viton GF (FKM)	308	7.32	345	21.0

Table 2.3. Hydrogen transport properties for some common elastomeric polymers from Ref. [1]; abbreviations from Table 1.1.1.

Material	Temperature (K)	$\Phi \times 10^{9}$ $\left(\frac{\text{mol } H_2}{\text{m} \cdot \text{s} \cdot \text{MPa}}\right)$	$D \times 10^{12}$ $\left(\frac{\text{m}^2}{\text{s}}\right)$	S $\left(\frac{\text{mol } H_2}{\text{m}^3 \cdot \text{MPa}}\right)$
Poly(butadiene) (BR)	298	14.1	960	14.5
CIIR shore 70‡	293 353	0.857 11.6	—	—
CR shore 42‡	293 353	2.23 27.3	—	—
Neoprene (CR) Neoprene G (CR)	308 298	9.24 4.55	933 380	9.9 12.8
Poly(isobutene-*co*-isoprene) (IIR) 98/2	298	2.42	152	15.8
Poly(butadiene-*co*-acrylonitrile) (NBR) 80/20 (Perbunan†) 61/39 (Hycar†)	 298 298	 8.43 2.39	 643 243	 13.2 9.7
NBR shore 70‡	293 353	1.45 12.1	—	—
NBR shore 60‡	293 353	1.67 21.1	—	—
NBR shore 50‡	293 353	2.04 17.1	—	—
Poly(isoprene-*co*- acrylonitrile) (NIR) 74/26	298	2.49	247	10.1
NR shore 66‡	293 353	4.09 38.4	—	—
SBR shore 52‡	293 353	2.98 21.7	—	—
CSM shore 70‡	293 353	1.31 9.28	—	—
EPDM shore 68‡	293 353	6.96 38.4	—	—
FKM shore 70‡	293 353	1.51 18.6	—	—
VMQ shore 50‡	293 353	100 260	—	—

† trade names
‡ shore durometer (hardness)

Table 2.4. Relationships for temperature dependence of hydrogen transport properties for some common polymers from Ref. [1]; abbreviations from Table 1.1.1. Values in parenthesis are not given in Ref. [1], and were calculated using equations 1 and 4 with values reported in the other tables.

Material	Temperature Range (K)	Permeability $\Phi = \Phi_o \exp(-H_\Phi / RT)$		Diffusivity $D = D_o \exp(-H_D / RT)$		Solubility, $S = \Phi/D$ $S = S_o \exp(-\Delta H_s / RT)$	
		Φ_o x 10^3 $\left(\frac{\text{mol H}_2}{\text{m}\cdot\text{s}\cdot\text{MPa}}\right)$	H_Φ $\left(\frac{\text{kJ}}{\text{mol}}\right)$	D_o x 10^6 $\left(\frac{\text{m}^2}{\text{s}}\right)$	H_D $\left(\frac{\text{kJ}}{\text{mol}}\right)$	S_o $\left(\frac{\text{mol H}_2}{\text{m}^3\cdot\text{MPa}}\right)$	ΔH_s $\left(\frac{\text{kJ}}{\text{mol}}\right)$
PP 0.907 g/cm^3, 50% crystallinity	293 - 343	99.9	38.5	—	—	—	—
PVC unplasticized	298 - 353	0.651	34.5	(55.7)	34.5	(11.7)	0
PTFE	293 - 403	0.0185	21.4	—	—	—	—
Poly(butadiene) (BR)	298 - 323	0.959	27.6	(5.20)	21.3	(185)	6.3
Neoprene G (CR)	288 - 323	3.93	33.9	(26.2)	27.6	(162)	6.3
Poly(isobutene-*co*-isoprene) (IIR) 98/2	298 - 323	5.71	36.4	(133)	33.9	(43.4)	2.5
Poly(butadiene-*co*-acrylonitrile) (NBR) 80/20 (Perbunan†) 61/39 (Hycar†)	298 - 323	 1.57 6.65	 30.1 36.8	 (23.2) (91.1)	 26.0 31.8	 (69.1) (72.8)	 4.1 5.0
Poly(isoprene-*co*- acrylonitrile) (NIR) 74/26	298 - 323	11.7	38.1	(67.1)	31.0	(178)	7.1

† trade names

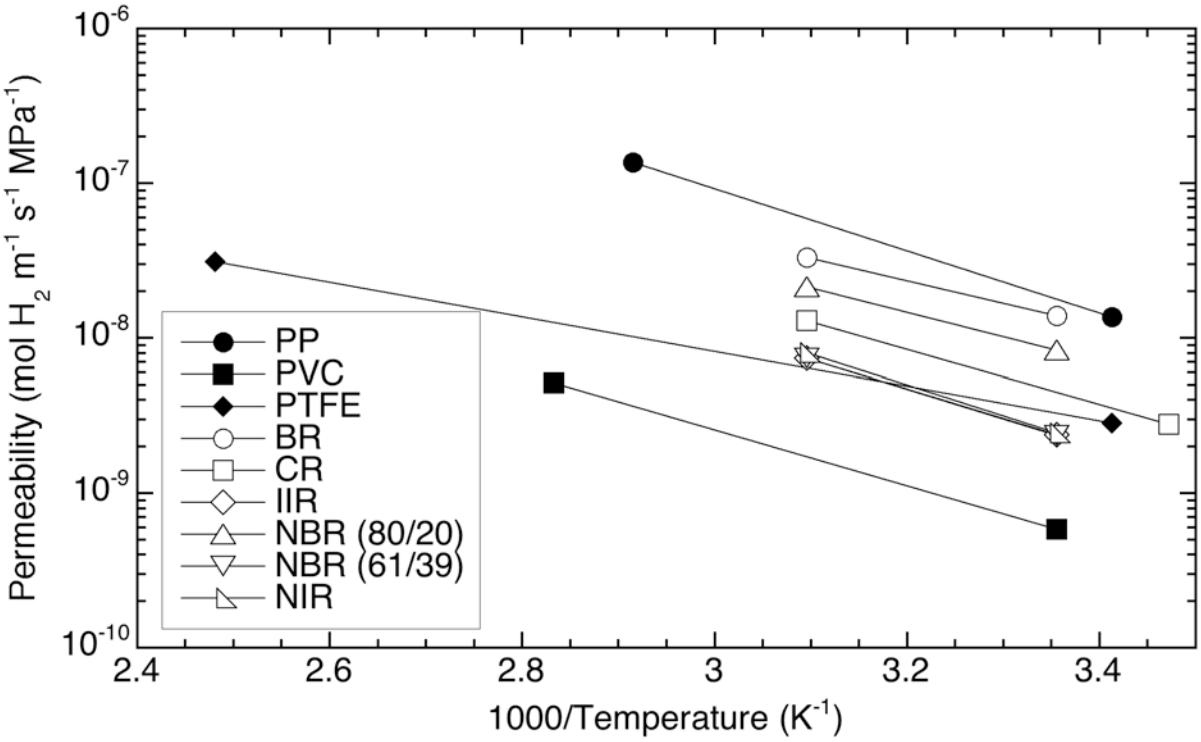

Figure 2.1. Permeability relationships (from Table 2.4) for several polymers.

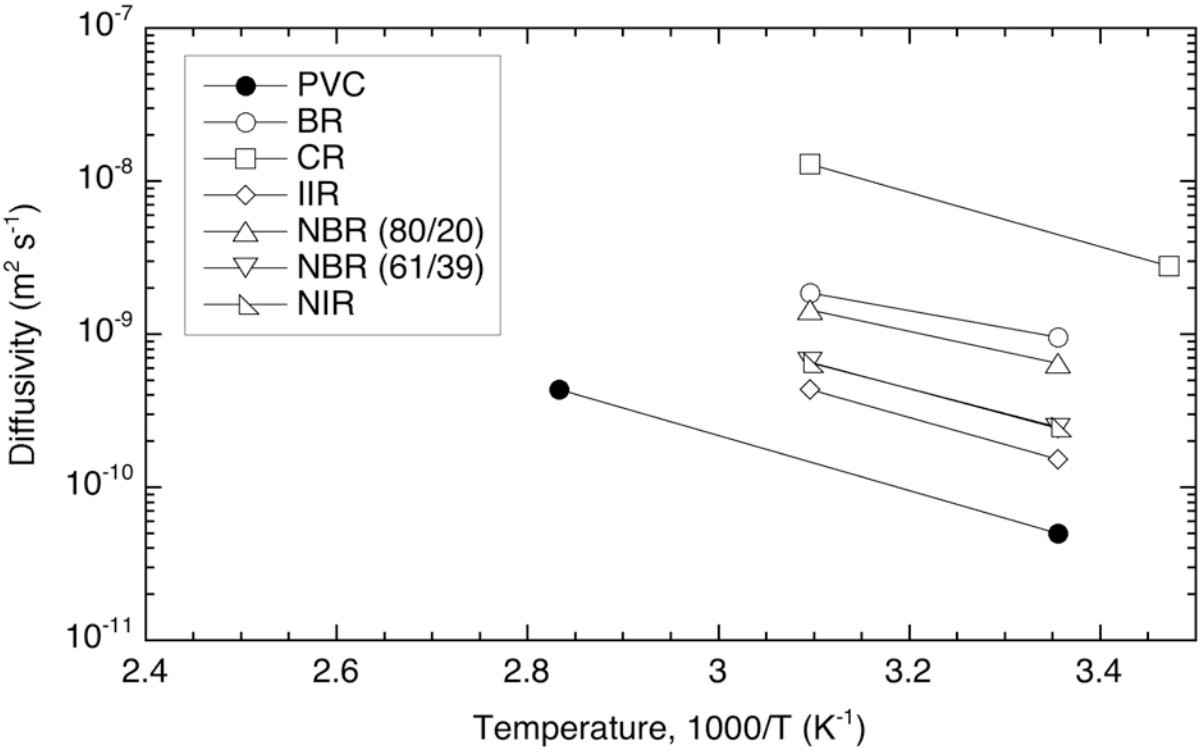

Figure 2.2. Diffusivity relationships (from Table 2.4) for several polymers.

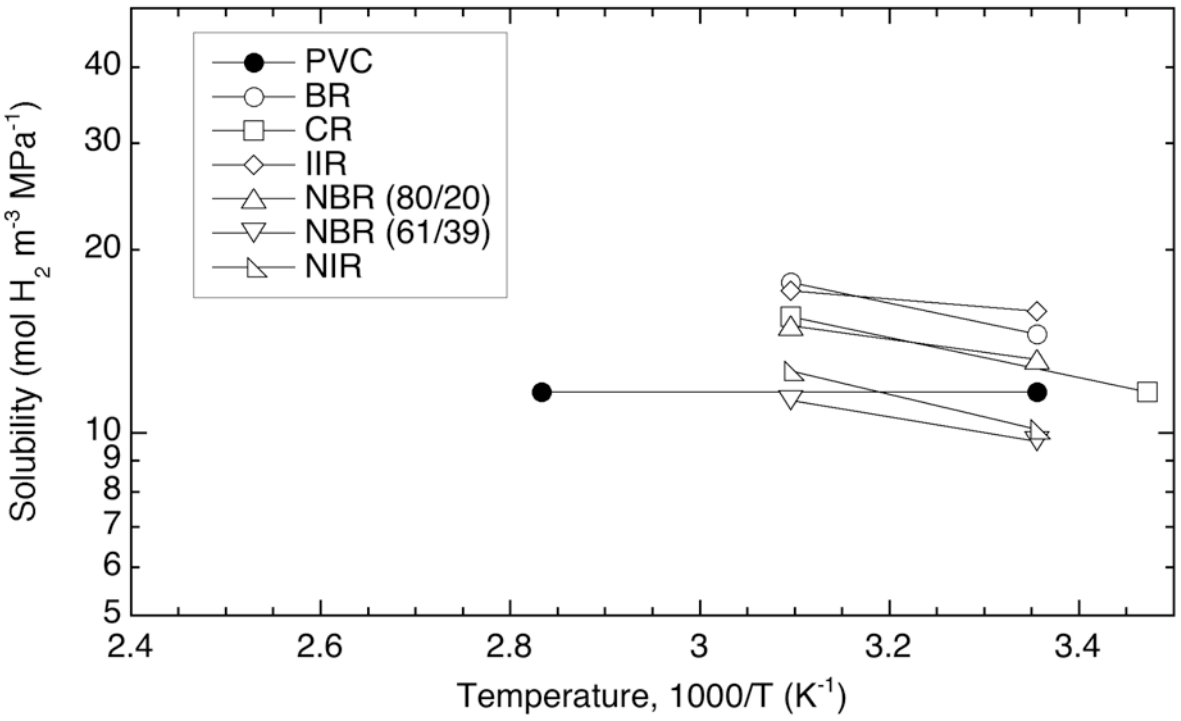

Figure 2.3. Solubility relationships (from Table 2.4) for several polymers.

DISTRIBUTION

1	MS0899	Technical Library	9536 (electronic copy)

This report in intended to be distributed electronically from the external website:
www.sandia.gov/matlsTechRef/

Electronic copies may also be requested from the authors or Sandia Technical Library.

This page intentionally left blank.